Instituto Politécnico de Tomar
(Unidade Departamental de Arqueologia, Conservação e Restauro e Património)

Istruzione e cultura
Erasmus Mundus

Master Erasmus Mundus em
QUATERNARIO E PRÉ HISTÓRIA

Gruta do Morgado Superior: A bioarchaeological analysis of the Chrono-cultural Periods in Square K51

H. Alejandro Delgado Ortega

Orientadores:
Luiz Oosterbeek
Francisco Curate

Ano académico 2022 /2023

Abstract: The bioarchaeological analysis of Gruta de Morgado Superior (Square 51) was conceived as a holistic analysis performed on a fraction (28%) of one of the biggest skeletal assemblages in Portugal for its chronology. The main objective was to characterize the chrono-cultural traditions that were already identified by the archaeologist in charge of the Excavation, Ana Rosa Cruz, and understand the sequence that led to its morphology. The context is a highly fragmented and disturbed collective inhumation that required the implementation of numerous anthropometric techniques for the elaboration of its paleodemographic profile and determination of its morphometric traits The analysis consisted in the consolidation of a global database that, hopefully, serves as the starting point for the analysis of the remaining material. GIS tools were used for dispersion analysis of every type of material, on the site and on the square. Results confirm that three culturally differentiated communities used the site as a funerary space, and that cultural traits associated to the Mesolithic survived well into the Chalcolithic. Lastly, the theory that places human intervention as the main taphonomic agent for the breakage and dislocation of the material was not entirely denied, even though there was no evidence that supported it.

Resumen: El análisis bioarqueológico de Gruta do Morgado Superior (Cuadrado 51) fue concebido como un análisis holístico llevado a cabo en una fracción (28%) de una de las colecciones esqueléticas más grandes para esa cronología. El principal objetivo del análisis fue caracterizar las tradiciones crono-culturales, ya identificadas por la líder de excavación, Ana Rosa Cruz, y comprender la secuencia de eventos que construyó su morfología. El contexto de inhumación colectiva, que se encuentra altamente fragmentado y perturbado, requirió de la implementación de técnicas antropométricas para la elaboración de un perfil paleodemográfico y la determinación de sus caracteristicas morfométricas. El análisis consistió en la consolidación de una base de datos global que pueda server como base de análisis para el material restante. Herramientas SIG fueron implementadas para análisis de dispersion de material global y local. Los resultados confirman que tres comunidades culturalmente diferenciadas usaron el sitio como espacio funerario, y que algunos rasgos culturales, asociados al Mesolítico, sobrevivieron hasta bien entrado el Calcolítico. Por último, la teoría de bioturbación por agentes antrópicos no fue totalmente descartada, aunque tampoco se encontró evidencia de que sea la principal causa tafonómica de fragmentación y dislocación.

Acknowledgements

I would like to thank Professor Ana Rosa Cruz for her arduous work in Gruta do Morgado Superior. I hope I have contributed to her years of research. I would also like to thank Prof. Luiz Oosterbeek for his patience and guidance, as well as Prof. Francisco Curate and Prof. Carlos Lorenzo.

Contents

List of Tables

List of Figures

List of Charts

List of Photos

List of Maps

1. Introduction

Funerary contexts brim with intentionality and purpose. Even when their layout seems chaotic, they serve as a testament to the will and prowess of the living (Tomé, 2010). Gruta do Morgado Superior is a challenge from different perspectives; it does not present a clear pattern of funerary architecture at first glance; most of the grave goods, as well as the skeletal elements, are shattered and intermingled in what seems to be an amorphous block of sediment. Archaeologist Ana Cruz faced the convoluted site for over a decade, trying to understand how it was constructed and by whom. Cruz was forced to adapt different methodologies to better approach the site, creating a stratigraphic model that would prove to be the key for an accurate description and interpretation of the inhumations that laid within the cave.

However, many questions remain unanswered; the sheer volume of material, most of which is comprised by human skeletal remains, dwarfed famous neighbouring sites as Gruta dos Ossos, Gruta do Cadaval, and Gruta de Nossa Senhora das Lapas. This brings us to the main objective of this study, which is to define the characteristics of three chrono-cultural periods that have been identified within the cave: the Neolithic, the Chalcolithic, and the Early Bronze Age. The trifecta represents one of the greatest transitions in human history that would eventually set the foundations upon which hierarchized societies would flourish, thanks to the introduction of farming, herding, food storage, and production excess. However, just as the cave, this process has been difficult to characterize in Western Europe, as Eastern models fail to befit the unearthed evidence, especially in Portugal.

The main objective of this academic endeavour is to determine if it is possible to characterize said cultures by performing a bioarchaeological analysis, in a holistic way, that incorporates a global overview of the context into the local archaeological context. As a secondary objective, a taphonomical catalogue will be presented to obtain information about the primary suspects behind the breakage of material in the cave, also considering their spatial distribution.

The analysis could only be performed on one square of the excavation due to time constraints. While samples may not represent the population accurately most of the time, “random sampling provides a basis for estimating how likely it is that our inferences about the population are wrong, and thus tells us how much confidence we should place in these inferences” (Drennan, 2010, P. 85).

The collection of Gruta do Morgado Superior is the result of a series of excavations, undertaken in recent years by Prof. Ana Rosa Cruz, who became my first co-supervisor. The general proposal I had received was to organize the collection and characterize in bioarchaeological terms. In the following chapters I present the results of such research. Unfortunately, Professor Ana Rosa Cruz passed away and could not see the results, but I think the main purpose has been achieved.

This work, besides the introductory and concluding chapters, is organized through four chapters, numbered 2 to 5.

Chapter 2 presents the site, within its natural and archaeological context, also clarifying the driving research questions.

Chapter 3 characterizes in detail the collection and explains the methods that have been selected to be used to address the research questions.

Chapter 4 presents the data obtained and related results.

Chapter 5 discusses the obtained results when confronted with the initial research questions and other issues raised throughout the research itself.

The thesis concludes with a discussion of the results within the wider regional context.

2. Gruta do Morgado Superior

Gruta do Morgado Superior, whose name roughly translates to Upper Morgado Cave, is a karstic rock shelter that harbours one of the largest prehistorical sites in the Ribatejo region, Portugal. Nowadays it is predominantly known as Abrigo do Morgado Superior (or AMS) (Upper Morgado Rock Shelter), although it behaves as a cave from the stratigraphic and speleological point of view (Cruz, 2017). GMS has a sister opening called Gruta do Morgado Inferior, which is located at the bottom of the cliff; hence earning the 'Inferior' component of its name. Morgado has been interpreted as a convergent location for past communities who wove it into their cultural practices as funerary space. Starting from the Neolithic and going all the way through the Chalcolithic, up until the Bronze Age, the cave witnessed countless funerary rites amalgamate and shape its peculiar layout. Its interaction with humans would not end there, although the nature of their relationship would; the rock shelter would continue to offer haven to occasional visitors in historic times, among whose most prominent guests include soldiers from the Napoleonic wars and fisherman from the 80's.

2.1. Geology and Geomorphology: The Alto Ribatejo Region

Gruta do Morgado Superior is embedded on the base of limestone cliff, located in the Alto Ribatejo (High Ribatejo, i.e., the northernmost part of the Middle Tagus Basin in Portugal). The Alto Ribatejo region is characterized by its heterogeneous geomorphologic landscape (Oosterbeek, 1994b) that was most likely consolidated during the Holocene. A gravitational axis aligned to the Lower Tagus region seems to have dominated the Alto Ribatejo, consolidating a tripartite orographic reign between the watercourses of the Zêzere, Almonda (both of which flow directly into the Tagus, the former being its main tributary) and Nabão (a current tributary of the Zêzere that used to flow directly into the Tagus before its capture over a million years ago) (Oosterbeek, 1994b). These rivers flow into a geological fringe zone where three great geomorphological formations clash onto each other: the Meso-Cenozoic western fringe, the Miocene basin of the Tagus (infilled with detrital sediments deposited in numerous terraces during the Quaternary), and the Central Iberic Massif. The convoluted geomorphological design has been correlated to prehistoric human occupation patterns on the area (Cruz et al., 2013; Oosterbeek, 1997). Elements such as soil composition, types of biomes, and climatic variables have yet to be included into the system (Cruz et al., 2013).

Nabão's orography is constituted by Cenozoic formations from the Miocene, covered occasionally by Holocene or Quaternary alluvial deposits. From the lithological point of view, its components are dominated by conglomerates, sandstone, dolomite limestones (West and Northeast). The central, Eastern, and Northeastern sections display outcrops of schist, amphibolite, greywacke, quartzite, gneiss, and granites. The broader areas near the Tagus, the lower Nabão, and the Zêzere are composed by sandstone, marl limestone, sands, gravel beds, clays and alluvions (Cruz, 1997). Archaeological sites along the Nabão are concentrated on a reduced number of geological formations: The Upper Nabão sites and Canteirões are embedded on Jurassic limestone formations; the open air sites that are located on Quaternary fluvial deposits from the Tagus valley; and the last group, all sites located along the Zêzere valley emplaced on Pre-Cambric formations.

Morgado owes most of its physicochemical characteristics to the limestone Massif of Sicó-Alviázere, which is composed by carbonated units dated to the Middle and Lower Jurassic (i.e., limestones of Sicó and Oolithic limestones of Santo António das Lapas). The underlying carbonated bedrock stretch starts in the municipality of Condeixa and elongates up until the council of Tomar. A wavy orography dominates the landscape, in which rarely the altitude exceeds 150 meters a.s.l. The surface showcases fissured and compressed formations with varied degrees of permeability, typical of the Orogenic Alpine cycle (Cruz et al., 2018).

Map 1 Landforms of Alto Ribatejo according to Frye (2023). Note how GMS is located within an area with a wide arrange of landforms that clash towards the centre.

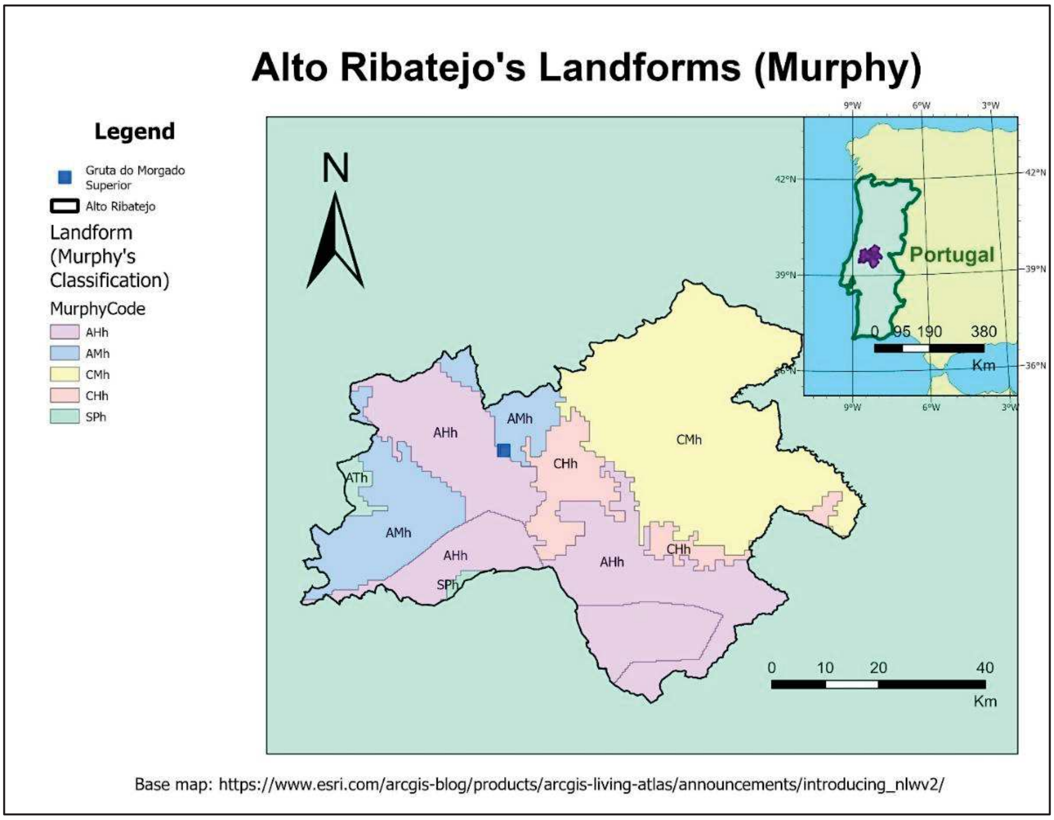

Most attempts to describe the geological landforms in the area have proven difficult due to its diversity. Generally, the Tagus basin is associated with a hill-shaped topography related to generic European wet lowlands, while the mountainous landscape from the Central Iberic Massiff and the Meso-Cenozoic western fringe are classified as hill-shaped topographic features (Frye et al., 2023) (see **Map 1**). Some categories geomorphological categories that have been used in the past include: *i*) orogenic processes related to the Iberian Plateau (i.e., Meseta), which are categorised as moist soils with either a hill-like (**AHh**) or mountain like (**AMh**) topography; orogenic processes related to the Alentejo Plateau that can also be hill-like (**CHh**) or mountain-like (**CMh**); and *iii*) orogenic processes related to the Ribatejo Plateau lowland (**SPh**) (see **Map 1**).

Nonetheless, from a geological perspective, most attempts to characterize the Alto Ribatejo's subregions has been hampered thanks to a complex series of neotectonic faults that shape its irregular landscape (Cruz et al., 2018). The encompassing term of Alto Ribatejo, as proposed by PhD Luiz Oosterbeek (1994b), overcomes this difficulty by using a combination of geomorphologic, ecologic, and anthropic criteria: an ecotonal zone peopled by communities that could dwell on it exploiting its diversity. In this sense, the region limits respond not only to its orogenesis but to anthropic processes of occupation as well. When compared with historic and administrative frontiers, it roughly includes the current Middle Tagus administrative unit, spreading towards Alviázere to the North, Golegã in the centre, and parts of the municipalities of Gavião and Chamusca in the South.

2.1.1. Climate

Paleoenvironmental reconstruction analysis has suggested that there was a progressive degradation of the environment during the Holocene, associated to the decline of arboreal species and their gradual replacement by herbaceous plants and shrubs. It is hypothesized that this process was the result of the intensification of human activity on the region, which fuelled by a deforestation event that had already been set in motion by climate change (Ferreira et al., 2013). Thus, the Holocene was witness of a continuous deforestation phenomena, which precedes the first appearance of Neolithic traits, and being followed by the consolidation of agropastoralism. Chalcolithic soils seem to have been preserved better than other soils used for agriculture, suggesting the development of a rich paleosol by the end of the 4th millennium BC, possibly associated to an acceleration of husbandry and farming activities in the region.

Climate patterns were most likely cold by the end of the 4th millennium (Middle Neolithic) and then succeeded by a warmer and more humid weather. This change could have been implicated in a series of cave ceiling collapses among the Canteirões region (Oosterbeek, 1993a).

2.1.2. Palaeobotany

The Nabão valley has provided complete sequences of sediment that, unlike those from the Tagus and Zêzere, are continuous and can be linked to the formation of thick stalagmitic mantles inside nearby caves and rock shelters. These formations are often associated to hot and humid weathers. Climate change turned the valley drier after this phase, resulting on the erosion of sandstones that mixed with the local clay. These climatic events are supported by palaeobotanic findings.

Palynological and anthracological analysis have recreated the spread and contribution of botanical specimens in the past, leading to the identification of three types of ecosystems: *i*) the flora from the late 6th Millennium BC (based on data collected at Armoreira and Gruta de Nossa Senhora das Lapas) was characterized by the presence of *Quercus ilex*/*coccifera* (evergreen oak/kermes oak bush) (25%), *Pistacia lentiscus* (lentisk or mastic) (20%), *Quercus suber* (cork oak) (18%), *Olea europaea* (olive), *Arbustus unedo* (strawberry tree) (10%), and the predominant genus *Juniperus* sp.; ii) the flora from the 5th millennium BC (based on information from Gruta de Nossa Senhora das Lapas, Gruta do Cadaval, and Anta 1 de Val da Laje) had a major contribution of *Pinus* sp. (17%), *Quercus* (9%), shrubs and herbs; lastly, iii) the flora from the 4th and 3rd millennium (based on information from all the sites at Canteirões de Nabão) was dominated by *Olea europapaea* (olive) and *Arbustus unedo* (strawberry tree) (30% each) (Oosterbeek et al., 2000). Data extracted from the caves was found in a continuous sediment that was somehow protected from the most aggressive erosion phenomena that abates its open-air counterparts (Allué, 2000).

Nonetheless, palynological and anthracological samples collected from cave-contexts face several methodological obstacles such as their overall poor conservation state, their high fragmentation rate, and their aleatory distribution patterns along different horizons. When properly collected, samples from these sites not only showcases the general distribution of botanical elements (palynology) but also cultural patterns of selection and usage of certain species(anthracology and palynology) (Allué, 2000). Results from studies performed on layers I/III and IV from Gruta dos Ossos (associated to anthropogenic alterations (Oosterbeek, 1993a)) identified the most common species on the landscape the Neolithic (see **Table 1**).

Table 1.Taxa identified at the Late Neolithic site, Gruta dos Ossos, Layers I, III, and IV (Allué, 2000, p. 54, Table 3).

Taxa	I/III	IV
Arbutus unedo	10	34
Erica sp.	1	-
Olea europaea	12	4
Pistacia lentiscus	4	1
Quercus ilex/coccifera	3	-
Quercus sp. Deciduous	-	1
Rhamnus/Phillyrea	3	-
Leguminosae	-	1
Indeterminable[1]	4	5
Undetermined 1	-	1
Undetermined	1	-
Total	**35**	**50**

Hence, the Nabão valley would likely have been dominated by oaks, pines, and olives (*zambuijero* variant), and strawberry trees (arbutus berry[2]). Eventually, the deforestation process would take a toll in the frequency of oaks and pines, akin to the one on the Zêzere valley. In conclusion, the arboreal landscape (during the Late Mesolithic) would end up transforming into a shrub-dominated one by the advent of the Chalcolithic (Oosterbeek et al., 2000). Communities living during the Neolithic probably exploited all available biotopes (e.g., riverside forests, evergreen oak forests, thickets, etc.). Use and intensity

[1] It is unclear whether *Indeterminable* and *Undetermined* are different categories, or if they refer to a specific layer.
[2] Although the fruit is referenced as a “strawberry” in Portuguese, the fruits are not real strawberries, hence the clarification.

varied depending on the related activity, whether it included extraction for fuelwood, construction, or manufacturing. These populations had a particular preference for the use of shrubs (Allué, 2000).

2.2. Archaeological Research on the Nabão Valley

The Nabão river receives the waters of the Fetal stream within a short meandric gorge known as Canteirões (Cruz et al., 2018). The ravine is dotted with karstic openings found along the riverbanks, some of which have yielded the most important prehistoric sites in area (Tomé & Silva, 2013). Archaeologists have conducted excavations at cave sites such as Gruta do Caldeirão, Gruta do Cadaval, Gruta dos Ossos, Gruta de Nossa Senhora das Lapas, and Gruta do Morgado Superior (see **Map 2**). Other prehistoric contexts have been only identified at Gruta das Andorinhas, Gruta do Sobreinnho, Gruta dos Morcegos and on top of the hill of Casais Novos.

Canteirões de Nabão presents evidence of communities from the Neolithic, Chalcolithic and Early Bronze Age, with some sites displaying a continuous occupation along the whole sequence (see **Figure 1** and **Table 2**).

Map 2. Location of some of the archaeological sites in the Canteirões do Nabão sector. Based on the coordinates presented in Cruz (1997) 1996. Hypsometric data provided by the USGS (https://earthexplorer.usgs.gov).

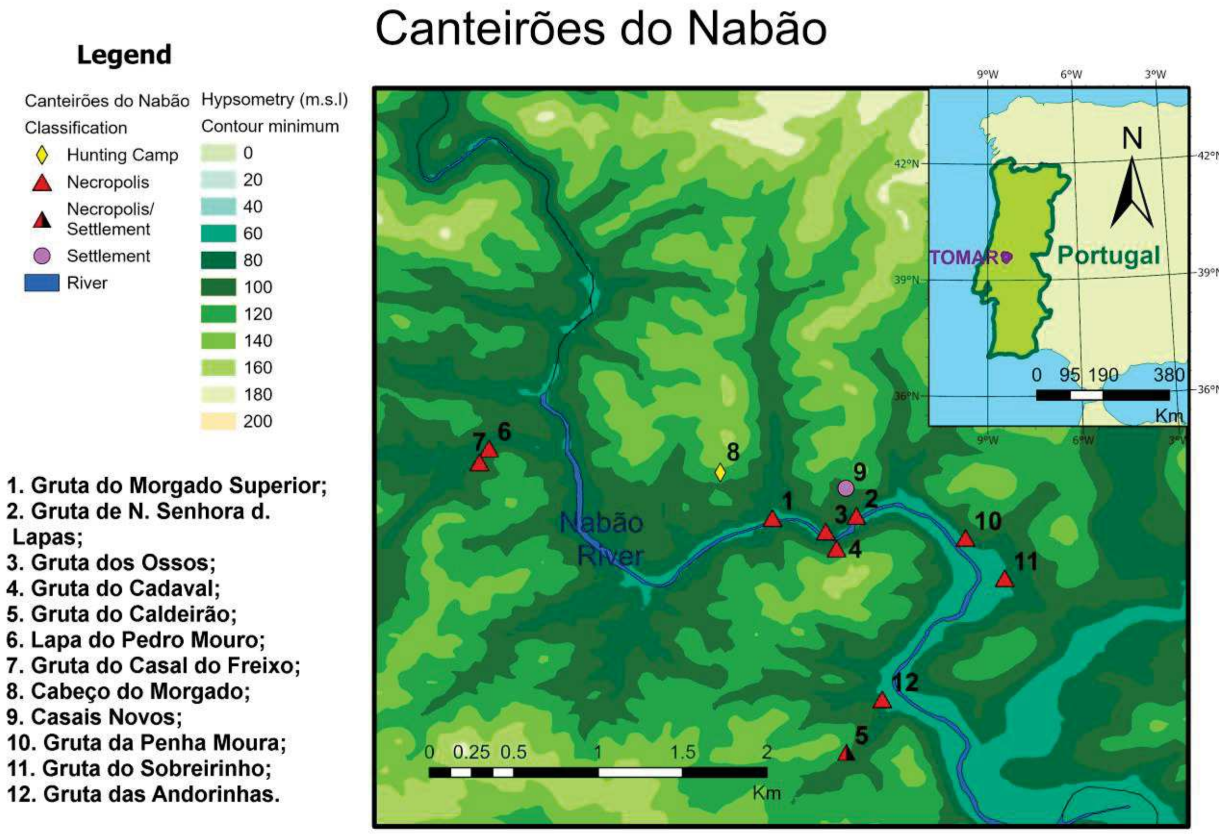

Figure 1. Comparison between some of the first radiocarbon dates from the Canteirões do Nabão group that includes Gruta dos Ossos, Gruta do Caldeirão, and Gruta de Nossa Senhora das Lapas(Cruz et al., 2013, p. 165, Grafico 8).

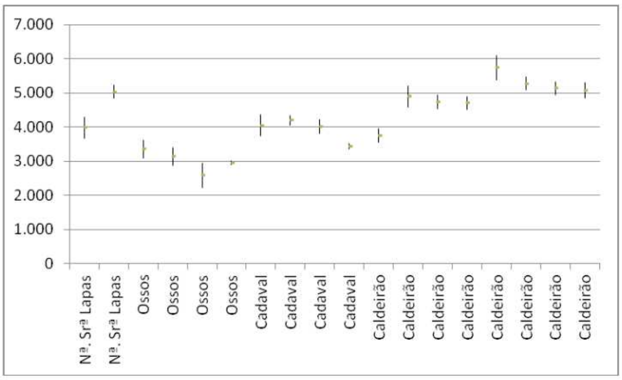

Table 2. Absolute dates taken from NSL-Gruta de Nossa Senhora das Lapas; CDV-Gruta do Cadaval, and GRO- Gruta dos Ossos (Tomé & Silva, 2013, personal translation, updated).

Site	Stratigraphic Unit	Reference	BP	Cal BC 2 sigma	Publication
NSL	Layer B (base)	ICEN-805	6100 ± 70	5220-4880	(Oosterbeek, 1993b)
NSL	Layer B	I-17247	5130 ± 140	4260-3650	(Cruz, 1997)
CDV	Layer D (S1)	ICEN-803	5390 ± 50	4340-4220	(Oosterbeek, 2003)
CDV	Layer C	I-17241	5180 ± 140	4270-3700	(Oosterbeek, 2003)
CDV	Layer D (S2)	ICEN-464	5160 ± 50	4050-3890	(Oosterbeek, 1994a)
CDV	F30 Layer C	Beta 189995	4640 ± 40	3520-3350	(Oosterbeek, 2003)
CDV	N/A	Thermoluminescence	3260±500	N/A	(Oosterbeek et al., 2020)
CDV	N/A	Thermoluminescence	1460±350	N/A	(Oosterbeek et al., 2020)
GRO	Layer I–III	ICEN-465	4630 ± 80	3540-3260	(Oosterbeek, 1993a)
GRO	Layer I-III	I-17368	4460 ± 110	3380-2890	(Oosterbeek, 1993a)
GRO	Layer I-III	Beta 189996	4330 ± 40	3030-2890	(Tomé, 2006)
GRO	Layer IV	I-17248	3970 ± 140	2880-2130	(Oosterbeek, 1993a)
GRO	N/A	N/A	N/A	5582-5053	Carvalho, 2014
GRO	N/A	N/A	N/A	5447-4840	Carvalho, 2014

Based on the information collected at the sites, it is likely that local communities constructed several socio-economic networks with their contemporary neighbours that spanned since the Epi-Palaeolithic and endured until the Bronze Age. The extent of these networks was large enough to connect them to societies living in Estremadura, the southern regions, and the coastline. In the archaeological record such commercial bonds can be seen through traded objects made of flint, shells, quartz, amphibolite, and shale. During the Bronze age, similar intracommunal exchange routes would allow for the acquisition of amber, copper, and tin (Cruz et al., 2018). Materials obtained through these networks have yet to be subjected to a systematic physical or chemical analysis that may link them to probable sources. Nonetheless, a preliminary inventory of possible natural flint quarries has been recorded, so possible trading routes can be mapped when new data comes to light. There are several sites that meet the necessary conditions: *i*) The westernmost range of the middle Tagus (11 km away from Tomar); *ii*) near Ribeira da

Sabacheira, in the margin of the Nabão river; *iii*) Ferreira do Zêzere, 3 km from the Avecasta Cave; and *iv*) the Municipality of Alcanena and Rio Maior. When pondering all possible sources, a reasonably ample exchange network, with a diameter of 100 km, can be inferred. This network may have included sites such as Laranjal de Cabeço das Pias (Torres Novas), Cerradinho do Ginete (Torres Novas), Gruta do Caldeirão (Tomar), Gruta do Cadaval (Tomar), Gruta dos Ossos (Tomar), Gruta do Nossa Senhora das Lapas (Tomar), Gruta do Morgado Superior (Tomar), Fonte Quente's I and II settlements (Tomar), Covão da Arrascada (Tomar), Algar do Barrão (Alcanena), Marmota Cave (Alcanena), Carrascos Cave (Alcanena), and Colos Hypogeum, among others (Cruz et al., 2018).

2.2.1. Theoretical Framework: The Neolithic, Chalcolithic, and the Bronze Age

The Golden Age of Portuguese Archaeology saw the description of skeletal remains relegated to a mere typological analysis, focusing mostly on long bones and cranial elements for a long time. The resulting information gaps started to weigh on the interpretation of funerary contexts, which led to the overhaul of the techniques and methodologies applied for their study in the last decades. The resulting methodologies inspired by the new approaches generated a promising corpus of information, especially constituted for the study of the transition to agropastoralism located chronologically between the Mesolithic and the Chalcolithic. Mesolithic communities became fundamental to understand their role in the process, whether they were considered the catalyst (diffusionist approach) or the direct ancestors (evolutionary approach) of the agropastoral socio-economic system. Neolithic and Chalcolithic human groups were regarded as the ones that eventually implemented said system, in a process that is formally known as the *Secondary Products Revoultion* (Tomé, 2010). I

The tripartite chronological division of the Stone Age would prove elusive in prehistoric communities from the Iberian Peninsula, even more so when trying to individualize the Mesolithic boundaries. Additionally, the transition between the 4th and 3rd millennium BC saw an unusual surge of collective burials that were not limited to megaliths or caves (Tomé, 2010). Although the attempts of delimiting the chrono-cultural frontiers among these populations have been arduous, the existence of an insurmountable barrier between the hunter-gatherer communities and the agropastoral ones may not ultimately exist, at least in such stern terms (Cruz, 1997).

Recent findings obtained through ancient DNA techniques (Szécsényi-Nagy et al., 2017) have found a significant presence of hunter-gatherer DNA within the genetic make-up of Neolithic communities, suggesting that these groups did not clash nor replaced each other, but built a network of exchange of goods and people that, in a way, could have kept ancient hunter-gatherer cultural traits alive. The interpretation of burial contexts could change as well, since these funerary contexts on megaliths and caves may be passage graves that integrate elements of local and regional cultures. These structures are therefore manifestations of the economy, social structure, mobility, subsistence and funerary patterns of both societies (Stojanovski et al., 2020).

Another aspect worth analysing is the modification of the landscape, namely the construction of physical structures that are ultimately a projection of the interpretation of the landscape itself, through the cultural lenses that reflects interpretative narratives based on symbolism and territory. Such modifications may take the form of habitational architecture, rock art, monuments, and burials. Neolithic traits probably required a preliminary change in climate and environmental composition, that coupled with foreign economic trends, produced the biggest changes in a relatively peaceful fashion. Thus, landscape cultural markers are the result of underlying notions space (distance), of time (change), and causality (consequence) that converge in a socio-economic system and end up shaping the surrounding landscape (Oosterbeek et al., 2018).

Before continuing with a summary of the most important archaeological studies in the Canteirões area, some concepts and their historical evolution must be revisited. Notions of the archaeological significance of the Neolithic, Chalcolithic and Bronze Age in Europe, and their implications for the Alto Ribatejo region (Portugal) will be presented next.

2.2.1.1. *Neolithization process*

Several authors have constructed their own variation of what the advent of the Neolithic meant for prehistoric people and those that came after. The Neolithic has been interpreted as a revolution, a process, an ideal. It is arguably the moment in which the foundations of hierarchical societies that relied on a socio-economic model based on accumulation and growth was laid down.

Robert Dennel (1972) (cited by Cruz, 1997) proposed three phases of neolithization: the Holocene expansion of herbaceous species, the expansion of the forests that in turn relocated herbaceous resources, and the consolidation of permanent agricultural centres that started to select animal species, botanical resources, and soils for domestication, and developed methods of harvesting. This model accepts a non-colonizer diffusion. Zvelebil and Rowley (1984) (cited by Cruz, 1997) tried to delimit a mobile and mutating frontier, or a sequence of frontiers, in opposition to a diffusionist and expansionist frontier. that This theory was founded on three phases: availability, substitution, and consolidation. They argued that diffusionist explanations are based upon arbitrary -and dubious- prejudices such as: i) the dichotomy between Europe and the Near East; *ii*) that cereals, leguminous plants, sheep, and goats originated only in the Near East; and *iii*) that the diffusion of products was done exclusively by humans (Cruz, 1997).

A.J. Ammerman and L.L. Cavalli-Sforza (1971) strongly believe that the Neolithic should approached purely on its economic sphere. Farming techniques would theoretically have emerged from single centres of diffusion that started in the Near East and Greece and expanded to the West. One of their fundamental axioms is that European ceramic traditions appear to have been imported along these colonization waves. The wild progenitors for emmer (*Triticum dicoccoides*) and barley (*Hordeum spontaneum*) do not appear to have extended to Europe (with no evidence of local domestication for *Triticum dicoccum* or *Hordeum distichim* and *Hordeum vulgare*), which implies that knowledge was also imported. Therefore, the Neolithic ideals would have been expanded by a process denominated as demic diffusion in three stages: *i*) population growth prompted by new available resources; *ii*) dispersal into regions with low population density; and *iii*) a limited initial admixture with the local populations followed by the triumph of Neolithic traits (Tomé, 2010). This spread could be considered a demi diffusion, being carried out by the farmers themselves at a spread rate of 15 km per generation, baptized as the wave front theory. Such take on the matter does not support the theory that interprets environmental factors (e.g., changes in climate, soils, forest cover, etc.) as determining agents with a significant role in the diffusion of farming (Ammerman & Cavalli-Sforza, 1984).

J.G. Rozoy (1971), Rowley-Conwy (1984) and Tortosa & Ripoli (1992) (cited by Cruz, 1997) considered the process as a mixture of traits with a strong component of local and regional variability. This was made thanks to the attachment of chronologic, geographic, and typological characteristics to each phenomenon. Authors consider that the process of transition was marked by a considerable regional variation, based on several principles: the diffusion of agriculture must have happened through ideas instead of people; the emergence of agriculture must have taken place in rich areas with abundant resources; the expansion was faster in areas with pre-existing hunter-gatherer societies; colonization tended to happen in inhabited areas; the process tends to happen faster in more complex hunter-gatherer societies that have already started to show signs of sedentarism; the period before the substitution is long, because the agropastoral resources were considered complementary activities to hunting and gathering; the transition seems to bring about a shift from communal to familiar habitats, which could imply a possible social hierarchization process; regional variability influences shared characteristics between central and peripheral expansion frontiers; and finally, the Neolithic is characterized by the existence of a numerous population, a territorial settling in course, abundance of resources, and proximity of domestic species or species with the possibility of domestication.

Although flawed, L.R. Binford's methodology refines the idea into a densification model that places population growth as the main cause for environmental degradation and the eventual adoption of farming as a sustenance mechanism (Tomé, 2010). S. Gregg (1998) (cited by Cruz, 1997) took theoretical elements on Binford's work, such as residential and logistic mobility, and constructed their own interpretation. Gregg considers that small groups of hunter-gatherers with residential mobility tended not accumulate property, kept a low population density, did not claim exclusivity to natural resources, did not store nor collect alimentary excess, did not dispose of a specific encampment, and reacted to eventual resource crisis or internal conflict through social fission. On the other hand, similar communities with permanent or semi-permanent dwellings tended to accumulate property, kept an elevated populational density, restricted access to certain resources, restricted hunting, produced and stored alimentary excess, and created social mechanisms to resolve internal conflict other than social fission. An incipient horticulture, that eventually would be the base for Neolithic-related behaviour, would emerge from the second group (thus giving birth to the Neolithic). This approach is heavily influenced by the evolutionist perspective.

Returning to the Iberian Peninsula, Ammerman and Sforza (1984) acknowledged that the least known European region was the Western Mediterranean, blaming the landscape. They argue that the type of sites studied (caves) and the presence of rugged limestone areas not suited for early farming made the verification of their theory difficult. Regarding their theory of gradual *cline* of gene association, results from the Western Mediterranean fit their model as the further away a population is from a neolithization centre, the less related their genetic components are from the earliest farmers. The southern half of the Iberian Peninsula seems is indeed one of the most genetically distant from Eastern populations when analysing certain genomes (e.g., ABO, Rh, MNS, Le, Fy, Hp, AP, PGM, HLA-A, HLA-B), producing subgroups that either stand alone or group with the rest of the peninsula and Southern France (Ammerman & Cavalli-Sforza, 1984). Finally, principal component analysis and other statistical methods do not rule out the existence of other neolithization centres that are not located in the Near East, such as England, which complicates the matter even further.

Even though the model of demic diffusion (advance wave) befits some Easter European regions, concerns regarding its continental application have resurfaced with the advent of new techniques that focus on ancient DNA. Sampietro and their team (2007) warned that the Neolithic spread process was neither genetically nor geographically uniform in the whole continent, pleading for further research in areas such as the Iberian Peninsula and Central Europe, where the Neolithic traits seem to either have existed before, or did not imply the import of genes.

Information extracted through these methodologies in Portugal have also suggested that the demic wave front may have behaved differently in Portugal. New data obtained through mitochondrial and nuclear STR DNA analysis, indicates during the Neolithic internal migration waves within Portugal were common between the coastlines and the continental territory (e.g., Bom Santo). It also proves that there was individual exchange between communities and that a simultaneous exploitation of marine, estuarine, and inland environments took place during (at least) the Early Neolithic (Carvalho et al., 2016). Analysis of haplogroup frequencies from Mesolithic sites (e.g., Arapouco, Vale de Romeiras, Poças de São Bento, Cabeço de Pez and Caveço das Amoreiras) and Neolithic contexts (e.g., Gruta do Caldeirão, Algar do Bom Santo and Perdigões) exhibited a high frequency of haplogroups *H* and *U5*, lower values for *U* and *V*, and -the most important finding- the absence of haplogroup J, also called the 'Neolithic Marker'. Considering the small size of the sample, results must be taken cautiously, but they may support yet again that the Neolithic spread followed a different pattern in Portugal (Silva, 2007). Hunter-gatherer genetic material has also demonstrated a stronger presence in Central Iberia, as the further farming communities moved inland, the stronger the presence of MLN haplogroups becomes. The Chalcolithic on the other hand seems to be a period of higher interaction and intermixing, resulting in a somehow homogeneous genetic constitution. The last phenomenon could be linked to the introduction of the Bell Beaker culture, but further analysis on Chalcolithic samples is needed. It is interesting to note that evidence for influx in the East to West direction was not found during this analysis. Be that as it may, there is enough evidence to suggest that local hunter-gatherer groups and early farmers were tightly linked from the beginning of the neolithization process, a trait that is missing from Central European farmers (Szécsényi-Nagy et al., 2017).

When tackling this issue using stable isotopic analysis (on elements such as carbon ($\delta^{13}C$), nitrogen ($\delta^{15}N$) and strontium ($^{87}Sr/^{86}Sr$)), it seems that there was in fact an implementation of certain Neolithic traits before the advent of the theoretical wave front from the East. Mesolithic sites from Muge and El Sado Valley, which encompass one of the most representative skeletal assemblages for this period, were compared to Neolithic sites. Individually, El Muge and Sado exhibited a concentration of $\delta^{13}C$ around -18.6±‰, which can be interpreted essentially as a terrestrial diet, since the average for land-based diets in Southern Europe is around 19‰. This implies that the shift towards a terrestrial plant-based diet in Portuguese societies was underway before the Neolithic. When compared with data obtained from 22 Neolithic sites (which included specimens from Gruta de Nossa Senhora das Lapas, Gruta dos Ossos, and Gruta do Cadaval), Mesolithic and Neolithic diets showed no significant variation. Additionally, sites such as Gruta de Lagar 1 and Cerca do Zambujal included individuals with strong evidence of a main marine-based diet. Such outcome could imply the coexistence of both diets up until the Neolithic (Guiry et al., 2016). This pattern may also be present at the local level, translated into hierarchization or social distinction between members of the same group. Waterman, Tykot, and Silva (2016) sampled eight archaeological sites ascribed to the Neolithic and Chalcolithic in the lower Tagus in a similar study. The results showcased a dominion of plant-based diets among the population, but also indicated that marine-based restrictions were applied differentially to juveniles. Not jumping into hasty conclusions, this may indicate that surviving cultural activities may have taken other forms in the Neolithic. In conclusion, the shift towards terrestrial diets would probably have coexisted with neolithic practices, starting before the advent of the Eastern wave advance, and probably being adapted differentially according to the region and/or social status (Carvalho et al., 2016).

On the other hand, animal domestication seemingly started with local populations (mainly goats), while plant domestication seems to be part of past population's efforts. Cereals present two distinct patterns between the species cultivated in the initial phase of neolithization and those cultivated in the same period in the Near East, contradicting the diffusionist theory. Ceramic ware behaves similarly, displaying types predating the Cardium tradition. Consequently, Portuguese archaeologists have turned to a different explanation system called *capillarity* or *percolation model* that seems to befit better the process of neolithization in the Iberian Peninsula. This model understands that environmental pressure influenced the first Neolithic transformations (goat domestication, gramineous and fruit plants horticulture, pottery traditions) and created strong social networks that eventually would articulate to their counterparts from the East, in a slow and peaceful process of social integration (Tomé, 2010).

PhD Ana Rosa Cruz (1997) concluded that the advent of the Neolithic practices should be understood as a cultural process in which there was a tendency to enforce certain mechanisms that, once articulated, would transform the socio-economic fabric, leading to an economy of production and social segmentation. Said mechanisms can be verified in different cultural spheres such as the economic (domestication), social (sedentarism), technological (artifacts typology), and symbolic (funerary practices).

On a similar academic quest, PhD Luiz Oosterbeek (Oosterbeek, 1994b) also understood the Neolithic as a cultural process that started within the ranks of Late Mesolithic communities (from the 7th millennium BC until the 3rd millennium BC). The process of neolithization took place on the prehistoric West Mediterranean landscape, as part of a single, alas uneven, campaign. As such, the acceptance and implementation of Neolithic socio-economic practices may have not fully occurred up until the 3rd millennium BC, and even then, both economic modes would have necessarily coexisted and even cooperated through the transition period. Oosterbeek argues that the different stages of the Neolithic can be summarized in a genetic phase (acquisition of characteristics), an integration phase, and an accomplishment phase. The possible routes followed by the dissemination of Neolithic traits were the coastal, through the current territories of French and Spanish Catalunya, characterized by the so-called cardial or impressed ware culture (which later would result into epicardia stages in the littoral and later inland) and a secondary fluvial spread through the southwestern main drainage basins of Iberia (i.e., Gualdalquivir, Guadiana, and Tagus basins)l, which would evolve into a different set of interactions with pre-existing local Mesolithic communities.

In their view, the neolithization process is marked by demographic growth, the reinforcement of agropastoral tendencies, and the emergence of megaliths and collective burials. These traits, coupled with the persistence of ancient traditions, were reflected in artifact technology and typology, and a great variability of economic strategies. Global trends were represented as collective burials, technological innovation, enlargement of settlements, and an increased complexity and variability of material (Oosterbeek, 1994b).

When structural and ideological complexity is understood as a fundamentally political process that materializes in the form of socio-economic transformation, the appropriation of the Mediterranean network by emerging local elites in search of profit and power would turn out to be the main driver of the neolithization process.

In such a context, if the emergence of the Neolithic was marked by innovation, diversification, and collectivization of socio-cultural traits, whereas its dawn manifested through the introduction of Bell Beaker pottery (i.e., Pamela-Ciempozuelos) that foresaw the emergency of a new administrative power and social organization. This ultimately led to the appearance of individual burials, the abandonment of hillforts, and the occupation of high fertile land (Oosterbeek, 1994b).

2.2.1.2. *The Chalcolithic*

The Chalcolithic is a socio-economic model based on agropastoral production and characterized by the emergence of metallurgy and social hierarchization. It is usually used as a categorical variable into which archaeologists can locate the antechamber to the Bronze Age. Historically, the term is rooted on economic and evolutionist perspectives, dominant in the 19th century.

The Chalcolithic is thus characterized by agricultural intensification, demographic growth, and eventual colonization of new areas. Superstructural indicators of this period include schist plates, horn idols, and solar motifs. This could indicate that there are new relationships between elites and commoners. In Portugal, this expansion seems to be supported by evidence husbandry practices. Perdigões, considered a continuous occupation from the Neolithic to the Early Bronze Age, was subjected to a stable isotope analysis focused on domestic animals. Results demonstrate that most of them fed within a large grazing area with a radius of at least 810km. It could also indicate the existence of exchange networks of cattle trade during the same period (Žalaitė et al., 2018).

2.2.1.3. *The Early Bronze Age*

Due to the advent of the Bell Beaker pottery and the generalized spread of metal smelting, the Early Bronze Age main achievement is the consolidation of the changes brought about by the Chalcolithic, including the intensification of agropastoral activity, the widespread domestication of bovids, milling and weaving, settlements expansion, and the privatization of funerary contexts. Cultural expressions in the Bronze Age seem to support claims of a highly hierarchic society that tends to hoard resources in a familiar-based organization. A further exploration of the Early Bronze Age in Portugal will be given in the next section.

2.2.1.4. *Archaeological research on the Nabão valley*

Several models of prehistoric settlement patterns have been proposed for the peopling of the Nabão valley, following theoretical approaches such as the Neo-Marxism, the Historical materialism, and the Dialectical materialism. PhD Ana Rosa Cruz (1997), an investigator that dedicated her life to the study of prehistoric sites in the Nabão and Alentejo regions, summarized a concise recapitulation of the three most influential models proposed in the 90's by local archaeologists.

Katrina Lillios (1991) (cited by Cruz, 1997) analysed the cultural shift that took place between the Chalcolithic to the Bronze Age through a Neo-Marxist approach. This method waged for a confrontational perspective, in a scenario where prehistoric communities competed aggressively for resources during the Chalcolithic, resulting in a social fission event around 2000 b.C. This setup would explain the sudden occupation of previously vacant territories and the subsequent abandonment of fortified hills after the Bronze Age. Their argument was based upon seven pillars: 1) Differentiated settlement patterns: instead of a "collapsing" theory they proposed a "fission" model, i.e., a diaspora forced by the environment. 2) Villages dissolution: fortified settlements built on top of hills during the Bronze Age were replaced by the end of the 3rd millennium b.C. by non-fortified villages. 3) Emergence of decentralized settlements (i.e., population diaspora); 4) A decline in the consumption of prestige objects. 5) Technologic continuity; 6) Substitution of the Chalcolithic large spectrum economy by one specialized on intensive domestication and agriculture. and 7) Substitution of collective burials by individual ones. Funerary behaviour changed dramatically during this period as most burials went through a relocation process. The author argues that Chalcolithic [3] saw the dawn of collective inhumations that started to concentrate in megaliths or tumuli with a false cupula, whereas the Bronze Age was characterized by small and individual burials placed upon modest grottos, accompanied by a lesser volume and complexity of grave goods.

K. Lillios theorizes that the funerary behaviour changed due to the toll left by the environmental degradation resulting from the massive deforestation of the Late Chalcolithic took a toll and the (apparent) decline of the Chalcolithic conflict for the land, which would translate into the disappearance of symbolic modifications on the landscape (e.g., rock art, walls, funerary monuments, prestige objects and decorations). Lllios' model, according to Cruz, exhibits some issues that must be resolved, namely: *i*) the identified frontiers in the high and low ground are debatable, as they do not account for landscape variation between the coastline and the interior; *ii*) intrinsic characteristics of the 17 sites selected for the analysis were either ignored or added to fit the model; and *iii*) the model does not allow for any variation, whether it is local or regional in nature.

João Zilhão (1992) (cited by Cruz, 1997) proposed a settlement model aligned with the school of Historical materialism. Their work was primarily based on Neolithic material

[3] She uses the term Copper Age in the original Personal translation from Portuguese to English.

unearthed at Gruta do Caldeirão. In summary, their argument oscillated between the approval and disproval of a series of dichotomous explanations for the emergence of the Neolithic and the every-day life of Middle Palaeolithic communities, as well as the dispersion of Cardial ware traditions. The first explored theory was that hunter-gatherer communities of the Nabão acquired pottery and domesticated animals through exchange relations with distant groups. This hypothesis was rejected because, according to Zilhão, Mesolithic peopling patterns followed coastline estuaries, relegating interior portions of the country to be seasonal occupation sites dedicated to hunting and foraging of resources. Such argument would necessarily imply that the valley did not sustain a continuous human occupation during the Mesolithic. The second theory was that the Nabão valley was a complementary territory, seasonally employed by hunter-gatherers from other regions as an exchange enclave. Such notion was rejected as well, based on the analysis of stable isotopes of carbon and nitrogen in skeletal elements, that revealed a primarily land-based diet, thus indicating a permanent occupation of the inlands. The third and final theory proposed by them was that the Nabão area was a grazing and hunting zone inhabited by herders and farmers coming from villages founded on nearby fertile soils. This hypothesis admits that there was a sedimentary hiatus prior the Early Neolithic (Cardial) that is often associated with dense forests, thus the subsequent depositions would align with the process of deforestation. Zilhão favours this hypothesis over the first two, arguing that the mortality pattern on Gruta do Caldeirão does not fit expected mortality rates, and implying that the burial contained individuals selected by age (providing no further evidence). Finally, he argued that the extended networks that imported rare materials such as variscite, muscovite, seashells, etc., would prove the stability degree of intercommunity relationships. Their take on impressed ware interpreted the tradition as a result of demic intrusion (and therefore not a local development) was used to support this claim (Sampietro et al., 2007).

Zilhão's model, according to Cruz, assumes the peopling of the Nabão area during the Early Neolithic in sections where there is not enough supporting evidence. It also implies that the fertile, yet hard, soils of the valley were tilled only using stone and wood tools. There is a contradiction between the hypothesis of deforestation and the interpretation of *Layer E* at Gruta do Caldeirão, as the former would inevitably have caused an accelerated erosion pattern that would have been noticeable in the cave´s sediment. Finally, there is no evidence of a sedimentary hiatus in most of the Nabão sites, as older sediments are only found at Gruta do Cadaval.

A third model of social evolution, focused on the process of neolithization and chalcolithization, was proposed by PhD Luiz Miguel Oosterbeek (1994b). This model could be theoretically framed within the Dialectical materialism. Oosterbeek proposes a theory in which various scenarios would have necessarily converged to catalyse the emergence and consolidation of the Neolithic in Portugal. Thus, the Neolithization process came about through capillarity, i.e., the Mesolithic communities that lived in the interior of the Iberian Peninsula were exposed to Neolithic cultural practices at a slow yet continuous rate, which resulted in differentiated mechanisms of adaptation and resistance to foreign practices that lasted well into the 3rd millennium AC.

For this thesis to work, an information and populational network had to be already in place before the advent of the Neolithic in the Mediterranean ideals, albeit manifesting itself through regional variants. Processes of growing complexity would eventually lead to the emergency of State-like administrative patterns. This argument implies that the complexification of economic activities was a result of an analogous process on the social structure. Eventually, Eastern Mediterranean communities built more powerful socio-economic networks over the ones that already existed.

During this stage, social differentiation was structured and supported by the implementation of bloodlines and their relative power – while still collective in nature-anchoring the status of the living to that of the dead. Modest villages emplaced in open-air sites would start to control the landscape, ready to be moved into territories already delimited by the necropolises. The latter would prove to be the most important collective investment of this period. By the beginning of the 3rd millennium, the increasing complexity and power of the social networks allowed certain bloodlines to impose an administrative organization of the landscape, initiating a new investment stage with higher investments. This time, collective resources were also poured onto structures for the living, consolidating true centres of power. Subsequently, power relations would become more stable, welcoming a third and decisive stage where the construction of monumental structures would result into the erection of greater monuments. Additionally, internally differentiated villages began to appear, along with individual burials. From this moment onwards a new type of power directive regulated (or imposed) inter- and intracommunal socio-economic relationships; the foundations for proto states were thus laid.

Another aspect to consider is the differentiated focus that some theoretical approaches imprint on prehistoric peopling models through to their own lenses. For example, the diffusionist model privileges the existence of one single point of diffusion, rather than a network, while the evolutionist models endow a higher value to regional variances. Evidence suggests that the diffusion of Neolithic patterns played a smaller role than previously thought in the neolithization process, as it becomes evident that several societies had already developed traits that could be considered proto-Neolithic beforehand (e.g., proto-sedentarism, specialized hunt involving symbiotic relations with certain species, etc.). In a similar trend, linear models allow a clearer overview phasing that can be easily tested, at the cost of losing any trace of complexity. Finally, Historic and Multilinear approaches conceive that the process of neolithization was continuous, the fundamental dimension of study of the communities involved in the process was space and not time, and the spatial analysis is essential to study and recognize the frontiers of the observed units (Oosterbeek, 1994b).

In conclusion. the Alto Ribatejo was part of a prehistoric Mediterranean network (an echo of Extremadura or Southwest Spain). This network was an expanding system with various interactive centres (some competitive in nature) which tended to generate local and regional hierarchization processes. Under this model, only one centre was dominant, causing the network to evolve through the constant dislocation of dominant centres. Thus, five stages for the emergence of the Neolithic can be identified: *i*) Aceramic Languedocian, until the 6th millennium a.C.: *ii*) Early Neolithic, which oscillates between two main centres, the Tejo (ceramic Languedocian) and Maciço Calcáreo (Cardial), up until the beginning of the 5th millennium a.C. *iii*) Megalithic period, assimilated by the Languedocien tradition (until the beginning of the 4th millennium a.C.); *iv*) collective burials and fortified villages in the periphery of an extensive long distance contact network; *v*) alteration in the burials, fortifications, metallurgy etc, (caused by the introduction of the Bell Beaker tradition). The last one would be the first sub-phase of a stage that would last until the middle of the 2nd millennium a.C. Cruz finds that the definition of the Languedocian is problematic, at best, as it ignores local differences among the sites.

Cruz (1997) would eventually point out that even though these theories have plenty of evidence to support their claims, a new revision of the archaeological sites that evaluates their excavation methodology, stratigraphic complexity, type of context and usage, with the main objective of create a hierarchical arrangement of sites that can effectively value them in similar (and comparable) categories.

2.2.2. Canteirões do Nabão

PhD Ana Rosa Cruz (1997) proposed a hierarchical classification for the study of archaeological sites within the Nabão region. This model was based on a scoring system that evaluated 72 prehistoric contexts, from which 28 were suitable for a regional characterization. The group scored positively in traits such as localization (i.e., geographic, administrative), physiographic characteristics (i.e., climate, geomorphology, edaphology, and morphology), archaeological methodology (e.g., stratigraphy, structures, artifacts, absolute dates, ecofacts, etc.), spatial relationships (e.g., dispersion of the settlements, inferred extension of the territories, and resource sources –the last one measured up until 60 minutes by foot-), interpretation of the sites, bibliography, and cartography. After they were selected, an additional variable classified them according to their usage either as a necropolis, a settlement, a workshop, or an indetermined site.

The result of Cruz' endeavour was the consolidation of three *Chrono-Cultural Groups*[4] that encompass the Neolithic, Chalcolithic, and the Early Bronze Age. Cruz understood that each of them responded to cultural transformations that were related to chronological events. Such premise allows certain flexibility when approaching prehistoric Nabão communities, as researchers can avoid a priori assumptions that force cultural characteristics based only on relative and absolute dating.

The first chrono-cultural group (*Group 1*) spans from 6000 to 4500 AC and coincides with the beginning of the neolithization process. Its most prominent members are Gruta de Nossa Senhora das Lapas (NSL), Gruta do Caldeirão, Anta 1 de Val da Laje, and Povoado da Amoreira. Anta 1 de Val de Laje stands out as one of the few sites with direct evidence of meat and milk exploitation and processing. The results were obtained using lipid residue analysis compound-specific radiocarbon dating; indicating that during the late 4th / early 3rd millennium BC meat consumption from domesticated cattle was wildly spread, while dairy products were consumed at a lesser extent (Stojanovski et al., 2020). Geological activity during this period, coupled with climatic and environmental phenomena, produced several cave ceiling collapses (cave-ins) that affected most karstic caves and rock shelters. Flows of sediment may have been deposited thanks to the orientation of the caves, creating layers formed by aeolian or fluvial erosion. Apparently, prehistoric communities separated funerary and habitational spaces, building them near water sources. Evidence of their economic activities is scarce, but there is enough to conclude that there was unequivocal domestication of animals (e.g., zooarchaeological

[4] The original Portuguese name is *Mancha*, which was translated thanks to persona communications with PhD Luiz Oosterbeek.

remains of sheep, pigs, and goats) and plants (e.g., milling sites for starch processing). Discontinuities in population patterns and low habitational density obstruct drawing geographic frontiers among human populations. Additionally, there is evidence of ceramic ware use in all contexts, often accompanied to lithic assemblages that include macrolithics.

The second chrono-cultural group (*Group 2*) spans from around 4500 to 2500 AC and coincides with the transition between the Late Neolithic and the Early Chalcolithic. Its most important sites are Gruta do Morgado Superior (GRO), NSL, Gruta dos Ossos (GRO), Gruta do Cadaval (CDV), Gruta do Caldeirão, and Anta 1 de Val da Laje. The second phase exhibits two distinct moments that may be a result of cultural variation: one associated to the Middle-Late Neolithic and the other to the Chalcolithic. A geological event of great magnitude caused several cave ceiling collapses. Archaeological sequences are much more clearly defined that in the previous group, which may suggest a deacceleration of the natural erosive processes in the region. This group is more diverse than the first, encompassing burial sites, workshops and (probable) settlements. Pigs and sheep keep showing up in archaeological sites, while bovids disappear and deer remains are present only within funerary contexts. There is ample evidence of weaving, milling, and, while copper elements are scarce, their existence can be inferred through ceramic typologies that are usually associated to the Chalcolithic. In general, there is a significant increase in archaeological sites containing pottery (all of which displays a qualitative and quantitative continuity with Group 1) as new ceramic styles emerge (e.g., carinated, geometric patterns, grooved surfaces, almond-shaped plates, incised decoration, etc.). Other items increase in frequency such as portable rock art and adornments, which also have a continuous relationship with those found in the previous group. Lithic technology shifts from the use of macro-utensils towards bladelets and blades that become more prominent, as the use of arrowpoints and utensils for agriculture increases. Thus, there is a growing importance and diversification of tools, which reflects the growing complexity of the economic activities. Group 2 may be further divided into sites that still display Group 1 characteristics and those that start to display proper Chalcolithic traits. Cumulative innovations are accompanied by the emergence of bigger settlements that may indicate exchange of goods and interdependence among local communities, as evidence of long-distance trade diminishes.

The last chrono-cultural group (*Group 3*) spans from 2500 to 1500 AC and coincides with the transition between the Late Chalcolithic and the Early Bronze Age. Most of the deposits analysed suggest an intense agropastoral use of the land, with a low prevalence of soil erosion due its fixation. Its most important sites include Lapa dos Furos, NSL, and Povoados do Agroal, Arrascada, Fonta, and Juncais de Baixo. This period is characterized by large settlements emplaced over locations with visual control of the landscape that are close to water sources and soils fit for intensive agriculture. Economic activity is marked by the domestication of bovids, weaving, milling, and copper smelting. Most ceramic styles are replaced by the Bell Beaker tradition, decorated with dots and wave motifs. Lithic technology starts to lose volume and diversity on the archaeological record, being dominated by blades and bladelets. Following the pattern seen in Group II, long-distance trade is reduced to essential items. Finally, funerary contexts start to present variability in form and location.

The ravine of Canteirões do Nabão has yielded several archaeological sites that bear striking similarities, enough to be considered sibling caves/openings. Among the prehistoric contexts that bear the most parallels with Gruta do Morgado Superior three sites stand out: Gruta de Nossa Senhora das Lapas, Gruta do Cadaval, and Gruta dos Ossos.

Gruta de Nossa Senhora das Lapas (**NSL**) contained a circular burial delimited by limestone blocks (Cruz et al., 2013). The tomb contained two individual inhumations that were deposited as early as 6000-7000 BP. The earliest burial, found within the base of *Layer B*, had an absolute date that placed it in the second half of the 4th millennium BC. The more recent inhumation, deposited within *Layer A*, had a relative date that places it within the 3rd millennium BC. After a bioarchaeological analysis was performed, the Minimal Number of Individuals (MNI) reached a value of at least 10 (5 adults and 5 juveniles, nine of which were identified in Layer B (Tomé et al., 2013; Tomé & Silva, 2013). Although the sample was excessively reduced to perform certain types of analyses, the representation of weak skeletal joints suggests that the collective burial was a primary context.

The unearthed material at NSL was associated with pottery traditions found on neighbouring and remote archaeological sites: beads carved on *Glycymeris glycymeris* shells present parallels by sediment affinity with those present in Gruta do Caldeirão's, associated to the Early Neolithic; a spheric ceramic vessel was linked to ware found in a Neolithic burial in Gruta do Cadaval; discoid beads bear similarities with those associated to Early and Middle Neolithic contexts in Caldeirão and Cadaval; and beads carved on *Theodoxus fluviatilis* shells were found in the same strata in Gruta do Caldeirão. Lithic technology was dominated by silex tools (scrapers, burins, points, blades and bladelets) and some macrolithic cores. Ceramic ware was mostly associated to the Early Neolithic, while some pieces were ascribed to the Bell Beaker tradition seating in the transition between the 5th and 4th millennium BP. Thus, the site was interpreted as a necropolis that had various moments of usage, from the Neolithic up until the Chalcolithic. (Cruz et al., 2013).

The necropolis of **Gruta do Cadaval** (**CDV**) was chronologically allocated to the 5th /4th millennium BP. The stratigraphy analysis revealed 19 occupation moments, from which some stand out: **Layer Fb** was interpreted as a domestic feature with a hearth; **Layer F** has been related to lithic industries from the Middle Palaeolithic that can also be found in open air sites such as Estrada do Prado and Santa Cita (Cruz et al., 2000); **Layer D** was classified as an individual burial; **Layer C** was classified as a collective burial; **Layer B** is represented by a hearth; and **Layer A3** was interpreted an intermittent hunting camp. The individual burials were covered in a sandy-clay deposit, while the collective burials were embedded in a clay-silty soil. Pottery artifacts included smooth ceramic vessels, some decorated with incisions, punctured or with plastic adornments. The assemblage exhibited other materials such as bone artifacts and adornments (Cruz et al., 2013). The Minimal Number of Individuals recently ascended to 33 (16 adults and 17 subadults). The fragmentation profile of the human remains is higher in large bones, cranial bones, pelvic and shoulder girdles, while hand and foot, bones and patellae were well-preserved. Layers (Tomé & Silva, 2013).

Gruta dos Ossos (**GRO**) is a Late Neolithic site that exhibited a rather unusual set of funerary practices characterized by the intentional rearrangement of buried skeletal elements. Each bone was grouped by type, and then stacked on a crescent-shaped pile. The site was identified thanks to an accumulation of cranial elements exposed in the surface of the cave's floor (Oosterbeek, 1993a). The spatial disposition seems to extend to the ceramic record, which was deposited in areas surrounding the bioarchaeological material. The site is often considered as one of the clearest funerary contexts of the Nabão valley in the sense that its usage is apparently limited to the 4th millennium BC (Tomé & Silva, 2013). Four layers were identified (aside the organic sediment): **Layer 1** contains a group of seven skulls located in the Southwest sector within a cohesive sediment characterized by a sandy-clay texture and some vestiges of erosion; it also presents a sublayer that showcased evidence of carbonates dissolution (Oosterbeek, 1987). **Layer 2** contains the base of the human remains, represented by a deposition of long bones buried within a sandy-clay soil, highly disturbed by anthropogenic and biological agents. This layer was chronologically situated between the Neolithic (i.e., it was older than Gruta do Caldeirão's) and the Chalcolithic (i.e., the Bell Beaker tradition) (I.e., it was younger than Fonte Quente). **Layer 3** was a product of disturbed soil in which some ceramic fragments and silex chips were found. It bears no human remains, but the artifacts within do not bear a striking difference to the ones in Layer 2. Finally, **Layer 4** was identified under a series of blocks, probably deposited by a previous collapse of the cave's ceiling. This layer contains the earliest burials on the site since the individuals were found in anatomical position along grave goods such as ceramic ware and some ornaments. Lithic technology was composed by flake points, blades, bladelets, scrappers, a burin, a polished hand-axe, and macro-lithic tools. Isotopic analysis of the biological material suggest that the necropolis dates back to a point between the 4th and 3rd millennium BP (Cruz et al., 2013). A total of fourteen sedimentary moments were described within a series of natural occurrences (including two ceiling collapses by thermal disruption (thermoclastic)).

The preliminary analysis of the human remains confirmed an overrepresentation of skeletal elements such as long bones, cranial and mandibular elements, patellae, hand and foot bones, and clavicles. On the contrary, skeletal regions such as the spine, pelvic girdle, thorax, and scapulae were scarce. Their absence may respond to the inherent taphonomic resilience of the bones mentioned above. The site presents the expected volume of material that was inferred by dental analysis, which becomes clearer once compatibility between bones from opposite literalities was demonstrated among juvenile and adult individuals (Tomé, 2010).

2.3. Gruta do Morgado Superior

Gruta do Morgado Superior is located at the coordinates: 39.659502 (Latitude) and -8.420149 (Longitude) [UTM (29N) M 549741 P 4390127]. It was excavated under the archaeological authorization ID **S-11334**. The cave is under the jurisdiction of Casais Novos, civil parish of Além da Ribbeira, Municipality of Tomar, Santarém District (Cruz & Oosterbeek, 2012). Formerly, this district was part of the now dissolved province of Ribatejo. This province was instituted by a reform in 1936 and dissolved in 1976. Even so, locals still use its name to describe the region to this day. It limited the provinces of Beira Litoral and Estremadura which coincided with the geographic limits of the mountain ranges of Serra de Aire e Candeeiros, Serra de Montejunto, Serra de Ansião, Serra Vermelha, Serra de Alvéolos and Serra do Moradal. To the south, it limited the Alentejo's plains.

The karstic opening can be found on the right bank of the Fetal stream, very close to where it meets the Nabão valley, to where it flows. The city of Tomar is only 11km away, to the Southeast.

Gruta do Morgado Superior contained a homogeneous assemble of human remains, which is why it was interpreted as a necropolis and a primary inhumation. Pottery traditions seem to be analogous to the ones found in CDV (Layers C and D) and GRO (Layers 1 and 3). Arrowheads carved on silex are the most abundant lithic tool type, including 13 different typologies (classified by hafting), some of which share features to counterparts on the region (Berruti & Daffara, 2014). The former Layer B (now subdivided into various Stratigraphic Units) was associated to prehistoric burials from the Neolithic and/or Early Chalcolithic during the first years of excavation. (Cruz et al., 2013).

The absolute dates obtained from the site oscillate form the Neolithic to the Early Bronze Age (see **Table 1**). Four additional dates were obtained for this study and will be presented in the results section (see section Error! Reference source not found.).

Table 3. Absolute dates taken at Gruta do Morgado Superior up until 2019 (Cruz, 2020, p. 48, Table 11 (modified))

Year	ID	SU	Chron.	Laboratory	Radiocarbon	Calibrated 2δ	Method
2013	J51-0904	[002]	Chalc.	Beta –359086	4260±30	2910-2880 calBC	A.M.S. – *bone - Homo*
	J51-0997	[002]	Chalc.	Beta –359087	4180±30	2640-2640 calBC	A.M.S. – *bone - Homo*
2014	J50-0574	[002]	Chalc.	Wk- 40440	4505±20	3244-3102 calBC	A.M.S. – *bone - Homo*
	J50-0946	[002]	Chalc.	Wk- 40441	4168±20	2816-2671 calBC	A.M.S. – *bone - Homo*. Could indicate Land-based diet
2015	F53-0023	[001]	Chalc.	Beta -423526	5960±30	4930- 4780 calBC	A.M.S. – *bone - Homo*
	G54-0012	[004]	Neo./Chalc.	Beta -423527	4610±30	3495-3435 calBC	A.M.S. – *bone - Homo*
	F53-0003	[006]	Neolithic	Wk- 42854	5214±20	4050-3970 calBC	A.M.S. – *bone - Homo*
	G54-0012	[004]	Neo./Chalc	Wk-42855	5960±20	4930-4920 calBC	A.M.S. – *bone - Homo*
2019	J50-0487	[002]	Chalc.	Beta -538888	4910±30	3763-3725 calBC	A.M.S. – *bone - Homo*
	J50-513	[002]	Chalc.	Beta -538887	4040±30	2832-2821 calBC	A.M.S. – *bone - Homo*
	L51-0768	[002]	Chalc.	Beta -538886	4150±30	2876-2829 calBC	A.M.S. – *bone - Homo*
	K50-0649	[060]	N/A	Beta -538885	4500±30	3347-3097 calBC	A.M.S. – *bone - Homo*

2.3.1. Archaeological Campaigns

Gruta do Morgado Superior was discovered in 1980 during an archaeological campaign conducted in the nearby cave of Gruta dos Ossos. The first official survey took place in 1988, and was subsequently excavated in the years of 2012, 2013, 2015, 1016, 2017, 2018, and 2019 under the coordination of PhD Ana Rosa Cruz. The site proved to be one of the most relevant sites in the region, considering the quantity and cultural affiliation of its materials that include a rich lithic technology (e.g., cores, composite tools –a trapezoid -, arrowpoints, blades, bladelets, hammerstones, splinters and spicules in flint, hyaline quartz, quartzite, amphibolite and shale), a prolific bone industry (e.g., spatulas, punches, and hairpins), various pottery elements (e.g., open and closed, with wide rims that are round, flat and pointed, no decoration having been found so far), adornments (e.g., perforated shells with a single, double or quadruple pierce, rings, polished bone pendants, stone pendants, schist beads, hair pins – both with body and false head - and incised or corrugated decoration), ideotechnical artifacts (polished bone artifacts, one of them decorated with ochre, and idols), metal artifacts (e.g., a cast and arrowheads on copper and arsenic copper), a wide assemblage of faunal remains, and, finally, one of the largest human remain collections in Iberia for these periods, with a Minimal Number of Individuals that may exceed the 200 mark.

Several of these artifacts can be considered as evidence of a link between the late Neolithic and Chalcolithic socioeconomic exchange network centred between Alentejo and Eastern Andalucía, Spain. Metallic elements have been linked to traditions in the Portuguese Estremadura, the Central Mesetas, and the Galician Roufeiro's site, also in Spain. The double awl may be a variant from the '*furadores lozângicos*', present in other Portuguese sites from Estremadura such as Vila Nova de S. Pedro and Abrigo Grande das Bocas. Additionally, it has been reported on sites in Alentejo (e.g., Monte Novo dos Albardeiros), and, internationally, in France (e.g., Languedoc, Pyrenees) and Spain (e.g., Catalonia) (Cruz et al., 2018).

Figure 2. Photographic mosaic displaying Gruta do Morgado Superior. Author: Fernando Pimienta. Published in Cruz (2020, P. 54).

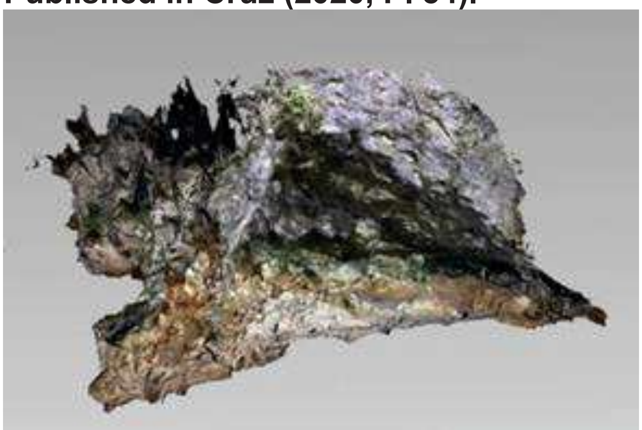

2.3.2. Excavation Methodology

The first step before the intervention of the site was the placement of an arbitrary grill, oriented to the magnetic North, along two axes: the *y* axis was placed along a North-South direction, and the *x* axis followed an East-West orientation (see **Map 3**).

At first, the excavation followed arbitrary levels of two centimetres each. Sediments were sieved in a two-millimetre net. Once the osteological material started to appear in a scant disposition, the levels were shrunk. During the recovery process most of the material was registered in three dimensions (along the *x*, *y*, and *z* (altitude) axis), differentiating *Lithic Industry* (all raw materials, type of industry, and typological classifications), *Ceramic Fragments* (including rims, bases, profiles and decorations), *Bone Industry*, *Mobile Art*, *Human Remains* (all types with the exception of long bones splinters that could not be identified), *Faunal Remains* (specifically species bigger than rabbits; microfaunal remains were recovered in the sieve), *Adornments*, and *Metallic Artifacts* (Cruz et al., 2013).

Map 3. Surface layout as it was at the end of 2019's campaign. Mosaic made by Fernando Pimienta, and in published in Cruz, (2020, P. 63). Slightly modified, adjusted, and georeferenced.

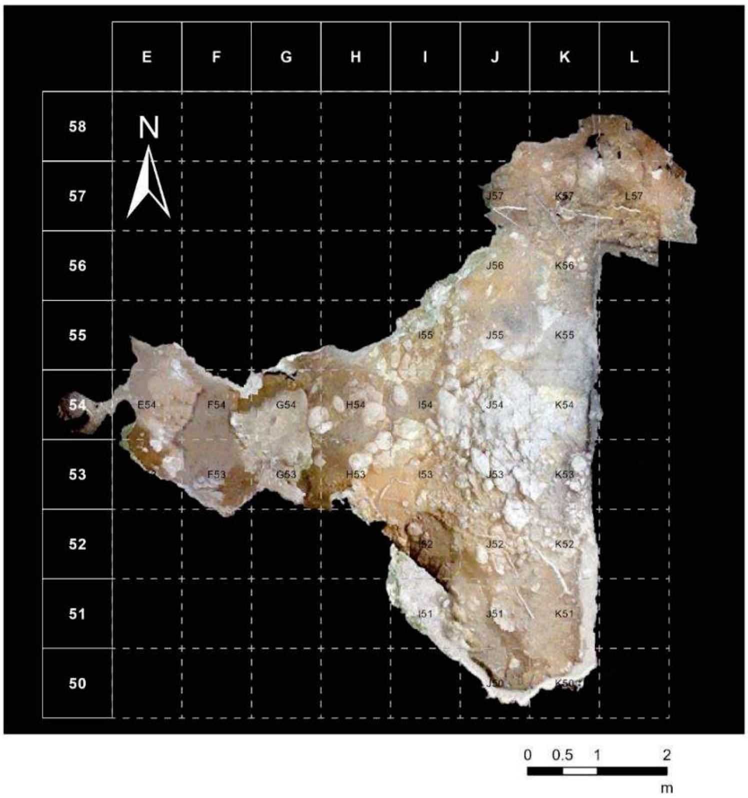

2.3.2.1. *First survey (1988)*

The first archaeological intervention took place in 1988, limited to the excavation of a considerably small sized testimonial survey, under the coordination of archaeologists Ana Rosa Cruz and Luiz Miguel Oosterbeek. The site did not yield enough material to deem necessary an additional campaign, which halted excavations for more than a decade (Cruz et al., 2013).

2.3.2.2. *2012's Campaign*

The second intervention lasted from the 1st to the 31st of October 2012. It was led by PhD Ana Rosa Cruz and financed by the Centro de Pré-História do Instituto Politécnico de Tomar (IPT) and the Centro de Investigação da Pré-história do Alto Ribatejo. A plea made alert by the speleology group GPS warned the authorities of Torres Novas about a possible case of pillaging of the site, which prompted a salvage intervention by the (Cruz & Oosterbeek, 2012). Eleven (11) square meters were intervened, from which two inhumation assemblages were found three meters apart from each other. The first assemblage included the squares F53, E53, F52, and F54 while the second included J50, J51, and K51.The Sepulchral Pit II (that includes the squares J50, J51, K50, K51) was the first to be intervened.

The intervention expanded to new areas that include the squares J52, J53, J54, J55, K57, and L57, all of which yielded similar results as the ones excavated before. This location would then be named **Sepulchral Pit II**[5] contained a great volume of material with a high density spread, which forced the team to expand towards contiguous squares (e.g., I51, I52, J52, and L52) (Cruz et al., 2013).

Four stages of occupation were identified during the excavation: **Stage 1** is composed by the most recently deposited sediments formed by **Layer A**; this stage was associated with the Late Chalcolithic/Middle Bronze Age; **Stage 2** is represented by the cave's ceiling collapse evidenced by limestone blocks; **Stage 3** is composed by the sediments classified as **Layer B**, and contained some of the archaeological material was recovered *in situ*; reason why it was ascribed to the Neolithic/ Chalcolithic transition; **Stage 4** is characterized by the formation of the stalagmitic mantle during the Early Holocene (Cruz et al., 2013).

In 2012 the team recovered 1980 human skeletal elements from which 789 were dental elements. The overall conservation status of the material was poor, as most of the bones were fragmented and disarticulated (see **Photograph 1**). No discernible trends in the disposition of elements were found. The dispersal pattern was interpreted as evidence of a constant reuse and rearrangement of the funerary site in different moments in time. Taphonomic alterations were attributed to biotic agents, namely plants (roots). Chemical alterations were mostly attributed calcium carbonate depositions on the bone's surface

[5] 'The original term in Portuguese is "*fossa sepulchral* 2".

that negatively affected the osteological analysis. Nonetheless, the sediment's conditions had a positive effect on the conservation state of small objects (Cruz et al., 2013).

Photograph 1. Dispersion of osteological materials (Cruz & Oosterbeek, 2012, p. 5, Annex III, Figura 9)

The bioanthropological analysis was conducted by PhD Tiago Tomé (2012) during this campaign, who employed a wide array of methodologies for the study. The calculation of the Minimal Number of Individuals (MNI) followed Silva's (1996) methodology using long bones, which in turn was an adaptation of Herrmann et al. (1990, p. 327); other skeletal regions followed Buikstra and Ubelaker's (1994) method. Sexual allocation followed Buikstra and Ubelaker's methodology based on mandibular and pelvic inspection. Morphologic analyses were divided into metric and nonmetric: metric methods were used to estimate the stature following Holland's (1995) technique employing measurements on the talus and the calcaneus. The platy-brachial, platymeric and cnemic indexes were taken from Martin & Saller (1957) and Oliver & Demoulin (1990). Nonmetric analysis of variation of postcranial elements was extracted from Finnegan (1978). Oral pathologies were registered according to Lukacks, (1989) – prevalence and dimension of dental cavities-, Moore & Corbett (1971) - location of dental cavities, Smith (1984) and Silva (1996) – occlusal dental wear analysis-, Martin & Saller (1957)– frequency of tartar (dental calculus), and Hillson (1996) - periodontal pathologies. Degenerative articular pathologies were scored using the scale of Crubézy, Morlock and Zammit. (1978)[6] (Tomé, 2012).

Tomé analysed 3050 osteological fragments. Their distribution was mainly tilted towards the Sepulchral Pit II. Sepulchral Pit I had a MNI of 2 individuals identified by the 1st right cuneiform, and two subadults identified by the upper lateral incisor. Sepulchral Pit II yielded 33 individuals identified by the right maxillary central incisor and 11 subadults identified by the right maxillary first molar(Tomé, 2012). These results differ from the official field report, in which the numbers are lower.

The distribution of sex in the Sepulchral Pit I was one male, and age determination was available only for one subadult (right ulna's unconsolidated diaphysis). The results in Sepulchral Pit II varied from one skeletal element to another, but the maximum number of males was 10 and the minimum 2, while the maximum value for females was 10 and the minimum 4. Age estimation was performed measuring eruption of teeth and epiphyseal fusion (Tomé, 2012).

Degenerative Pathologies were observed in 33 fragments that presented marginal osteophytes, from which 23 belonged to the hands and feet, and 10 to the spine. Most of the elements (87.88%) presented a moderate to low degree. From the upper limb assemblage, the prevalence was greater in distal phalanges (*n*=10 - 8.7%). The most affected elements were the proximal foot phalanges. Most vertebrae belonged to the lumbar section (18.75%). Some articular surfaces displayed alterations on the muscular insertions in the patella (*n*=30 - 30%), tibia (*n*=2, 100%), the calcaneus (*n*=6 - 83.33 %, *Achilles* tendon), and femur (*n*=4 - 50%, gluteus maximus). When divided by skeletal region, the most affected areas were the lower limbs which was interpreted as the result of stress-related behaviour and mobility patterns. Stress markers in the upper limbs were related to the intensity of biomechanical loads and/or activity patterns (Tomé, 2012).

Nonetheless, the analysis of human remains was clouded by the overall lack of well-preserved articular surfaces. Among the few that were well preserved, arthrosis (level 1 and 2) was identified in hand and foot bones (Cruz et al., 2013). Evidence of trauma was identified in a right metatarsal (*J51-0182*). Four cases of ankylosis were observed in some of the phalanges from hand and foot. A metacarpal presents deformation in the diaphysis, and a traumatic lesion. A fourth right metatarsal and a fifth left metacarpal exhibited bone calluses in the proximal area of the diaphysis (Tomé, 2012). Cavities were found on 25 teeth (mostly in premolars and molars), and dental wear identified in 397 teeth (with intensities from mild, moderate, and mildly moderate). Finally, tartar displayed a moderate prevalence (Cruz et al., 2013, p. 43).

The faunal assemblage was composed by ovicaprids and suids (46%). About 30% of the fragments correspond to micro-faunal remains, 12% to malacological species, 7% to carpological samples, 4% to anthracological samples and 1% for entomological specimens (the latter being contemporaneous).

Most of the adornments recovered were dominated by discoid bone beads (50%), discoid green-stone beads (48%), and a circular perforation in a faunal tooth (2%). It is

[6] This reference has a discrepancy between Tomé and Curto regarding its year of publication and number, the latter placing it as an individual thesis from 1988. Additionally, Tomé does not provide the exact reference. At any rate, the text is missing from most online databases.

worth mentioning a fragmented corrugated pinhead and its pin made in bone, and a polished bone ring (fragmented).

Lithic technology was carved mostly on silex (68%), followed by quartzite (30%) and amphibolite (2%). The assemblage was mostly composed by silex arrowheads (45%) (see **Figure 3**), quartz flakes (18%), blades and bladelets in silex (16%). Choppers and debitage fragments have each a 5% of representation. A quartzite hammer and a composite tool (trapezoid) were also found.

Figure 3. Arrowheads found in 2012's campaign: 6: J51-0394; 7: K51-0335, 8: J51-0416, 9:K51-420 (Cruz & Oosterbeek, 2012, p. 4, Annex II, modified).

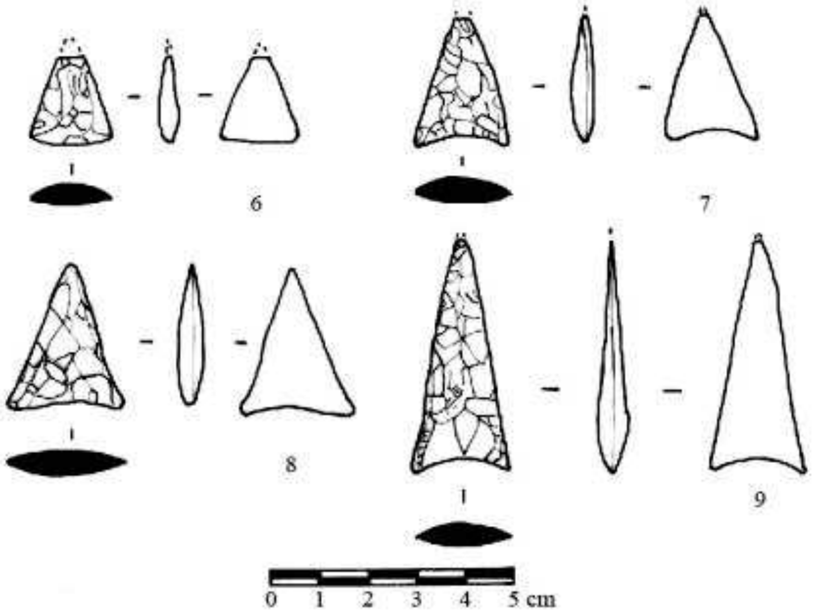

Pottery traditions were divided between two types of manufacture: *manual* (45%, from with 2% were diagnostic) and *potter's wheel* (48%, from which 1% were diagnostic). The paste's burning atmosphere (oxidised or reduced) was not clearly defined due to the irregularity of the fragments. Most of the fragments share similarities with the Lower Carinated style, which are parallel to contexts typically associated to the Chalcolithic/Bronze Age transition. Rim analysis indicates vessels with ample diameters, that could be comparable to those in Gruta do Cadaval's Layers C and D.

The bone industry is represented by a small, polished burin and a polished spatula (Cruz et al., 2013). Ideotechnic material found during this campaign includes one petite zoomorphic statue that resembles a lagomorph and one idol classified as *Almeriense*, both carved in bone.

A barbed arrowhead (*espigão e barbelas*) smelted in arsenic copper was recovered. This artifact is considered typical from sites such as Abrigo Grande das Bocas, which is associated with the Early Bronze Age. Similar arrowheads were also found in Spanish sites such as El Acequión (Albacete) coupled with other metal objects such as daggers and flat axes. The thorn-like structure has been interpreted as a modification that was designed for warfare.

2.3.2.3. *2013's Campaign*

For a funerary context that was once deemed to be too reduced fill more than a couple of pages on regional and local analysis (Tomé, 2010), the archaeological material retrieved in 2012 quickly eclipsed some neighbouring prehistoric sites. The site gained a privileged relevance for the investigation of regional socio-economic dynamics focused on the emergence of agropastoralism (Neolithic) and its consolidation (Chalcolithic).

Bearing this in mind, the main objectives of 2013's campaign were: 1) to delimit vertically and horizontally the extension of Sepulchral Pit II; and 2) define and expose the -archaeologically sterile- layer below the assemblage. To achieve these goals most of the digging effort was focused on the squares from the grid where the Sepulchral Pit II had been identified (central-southern section) (Cruz & Oosterbeek, 2013).

The most relevant finding was the identification of a positive structure near the southern wall for the first time, composed by a semi-circular alignment of cave-in limestone blocks. A total of 369 artifacts was found from which 50% were ornaments, 24% were ceramic fragments, 13% were lithic fragments, 12% were faunal bone artifacts, and 1% of ideotechnic artifacts. Once again, the most abundant material corresponded to human remains which amounted to 6761 pieces, from which 1597 were dental elements. Once again, **all** bone fragments presented different degrees of conservation and fragmentation. It is worth noting that the total number of elements by category, described by all field reports, refers only to a georeferenced position in a three-dimensional space. Hence, **one entry** (as they will be called from now on) may represent a complete element[7], two or more complete elements that are related and/or articulated, fragments that may or not be part of a single element, fragments that are part of different elements, fragments found on sieves from a whole square, or fragments labelled incorrectly and given new denominations with shared coordinates. **Entries are not analogous to** the number of **bags**, **boxes**, **elements**, or **fragments**.

Lithic technology was represented by arrowpoints (51%), blades (12%), bladelets (7%), flakes and chips (7%), and cores (2%). Most artifacts were affected by chemical taphonomic agents and presented calcite crusts and patina. Lithic tools were manufactured by direct percussion or by pressure. Regarding typology, flakes were considered cortical, with a percussion plane that presents as cortical, faceted, or straight; bulbs are present at the medium, and the orientation of the platform was always perpendicular. The presence of chips indicated that the lithic reduction process was done locally. Blades and bladelets vary in shape, being convex, straight, and trapezoidal, with percussion planes that were usually smooth or faceted, and reduced or absent bulbs. The orientation of the platforms was perpendicular, and its profile varied between a trapezoidal or triangular shape. Retouch types varies between unifacial, bifacial, invasive, alternate, or direct. Arrowheads seemed to lack of any typological directive, fact that was also noted by Berruti and Daffara (2014), who eventually identified thirteen types and two main families. Some of the arrowheads were triangular (without a perceivable bulb), convex, plain, pedunculated, and concave. Their edges were unifacially or bifacially retouched in the back side on the right or left edge, using a triangular delimitation. Their extension was

[7] The term element refers to any type of archaeological material, geological sample, biological sample, or anything that was considered worthy enough to register on the field formats or database.

unifacial and invasive in one of the edges with a continuous spread, a flat slope, and a scale-like shape. Additionally, one sickle carved on a flake was identified, and it seems to have been crafted by direct percussion on a smooth plane, with a cortical platform, a trapezoidal profile, unifacial retouch on the right edge, and a continuous and parallel morphology. The small core was obtained by direct percussion and completely used.

Bone artifacts were classified into three groups: spatulas (73%), burins (20%) and polished faunal teeth (7%). A polished tooth may have belonged to a wild boar (*Sus scrofa*) Spatulas were flat with elongated distal extremities (akin to a baker's shovel), exhibiting different degrees of polishing and fragmentation, probably related to taphonomic alterations. Cruz related their peculiar shapes to anthropomorphic figures, effectively classifying them as 'idols'. Bone burins also suffered from severe surface erosion, which hindered their proper classification.

Adornments were represented by a perforated shell (1%), polished earrings (2%), headpins (body and false head) (20%) and beads (77%). The perforated shells had quadrangular and elliptical punctures, with only one exhibiting a double perforation. Shells were classified by taxa, succesfully identifying *Helix pomatia*, *Solecurtus chamasolen*, *Trivia arctica*, and *Pecten maximus*. Earrings were carved out of muscovite and enamel, with double perforation and incisions. Headpins are highly fragmented, with two artifacts decorated with incisions and corrugations. Discoidal beads were made on muscovite and bone (see **Figure 4**). Atypical beads presented cylindrical and ovoid shapes, while one ceramic bead was tubular, with incisions on the surface.

Figure 4. Discoid beads carved on muscovite (1 to 31); semi-cylindrical beads (32 to 34), and elliptical perforated earring (35) (Cruz & Oosterbeek, 2013, p. 25, Annex II, Figure 29)

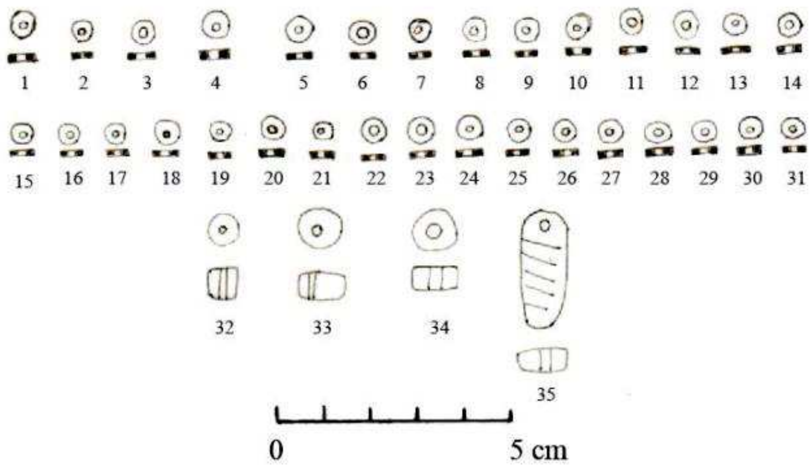

Pottery was classified according to its fragmentation level; atypical sherds fabricated using a potter's wheel (20th Century) (4%), and fragments manufactured manually[8], which included bases (4%), complete profiles (6%), rims (12%) and sherds (78%). Ware fragments that present a complete profile were subdivided in two groups: open vessels (everted rim) and closed vessels (inverted rim), globular vessels (with a convex or flat base), and vessels presenting low keel and flat base (typical of the Early Bronze Age).

[8] The name of the technique is not specified (e.g., coiling).

Just one of the fragments presented a perforation for suspension. Most rims have a shape that ranges from rounded, flat, and pointed, most straight, or everted. Pottery analysis did not extent to unclassified sherds. Regarding the fabric, most fragment were well baked, with oxidizing, irregular and reduced atmospheres. Inclusions' density varies from 25 to 50 and 50 to 75 percent, distributed homogenously, and composed mostly by inorganic elements such as quartz, limestone, and feldspar. The fabric's hardness was optimal, glazed finishes were smooth in both internal and external surfaces. Most of the colour varied due to the atmospheric conditions during baking, exhibiting mainly dark brown, reddish brown, yellowish brown, and dark red hues.

This year's bioanthropological studies were conducted by Tiago Tomé and Claudia Cunha (2013). Since the excavation efforts were focused on Sepulchral Pit 2, the bioanthropological analysis was divided among each pit to reflect their provenance. Sepulchral Pit II had a MNI of 151 (95 adults identified by the right and left maxillary central incisor and 56 subadults identified by the right maxillary lateral incisor and the left maxillary canine), from both sexes, and several age groups. Pathological analysis revealed a low prevalence of cariogenic lesions and a moderate degree of occlusal dental wear (2.94%). Other pathologies included articular degenerative lesions, located mostly in the feet and spine (Tomé & Cunha, 2013). Paleodemographic profiling led to the classification by age group: 1 to 4 years had 13 individuals; 5 to 9 years had 20 individuals, 10 to 14 years had 15 individuals; 15 to 19 years had 8 individuals. No perinatal cases were identified. Stature was determined measuring the talus and the calcaneus, each resulting on ranges of 157.02 and 155.64 cm for females, and 168.43 to 169.07 cm for males. The 10 cm difference was interpreted as a sexually dimorphic trait.

Cariogenic lesions were present on 123 permanent teeth (7.3%), located mostly on posterior dentition (*n*=94), and on interproximal (*n*=57) and cervical (*n*=35) surfaces. The lesions ranged in size from small to medium. Deciduous dentition reached a prevalence of 2.4% (*n*=5), distributed on a central incisor, three first molars and a second molar. Tartar was present on permanent teeth in 21.9% (*n*=362). Dental Wear was classified using Smith's scale: most of them presented a 2.94 value (99.3% of the sample). Even though the average occlusal dental wear is not above the expected levels for a prehistoric population, the number and type of wear (asymmetric and in more than one plane) is pronounced. This finding will lead to further conclusions *below* (Tomé & Cunha, 2013).

From the bones that presented signs of degenerative pathologies, most of the pieces belonged to the foot, spine, and hand. Identified alterations were found mostly around insertions of tendons in areas such as the patella (quadricipital tendon, 32.95%), the ankle (25.58%), and the proximal and intermediate phalanges (26.83 and 26.35%). Signs of infectious pathology were observed in only four fragments.

2.3.2.4. *2015's Campaign*

Previous campaigns forced the PhD Ana Cruz to restructure the methodology use for the registration of the archaeological record, namely the stratigraphic profiles. Two new objectives were set for this campaign: 1) continuing the excavation of Sepulchral Pit II; and 2) the launch of a horizontal excavation (i.e., area excavation) that would allow for a more holistic comprehension of the size and importance of Sepulchral Pits I and II. Thus, the classification of the stratigraphic layers had to be revamped, creating new

Stratigraphic Units (SU)[9] which facilitated the interpretation of various occupation moments within the rock shelter. A thorough list including the newly defined SUs can be found on the **Stratigraphy** section. Ultimately, the goal of the implementation of SU was to create comprehensive matrix that separated each layer according to their chrono-cultural characteristics.

Excavation efforts were focused on the rows 50, 51, 52, 53, 54, 55, 56, 57, and 58. This time a total of 725 ecofacts and artifacts were recovered from the site. Human remains were the most abundant (*n*=634/ 87.5%), followed by pottery (*n*=44/ 6%), adornments (*n*=26/ 3.6%), lithic artifacts (*n*=14/ 1.9%), bone artifacts (*n*=5/ 0.7%), symbolic artifacts (*n*=1/ 0.15%), and metallic artifacts (*n*=1/ 0.15%) (Cruz, 2015).

Sepulchral Pit II was interpreted as collective burial with material from the Chalcolithic and Neolithic. The slither of soil (Layer B) that was initially identified within the Sepulchral Pit II corresponded to an anthropogenic filling that included the newly defined SU [004] and extended along the walls of the rock shelter, all the way until the lower chamber.

Photograph 2. Sepulchral Pit I during excavation (western profile) (Cruz, 2015, p. 3, Annex II, Figure 3).

The number of beads that accompanied the bones seem to suggest that these items were buried with the individuals, and thus, they were originally in anatomical position. GMS was therefore tentatively classified as a “communal cemetery” that was functional for at least 4000 years. One of the new architectonic features discovered was a hearth surrounded by limestone boulders. This feature was interpreted as a temporary shelter.

The assemblage of human remains was composed mostly by small or fragmented bones from individuals of all ages. Ana Curto was this campaign’s bioanthropological researcher. Curto (2015) used roughly the same methodology as Tomé and Cunha with few additions: morphologic analysis followed the methodologies of Mendonça (2000) when analysing femora, Oliver et. Al. (1978) when analysing tibiae, and Santos (2002) and Cordeiro(2009) when analysing metatarsal elements. Arthrosis was identified utilizing

[9] Originally coined as “Unidades estratigráficas -UE” (Portuguese).

the website *Global History Health Project*, while non-articular degenerative pathologies were analysed using Crubézy's (1988) methods.

A total of 634 skeletal elements were unearthed from which 89 were associated with dental elements. The reason behind the homogenization of data from all skeletal elements, regardless of their SU or Sepulchral Pit is not stated clearly, although implicitly may be a result of the new methodology. The low count of human remains (when compared to 2013) is result of the change in methodology, as this campaign was focused on the characterization and delimitation of the funerary space. Thanks to this new approach, the southern wall was identified as a predilected site for burials. It also permitted the identification of human remains that probably were deposited earlier than most of the burials nearby the southern wall, both located close to it and in the north wall (Curto, 2015). Paleodemographic classification of age groups at the time of dead was once again focused on subadults with one individual under two years of age, three individuals under four years of age, two individuals under five years of age, one individual that ranged between eleven and sixteen years of age, and another one from fifteen to twenty-four years of age. Five individuals presented a greater range, from two to 20 years of age. In this campaign the most represented tooth was the second inferior molar (47). However, the most represented bone in previous campaign was the right maxillary central incisor, therefore the MNI of the rock shelter rose to 131. The fact that deciduous teeth display a skewed distribution towards the range between 5 and 9 years may be result of a higher mortality rate, caused by broader mobility patterns and factors related to it (e.g., accidents). Sexual allocation resulted in the identification of four females and one male(Curto, 2015).

Paleopathological analysis yielded 57 affected elements with degenerative lesions on the upper limbs and 40 in the lower limbs. Dental cariogenic lesions were identified on 12 pieces, hypoplasia on 34 and tartar in different degrees on 58. Other pathologies include the ossification of the apical odontoid ligament (GMSJ51-2205), bipartition of the navicular (GMSK511464), and congenital anomaly in ribs (GMSI52-987) (Curto, 2015).

The material recovered during 2015 was severely fragmented due to mechanic and chemical factors. Curto concludes that GMS is a primary funerary archaeological context where individuals of all ages were buried. It is possible that the southern wall burial corresponds to a concrete chrono-cultural society that is differentiated from the other burials (Curto, 2015).

2.3.2.5. *2016's Campaign*

During the field campaign of 2016 new stratigraphic units were detected. The funerary context in SU [002] was attributed to the Chalcolithic/ Early Bronze Age. What seems like a recognizable ossuary was found delimited by a wall made of boulders within SU [013], in an area of 2 m^2. Next to the ossuary, a similar structure embedded in SU [014] was classified as the remnant of a disturbed individual burial, as bones of a foot were found in anatomical position (indicating a flexed inhumation) (see **Photograph 3**). Other small structures, limited with limestone blocks, appeared also in the vicinity, although their contents were composed by disarticulated elements.

Photograph 3. Foot bones in anatomical position (*left*) (J52-????), anterior portion of a skull without reference (*right*) (Relvado & Anselmo, 2016, pp. 8-10, Figures 3 and 4)

Recovered artifacts, aside from beads, were scarcer than in previous years. The beads were linked to the existence of a cultural network in the Portuguese Estremadura, as they share their typology with those found within megalithic contexts, including the Alejntejo region.

This intervention was focused on the excavation process in SU [002], hoping to compare it with SU [003], SU [004] and SU [005]. Squares intervened included: L 50, 51, 52, and 23: K 50, 51, 52, 53, and 54; J50, 51, 52, 53, and 54; I 51, 52, and 53; H 51, 52, and 53; G 52, 53, and 54; and E 53 and 54.

A new field formulary was elaborated to record and describe Stratigraphic Units. The overall value of the usage of SU over layers improved the capacity of interpretation of most of the moments of occupation on the cave.

Rows 50, 51, 52, 53 and 54 were excavated. During the excavation 2872 artifacts were recovered uncovering lithic technology (represented by arrowpoints, geometric truncations, a polished hand axe, and an adze), bone industry (composed by spatulas and a burin made out of an ungulate's tarsal), pottery (included mostly sherds, and a rim fragment with a straight profile), adornments (represented by bone beads, earrings made out of a carnivore's tooth, a tubular bone pendant, and a green stone pendant), symbolic material (which yielded one rectangular pottery plaque), faunal remains (which were sent for a specialized study by Cláudia Revaldo from the Évora University.

In general, artifacts were scarce, continuing a trend identified during the previous excavations It is likely that most of them belong to the Middle/Late Neolithic. It was the first time in which a partially complete foot was found in anatomical position. The SU [013] was identified as a circular petrous structure under SU [002], that could belong to the Late Neolithic/Early Chalcolithic period. A metacarpal that belongs to this SU [K512820] was sent for radiocarbon dating (see **section** Error! Reference source not found.) with values between 3354 and 3092 calBC (2σ).

Palaeoanthropologists Cláudia Revaldo and Daniela Anselmo (2016) analysed 3747 records of skeletal elements that elevated the MNI to 224. The presence of anatomic articulation in situ and the retrieval of teeth and small-sized bones points to the presence of individuals of both sexes and a diverse age range. This evidence supports the theory that the site was a primary inhumation context for all kinds of people. Dental pieces presented a low frequency of oral and degenerative pathologies.

The MNI was obtained adapting the methodologies of Hermann et al. (1990, adapted by Silva1996) for the long bones, and Buikstra & Ubelaker for all other elements (1974). To establish age at the time of death two methodologies were used: for the *os coxae* the pubic symphysis method (Brooks & Suchey, 1990) and for subadults the epiphyseal fusion and maximum length of the clavicle technique (Sheuer & Black, 2004). Dental growth and eruption were estimated using AlQuahtani et al.'s method (2010). Sexual allocation followed Buikstra and Ubelaker (1994), applied only to adult individuals. Estimation using the talus and the calcaneus followed Silva's (1995) technique, and the methods used by Wasterlain and Cunha (200) for the humerus. To determine stature a metric analysis proposed by Santos (2002) and Cordeiro (2009) were used.

Age determination was applied to two adult individuals: one represented by a pubic symphysis GMS K51-1665b Indetermined sex, and age if female 38.2 ± 10.9 if male 35.2 ±9.4; another represented by a Clavicle [GMS L52 0069] – without complete fusion of the proximal epiphysis (<30). The rest were 104 juveniles ranging from 1.5 to 21 years. Sex allocation by morphology and anthropometry identified 14 males, 16 females, and 4 undetermined, using the skull, humerus, talus, and calcaneus. Estimation of stature was performed on 20 individuals with a mean of 156.1 cm.

A total of 441 dental elements were analysed, from which cariogenic lesions were mostly found on central incisors (39 out of 136 cases), while hypoplasia was discovered in just one case. Trauma was present in two metatarsals, and infectious processes on a rib, a femur, and a first right metatarsal. Among these, the first metatarsal (K51-2073) was unfortunately not found in the current collection.

2.3.2.6. *2017's Campaign*

PhD Cheila Ribeiro (2018) analysed the human remains recovered during the 2017's campaign. A total of 944 human skeletal elements were recovered, raising the MNI to 236 (counting the left central incisor[10]). Bones in anatomic position were uncovered again and correspond to the middle hand phalanx belonging to a subadult that had not yet fused with the proximal epiphysis. 944 fragments were recovered in total from which 87 were teeth. A total of 13361 human bone fragments were recovered from 2012 to 2017.

The palaeodemographic profile was scarcer than in previous reports. When determining age, only three juvenile age groups were identified: [1-4] included 4 individuals, [5-9] included 3 individuals, [10-14] included 2 individuals. Sex allocation added two individuals were identified, one [probably male] by the *os coxae* [K51-3322] and another [probably female] by the calcaneus. The innominate [K51-3322] was analysed in this study, and it was only represented by five fragments that were highly eroded and corresponded to the upper acetabular region, reason why sex determination with the piece was deemed too biased. A calcaneus, two first metatarsals and two second metatarsals were used to estimate stature, resulting on an average of 158 cm.

Regarding the health conditions of the sample, cariogenic lesions were found on 39 individuals, from which the highest value was present -again- on the central incisor. Other

[10] Ribeiro's tables do not take previous counts on other bones into account, and only present data for teeth.

pathologies included articular degenerative lesions, and ankylosing formations on foot phalanges.

A new discovery of elements in anatomical position is mentioned, but not specified.

2.3.2.7. *2018's Campaign*

Bioanthropologists Ana Curto and Cheila (2019) Ribero oversaw the analysis of the bioarchaeological material unearthed during 2018. The excavation was focused on squares J51, J52, K51, K52, L51, L52, L53, and L54. During this campaign 3078 human skeletal elements were recovered, including 318 dental elements.

The MNI for adults was raised to 163, with the discovery of nine left maxillary central incisors (permanent). The MNI of subadults was raised by 5, but the results are presented as an age-group table that would raise each age stage to 26 [1-4], 36 [5-9], 24 [10-14], and 12 [15-19]. Stature determination was subtracted from six metatarsals, with an average of 157.7 cm. Cariogenic lesions reached a 0.125 to 0.18% of Prevalence, with similar values for tartar. Other pathological conditions included arthritis and ankylosing of foot phalanges., traumas on a scaphoid and a compression fracture on a vertebral body.

2.3.2.8. *2019's Campaign*

The 2019's campaign persisted on the excavation of the southern wall. Its main objective was to unveil the contextual relationship between the positive structures and the material that, apparently, had no context. The archaeological layers that were located on the fringe squares H, I, J, K, and L 51 appeared to continue below the southern wall into the row 50. The distribution seems to suggest that the layer belongs to the Middle-Early Neolithic and its contents were uncovered *in situ* (Cruz, 2020). A total of 332 records were excavated in this campaign.

During the 2019's campaign a series of administrative and bureaucratic impasses made it impossible to continue the excavation of human remains after the month of June (Cruz, 2020). As of 2018, the Minimal Number of Individuals (MNI) for the whole collection was set at 216. Inferred stature from 10 individuals had a mean value of 1.6 m, 17 individuals with a mean value of 1.5 m, and 5 individuals with a mean value of 1.4 m. Sexual dimorphism was greater during the 2015 campaign, while insignificant in subsequent campaigns.

2.3.3. Interpretation of the site

A series of possible interpretations for Gruta do Morgado Superior's role in prehistoric times have been suggested through the last decades. These interpretations were concerned with its architecture, the volume and distribution of its material, the taphonomic alterations to which it was subjected, and its relation to other sites in the region.

While dolmens and necropolis coexisted during the Neolithic-Chalcolithic transition, only 6% of the burials have been found in rock shelters and caves against 94% found in funerary monuments. The disproportion may be due to the existence of a reduced number of available caves and openings that encouraged their repeated usage and resulted in the opportunistic behaviour seen in the archaeological record. Although both depositions exhibit different types of architecture, some have argued that caves lack of a differentiated organization that is limited by the cave's morphology. However, it is possible that funerary contexts on caves did in fact possessed differentiated structures that were destroyed by the most recent depositions (Cruz, 2020). Various structures have been found in the centre-South sectors of Gruta do Morgado Superior, albeit badly damaged. Density patterns suggest that the inhumations were primarily placed nearby the southern wall, but the sector presents a small depression when compared to the central or eastern flanks. These deteriorated structures correspond to single-burial activities from the early Neolithic (Cruz et al., 2013).

Only two cases of remains found in anatomical connection was registered: i) J52- The 1st, 3rd, 4th, and 5th metatarsals, a left navicular, and a left cuboid; ii) K51 – Medial hand phalange from a subadult and its epiphysis(Cruz et al., 2018), leading to the conclusion that Neolithic primary inhumations were disturbed by collective ones during the Chalcolithic. This number would rise as more elements seem to exhibit the same trait (see **section 4.4**).

Cruz (2018) suggested that the Gruta do Morgado Superior presents a confounding lack of artifacts when considering the number of buried individuals. This characteristic may result from socioeconomic factors such as lack of resources, social status, or funerary practices of recycling.

Among the taphonomic agents that were identified at GMS, the anthropic modifications stand out the most. They began during the Chalcolithic through the Bronze Age, and most recently by local communities. Thanks to an army's handcuff found in the cave and a fireplace in the base of the cave it is suggested that soldiers used the cave as a temporary shelter during the Napoleonic invasions.

After the anthropogenic modifications the second most important taphonomic agents are the chemical and physical modifications that include the patinas and calcite films that were found stuck to lithic and bone material (Cruz et al., 2018; Curto, 2015).

Bones buried at Morgado had a differentiated preservation grade that favoured small elements and teeth, while badly damaging long, pelvic, shoulder and cranial bones. This pattern reinforces the hypothesis that the cave is a primary context, and it was constantly modified by mechanical forces, which specially affect long bone conservation (Curto, 2015). Although all skeletal regions are represented, their proportions are not typical. elements such as the mandible, long bones, patella and hand and feet bones are overrepresented, while regions such as the skull, cranium, scapula, pelvic bones, sternum, and the vertebral column are underrepresented. It has been suggested that since these elements are composed mostly by trabecular tissue (except for the skull), they are prone to disintegration by different erosive agents. This would also explain why their conservation score is lower in contexts with high rates of mechanical alterations. Heat-exposed bones have been identified in the cave as well but considering evidence of recent campfires in the interior and the relatively thin layer of sediment, it is possible that they were burnt recently. Although human remains in the assemblage do not exhibit gnawing marks, the cave is used frequently by small animals such as reptiles and mammals. It is unclear why is no evidence of at least gnawing of the bones considering the overall depth of the skeletal elements. (Tomé & Cunha, 2013).

Dental wear values are atypical from those recorded in nearby caves; some researchers suggest that teeth (especially anterior incisors) were used as tools in everyday activities. The arrowpoints are a novelty in the area when comparing it to their neighbours (Gruta do Cadaval, Gruta dos Ossos and Gruta de Nossa Senhora das Lapas), and very similar to the post Neolithic layers of Gruta do Caldeirão. The pottery tradition is very similar to the one found in Gruta do Cadaval (Layers C and D – associated with the Middle Neolithic) (Cruz & Oosterbeek, 2013).

Finally, Gruta do Morgado Superior seems to have been closely linked to local and regional cultures in the past. Lithic technology displays similarities with other sites of the Portuguese Estremadura such as Lugar do Canto, Lapa da Galinha, Lapa do Carrascos, as well as megalithic sites. The grave goods present on the cave are analogous to the one found in Anta 1 de Val de Laje (Chalcolithic). This may suggest a wide spread of technological industries (Cruz & Oosterbeek, 2013).

Adornments may be an indicator of a wide area of goods-circulation that reached as far as the megaliths of Alto Alentejo (100 km) and the Portugues Estremadura (50 km). The small lagomorph-like statue has similarities with other symbolic artifacts found in Gruta da Galinha, Lapa do Suão, Cova da Moura, Cabeço da Arruda, Gruta da Carrasca, Quinta das Lapas, Castro da Ota, Portalegre, Vila Franca de Xira, Elvas, Monumento de Casainhos, Gruta de Carenque, Monumento das Conchadas, Grutas de Cascais, Montemor-o-Novo, Lapa do Bugio, Anta da Comenda da Igreja e Anta do Olival da Pega. The Almeriense Idol may bear similarities to artifacts found in Lapa do Bugio and Anta Grande do Olival de Paga. Headpins have analogous counterparts in Lapa do Bugio and Monumento da Praia das Maçãs (Cruz & Oosterbeek, 2013). Societies in Gruta do Morgado Superior may have led primarily a hunter-gatherer economic lifestyle, coupled with some complementary agropastoral activities. They also maintained close cultural and economic relationships with other communities in the region.

2.3.4. Stratigraphy

Throughout the process of excavation, the site became more and more complex with time. From 1988 to 2014 the identified archaeological stratigraphy consisted of only two layers (A and B), that was often related to two sepulchral pits that were delimited during the first interventions (Cruz et al., 2013) (see **Table 4**).

Table 4. Archaeological layers as described in 2013 (Cruz et al., 2013).

Name	Thickness (cm)	Characteristics	Adscription
Layer A (*Camada A*)	5- 50	Sandy-silty composition, with a grey-yellow hue (Cailleux = L73)	Sepulchral Pit II
Layer B (*Camada B*)	5-20	Partially brechified limestone layer, full of carbonated calcium precipitations. It displayed a concretion-like clay sediment within. It presented a light brown/orange hue (Cailleux = M69)	Sepulchral Pit I: Usually found surrounding human remains.

As the volume of material increased exponentially, PhD Ana Cruz saw the necessity of elaborating a methodology that shifted apart from arbitrary levels of excavation to digging using the help of Stratigraphic Units (SU) (Cruz, 2017).

Over 63 SUs were identified and/or described in different field reports from 2015 to 2019, with an additional 14 SU that were recorded only on the database, bringing up the total to 76 (see **Table 5**).

Table 5. List of all the Archaeological Stratigraphic Units (SU) identified at Gruta do Morgado Superior. From SU [001] to SU [009] the information was translated and slightly modified from Table 1 in Cruz (2015, Pages 7 to 10). From SU [010] to SU [024] the data was translated and summarized from Cruz (2017, Pages 5 to 6). Complementary information in other reports regarding the SU are cited directly. The translation includes standard nomenclature by Schoeneberger et al. (2012).

Square	1988 & 2012	2013	From 2015 to 2020	Relative Chronology	Location	Description
K53	Layer A	Sepulchral Pit II	SU 001	Chalcolithic/ Early Bronze Age	On top of the surface, contiguous to SU 003	**Horizon O**. Sandy soil with a very fine texture (like dust). Colour: 5 YR 4/4 (Reddish brown) – Munsell; S 47 - *Brun Rouge* - Cailleux.
J51 K51	Layer A	Sepulchral Pit II	SU 001i2i3i4iI	Chalcolithic/ Early Bronze Age	Contained within SU 001, 002, 003 and 004	Loosely cemented sediment, with a sandy texture. Colour 5 YR 3/4 (Dark reddish brown) - Munsell; S 45 – *Brun Rouge* - Cailleux (Cruz, 2020). Limestones with varying dimensions (Cruz, 2017).
I52 J51 J52 J53 K51 K52	Layer A	Sepulchral Pit II	SU 002	Chalcolithic	Under SU 001 and on top of SU 004.	Sandy texture, poorly cemented. Colour: 5 YR 4/4 (Reddish brown) -Munsell; S 47 *Brun Rouge* - Cailleux.
K52	(?)	Sepulchral Pit II	SU 002ii	Chalcolithic	Contained within SU 002.	Clogged burrow. Colour: 7.5 YR 5/4 (Brown)-Munsell; P 67 - *Brun Rouge* - Cailleux.
I51 I52 J51 J52 K51 K50	(?)	Sepulchral Pit II	SU 002i4i	Chalcolithic	Interface between UE 002 and UE 004	Sandy texture, poorly cemented. Colour: 5 YR 4/4 (Reddish brown) - Munsell; S 47 *Brun Rouge* - Cailleux.
J51 J52 K51	(?)	Sepulchral Pit II	SU 00214iII	Neolithic/ Chalcolithic	Contained within SU 002 and SU 004. Constructed originally on SU 004.	Limestone blocks *in situ*, placed in a semi-circle. Positive structure.
I53 I54 J53 J54 K53 K54	Layer A	Sepulchral Pit II	SU 003	Chalcolithic/ Early Bronze Age	On top of the surface and contiguous to SU 001 and SU 002.	Sandy loam texture, sediment with a granular structure. Colour: 7.5 YR 5/4 (Brown) Munsell; P 67 – *Brun* - Cailleux.
I53 I54	Layer A	Sepulchral Pit II	SU 003iI	Neolithic/ Chalcolithic	Contained within SU 003	Layer of large cave-in blocks, all heavily debilitated and meteorized. s
I53 J53 J54	Layer A	Sepulchral Pit II	SU 003iII	Neolithic/ Chalcolithic	Contained within SU 003	Anthropic filling of large rock blocks, accompanied by small limestone fragments. This task required the construction of an artificial floor for circulation. Colour: 5 YR 5/3 (Reddish Brown) – Munsell; P 27 -*Brun Rouge* - Cailleux.

Square	1988 & 2012	2013	From 2015 to 2020	Relative Chronology	Location	Description
G53 G54 H52 I51 I52 I53	Layer B	Sepulchral Pit I / Sepulchral Pit II	SU 004	Neolithic/ Chalcolithic	Under the stalagmitic mantle in the Northern Wall, on top of the surface on the Southern Wall, and under SU 002.	Strongly cemented soil with a silty clay texture, with a granular structure. It may correspond to earlier burials that were destroyed to make way for new ones during the Neolithic. It remained protected near the cave walls due to the formation of a stalagmitic mantle. Sediment with a silty texture, a plastic consistence and an abundance of rock and artifacts such as gravel, pebbles and calcite crystals; it is moderately cemented. Colour: 5 YR 5/4 (Reddish Brown); P 55 - *Brun Rouge* - Cailleux.
H53	Layer B	Sepulchral Pit I	SU 004i	Neolithic	Contained within SU 004	Clogged burrow. Colour: 5 YR 5/3 (Reddish brown)-Munsell; R53- *Brun Rouge*.
H53 H54 I54	Layer B	Sepulchral Pit I	SU 005	*Arch. Sterile*. **However, it has material on database**.	On top of the surface, contiguous to SU 003 and SU 004.	Strongly sedimented soil, with a clay texture, with a breccia-like structure. Colour: - 5 YR 6/4 (light reddish brown) – Munsell; N 55 - *Brun Rouge clair.*
H53	Layer B	Sepulchral Pit I	SU 005iI	N/A	Contained within SU 004 and SU 005	Stalagmitic Mantle formation.
G54 H54 I54	Layer B	Sepulchral Pit I	SU 005iII	N/A	Contained within SU 004 and SU 005	Stalagmitic Mantle formation.
G53 G54	Layer B	Sepulchral Pit I	SU 005iIII	N/A	Contained within SU 005	Stalagmitic Mantle formation.
G53 G54	Layer B	Sepulchral Pit I	SU 005iIV	N/A	Contained within SU 005, under a large cave-in block (5iiI).	Stalagmitic Mantle formation.
G54	Layer B	Sepulchral Pit I	SU 005iV		Contained within SU 006, contiguous to the Stalagmitic Mantle (5iiIV)	Stalagmitic Mantle formation.
G53	Layer B	Sepulchral Pit I	SU 005iII	Arch. Sterile	On top the surface, at the convergence between the wall and the cave.	Unspecified sediment. Colour: 5 YR 6/3 (light reddish brown) – Munsell; N 30 - *Brun Rouge clair* - Cailleux. (The homonymous relationship with another layer was left unexplained).
E53 E54 F53 F54 G53	Layer B	Sepulchral Pit I	SU 006	Neolithic	On top of the surface, next to the Stalagmitic Mantle (5iIV).	Strongly cemented soil, with a sandy texture. Colour: 2.5 YR 6/2 (Pale red) - Munsell; M 50 *Rouge pale* - Cailleux.
E54	Layer B	Sepulchral Pit I	SU 006i	Neolithic	Contained within SU 006	Clogged burrow. Colour: 2.5 YR 6/2 - Munsell; M 50- *Rouge pâle*- Cailleux.
E54	Layer B	Sepulchral Pit I	SU 006ii	Neolithic	Contained within SU 006	Clogged burrow. Colour: 5 YR 6/3 (Light reddish brown) – Munsell; N 30 - *Brun Rouge clair* - Cailleux.
J55 J56 K55 K56	Layer B	Sepulchral pit I	SU 007	Possibly modern – Napoleonic Invasions	On top of the surface, contiguous to SU 003, SU 005 and SU 009	Strongly cemented soil, with a sandy loam structure. Colour: 5 YR 5/6 (Yellowish red) Munsell; P57 *Rouge jaune* - Cailleux.
J56 K56	Layer B	Sepulchral Pit I	SU 007i	N/A	Contained within SU 007	Clogged burrow. Colour: 5 YR 5/4 (Reddish brown) – Munsell; P 55 -B*run Rouge* - Cailleux.
J56 K56	Layer B	Sepulchral Pit I	SU 007iI	N/A	Contained within SU 007	Limestone blocks with various dimensions.
J55 K56	Layer B	Sepulchral Pit I	SU 007iiI	Restoration of Independ.	Contained within SU 007.	Limestone blocks *in situ*, placed in a semi-circle. Positive structure.

Square	1988 & 2012	2013	From 2015 to 2020	Relative Chronology	Location	Description
					Originally constructed over SU 007, taking advantage of the wall and the limestone pavement.	
J55 K56	Layer B	Sepulchral Pit I	SU 007iiil	N/A	Contained within SU 007	Circular Hearth. Colour: 7,5 YR 5/2 (Brown) - Munsell; P 30 – *Brun* - Cailleux. Strongly cemented sediment. Colour 5 YR 5/6 (Yellowish red) – Munsell; P 29 *Brun Rouge* (Cruz, 2020).
K55 K56	Layer B	Sepulchral Pit I	SU 007iII	Modern –19th Century	Under SU 007, contiguous to SU 008	Strongly cemented sediment. Colour: 5 YR 5/6 (Yellowish red) – Munsell; P 57 - *Rouge jaune*- Cailleux.
K54 K55	Layer B	Sepulchral Pit I	SU 008	Probably a modern deposit, in the 20th century – N/A (Cruz, 2020)	Under SU 007, on top of a cave-in block	Strongly cemented sediment with a clayey texture. Possible mudbrick (*Adobe*) (?)set in place to level the cavity's floor. Colour: 5 YR 5/3 (*Reddish brown*)- P 29 - *Brun rouge*. Also described as a loosely cemented sediment with a sandy texture and a (fine) granular structure. Colour 7.5 YR 5/4 (Brown) – Musell; P67 - *Brun*– Cailleux (Cruz, 2020) .
J57 K57 K58 L57 L58 M57	Layer B	Sepulchral Pit I	SU 009	N/A	On the top layer, contiguous to SU 007	Weakly cemented soil, with a sandy texture and a granular structure with very fine particles. Colour: 7,5 YR 5/4 (*Brown*); P 67 – *Brun* - Cailleux.
J57 L57 L58	Layer B	Sepulchral Pit I	SU 009i	N/A	Contained within SU 009	Clogged burrow. Colour: 5 YR 6/3 (Light reddish brown) - Munsell; N 33 - *Brun rouge clair* - Cailleux.
K58 L58	Layer B	Sepulchral Pit I	SU 009ii	N/A	Contained within SU 009	Burrow (unclogged). Colour 5 YR - 5/6 (Yellowish red) - Munsell; P 57 -*Rouge jaune* - Cailleux.
K57	Layer B	Sepulchral Pit I	SU 009iii	N/A	Contained within SU 009	Large-sized cave-in block.
K57 K58 L57 L58 M57	Layer B	Sepulchral Pit I	SU 009iI	N/A	Contained within SU 009	Limestone blocks *in situ*, placed in a semi-circle. Positive structure.
K57	Layer B	Sepulchral Pit I	SU 009iII	N/A	Contained within SU 009	Limestone blocks *in situ*, placed in a semi-circle. Positive structure.
K51 K52	Layer A	Sepulchral Pit II	SU 010*	Chalcolithic	Under SU 002	Strongly cemented sediment. Contains SU17 and SU19. Within it a probable individual burial was found since some bones are in anatomic position. On the left margin of the square a mandible was recovered. Colour: R49 – Cailleux.
J51 K51 L50 L51	N/A	Sepulchral Pit II	SU 011*	*Arch. Sterile*. **However, it has material on database**.	Contiguous to SU 002 and SU 0010.	Horizon O. Poorly cemented sediment with a silty texture.
J50 ** I51	N/A	Sepulchral Pit II	SU 012*	Neolithic/ Chalcolithic (Cruz, 2020)	Under SU 004 and SU 13	Moderately cemented soil. It contains a positive fraction of a structure (anterior section of an individual burial) that was eroded by the anthropic activity on SU2. An artificial floor was found within it. The section within I51 presented a sediment with a silt texture, plastic consistence,

Square	1988 & 2012	2013	From 2015 to 2020	Relative Chronology	Location	Description
						and massive grain structure. It contains inorganic (soil) artifacts such as stalagmitic fragments and pebbles, as well as roots and human remains. Colour: Between R49 and R50 – Calliwux.
K51 K52 L51 L52 ** L53 (b)	N/A	Sepulchral Pit II	SU 013*	Chalcolithic	N/A	Ossuary characterized delimited by a small to medium-sized block wall. Sediment with a granular (fine) structure. Colour: Variation between N 53 to N 50, and P 30 to S 67.
G50 K51	N/A	Sepulchral Pit II	SU 013a SU 013 b	Neolithic/ Chalcolithic	Contained within SU 013. K51 section is covered by SU019, and delimited by SY 002, SU 004, SU 005, SU 011, and SU14.	Sedimentary pocket that contains calcite crystals and blocks, roots and human remains. The sediment presents a silt texture, moderately cemented. Colour: P 30 – S 67 - Callieux.
J52 **	N/A	Sepulchral Pit II	SU 014*	Late Neolithic/ Early Chalcolithic	Contiguous to SU 004, SU 002, SU 011, SU 010, SU 019, and SU 020	Small niche-ossuary. Lithic and pottery artifacts selected for chemical analysis. Colour: N49 - Cailleux.
J50, K50 K51 **	N/A	Sepulchral Pit II	SU 015*	Late Neolithic/ Early Chalcolithic	Under SU 002, next to SU 004, SU 002, SU 011, and SU 005	Niche-ossuary Lithic and pottery artifacts selected for chemical analysis. Colour: N65 - Cailleux
L51 L52 **	N/A	Sepulchral Pit II	SU 016*	Late Neolithic/ Early Chalcolithic	Under SU 002, next to SU 004, SU 002, SU 011, and SU 005	Niche-ossuary Lithic and pottery artifacts selected for chemical analysis. Colour: N65 - Cailleux.
J51 **	N/A	Sepulchral Pit II	SU 017*	Late Neolithic/ Early Chalcolithic	Under SU 002, contiguous to SU 018 and SU 016	Niche-ossuary Lithic and pottery artifacts selected for chemical analysis. Colour: R35 - Cailleux.
K51	N/A	Sepulchral Pit II	SU 018*	Late Neolithic/ Early Chalcolithic	Under SU 002, contiguous to SU 017, SU 016, SU 004, SU 011, and SU 021	Niche-ossuary Lithic and pottery artifacts selected for chemical analysis. Colour: R35 - Cailleux.
H51 H52 I51 I52 J51 J52**	N/A	Sepulchral Pit II	SU 019*	(?)	Under SU 002, contiguous to SU 005, SU 004, SU 002, SU 011, and SU 014	Niche-ossuary. Colour: M65 - Cailleux.
J52 K51 K52**	N/A	Sepulchral Pit II	SU 020*	(?)	Under SU 002, contiguous to SU 002 and SU 010, and SU 013	Niche-ossuary. Colour: M29 - Cailleux.
J51 L52 **	N/A	Sepulchral Pit II	SU 021*	(?)	Under SU 002 and SU 013, contiguous to SU 010.	Niche-ossuary. Colour: L25 - Cailleux.
J51 K51	N/A	Sepulchral Pit II	SU 022*	(?)	Under SU 002, contiguous to SU 018.	Niche-ossuary. Colour: M27 - Cailleux.
J51 K51	N/A	Sepulchral Pit II	SU 023*	(?)	Under SU 002, contiguous to SU 017.	Niche-ossuary. Colour: M20 - Cailleux.

Square	1988 & 2012	2013	From 2015 to 2020	Relative Chronology	Location	Description
K51 K52 L52 L53 **	N/A	Sepulchral Pit II	SU 024*	*Arch. Sterile*. **However, it has material on database**.	On top of SU 005	Sediment with a breccia-like structure.
K51	N/A	Sepulchral Pit II	SU 025	Neolithic/ Chalcolithic	Contained within SU 13	Sediment with a sandy texture, cemented and homogeneous. Contains pebbles, human and troglofaunal remains. Colour: T29 and T 30 – Callieux.
K51	N/A	Sepulchral Pit II	SU 026	Neolithic/ Chalcolithic	Contained within SU 025	Sediment with a silt texture, moderately cemented and a massive grain structure. Contains human remains, calcareous stones, pebbles, and roots. Colour between T29 and T 30 – Callieux.
I51	N/A	Sepulchral Pit II	SU 027	Neolithic/ Chalcolithic	On top of SU 005 and SU 28	Sediment with a sandy/ sandy loam texture with pockets of silt (Sandy loam (Schoeneberger et al., 2012)), moderately cemented and with a massive structure. The ossuary was built over a calcareous stone structure with a semi-circular shape. It contains calcite crystals and human remains. Colour: Between R20 and R21, Callieux.
(?)	(?)	(?)	SU 028	(?)	Adjoined to SU 029	(?)
I51	N/A	Sepulchral Pit II	SU 029	Neolithic/ Chalcolithic	Adjoined to SU 027 and 028	Sediment with a sandy texture with pockets of silt (Sandy loam (Schoeneberger et al., 2012)), moderately cemented and with a massive structure. Colour: R39 – R49, Callieux.
(?)	(?)	(?)	SU 030	(?)	(?)	(?)
(?)	(?)	(?)	SU 031	(?)	(?)	(?)
K51	N/A	Sepulchral Pit II	SU 032	Neolithic/ Chalcolithic	Under SU 026	Sediment with a sandy loamy texture, moderately cemented. Contains charcoal, microfauna, malacofauna, and calcareous rocks and crystals. Colour: R10 and R4/3 – Callieux.
K51	N/A	Sepulchral Pit II	SU 033	Neolithic/ Chalcolithic	Under SU 032	Sediment with a sandy texture and no discernible structure. Contains charcoal, microfauna, roots, and calcareous rocks and crystals. Colour: between T29 and T30 – Callieux.
(?)	(?)	(?)	SU 034	(?)	(?)	Similar to SU 036
K51	N/A	Sepulchral Pit II	SU 035	Neolithic/ Chalcolithic	Under SU 033	Sediment with a sandy texture and no discernible structure. Contains charcoal, microfauna, and calcareous rocks and crystals. Colour: between U29 and U30 – Callieux.
K51	N/A	Sepulchral Pit II	SU 036	Neolithic/ Chalcolithic	Adjoined and contained within SU 035	Part of the Chalcolithic Ossuary, with human remains from both periods. The sediment has a silt texture, moderately cemented. It contains calcite crystals and human remains. Colour: P 30 to S67 – Callieux.
K51	N/A	Sepulchral Pit II	SU 037	Neolithic/ Chalcolithic	Under SU 036	Disturbed soil with a sandy loam texture, without a discernible structure. Contains calcareous rocks, roots, and human remains. Colour: between S69 and S71.
K51	N/A	Sepulchral Pit II	SU 038	Neolithic/ Chalcolithic	Adjoined and contained within SU 039.	Sediment with a sandy texture, cemented and with a massive grain structure.
K51	N/A	Sepulchral Pit II	SU0 39	Neolithic/ Chalcolithic	Contained within SU 041	Sediment with a silt texture, cemented and with a massive grain structure. Contains calcareous rocks, pebbles, roots, and human remains. Colour: Between T29 and T30.

Square	1988 & 2012	2013	From 2015 to 2020	Relative Chronology	Location	Description
K51	N/A	Sepulchral Pit II	SU 040	Neolithic/ Chalcolithic	Under SU 039	Sediment with a sandy loam texture, moderately cemented. Contains charcoal, microfauna, malacofauna, and calcareous rocks and crystals. Colour: between R10 and R 4/3 – Callieux.
K51	N/A	Sepulchral Pit II	SU 041	Neolithic/ Chalcolithic	Under SU 040 and SU 039	Sediment with a sandy texture and no discernible structure. Contains charcoal, microfauna, roots, and calcareous rocks and crystals. Colour: between T29 and T 30 – Callieux.
K51	N/A	Sepulchral Pit II	SU 042	Neolithic/ Chalcolithic	Under SU 041	Sediment with a sandy texture and no discernible structure. Contains charcoal, microfauna, and calcareous rocks and crystals. Its colour is a combination between the ones observed in SU 029 and SY 030.

(*) These SU were described in The Field Report from Cruz (2017).

(**) Information extracted from annex no. 1., in Cruz (2017).

The SUs found on field formats and databases have no description available on the field reports and belong mostly to the 2019's Field Campaign. These include all SUs from [043] to [060] and SU [013b]. The latter belongs to the square L53 while the others are part of the Sepulchral Pit II, which includes the squares J50, J51, K50 and K51. These SUs seem to be smaller by comparison as only 118 entries were recorded in them. Most of the SU are depositions formed by geological, biological, or anthropogenic activity. Only four SUs were officially classified as archaeologically sterile (0[05], [005iII], [011] and 024).

The chronological periods associated with each SU are diverse as well, spanning from the Neolithic to the 20th Century. Starting with the Neolithic, five units were ascribed to it: SUs [002], [002ii], [002i4i], [010], and [013]. The transition between the Neolithic and Chalcolithic yielded 25 units (SUs [00214iII], [003iI]. [003iII]. [004], [012], [013a], [014], [015], [016], [017], [018]. [025], [026], [027], [029], [032], [033], [035], [036], [037], [038], [039], [040], [041], and [042]), from which SUs [014], [015], [016], [017] and [018] were specifically situated in the Late Neolithic – Early Chalcolithic transition. The Chalcolithic SUs include just four units ([002], [002ii], [002i4i], [010], and [013]), most of them associated/close to SU [002]. The transition between the Chalcolithic and the Early Bronze age corresponds to the first excavations on the site, including SUs [001], [001i2i3i4iI], and [003]. Layers associated with historic periods consist of SU [007] (Napoleonic Invasions), SU [007iiI] (Portugal's Restoration of Independence) and SU [008]. The remaining SUs ([019], [020], [021], [022] and [023]) correspond to ossuaries that were ultimately not attributed any specific chronological period on the field reports, although all of them were located under SU [002], which may suggest that they were constructed earlier or around the Chalcolithic.

Although most of the SUs were carefully described on the field reports, four layers were mentioned only by name (SU [029], SU [30]. SU [031] and SU [034]). Given that their consecutives belong to the 2017 to 2019 periods is safe to assume that they belong to the excavations on the southern wall of the cave, within the deepest layers.

3. Materials and Methods

According to the original data recorded by Ana Cruz, PhD, the collection recovered in Gruta do Morgado Superior was composed by at least 18089 records (18635 by the end of this research) distributed in categories such as adornments (313 entries1[11]), anthracological samples (17 entries), bone tools (48 entries), carpological samples (9 entries), entomological samples (1 entry), faunal bones (194 entries), figurines (12 entries), human remains (17249 entries), lithics (181 entries), malacological samples (47 entries), metal tools (2 entries), mineral samples (65 entries), portable rock art (2 entries), rock samples (43 entries), and ceramic ware (444 entries) (see **Table 6** and **Chart 1**).

Such estimates should be deemed modest at best, as demonstrated by the results obtained while elaborating the current inventory for square **K51**. An increase of 11.5% was recorded while consolidating data. Additionally, non-coordinated entries, usually comprised by elements obtained through sediment sieving, have dozens of fragments from different bones.

An analysis performed on the 18635 entries would have exceeded the time available for the current analysis, so it was deemed necessary to select a sample that best represented the collection and fitted the schedule. Square **K51** was chosen as the most representative sample due to its variety of material and its sheer size (see **Annex 1** and **Chart 2**).

Table 6. Recorded entries (including non-coordinated records) by category. The total value was calculated after the analysis of square K51.

Category	No. of Entries	Percentage
Adornment	313	1.68%
Anthracological Sample	17	0.09%
Bone Tool	48	0.26%
Carpological Sample	9	0.05%
Faunal Bone	194	1.04%
Figurine	12	0.06%
Human Remains	17249	92.56%
Lithic	181	0.97%
Malacological Sample	47	0.25%
Metal Tool	1	0.01%
Mineral	65	0.35%
Portable Rock Art	2	0.01%
Rock	43	0.23%
Ceramic Ware	444	2.38%
Undetermined/Entomologic	9	0.05%
Grand Total	**18635**	**100.00%**

[11] The term "entry" refers to one excel row that may or not represent one element. This denomination is used because In several occasions the rows represent mixed or fragmentary elements.

Chart 1. Recorded material (including non-coordinated records) by category. The most abundant categories are highlighted. Notice that it refers to number of bags, not fragments. The total value was calculated after the analysis of square K51.

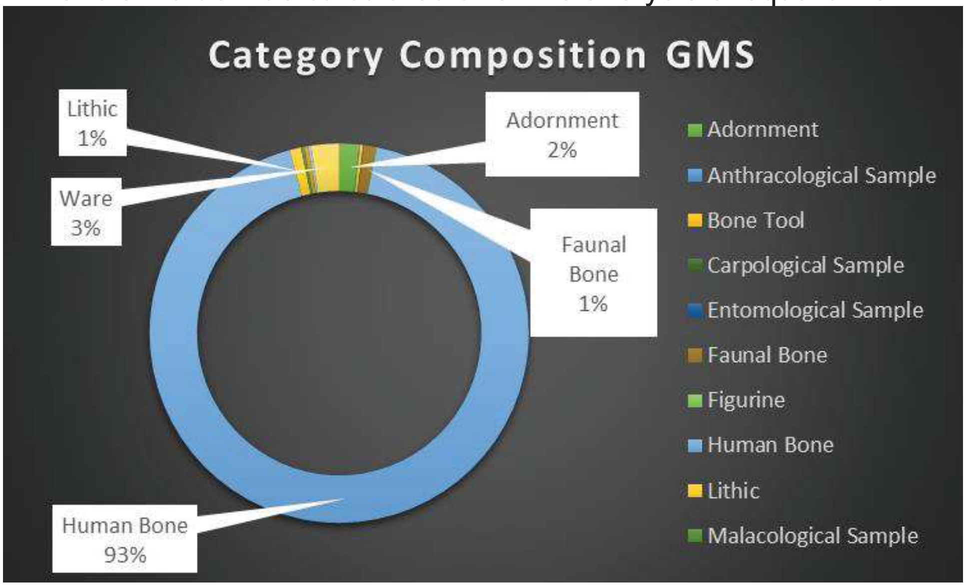

Chart 2. Distribution of GMS material (all categories) among the excavated squares. Squares with the most notable assemblages are highlighted. Note that those squares that end in "W" represent non-coordinated material from sieves.

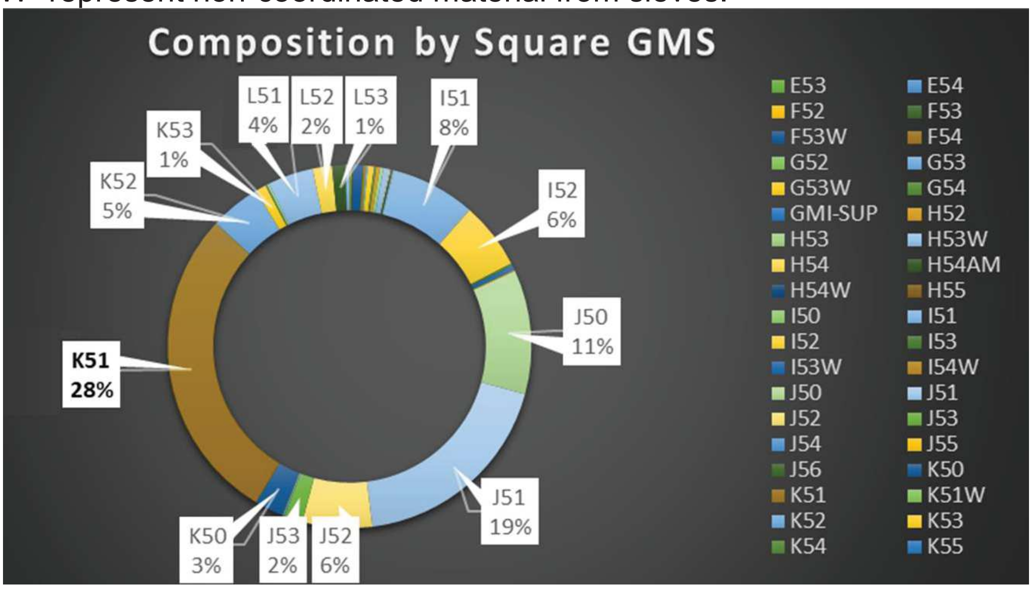

Coordinated elements on **Square K51** comprise 28.24% of the material collected. Although **K51** is a diverse square, its composition is not entirely analogous to the whole site. Firstly, none of the material within it qualified for a carpological or malacological study. From the artifact's perspective, metal tools or portable rock art elements were not recovered from it. The overall percentage of certain material categories is lower than their global trends, especially when observing *adornments* (-1.05%), *anthracological samples*

(-0.03%), *bone tools* (-0.13%), *faunal bones* (-0.72%), *figurines* (-0.02%), and *ceramic ware* (-1.35%). On the other hand, some material categories are more abundant such as of *human remains* (+3.37%), *lithic artifacts* (+0.13%), and *mineral and rock* samples (+0.07% for each). The latter may be a result of the excavation methodology as Square K51 was heavily target after 2015. In conclusion, leaving all supporting samples aside, the presence of human remains, and lithic artifacts is slightly higher than the overall trends, while the recovery rate of figurines, bone tools, ceramic ware, adornments, and fauna is slightly lower (see **Chart 3**). The absence of metal tools and portable rock art is a shared trait with most squares, given their uncommonness. Thus, the bioanthropological sample in **K51** was deemed representative enough of the whole Gruta do Morgado Superior Collection.

Chart 3. Stacked percentage of the categorical comparison between GMS's and Square K51's composition.

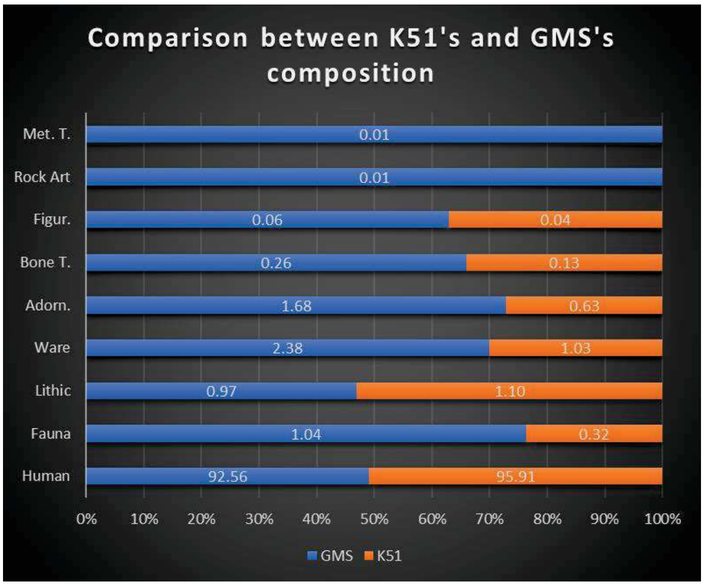

Originally, **K51** was supposed to contain 4718 entries from which 95.38 % (4500) were human skeletal remains. The final percentage of human bones and teeth ascended to 95.97% (5260 entries) after the inventory was completed. New entries include a mixture of homonymous records that were not registered on the previous database and/or to bags with different skeletal elements weighed as one (see **Table 7**). Generally, when one record was duplicated, Cruz would add a letter to the end denoting the order of appearance (e.g., 1509A, 1509B, etc.), so to avoid any confusion, new entries obtained during the analysis were denominated with a *prime* symbol (') used in succession (e.g., 1509A', 1509A'', etc.). Letters were not used because some bags already had them attached (even if the record was not on the previous database) In some cases the consecutives utilized all the alphabet until letter *z*, or had a composite with two letters (e.g., AB, AC, etc.), rendering impossible the use of alphabetic denominations. If only one square had an increase of 10.5% in data, it is plausible to assume that the remaining squares will behave similarly.

Table 7. Number of entries by category and their composition percentage on Square K51.

Row Labels	Entries (before analysis)	Entries (after analysis)	Percentage
Adornment	33	33	0.63%
Anthracological Sample	3	3	0.06%
Bone Tool	7	7	0.13%
Faunal Bone	26	17	0.32%
Figurine	2	2	0.04%
Human Remains	4500	5048	95.97%
Lithic	60	58	1.10%
Mineral	20	22	0.42%
Rock	13	16[12]	0.30%
Ware	54	54	1.03%
Grand Total	**4718**	**5260**	**100.00%**

The bioanthropological analysis was performed on 4351 human remains distributed along various skeletal regions (see **Table 8**). The remainder entries (703 -13.4%) that were not included were physically missing from the collection. They correspond mostly to 2015's campaign excavation material (422 entries), and an amalgamation of entries from the other campaigns. Their absence could have been caused by incorrect labelling of the bags (leading to duplicates), or difficulties during the digitalization process.

Table 8. List of the entries analysed for this research by skeletal region in the square K51.

Skeletal Region	Entries
Cranium and Mandible	149
Upper Dentition	309
Lower Dentition	298
Dentition (Und.)	1
Hyoid and Vertebrae	323
Thorax	282
Shoulder Girdle	44
Upper Limb	95
Hand	900
Pelvic Girdle	44
Lower Limb	155
Foot	801
Undetermined	944
Total	4351

[12] The increase in rocks corresponds to material misclassified classified as bone.

3.1. General state of the collection

Most of the human skeletal remains material was kept in hermetic plastic bags (at least from 2013), with a lower percentage being kept in regular plastic bags held together by metal clips. Teeth that were still embedded in alveolar tissue was kept in plastic boxes for extra protection in campaigns before 2014. From 2015 onwards there seems to be differentiation between delicate and regular material regarding its packaging. Most bags from earlier campaigns (2014-1015) present punctures to reduce damage by fungi. Elements collected before 2014 were already cleaned when this analysis was performed, whereas material labelled from 2015 onwards was prone to be accompanied by blocks of soil, roots, insects, and fungi (see **Photograph 4**).

Considering the importance of the site and the fragility of the bones, all the pieces that were had recognizable landmarks or were suitable for anthropometric measurement were cleaned with brushes and dental equipment, without using any alcohol or water during the process (see **Photograph 4**), it is advised that the whole collection is cleaned at some time in the future before it deteriorates further.

Photograph 4. (a) Example of material storage. (b) Cleaning process with brushes and dental equipment (without water or alcohol). (c) Example of a right femur with evidence of bioturbation (roots) (K51 -0908).

(a)

(b)

(c)

The problem regarding coordinated elements that were labelled with the same ID was surpassed by adding the original coordinates to further duplicates. According to the original team, each coordinate may represent one or more entries in a 10 cm radius.

Gruta do Morgado Superior contained an ensemble of archaeological remains that were highly fragmented within a severely disturbed sediment filling. This trait made it difficult for researchers to employ commonly used methodologies in palaeoanthropology, especially those that rely on clearly defined mortuary architecture and well-preserved bioanthropological material.

For the sake of answering some of the questions surrounding the assemblage's formation and chrono-cultural association(s) it was deemed necessary the construction of a multivariable approach in which the information could be easily analysed and compared. Each variable was then recorded within an additional database that could serve as the cornerstone of the analysis. Most of the variables were taken from studies in similar contexts in Portugal and Europe, keeping in mind the provenance of the raw material used to hone each technique.

The current chapter's objective is to define and describe in detail all the variables utilized in the database, the studies from which they were taken, and the modifications done for Gruta de Morgado Superior. Additional methods were described with the intent of constructing the framework for future analysis that can encompass the whole collection.

3.2. Database consolidation

The first step towards the creation of a cohesive inventory that allowed the collection of morphometric data and its standardization, was the consolidation of a general database. It had to be versatile enough so that all the information gathered in the last three decades could be integrated. This process was done by conducting *i*) the digitalization of missing information; *ii*) the elimination of gaps and repeated records; *iii*) the translation of the data from Portuguese to English; *iv*) the redistribution of data according to its scope and new classification; *v*) the revision of three-dimensionally coordinated elements; and *vi*) the addition of the variables necessary to perform the bioarchaeological analysis.

3.2.1. *Digitalization of data*

Throughout 2022's summer break, missing data from 2017, 2018 and 2019 that was still confined into field sheets was digitalized. A total of 3251 entries were added: 16 entries from square **I50**; 149 from **I51**; 116 from **I52**; 65 from **J50**; 850 from **J51**; 2 from **J56**; 11 from **K50**; 1940 from **K51**; 30 from **K52**; 38 from **K53**; 4 from **L50**; 420 from **L51**; 36 from **L52**; 218 from **L53**; 2 from **L57**; and 1 from **L58**.

3.2.2. *Elimination of gaps and repeated records*

During the addition of data some problems were detected, mostly the appearance of repeated records with the same information and the same coordinates within some squares. The decision to eliminate such entries proved to be correct once the analysis begun, as most duplicates corresponded to only one record. A total of 588 entries were removed from the original database. The gaps within rows were also eliminated, as most statistical software requires a continuous arrangement of data so that each variable can be compared with the ones before and after it (see **Figure 1**).

Figure 5. Original layout of the database. It used placeholder rows that acted as boundaries (information provided by PhD. Ana Cruz).

	A	B	C	D	E	F	G
1	1	ECOFACTO	HUMANO	OSSO	DETERMINÁVEL	1987	0
2	2	ECOFACTO	HUMANO	OSSO	DETERMINÁVEL	1987	0
3	3	ARTEFACTO	ADORNO	MOSCOVITE	CONTA DE COLAR - DISCÓIDE - PERFURAÇÃO CILÍNDRICA	1987	1
4	4	ARTEFACTO	ADORNO	MOSCOVITE	CONTA DE COLAR - DISCÓIDE - PERFURAÇÃO CILÍNDRICA	1987	1
5	5	ARTEFACTO	ADORNO	MOSCOVITE	CONTA DE COLAR - DISCÓIDE - PERFURAÇÃO CILÍNDRICA	1987	1
6	6	ARTEFACTO	ADORNO	MOSCOVITE	CONTA DE COLAR - DISCÓIDE - PERFURAÇÃO CILÍNDRICA	1987	1
7	7	ARTEFACTO	ADORNO	MOSCOVITE	CONTA DE COLAR - DISCÓIDE - PERFURAÇÃO CILÍNDRICA	1987	1
8	8	ARTEFACTO	ADORNO	MOSCOVITE	CONTA DE COLAR - DISCÓIDE - PERFURAÇÃO CILÍNDRICA	1987	1
9	28.07.2021	28.07.2021	28.07.2021	28.07.2021	28.07.2021	28.07.2021	28.07.2021
10	51-24	ECOFACTO	HUMANO	OSSO	COSTELA	2016	2_4
11	51-391	ECOFACTO	HUMANO	OSSO	VÉRTEBRA	2013	1
12	52-111	ECOFACTO	HUMANO	OSSO	DIAFISE	2016	2_3
13	851-862	ECOFACTO	HUMANO	OSSO	COSTELA	2013	1
14	CODIGO_INVENTARIO	TIPO_ACHADO	CATEGORIA_ACH	MATERIA_PRIMA_ACH	DESCRICAO	ANO	U.E.
15	CODIGO_INVENTARIO	TIPO_ACHADO	CATEGORIA_ACH	MATERIA_PRIMA_ACH	DESCRICAO	ANO	U.E.
16	CODIGO_INVENTARIO	TIPO_ACHADO	CATEGORIA_ACH	MATERIA_PRIMA_ACH	DESCRICAO	ANO	U.E.
17	CODIGO_INVENTARIO	TIPO_ACHADO	CATEGORIA_ACH	MATERIA_PRIMA_ACH	DESCRICAO	ANO	U.E.
18	E53-1	ECOFACTO	HUMANO	OSSO	DETERMINÁVEL	2012	1
19	E53-10	ECOFACTO	HUMANO	OSSO		2016	6
20	E53-10	ECOFACTO	HUMANO	OSSO	OSSO DETERMINÁVEL	2015	6

Most of the information kept in such placeholders and gaps was either transported to new variables (e.g., a new variable for year of excavation) (see Figure 6).

Figure 6. Original layout of the database. It used gaps to keep different excavation campaigns separated (information provided by PhD. Ana Cruz).

	A	B	C	D	E	F	G
16270	RECSUP-S/C6	ARTEFACTO	CERÂMICA	ARGILA	ATÍPICO - MANUAL	1988	1
16271	RECSUP-S/C6A	ECOFACTO	HUMANO	OSSO	MÃO -2ª FALANGE - ADULTO	1988	1
16272	RECSUP-S/C7	ARTEFACTO	CERÂMICA	ARGILA	ATÍPICO - MANUAL	1988	1
16273	RECSUP-S/C7A	ECOFACTO	HUMANO	OSSO	CRÂNEO - FRONTAL - FRAGMENTO	1988	1
16274	RECSUP-S/C8	ARTEFACTO	CERÂMICA	ARGILA	ATÍPICO - MANUAL	1988	1
16275	RECSUP-S/C8A	ECOFACTO	HUMANO	OSSO	VÉRTEBRA CERVICAL - FRAGMENTO	1988	1
16276	RECSUP-S/C9	ARTEFACTO	CERÂMICA	ARGILA	BASE - TORNO	1988	1
16277	RECSUP-S/C9A	ECOFACTO	HUMANO	OSSO	PÉ - METATARSO - V DEDO - ADULTO	1988	1
16278							
16279	K51-2771	ECOFACTO	HUMANO	OSSO	COSTELA	2017	13
16280	K51-2772	ECOFACTO	HUMANO	OSSO	METATARSO	2017	13
16281	K51-2773	ECOFACTO	HUMANO	OSSO	EPÍFISE DE OSSO LONGO	2017	13
16282	K51-2774	ECOFACTO	HUMANO	OSSO	DIÁFISE DE OSSO LONGO	2017	13
16283	K51-2775	ECOFACTO	HUMANO	OSSO	OSSO DETERMINÁVEL	2017	13
16284	K51-2776	ECOFACTO	HUMANO	OSSO	DIÁFISE DE OSSO LONGO	2017	13
16285	K51-2777	ECOFACTO	HUMANO	OSSO	FALANGE	2017	13
16286	K51-2778	ECOFACTO	HUMANO	OSSO	FALANGE	2017	13
16287	K51-2779	ECOFACTO	HUMANO	OSSO	FALANGE	2017	13
16288	K51-2780	ECOFACTO	HUMANO	OSSO	VÉRTEBRA	2017	13
16289	K51-2781	ECOFACTO	HUMANO	OSSO	OSSO DETERMINÁVEL	2017	13

Once the information was homogeneous, filters were applied to check their continuity. The previous process of digitalization was constructed following an availability clause in which each batch of field formularies was added independently, which led to the appearance of duplicates.

3.2.3. *Translation from Portuguese to English*

Being a Portuguese collection, the decision of translating each entry was done to facilitate the inclusion of new variables without leaving room for a term misuse or a mistranslation of core definitions. In this stage a backup file was created, with all the added information in the original language to keep local researchers from being forced to digitalize information a second time in the future. This process was relatively fluent given the amount of fieldwork manuals, papers and books of Luiz Oosterbeek, Ana Cruz and Telmo Pereira, which were generally published in both languages and allowed a one-to-one allocation of terms. The final database is intended to be translated back to Portuguese and delivered to the Instituto Politécnico de Tomar.

3.2.4. *Redistribution of data*

Once the data was translated, the main hierarchic tree was built and implemented so each entry had a specific classification system in line with a specific scope level (from the most general to the most specific). Although this study was principally aimed towards the analysis of human skeletal remains, all the material registered on the database went through the same process, even the mineralogical samples, as they are all intrinsically bound to one another (see **Figure 7**).

Figure 7. Example of the new distribution of variables after the previous phases.

	A	B	C	D	E	F	G	H	I	J	K	L	M	N	O	P	Q	R	S	T	U	V	W
1	ID	Square	Cons	SU	Chron.	Type	Categc	Form	Raw M	Class_	Class_	Lateral	Coi	Sec_	%	Sec_	%	Sec_	%	Sec_	%	Sec_	%
14831	K51-3415	K51	3415	[013]	Chalcolithic	Ecofact	Human Boi	Hyoid and	Bone	Splinter (bone)													
14832	K51-3416	K51	3416	[013]	Chalcolithic	Ecofact	Human Boi	Undetermir	Bone	Splinter (Long bone)													
14833	K51-3417	K51	3417	[013]	Chalcolithic	Ecofact	Human Boi	Hyoid and	Bone	Splinter (bone)													
14834	K51-3418	K51	3418	[013]	Chalcolithic	Ecofact	Human Boi	Undetermir	Bone	Splinter (Long bone)													
14835	K51-3419	K51	3419	[013]	Chalcolithic	Ecofact	Human Boi	Foot	Bone	Metatarsal	Undetermir	Undetermined			C		C						
14836	K51-3420	K51	3420	[013]	Chalcolithic	Ecofact	Human Boi	Hyoid and	Bone	Vertebrae													
14837	K51-3421	K51	3421	[013]	Chalcolithic	Ecofact	Human Boi	Undetermir	Bone	Splinter (Long bone)													
14838	K51-3422	K51	3422	[013]	Chalcolithic	Ecofact	Human Boi	Foot	Bone	Metatarsal	1	Left			P	5	C		C				
14839	K51-3423	K51	3423	[013]	Chalcolithic	Ecofact	Human Boi	Undetermir	Bone	Splinter (Long bone)													
14840	K51-3424	K51	3424	[013]	Chalcolithic	Ecofact	Human Boi	Foot	Bone	Calcaneus		Undetermined							P	60			
14841	K51-3425	K51	3425	[013]	Chalcolithic	Ecofact	Human Boi	Hand	Bone	Proximal H	Undetermir	Undetermined			C								
14842	K51-3426	K51	3426	[013]	Chalcolithic	Ecofact	Human Boi	Cranium ar	Bone	Temporal		Left			P	1							
14843	K51-3427	K51	3427	[013]	Chalcolithic	Ecofact	Human Boi	Hand	Bone	Proximal H	Undetermir	Undetermined					C		C				
14844	K51-3428	K51	3428	[013]	Chalcolithic	Ecofact	Human Boi	Undetermir	Bone	Splinter (Long bone)													
14845	K51-3429	K51	3429	[013]	Chalcolithic	Ecofact	Human Boi	Hyoid and	Bone	Cervical	2				C		P	3	C				
14846	K51-3430	K51	3430	[013]	Chalcolithic	Ecofact	Human Boi	Hyoid and	Bone	Vertebrae					P	4	P	5	P	5			
14847	K51-3431	K51	3431	[013]	Chalcolithic	Ecofact	Human Boi	Foot	Bone	Proximal Fi	Undetermir	Undetermined		C									
14848	K51-3432	K51	3432	[013]	Chalcolithic	Ecofact	Human Boi	Lower Der	Dentine/En	M	2	Left			C		F						
14849	K51-3433	K51	3433	[013]	Chalcolithic	Ecofact	Human Bone		Bone														
14850	K51-3434	K51	3434	[013]	Chalcolithic	Ecofact	Human Boi	Undetermir	Bone	Splinter (bone)													
14851	K51-3435	K51	3435	[013]	Chalcolithic	Ecofact	Human Boi	Foot	Bone	Navicular		Left		C									
14852	K51-3436	K51	3436	[020]	N/A	Artifact	Undetermir	Undetermir	Undetermined														
14853	K51-3437	K51	3437	[020]	N/A	Artifact	Adornmen	Hair Pin	Undetermir	Handle													
14854	K51-3438	K51	3438	[020]	N/A	Artifact	Adornmen	Hair Pin	Undetermir	Handle													
14855	K51-3439	K51	3439	[013]	Chalcolithic	Ecofact	FauUndeterminedl Boi		Bone														
14856	K51-3440	K51	3440	[013]	Chalcolithic	Ecofact	Human Boi	Foot	Bone	Proximal Fi	Undetermir	Undetermined		C									
14857	K51-3441	K51	3441	[013]	Chalcolithic	Ecofact	Human Boi	Upper Den	Dentine/En	I	2	Right			C		F						
14858	K51-3442	K51	3442	[013]	Chalcolithic	Ecofact	Human Boi	Thorax	Bone	Rib		Undetermined											

In some cases (often when dealing with ornaments, lithic material, and ceramic ware) the description found in observations was not specific enough to fill major and minor classifications. Missing information in these categories was recorded as '**Undetermined**', which is not completely accurate since most of the faunal and lithic assemblages have had proper studies conducted on them. However, gathering such information has proven rather difficult, which reinforces the need of creating a database that can be used by any future researchers that want to study the rock shelter or nearby sites. A more detailed explanation of the new hierarchy tree will be given further on (see **Section 3.3.4**). A total of 18090 entries were updated and classified within new variables.

3.2.5. *Revision of coordinated elements*

As stated in previous sections, most of the ecofacts and artifacts unearthed during the excavation campaigns were three-dimensionally coordinated, i.e., they had a point of origin from which an imaginary x axis (east-west), a y axis (north-south), and a z axis (up and down) sprouted. These elements were ultimately chosen for analysis in the current study, mainly because of this feature. If a specific element can be accurately located in space, the relationship between it and the ones surrounding it could help understand the process of formation of the site.

Keeping this in mind, all the records were drawn in a preliminary scatter plot before uploading them into a Geographic Information System software, using *Excel* (see **Graph 1**). The results were underwhelming; at some point the data was converted using faulty equations which resulted in *i*) the interchange between the x and y axis, which on paper treated north-south axis as the east-west axis; *ii*) some z values fluctuated more than 20 m (in an initial 8 m^2 site (Almeida et al., 2023)), and *iii*) the squares at the centre (i.e., I53, H53, I54 and H54) were stripped from coordinated material while the ones in the periphery, that should correspond to the rock shelter's walls, were overflooded.

Graph 1. Preliminary scatter plot of the coordinated elements in GMS. The most outlier values were eliminated.

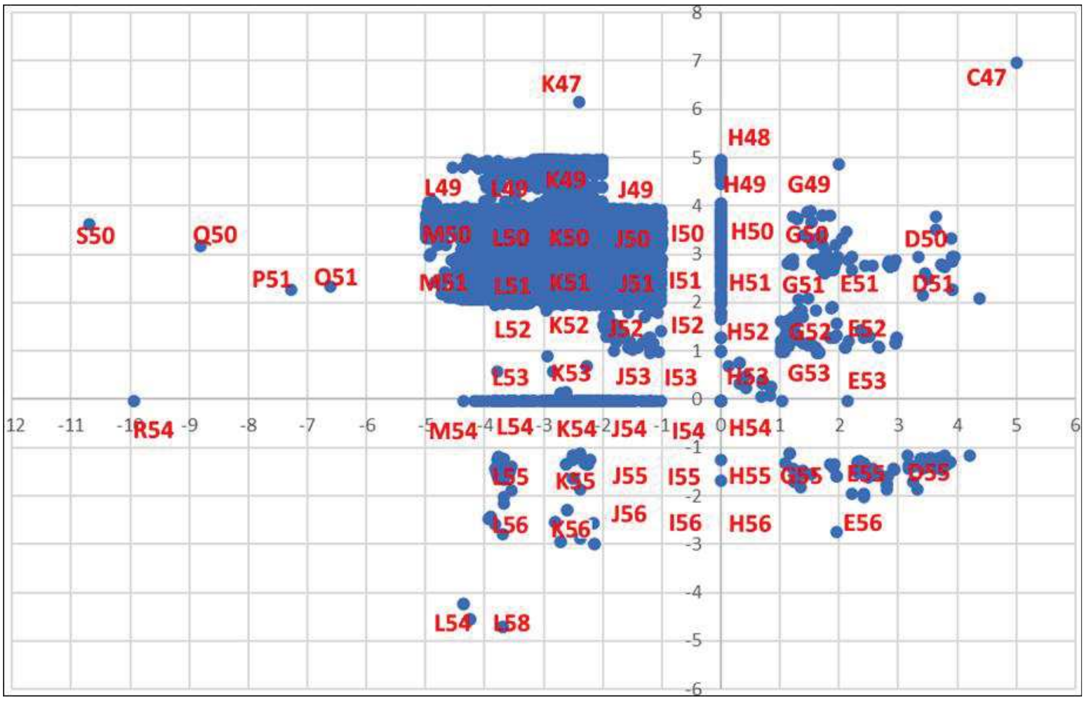

Digitalization mistakes accumulated, resulting in an area of excavation of 14 x 16 m area that did not retain the rock shelter's floor shape.

Tackling this issue required the application inverse equations in each square to obtain the original coordinates. In the field, each square was treated as an independent cut, i.e., each one had an x and a y value with an open range of (0, 1) m. Thanks to this precaution each original value was safely recovered. The outlier values that indisputably represented typos made during transcription were corrected as well, with the help of the original field sheets. Once every value had the appropriate range, new equivalence equations were implemented to obtain their real location (see **Figure 1**). Due to time constraints, it was impossible to take new topographic data to rectify the actual location of the rock shelter's walls. The contour was extrapolated from images presented in previous field reports by Ana Cruz (2015; 2013) and Geographic information system (GIS) software (namely the command "Georeferentiation" in ArcGis Pro 3.0.0).

Figure 8. Rectified equivalence equations for coordinated elements within the excavation grid. Each green square represents material coordinated and registered in the database. The green line represents the y axis while the red represents the x axis.

	E	F	G	H	I	J	K	L	M
58	X-5 Y+3	X-4 Y+3	X-3 Y+3	X-2 Y+3	X-1 Y+3	X(1) Y+3	X+1 Y+3	X+2 Y+3	X+3 Y+3
57	X-5 Y+2	X-4 Y+2	X-3 Y+2	X-2 Y+2	X-1 Y+2	X(1) Y+2	X+1 Y+2	X+2 Y+2	X+3 Y+2
56	X-5 Y+1	X-4 Y+1	X-3 Y+1	X-2 Y+1	X-1 Y+1	X(1) Y+1	X+1 Y+1	X+2 Y+1	X+3 Y+1
55	X-5 Y(1)	X-4 Y(1)	X-3 Y(1)	X-2 Y(1)	X-1 Y(1)	X(1) Y(1)	X+1 Y(1)	X+2 Y(1)	X+3 Y(1)
54	x-5 Y-1	X-4 Y-1	X-3 Y-1	X-2 Y-1	X-1 Y-1	X(1) Y -1	X+1 Y-1	X+2 Y-1	X+3 Y-1
53	x-5 Y-2	X-4 Y-2	X-3 Y-2	X-2 Y-2	X-1 Y-2	X(1) Y -2	X+1 Y-2	X+2 Y-2	X+3 Y-2
52	x-5 Y-3	X-4 Y-3	X-3 Y-3	X-2 Y-3	X-1 Y-3	X(1) Y -3	X+1 Y-3	X+2 Y-3	X+3 Y-3
51	x-5 Y-4	X-4 Y-4	X-3 Y-4	X-2 Y-4	X-1 Y-4	X(1) Y -4	X+1 Y-4	X+2 Y-4	X+3 Y-4
50	x-5 Y-5	X-4 Y-5	X-3 Y-5	X-2 Y-5	X-1 Y-5	X(1) Y -5	X+1 Y-5	X+2 Y-5	X+3 Y-5

Most of the entries at this point (17515) were subjected to a coordinate change in all, or at least, two axes. A summary of all the activities carried out during this phase can be found in **Table 9**. It is worth noting that backup files were created along every step, to allow tracking of any error in the final draft.

Table 9. Summary of the activities regarding the consolidation of the main database.

Activity	Summary	Notes
Digitalization (New Information)	3251 new entries	New entries from field formats added to the database.
Change: X and Y Coordinates	17515 Entries changed to fit the correct values.	All x and y values updated.
Change: Z Real Coordinates	6 oddities, various examples of misuse of the correct equation	Most outlier values revised (differences of more than 10 m in height).
Nameless Entries	4 entries pinpointed thanks to their coordinates	**NN51 – 0024**: Transformed into L51 (*) **NN51 – 0391**: Transformed into I51 – 0391 (*) **NN52 – 0111**: Transformed into L52 - 0111 (*) **NN51 – 0862**: Transformed into J51 - 0862 (*)
Duplicates	588 entries revised and updated with all values.	**J51**: Entries from 0708 to 2163 were eliminated. Duplicates from 2016 were deleted while 2013's entries kept. Duplicates from 2200 to 2219 were removed. **J52**: Three field formats were photocopied and marked as AA and AA and AAA were removed from the set. **L53**: Values from 1 to 4 were already in database. **L57**: Two values added already under A suffix because of different coordinates.
New Hierarchical Tree	18090 entries	All entries' information was categorized into new variables.

(*) It matches the coordinate information and was missing from the original database.

This phase marks the final step of preparing the digital materials needed for the current study: a total **18090** entries were adapted to the new database, from which an original estimate of **4500** records corresponding to human remains were chosen for the bioanthropological analysis. These totals would change over time with the addition of material not registered in the previous database and the absence of the portion corresponding to 2015's campaign.

Once all the information was uploaded, rectified, and classified in the new format, the selection of the variables necessary for the bioanthropological analysis begun. Each column in the new database represents a variable that is backed by specific methodological instruments. Each variable will be itemized thoroughly in the forthcoming sections in order of appearance on the database.

3.3. Data collection

The following variables were created considering the need of exporting data towards statistical software, registering simultaneous characteristics on the same entry (e.g., taphonomic or pathological alterations that occur in unison), and describing thoroughly diagnostic elements. Each variable was represented by on or more columns depending on their scope.

3.3.1. ID, Square and Consecutive

The variables that correspond to the ID of each entry respond to the necessity of being able to filter, organize and rearrange the data as needed. For this reason three columns were created: **Consecutive**: corresponds to a customized cell arrangement in which any 0 to the left of a number is left in place while allowing the use of alphabetical and special characters; **Square**: corresponds to the square to which the entry belongs; **ID**: corresponds to the denomination written on the bag that contains the entry, and depends on the other two variables by using the following equation (Excel): **=CONCAT(BX,"-",TEXT(CX,"0000"))**. This setup was necessary for filtering each section independently (e.g., square, and consecutive number) so that all the information was suitable for rearrangements in a correct alphanumeric order (most statistical software tends to misinterpret single digits as the highest value, for example a 1 may be interpreted as 1000 if there are entries with four digits) (See Figure 9). The use of filters also permits the user finding outliers and oddities within the seriation, such as repeated values, in a quicker way.

Figure 9. The first variables on the database: ID, Square and Consecutive.

	A	B	C	
1	ID	Square	Conse	$
2	E53-0001	E53	0001	[
3	E53-0002	E53	0002	[
4	E53-0003	E53	0003	[
5	E53-0004	E53	0004	[
6	E53-0005	E53	0005	[
7	E53-0006	E53	0006	[
8	E53-0007	E53	0007	[
9	E53-0008	E53	0008	[
10	E53-0009	E53	0009	[
11	E53-0010	E53	0010	[
12	E53-0010A	E53	0010A	[
13	E53-0011	E53	0011	[
14	E54-0001	E54	0001	[

3.3.2. Stratigraphic Unit and Chronological Period

The following nominal variables describe the stratigraphic unit (SU) in which the material was found and the chronological adscription to which said SU belongs. The values were taken mostly from the description provided by Cruz (2020), in which a summary of all the defined/ found SUs was presented. Each SU number was registered within brackets as they were in the original. For a specific list of each SU and its chronological adscription see **above**.

3.3.3. Archaeological Material Type

The **Archaeological Material Type** variable is a broad-spectrum classification tool that determines the main origin of an element depending on its relationship with human activity in the past. The types chosen were: Artefact, which contains any material modified directly as result of human agency (Price & Burton, 2011); **Ecofact**, or biofact in some literature, which refers to organic material that has not been technologically altered by humans, but has cultural relevance (Price & Burton, 2011), **Geological Material**, which refers to inorganic material that apparently has not been *technologically* altered by humans, but may bear information about the availability of resources and environment; and, lastly, **Undetermined**, which is a category that contains any entries with an unspecified type. The last grouping was already in use in the original database, although it was mixed with data regarding 'Raw Material' when used in a conjunction with geological material. Since raw material can be applied to all other categories, it was decided that a separate variable would contain it.

3.3.4. Category

Category is a grouping system that depends on the Type of Material and is more specific. If an entry were to be classified as an **Ecofact**, its tributaries included either **Human Remain**, **Faunal Remains**, **Malacological Sample**, **Anthracological Sample**, and **Carpological Sample**. If an entry were to be considered an **Artifact**, it could be classified as an **Adornment**, **Figurine**, **Portable Rock Art**, (Ceramic) **Ware**, **Lithic**, or **Bone Tool**. Finally, **Geological Material** has two categories that select between either **Mineral** (Unconsolidated material) or **Rock** (consolidated material). An optional **Undetermined** category was added for cases without any further information.

3.3.5. Subcategory

Subcategory is the first variable to behave differently on bioanthropological elements. For human remains, it refers to a skeletal region to which the bone belongs. Most osteology manuals present them, slightly modifying the location for certain skeletal element. The manuals written by Scheuer & Black (2004), Matshes (2005), and White et al. (2012) were considered, as well as Tiago Tomé's field reports (2012; 2013). The skeletal regions selected, from top to bottom, included **Cranium and Mandible**, **Upper**

Dentition, **Lower Dentition**, **Hyoid and Vertebrae**, **Thorax**, **Shoulder Girdle**, **Upper Limb**, **Hand**, **Pelvic Girdle**, **Lower Limb**, and **Foot**.

The remainder elements that belonged to the ecofact type were had no additional information except for **Scallop.**

The subcategories related to ceramic material (**Ware**) were selected according to the morphometric information available for study: **Sherd** is a group that contains any pottery fragment without any outstanding features, **Diagnostic** refers to all diagnostic material that may provide some sort of dimension, form, and/or style inferences, and a **Vessel** refers to a fragment or group of fragments that were complete enough to identify typological features and/or vessel profiles on a single container.

Adornments were subdivided into their morphological characteristics such as **Ring**, **Bead**, **Earring**, **Trinket**, **Cufflink**, and **Hair Pin**. The Figurine category may be present as either **Zoomorphic** or **Anthropomorphic**. Portable Rock art had only one further subcategory: **Plaque**. Lithic material was exhaustively described on the previous database as: **Axe**, **Chip**, **Core**, **Adze**, **Flake**, **Blade**, **Sickle**, **Chopper**, **Bladelet**, **Scrapper**, **Debitage**, **Composite**, **Arrowhead**, and **Hammerstone**. Bone tools can be classified as **Spatula**, **Stitching Awl**, and **Polishing Tool**. Geological material was grouped as **Pigment**, **Sediment**, **Aggregate**, and **Speleothem**. An optional **Undetermined** category was added for cases without any further information.

3.3.6. Raw Material

Raw material is a variable with entries that may be shared among multiple subcategories The list of materials was drawn from the original database and include **Bone**, **Dentine/Enamel**, **Shell**, **Charcoal**, **Seed**, **Bronze**, **Copper**, **Muscovite**, **Amphibolite**, **Schist**, **Clay**, **Silex**, **Quartz**, **Quartzite**, **Hyaline Quartz**, **Ivory**, **Calcite**, **Sandstone**, and **Limestone**. The last three groups are not the same as their homonyms in subcategory, because they are used exclusively for lithic artifacts. An optional **Undetermined** category was added for cases without any further information.

3.3.7. Major Classification

On human remains, Major Classification describes the skeletal element according to the region chosen in *subcategory*. If the latter was grouped as *Cranium and Mandible*, the options are **Frontal**, **Parietal Temporal**, **Occipital**, **Maxilla**, **Palatine**, **Vomer**, **Nasal Conchae**, **Ethmoid**, **Lacrimal**, **Nasal**, **Zygomatic**, **Sphenoid**, and **Mandible**. When choosing *Upper* or *Lower Dentition*, the variable depends on the dental element: **I** (incisor), **di** (deciduous incisor), **C** (canine), **dc** (deciduous canine), **P** (premolar), **M** (molar), **dm** (deciduous molar). When analysing *Hyoid and Vertebrae* the values are separated by region: **Hyoid**, **Cervical**, **Thoracic**, and **Lumbar**. In cases where an element was deemed to belong to a vertebra, but it is too fragmented or damaged to determine the region the only option is **Vertebra**. The *Thorax* encompasses the **Sternum** and **Rib**. Bones in the *Shoulder Girdle* contain the **Clavicle** and the **Scapula**. The *Upper Limb* has the categories of **Humerus**, **Radius** and **Ulna**. The *Hand* may be classified as **Carpal** (used for fragmented or subadult elements), **Scaphoid**, **Lunate**, **Triquetral**,

Pisiform, **Trapezium**, **Trapezoid**, **Capitate**, **Hamate**, **Metacarpal**, **Hand Phalanx** (used for fragmented pieces that lack specific landmarks), **Proximal Hand Phalanx**, **Intermediate Hand Phalanx**, and **Distal Hand Phalanx**. When describing the *Pelvic Girdle*, the options are **Sacrum**, **Coccyx**, **Os Coxae**, **Iliac Body**, **Ischial Body**, and **Pubic Body**. The *Lower Limb* includes the **Femur**, **Patella**, **Tibia**, and **Fibula**. The *Foot* behaves analogous to the *Hand* and contains the categories of **Tarsal** (for undetermined tarsal elements), **Talus**, **Calcaneus**, **Cuboid**, **Navicular**, **Medial (First) Cuneiform**, **Intermediate (Second) Cuneiform**, **Lateral (Third) Cuneiform**, **Metatarsal**, **Foot Phalanx** (for undetermined positioning of the foot phalanx), **Proximal Foot Phalanx**, **Intermediate Foot Phalanx**, and **Distal Foot Phalanx**. Additionally, the categories of **Undetermined**, **Splinter (bone)**, and **Splinter (Long bone)** were added for small and medium-sized bone fragments that had not observable landmarks.

When describing Artefacts, Major Classification was used to describe specific details about the material. *Adornments*, *Ware* ,and *Geological Material* may be classified in different categories according to their characteristics: *i*) The ones related to form such as **Discoidal**, **Head**, **Handle**, **Cup**, **Vase**; *ii*) the ones related to manufacture like **Manual** (for ceramic ware, it is not clear if it refers to the coiling technique), **Potter's Wheel** (for ceramic ware, it refers to the manufacturing technique that makes use of Tourneys / Slow Wheel / Fast Wheel), **Retouched**, **W. Retouch** (Without); and *iii*) natural forms or materials like **Ochre**, **Crystal**, **Pebble** (Schoeneberger et al., 2012), **Breccia**, **Stalagmite**, and **Thermoclastic** (element). An optional **Undetermined** category was added for cases without any further information.

3.3.8. Minor Classification

Minor Classification is a supplement for the previous entry and specifies any variation within. When dealing with Human Remains, it behaves as a **numeric value (1 to 12)**: on vertebrae it may be a number within specific ranges such as 1 to 7 [cervical], 1 to 12 [thoracic], 1 to 5 [lumbar], on the sacrum 1 to 5, on metacarpals/ metatarsals and Hand/ Foot Phalanx 1 to 5, on ribs 1 to 12, on incisors 1 or 2, on premolars 3 or 4, and on molars 1 to 3. On fragmented elements it was not used on elements with poor confidence rates.

For the remaining entries, it referred to specific characteristics of manufacture such as **Perforated**, **Incised**, **Indented**, **Idol**, **Glazed**, **Decorated**, **Plastic Decoration**, **Undone**, **Profile**, **Hemispherical**, **Complete Profile**, **Rim**, **Base**, **Bulge**, **Rim/ Bulge**, **Rim/ Bulge/ Base**, **Carinated**, **Trapezoid**, **Notched**, and **Polished**. An optional **Undetermined** category was added for cases without any further information.

3.3.9. Siding

Numerous skeletal pieces tend to have a mirrored counterpart in the opposite side of the body. Understanding the correct positioning of each bone is crucial to extract information about laterality (or the preference of usage of a homologous section of the body over the other), palaeopathology, and stress related to certain strenuous activities. In highly fragmented or mixed sites, correct siding is needed to obtain the Minimal Number of Individuals buried within.

In Gruta do Morgado Superior, the guidelines followed to accurately identify and lateralize each skeletal element came from texts of Black and Folkens (2012), Matshes (2005), Scheuer and Black (2004). Entries in this variable were **Right**, **Left**, and **Undetermined**. Bones found in a very poor conservation state were classified within the undetermined category unless specific landmarks were observable.

Although most bones can be easily sided when found in isolation, phalanges pose a methodological problem when sided. In such cases, specific guidelines were followed.

3.3.9.1. *Siding manual phalanges*

Phalanges pose a methodological challenge as they are difficult to allocate in the correct ray and type when found in isolation. In the case of Gruta do Morgado Superior, the methodology used for siding these elements followed Angi Christensen's (2009) guidelines (see **Annex 2**).

Christensen reviewed a previous methodology proposed by Case and Heilman (2000), adding new parameters. The allocation rate of phalanges reached 100% for the elements PP1, PP2, PP4, PP5, IP3, IP5, DP1; 97% when allocating PP3 and IP2; and a value of 81% for IP4. DP2-. Their results indicate that the more bones are present for study the more accurate is the identification of ray and side (Christensen, 2009). Some of the modifications to Case and Hellman's method are *i*) PP2 and PP4 can be distinguished based on their relative robusticities, with PP2 having a more robust base than PP4 (it is asymmetric); *ii*) IP2 had a more flared base than IP3 or IP4, which tended to be relatively more slender; *iii*) tubercles on the surface of PP4 had different heights (mostly), but it was also noted that the more angular a tubercle was the better indicator of side; *iv*) the extension of the superior-distal facet of PP5 was characterized by Case and Heilman as the most important trait for siding, however, their second-rated characteristic[13] was found to be easier to see and more confidently applied; *v*) the distal phalanges were the most difficult to side, mostly due to pathological conditions or difficulties when delineating both facets (Christensen, 2009).

Regardless of their success, phalanx allocation may prove deceitful when trying to obtain data regarding the Minimal Number of Individuals (MNI). Although the technique was used whenever possible, in well preserved elements, the results were not used for the final MNI count. This decision was made considering the accuracy loss when analysing isolated material, and the lack of undisturbed elements in anatomical position on the site. Christensen findings were useful when applying them to phalanges belonging to the first ray, as they were the easiest to identify in isolation.

[13] The distal most point of the distance between the articular region, when viewed from the dorsal side.

3.3.10. Completeness and Fragmentation

Archaeological materials are regularly subjected to preservation analyses that assess their completeness and level of fragmentation. Such information may be used to understand a site's stages of formation. Assessing the level of fragmentation of skeletal elements in funerary contexts is the cornerstone that enables researchers to calculate descriptive variables such as the Minimal Number of Individuals (MNI), identify different taphonomic agents and their impact upon the material, and infer social features associated with the funerary behaviour of the people represented in it.

Gruta do Morgado Superior presents a distinctive funerary pattern in which the elements are mostly disarticulated and highly fragmented. Additionally, the skeletal regions most affected include those that are usually considered to be the most valuable to determine paleodemographic and morphometric variables such as biological sex (e.g., the pelvic girdle and cranium), age at the time of death (e.g., the pubic symphysis), stature (e.g., the lower appendicular long bones), and pathologies.

On the database, the categories chosen to describe completeness and fragmentation were implemented to perform the MNI count. The first column is a general variable used only to identify the location and distribution of the skeletal elements that were complete. The following twelve columns were paired in six groups, each representing a (possible) section of the element. These variables are the result of a series of modifications on similar approaches used by Portuguese researchers in the past.

3.3.10.1. *Minimal Number of Individuals*

As mentioned in previous chapters, the determination of the Minimal Number of Individuals (MNI) relied on the methodology and guidelines utilized by Ana Maria Silva (1996), who adapted a similar technique developed by Herrmann et al. (1990). This method appears reiteratively on various Portuguese publications.

Herrman's method proposes that any MNI count has to consider that *i*) only the skeletal elements of the same anatomical region may be counted, noting that most bones occur in pairs, and bearing in mind that some contexts may consist of fragmented material; *ii*) if the latter is true, it is possible that some fragments may belong to the same skeletal element, representing different regions; and *iii*) in cases with large quantities of material it is considered *economically possible* to separate the contexts in burials and then choose an osteological piece to calculate the MNI (Herrmann et al., 1990, p. 318). In GMS's case, the last suggestion could not be applied as GMS's funerary architecture is not clearly defined by individual. The first two require the elaboration of specific methodology that allows the most accurate count.

The estimation of the MNI may use fragmented long bones, where the skeletal element is divided into several sections that are easily recognizable (see **Figure 10**). Whenever the counted element is paired, an accurate side allocation must be obtained. This approach would virtually eliminate any possible false positives that may arise from the same element being counted two or more times.

Figure 10. Example of the application of Herrmann et al.' methodology on a tibia. (1990, p. 318, Abb. 5.3.3.). Each vertical line represents the observed section(s) found in each fragment. Complete elements are represented by a continuous line that spans through all of them.

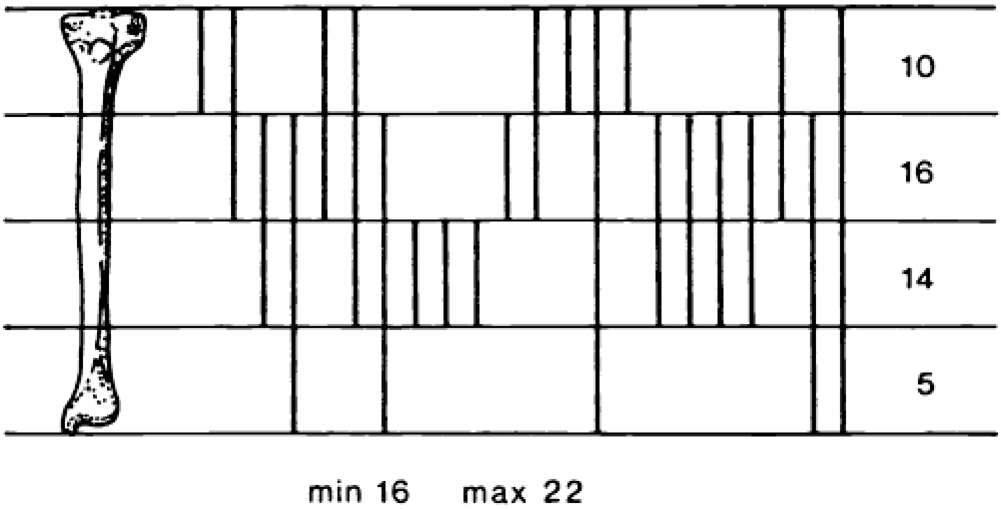

Silva(1996) employed the same visual guides to create her field sheets and calculate the MNI in most of her publications, as did several Portuguese researchers that continued her work.

Nevertheless, Gruta do Morgado Superior is a site in which complete long bones are a rare sight, if not a wonder, and the rates of fragmentation are such that a single portion can be found shattered into several pieces. Hermann et al.'s field formats lack traceability, as each line represented on them would have to be named physically. For these reasons the method was tweaked by *i*) generating adjusted bone sections instead of arbitrary ones, and *ii*) replacing the physical formats by digital counterparts. This way any fragment could be traced back to its ID easily. On the other hand, each section was given a score of completeness that on its own may seem redundant, but when paired with a other scores for elements located at the same anatomical region can be used to identify or differentiate individuals assigned (see **Table 10**).

Table 10. Completeness score for fragments and their description.

Completeness Score	Percentage	Description
1	1 to 25	Almost no landmarks are visible and/or less than a quarter of the skeletal element is present.
2	25 to 50	Some landmarks are visible and/or more than a quarter but less than a half of the element is present.
3	50	Half of the landmarks are visible and /or half of the skeletal element is present.
4	50 to 75	Several landmarks are visible and/or more than half but less than three quarters of the skeletal element is present.
5	75 to 99	Almost all landmarks are visible and/or most of the skeletal element is present.

The fragmentary lines were replaced by six paired variables, each pair with a general assessment of completeness (C=Complete, P=Present (bone)/F=Fragmented (dentine)), and a score. The continuous lines that represent complete bones used by Herrmann's team were transformed into an independent column that describes only complete elements. Thus, Herrmann's method remained virtually unchanged at its core elements, only adding a percentage of completeness score that helps understand better the relationship between isolated fragments. Contrary to Hermann's application, the technique was expanded to every skeletal element in the body.

Each bone was subsequently divided in sections that were delimited considering topographic and morphologic characteristics useful when identifying and describing each bone. Factors such as frailty (proneness to breakage) and complexity (whether the section is usually misclassified when found in isolation) were considered. Ontogenetical characteristics served as a final filter to create each one of them. The upcoming paragraphs will describe each skeletal element that was identified at GMS and the sections delimited to assess their completeness and count the MNI. Missing descriptions correspond to elements not found during the analysis (i.e., palatine, vomer, nasal conchae, ethmoid, lacrimal, nasal, hyoid, and coccyx).

The **frontal** bone develops from two separate ossification centres that collide into the metopic suture until their fusion about 2 to 4 years after birth. Because of this, this skeletal element has been divided into four sections: two general portions (right and left) that coincide with the ossification centres; each in turn subdivided in two smaller regions that are morphologically different (supraorbital and squama regions) (see **Figure 11**).

Figure 11. Sections chosen for the frontal bone (Original picture found in Mann, 2017, p. 35, slightly modified).

Frontal (anterior view)

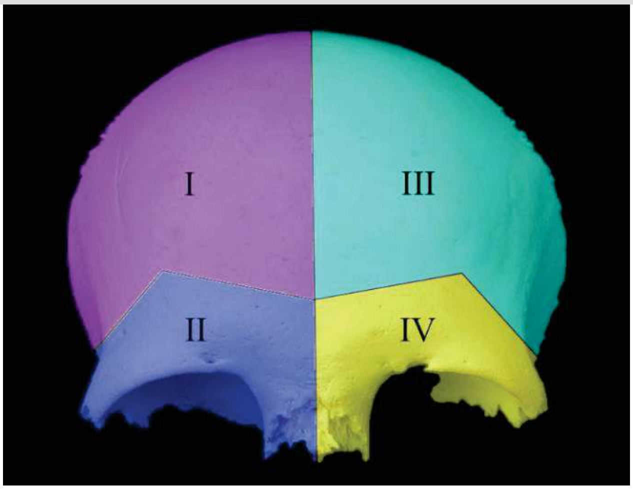

I. Squama (Right). Landmarks: articular surface for parietal, frontal eminence arachnoid foveae, sagittal sulcus (right section), meningeal grooves.	**III: Squama (Left).** Landmarks: articular surface for parietal, frontal eminence arachnoid foveae, sagittal sulcus (left section), meningeal grooves.
II: Horizontal portion (Right). Landmarks: temporal line, superciliary arch, supraorbital notch, supraorbital foramen, supraorbital margin, pars orbitalis, ethmoidal notch (right section), frontal sinus (right), glabella, zygomatic process, articular surface for nasal bones, frontal crest (right section), foramen cecum.	**IV. Horizontal portion (Left).** Landmarks: temporal line, superciliary arch, supraorbital notch, supraorbital foramen, supraorbital margin, pars orbitalis, ethmoidal notch (left section), frontal sinus (left), glabella, zygomatic process, articular surface for nasal bones, frontal crest (left section), foramen cecum.

The **parietal** bone was divided into two sections (see **Figure 12**), one anterior and one posterior. The sections are partially arbitrary as they are divided by a perpendicular imaginary line that starts at the midpoint of the sagittal suture and runs towards the most medial point of the notch in the sphenotemporal suture. Each one has well-enough differentiated landmarks such as the angles (that tend to be right in the anterior section and obtuse in the posterior section), the presence of features such as the arachnoid foveae in **Section I** (possibly shared with the frontal bone), and the sigmoid/ transverse sulcus in the **Section II**, which is also present in the temporal bone (Matshes et al., 2005). The meningeal grooves are shared among both sections, although their pattern, density, and direction allow a better identification of each.

Figure 12. Sections chosen for the parietal bone. (Original picture found in Mann, 2017, p. 48, slightly modified).

Right Parietal (medial/ endocranial view)

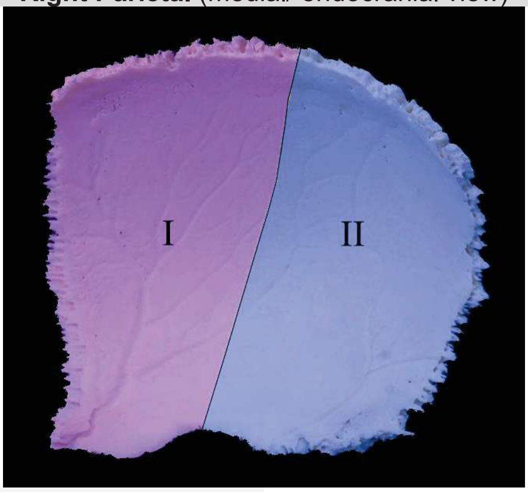

I. Anterior Squama. Landmarks: Coronal suture, meningeal grooves, articular surface for the sphenoid bone, frontal angle, sphenoidal angle, arachnoid foveae.	**II. Posterior Squama**. Landmarks: lambdoidal suture, meningeal grooves, parietal eminence, parietal notch, sigmoid/ transverse sulcus, mastoid angle, occipital angle.

The **temporal** bone serves as a transitional element between the calvaria and the skull base. It houses the auditory canal, and serves as anchor for the mandibular joint (White et al., 2012). This variety of functions ultimately shape its irregular form and diverse topography. The temporal was subdivided into three sections (see **Figure 13**), considering the general morphology and fragility of each part.

Section I is often referred to as the petrous portion of the temporal and is considered the densest area of the bone. While the endocranial and ectocranial topography of this region could have been divided into two distinct zones, its dense properties make it a very resilient element that tends to be found almost complete, as was the case in GMS. From the developmental point of view, it includes the petrous pyramid, the tympanic ring, and the mastoid portion. In fully developed individuals, the ectocranial section of the petrous section includes the external auditory canal (lower portion), the mastoid process, and the mastoid notch. The endocranial portion displays the petrous pyramid, the internal acoustic meatus, and the carotid canal.

Section II is denominated as the squamous region of the temporal. It includes most of the articular surfaces and sutures with the sphenoid, parietal, and the joint with the mandibular body. This section develops separately from the petrous area. Although the zygomatic process develops jointly with **Section II**, this region was separated into

Section III, due to its shape and frailty: it is easily broken off the main body when exposed to erosive and taphonomic agents, and usually it is found either fragmented (when isolated) or missing (from the main squama).

Figure 13. Sections chosen for the temporal bone (Original picture found in White & Folkens, 2005, p. 68, slightly modified).

Right Temporal (ectocranial view)

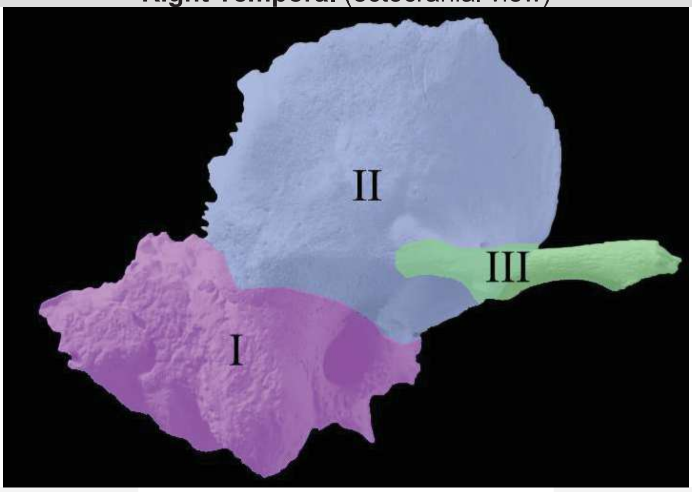

I. Petrous Portion. Landmarks: petrous portion, tympanic section of the temporal, tegmen tympani, suprameatal triangle, styloid process, mastoid process, arcuate eminence, groove for sigmoid sinus, apex of petrous temporal bone, internal auditory meatus, carotid canal, articular tubercle.	**II. Temporal Squama**. Landmarks: squamosal suture (includes the articular surface for the parietal), sphenotemporal suture (includes the articular surface for the sphenoid), occitomastoid suture (includes the articular surface for occipital bone), occipital groove, mandibular fossa, postglenoid tubercle.	**III. Zygomatic Section**. Landmarks: zygomatic process of the temporal bone, zygomaticotemporal suture (includes the articular surface for the zygomatic, articular tubercle.

The **occipital** bone was separated into four regions that correspond to the bones that compose it during its developmental stages (see **Figure 14**). This subdivision was made even though fragments on adults are usually not so easily located unless they have specific landmarks All sections play a role in the formation of the foramen magnum, being concentric to it.

The squama was labelled as **Section I**, and it comprises the large plate that raises posteriorly. This section contains landmarks that are usually associated with morphological traits, such as intrasutural bones, and sexual markers (e.g., the external occipital protuberance) (White et al., 2012). **Sections II** and **III** correspond to ossification centres known as pars lateralis (left and right), where the condyles are located and the articular surfaces for the superior portion of the atlas rest. Lastly, **Section IV** is shaped after the basilar portion of the occipital in which the joint with the sphenoid is located. The latter usually ossifies by the late twenties, creating a continuous bridge (Scheuer & Black, 2004).

Figure 14. Sections chosen for the occipital bone (Original picture found in Mann, 2017, p. 51, slightly modified).

Occipital (ectocranial view)
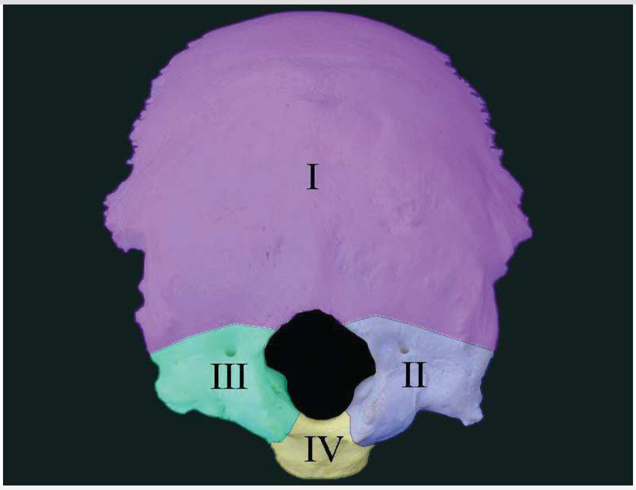
I. Squama. Landmarks: Occipital planum, external occipital protuberance, superior, inferior and median nuchal lines, nuchal planum, sagittal and transverse sulcus, cruciform eminence, internal protuberance, cerebral fossa, internal crest.
II. Pars lateralis (right). Landmarks: occipital condyle, condylar foramen, condylar fossa (inconstant), hypoglossal canal, jugular notch.
III. Pars lateralis (Left). Landmarks: occipital condyle, condylar foramen, condylar fossa (inconstant), hypoglossal canal, jugular notch.
VI. Pars basilaris. Landmarks: groove for the medulla oblongata, baciocciput, pharyngeal tubercle.

The **maxillae** bones were separated into three sections, chosen because of their proneness of breakage (or separation) from the main body (see **Figure 15**).

Figure 15. Sections chosen for the maxilla (Original picture found in White & Folkens, 2005, p. 76, slightly modified).

Right Maxilla (anterior view)	
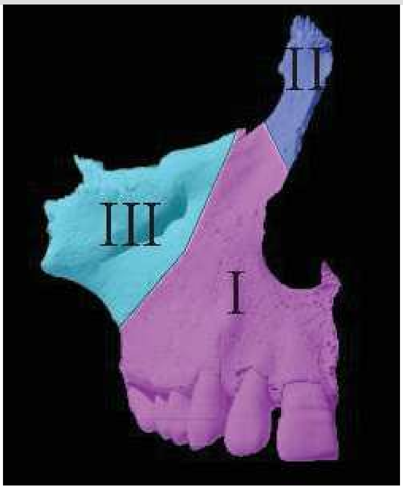	**I. Main body.** Landmarks. posterior surface, orbital surface, lacrimal groove, palatine process, alveolar process for maxillary teeth, infraorbital foramen, nasal aperture (inferior).
	II. Frontal Process. Landmarks: frontal process and suture, nasal aperture (superior), ethmoidal crest, frontal groove.
	III. Zygomatic Process. Landmarks: zygomatic process and suture.

Section II and **III** correspond to the frontal and zygomatic processes respectively, while **Section I** is comprised by most of the main body landmarks, the palatine process, and the alveolar process. Consensus regarding the number of ossification centres and the existence of a premaxillary bone (as is the case in other primates) in prenatal stages is still much debated (Scheuer & Black, 2004), which is part of the reason why ontogenetical development did not guide this bone's section delimitation. Additionally, maxillae present a recognizable shape around birth. Sections I and II do not match exactly the neural and alveolar natural regions defined in some manuals (Matshes et al., 2005; White et al., 2012) because the area is resilient to breakage.

Similarly, the **zygomatic** bone's sections were selected considering their proneness to breakage. The bone was divided into three sections (see **Figure 16**): *i*) The frontal process, which includes the frontal suture; *ii*) the orbital process that displays the most recognizable landmarks such as the zygomatico-orbital foramen, the articular surface for the maxilla, and the masseteric anchoring point; and *iii*) the temporal process. These sections do not reflect the zygomatic's ossification process, which starts from a single centre that develops inferiorly and laterally to each orbit. Evidence for any additional ossification centres is dubious, and the skeletal element resembles its mature form well enough in the second half of prenatal life (Scheuer & Black, 2004).

Figure 16. Sections chosen for the zygomatic bone (Original picture found in White & Folkens, 2005, p. 85, slightly modified).

Right Zygomatic (anterior view)

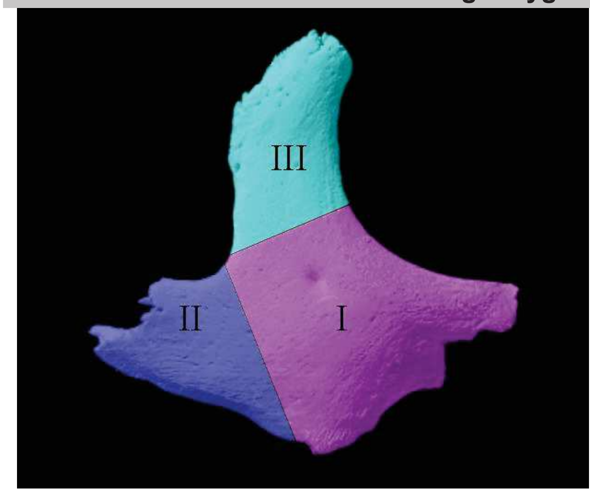

I. Orbital process. Landmarks: body, orbital margin, orbital surface, zygomatico-orbital foramen malar tubercle, zygomaticofacial foramen, articular surface for maxilla, masseteric origin.

II: Temporal Process. Landmarks: Temporal process of zygomatic bone, zygomaticotemporal foramen.

III. Frontal Process. Landmarks: frontal suture, frontal process.

The **sphenoid** is one of the most complex bones of the cranium, articulating to twelve other bones, and displaying an irregular shape that surfaces endocranially, inferiorly, laterally, and anteriorly. It is rarely complete when found in fragmented archaeological contexts, being seldomly represented by small pieces attached to adjacent cranial bones (White et al., 2012). Its developmental stages are equally intricated, growing from six differentiated ossification centres during the prenatal stage: two body parts -presphenoid and postsphenoid-, two lesser wings, and two greater wings. Around birth, the bone is represented by three elements that include the body (fused with the lesser wings) and the two greater wings. It is completely fused during the first year after birth (Scheuer & Black, 2004).

Considering its complexity and the difficulty it poses in the process of identification (in fragmentary contexts), the sphenoid was subdivided into three sections that resemble closely its composition around birth (see **Figure 17**). **Section I** includes the presphenoid part of the body and the right and left lesser wings, while **Section II** and **Section III** represent the right and left greater wings respectively, as well as their attachment points to the postsphenoid section of the body.

Figure 17. Sections chosen for the sphenoid bone (Original picture found in White & Folkens, 2005, p. 88, slightly modified).

Sphenoid (anterior view)

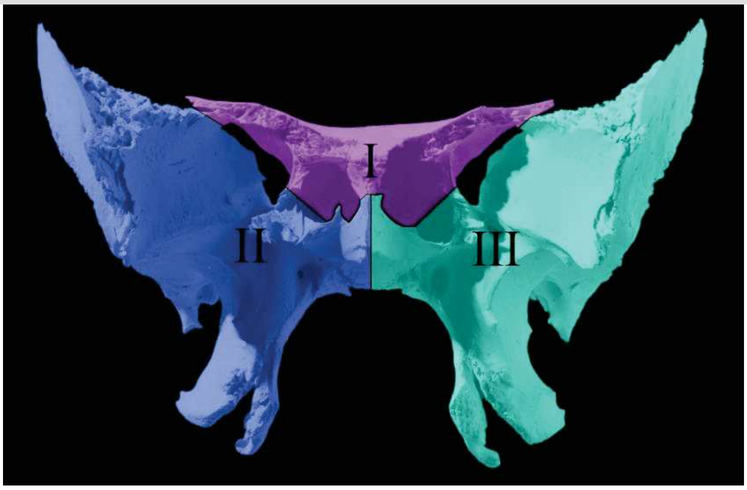

I. Body (Presphenoid). Landmarks: body, right and left lesser wings, sphenoidal sinuses, sphenoidal crest.

II. Great Wing (Right). Landmarks: great wing (right), sphenoidal crest, orbital surface, infratemporal crest, pterygoid process, pterygoid canal, lateral pterygoid plate, medial pterygoid plate, pterygoid hamulus, angular spine, hypophyseal fossa, posterior clinoid process, anterior clinoid process.

II. Great Wing (Left). Landmarks: great wing (left), sphenoidal crest, orbital surface, infratemporal crest, pterygoid process, pterygoid canal, lateral pterygoid plate, medial pterygoid plate, pterygoid hamulus, angular spine, hypophyseal fossa, posterior clinoid process, anterior clinoid process.

The lower jaw is one of the few skeletal elements belonging to the cranium that enjoys free movement. It holds the lower dentition and the insertion surfaces for strong mastication muscles. These two functions impact its topography, differentiating the corpus (alveolar) area from the ascending ramus. The **mandible** develops from two ossification points from which each hemi-mandible is formed. Both sections eventually fuse at the symphysis during the first postnatal year. Each half houses their side's respective dental arcade and condylar process.

When considering both the ossification process and its functional morphology, the mandible was subdivided similarly to the frontal bone. Four sections were delimited (see **Figure 18**): Section I and Section II represent the corpus, with the former being the right side and the latter the left one. Each group the lower dental arcade and the mental eminence, used frequently for sex allocation. The second group is formed by the ascending ramus of each side, including the articular surface with the temporal squamous region (condyle), the insertion points for mastication muscles such as the *masseter* and the *temporalis*, the glenoid angle, and pterygoid tuberosities.

The subdivision of the ramus from the corpus responded to the conservation state of this bone at GMS. Although the mandible is regarded as a resistant and heavy bone, it was usually found fragmented, mostly behind or around the extramolar sulcus, and rarely displaying both the alveolar and the ramus sections. It was also common to find only one side of the corpus.

Figure 18. Sections chosen for the mandible (Original picture found in White & Folkens, 2005, p. 91, slightly modified).

Mandible (superior view)

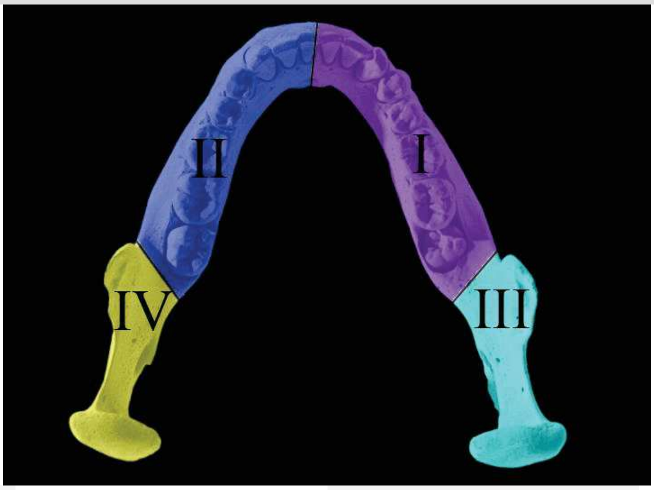

I. Corpus (Right). Landmarks: mental spines, alveolar portion, mental foramen, extramolar sulcus, digastric fossa, sublingual fossa, mental foramen, mental protuberance.	**II. Corpus (Left).** Landmarks: mental spines, alveolar portion, mental foramen, extramolar sulcus, digastric fossa, sublingual fossa, mental foramen, mental protuberance.	**III. Ascending Ramus (Right).** Landmarks: mandibular notch, mandibular condyle, condylar neck, lingula, coronoid process, mandibular foramen, masseteric tuberosity, masseteric fossa, gonial angle, pterygoid tuberosities, mylohyoid line, mylohyoid groove, coronoid process, mandibular notch.	**IV. Ascending Ramus (Left).** Landmarks: mandibular notch, mandibular condyle, condylar neck, lingula, coronoid process, mandibular foramen, masseteric tuberosity, masseteric fossa, gonial angle, pterygoid tuberosities, mylohyoid line, mylohyoid groove, coronoid process, mandibular notch.

Dentition's topography is the result of a process of evolutionary honing materialized into a variety of shapes and sizes that mostly depend on the species nourishing needs. However, their internal composition can be generally divided into the tooth's crown section and the root (see **Figure 19**).

Figure 19. Sections chosen for teeth (Original picture found in White & Folkens, 2005, p. 120, slightly modified).

Lower Right Molar 1 (mesial view)

I. Tooth Crown. Landmarks: cervix, cementoenamel, dentinoenamel junction, pulp, pulp chamber, cusp (protocone, hypocone, paracone, metacone, protoconid, hypoconid, metaconid, entoconid, hypoconulid, mamelons), crest, ridge, cingulum, tuberculum, fissure, groove, fovea, occlusal and interproximal facets.
II. Tooth Root. Landmarks: root canal, apical foramen.

When analysing human dentition, cultural behaviour plays a key role in understanding any modifications of a crown's original topography. Abrasive masticatory processes (attrition, abrasion and abfraction), breakage, intentional modification, and demineralization all influence the final state of a dental piece found within an archaeological context (Hillson, 2014). Having so many agents modelling a tooth's features requires a cautious approach when determining completeness and fragmentation of a tooth. In previous skeletal elements assessing the percentage missing from them was relatively straightforward, even considering developmental and individual variability. If one were to follow the same process, tooth completeness analysis would require the methodological assumption that the missing section or fragment did not undergo any morphological modification before its deposition.

Given the general state of dental elements in GMS, incomplete sections were not flagged with a percentage of completeness, since most of the adult teeth in the sample present a high prevalence dental wear in different degrees. Instead, visible (and post depositional) loss of material was registered with a "**Fragmented**/**F**" variable. The intention behind this category was avoiding the dilution of the real amount of tissue at the time of death within the percentages of missing tissue that are direct result of taphonomic events.

Vertebral elements display general morphologic traits that can be identified virtually in all of them with slight variations depending on the region, that is, if the bone is part of the cervical (C), thoracic (T), or lumbar (L) areas. A preliminary classification by region can be easily performed when a vertebra is found in isolation or in fragmentary contexts. The same argument might not hold true when trying to assign an individual nomenclature to the bone, as for most vertebrae this process requires comparisons with adjacent elements from the same individual.

Outstanding vertebral elements may be accurately classified by morphology alone such as C1 (i.e., Atlas) and C2 (i.e., Axis). Transitional elements, such as C7 and L5, can be identified with confidence to a lesser extent; there is a slight chance (around 10%) that population and individual variability among fringe elements may shift their morphological characteristics to those of an adjacent group (e.g., a C7 may become T1, or L1 a T12, and so on) (White et al., 2012). Additionally, C1 and C2's variability extends to their developmental stages, in which ossification centres behave differently to other vertebrae.

In GMS' case, most of the vertebral elements were found in isolation (except for *K51-2700* and *K51-2700' – Individual **A***) which made it difficult to assess an accurate identification of most bones, leaving only C1 and C2 as reliable elements that could be used for the MNI's count.

Vertebral elements were split into four sections: the first three are analogue to their developmental counterparts (i.e., body/ centrum and the vertebral arch divided in two), while adding a fourth one for the spinous process. The latter was defined during the classification process, as it seems to break-off regularly as a unit (see **Figure 20**).

The **first cervical** (**C1**) vertebra does not possess a vertebral body, while the posterior tubercle replaces the spinous process. When this element was classified *Section I* referred to its *anterior arch,* while *Section IV* was not used as the posterior tubercle does not break-off that easily, being recorded in sections II and III.

The **second cervical** (**C2**) vertebra develops from five primary ossification centres from which three behave similarly to other vertebral elements (e.g., two for neural arches and one for the centrum), and two are reserved for the body of the dens (Schaefer et al., 2009). The spinous process in this vertebra is not as pronounced as other cervical elements, thus it was recorded in sections II and III. When classifying a C2, *Section IV* was kept for the presence of the **dens** instead.

The vertebral bodies that compose the sacrum and coccyx will be explained in the section that deals with the pelvic region. When approaching recognizable vertebral elements that were too fragmented to determine the percentage of completeness the whole entry was treated with a value of "**U/ Undetermined**".

Figure 20. Sections chosen for the vertebrae (Original picture found in White & Folkens, 2005, p. 140, slightly modified).

Second Thoracic Vertebra (superior view)

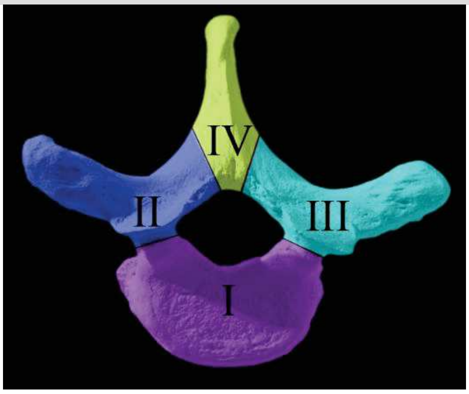

I. Vertebral centrum. Landmarks: articular surfaces (superior and inferior).

II. Neural Arch (Right). Landmarks: lamina, superior and inferior articular facets., transverse foramen (cervical), uncinate process (cervical), anterior and posterior transverse processes, superior, transverse, and inferior costal facets (thoracic), intervertebral notch, pedicle, accessory process (lumbar), mammillary process (lumbar).

III. Neural Arch (Right). Landmarks: lamina, superior and inferior articular facets., transverse foramen (cervical), uncinate process (cervical), anterior and posterior transverse processes, superior, transverse, and inferior costal facets (thoracic), intervertebral notch, pedicle, accessory process (lumbar), mammillary process (lumbar).

I. Spinous Process. Landmarks: spinous process.

The **sternum** develops prenatally from at least five ossification centres, the first one being the manubrium, and the other four being sternebrae. A sixth ossification centre, the xiphoid, will not commence ossification until the third to the sixth year of life. Morphological variation in this element has been attributed to its developmental variability, which is a direct result of the number of ossification centres per sternebrae; if the element has two ossification centres it turns into a wider bone, whereas if it develops from only one it tends to be narrower. At least three types of shapes have been categorized: Type I is the narrowest, Type II is widest, and Type III has a mixed pattern. Similarly, the constant interaction between the sternebrae and the ribs may influence the shape of the sternum and xiphoid process, forcing irregular shapes into the bone (Scheuer & Black, 2004).

From the morphological point of view, sternebrae will not be recognizable until about six months after birth. Though the patterns of fusion among sternebrae are diagnostic when determining age, variation among individuals results in wide age ranges (Scheuer & Black, 2004). Sternebrae 3 and 4 are the first elements that fuse together (4 to 10 years old) and sometimes form a midline sternal foramen that resembles a gunshot. Next, sternebrae 3-4 fuses with sternebrae 2 during puberty (11 to 16 years), and later with sternebrae 1 by the end of the first two decades of life (15 to 20 years). Up until this moment the sternum is divided in three sections and will remain virtually unchanged until the fourth decade of life, when the xiphoid process starts to fuse to the main body.

The sternum was divided into sections that reflected the elements present at a perinatal age (manubrium and four sternebrae), adding a sixth section in case an ossified xiphoid was found (see **Figure 21**).

Figure 21. Sections chosen for the sternum (Original picture found in White & Folkens, 2005, p. 150, slightly modified).

Sternum (anterior view)

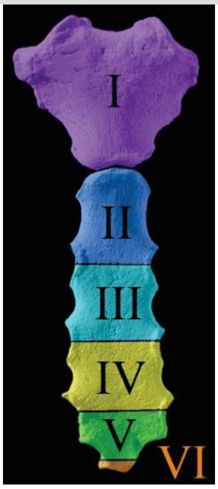

I. Manubrium. Landmarks: jugular, clavicular, first and second costal notches, stermal angle.

II. Sternebrae I. Landmarks: corpus sterni, second and third costal notches, lines of fusion.

III. Sternebrae II. Landmarks: corpus sterni, third and fourth costal notches, lines of fusion.

IV. Sternebrae III. Landmarks: corpus sterni, fourth and fifth costal notches, lines of fusion, sternal foramen (inconstant).

V. Sternebrae IV. Landmarks: corpus sterni, fifth, sixth, and seventh costal notches, lines of fusion, sternal foramen (inconstant).

VI. Xiphoid process. Landmarks: xiphoid process, seventh costal notch.

Akin to vertebral bodies, **ribs** have a differentiated morphology depending on the region in which they are located. Developmentally, most ribs grow out of a single primary centre of ossification while gaining secondary centres later, mostly located at articular sections such as the tubercle (Schaefer et al., 2009). Secondary ossification centres appear and fuse during puberty and do not seem to generate separate skeletal elements.

The rib was separated into four sections that correspond to the morphological regions known as its head, neck, body, and a distal portion (which can be present as a sternal end or distal point) (see **Figure 22**).

Figure 22. Sections chosen for the rib (Original picture found in White & Folkens, 2005, p. 157, slightly modified).

Right Second Rib (superior view)

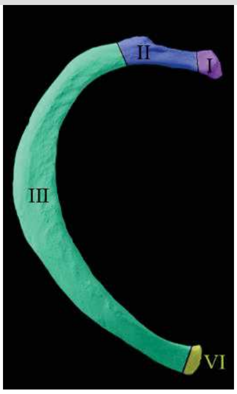

I. Head. Landmarks: head, articular surface of head.

II. Neck. Landmarks: neck, crest of the neck, tubercle, articular facet of the tubercle, angle

III. Body. Landmarks: costal groove, caudal and cranial edge. Only for the 1st rib: groove for subclavian artery and brachial plexus, scalene tubercle, and groove for subclavian vein. Only for the 2nd rib: tuberosity for serratus anterior

IV. Distal Section. Landmarks: sternal end, distal end (ribs 11th and 12th)

In general, ribs portrait a similar morphology which makes accurate identification difficult when found in isolation. However, R1 and R2 are easily identified, even when fragmented, which makes them eligible for the MNI's count. Other outstanding elements such as R10, R11 and R12 have unique characteristics as well, but R10 requires the presence of specific landmarks, while R11 and R12 involve comparison among each other to obtain reliable conclusions. These elements were only added to the final MNI's count if found whole.

The **clavicle** forms very early in development and acquires its distinctive 'S' shape around the 8th or 9th perinatal week. Apparently, it develops from a membranous ossification (acromial end) and a main ossification centre (sternal end) around the same time. Secondary ossification centres devoted to the constitution of the epiphyseal ends appear during puberty and fuse within a wide age range (20 to 30 years old) (Scheuer & Black, 2004).

Because its growth pattern, the clavicle was divided in three sections chosen thanks to their proneness to be separated in fragmentary contests (see **Figure 23**). The lateral and medial ones are analogue to the secondary ossification centres, making them a bit larger and including some landmarks that could be used for their identification. The epiphyseal area where the flat and tubular sections meet was deemed as the last section due its characteristic shape.

Figure 23. Sections chosen for the clavicle (Original picture found in White & Folkens, 2005, p. 162, slightly modified).

Right Clavicle (inferior view)

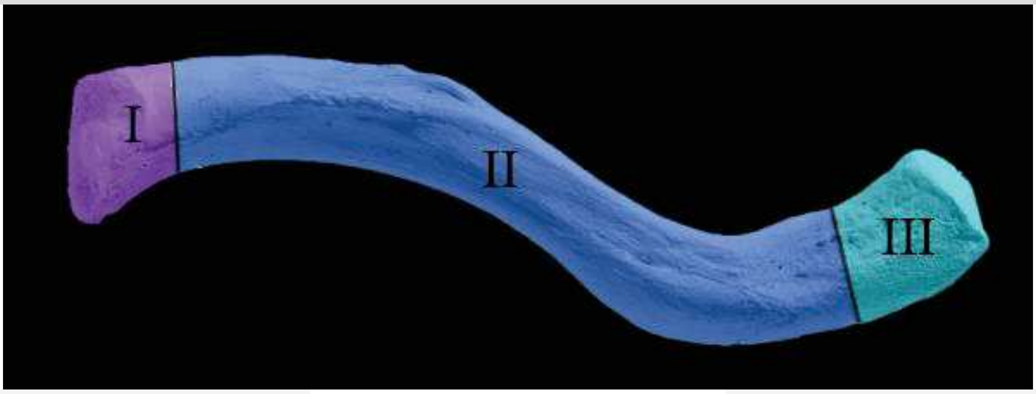

I. Sternal End. Landmarks: articular surfaces for the manubrium and the first costal cartilage, costoclavicular impression.	**I. Epiphysis.** Landmarks: subclavian sulcus, rugosities for the *pectoralis major*, coronoid tubercle, part of the trapezoid line, rugosity for the *trapezius*, nutrient foramen.	**I. Acromial End.** Landmarks: acromial facet for the scapula, part of the trapezoid line.

The **scapula** is a flat and triangular bone that develops prenatally from a single main ossification centre. Secondary ossification centres appear later in life, mostly in the acromial process, coracoid process, glenoid fossa, and the medial edge (Scheuer & Black, 2004). Unfortunately, when found in fragmentary contexts some of these areas are hard to identify correctly. The sections chosen for the scapula turned to morphological traits that were easily identified and had a somehow discernible post depositional breakage pattern (see **Figure 24**). Sections III and IV are specifically linked to the appearance and fusion of secondary centres that are deeply intertwined with the shoulder articulation. Both may be used as diagnostic elements age estimation.

Figure 24. Sections chosen for the scapula (Original picture found in White & Folkens, 2005, p. 167, slightly modified).

Right Scapula (posterior view)

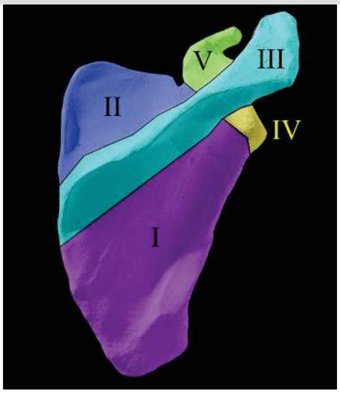

I. Body (Inferior). Landmarks: lateral border, infraspinous fossa, subscapular fossa, oblique ridges, inferior angle, medial border (inferior).

II. Body (Superior). Landmarks: superior border, superior angle, medial border (superior).

III. Spine/Acromion. Landmarks: scapular spine, acromion, clavicular facet.

IV. Glenoid Process. Landmarks: glenoid fossa, infraglenoid tubercle, supraglnoid tubercle, scapular neck.

V. Coracoid Process. Landmarks: coracoid process.

The **humerus**' diaphysis develops from a main ossification centre and acquires its characteristic form perinatally. Three additional centres appear shortly after birth around the proximal epiphysis: one for the head, and two for the greater and the lesser tubercles. The three coalesce to form a single structure before fusing with the shaft (Scheuer & Black, 2004). The distal epiphysis develops from four separate ossification centres (i.e., the capitulum, medial epicondyle, trochlea, and lateral epicondyle) that anchor themselves to the distal part of the diaphysis. The capitulum, trochlea and lateral epicondyle unify in a single component, but the medial condyle remains independent until its fusion with the diaphysis (Schaefer et al., 2009).The sections chosen for the humerus were delimited considering some developmental elements as groups (mostly those that coalesce), while the diaphysis was split in two to account for fragmentation postmortem (see **Figure 25**).

Figure 25. Sections chosen for the humerus (Original picture found in White & Folkens, 2005, p. 176, slightly modified).

Right Humerus (anterior view)

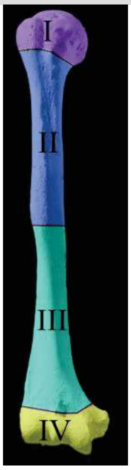

I. Proximal Epiphysis. Landmarks: humeral head, anatomical neck, greater and lesser tubercle, intertubercular groove, surgical neck.

II. Proximal Diaphysis. Landmarks: crest for the greater and lesser tubercle, anteromedial and anterolateral surfaces, deltoid tuberosity, crest for the *triceps brachii*, radial sulcus.

III. Distal Diaphysis. Landmarks: medial and lateral borders, posterior and anterior surfaces, lateral and medial supracondylar crests.

IV. Distal Epiphysis. Landmarks: radial, coronoid and olecranon fossa, lateral and medial epicondyles, trochlea, capitulum, groove for the ulnar nerve.

The **radius**'s shaft develops from a single ossification centre perinatally, which is complemented by two postnatal centres that form the head and the distal epiphysis. An occasional centre may develop around the radial tuberosity in some individuals (Scheuer

& Black, 2004). Akin to the humerus, the radius was segmented into four sections that represent its three primary components (head, diaphysis, and distal epiphysis) and subdivides its shaft into two (see **Figure 26**).

Figure 26. Sections chosen for the radius (Original picture found in White & Folkens, 2005, p. 185, slightly modified).

Right Radius (anterior view)

I. Proximal Epiphysis. Landmarks: radial head, radial neck, articular circumference.

II. Proximal Diaphysis. Landmarks: radial tuberosity, pronator tuberosity, anterior and posterior oblique lines, lateral and anterior surfaces, anterior border, interosseous border (superior).

III. Distal Diaphysis. Landmarks: interosseous border (inferior), anterior and lateral surfaces (inferior sections).

IV. Distal Epiphysis. Landmarks: radial styloid process, suprastyloid crest, dorsal tubercle, ulnar notch, grooves for *extensor carpi radialis*, *extensor pollicis longus*, and *extensor muscle tendons*, carpal articular surface.

The **ulna** was divided similarly to the radius and humerus, with the addition of a fifth section that reflects the juvenile partition of the olecranon (see **Figure 27**). This was done to separate the recognizable features of the distal epiphysis from the diaphysis.

Figure 27. Sections chosen for the ulna (Original picture found in White & Folkens, 2005, p. 194, slightly modified).

Right Ulna (lateral view)

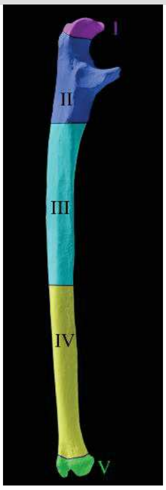

I. Olecranon. Landmarks: olecranon, trochlear notch, guiding ridge.

II. Proximal Epiphysis. Landmarks: coronoid process, ulnar tuberosity, radial notch, supinator crest.

III. Proximal Diaphysis. Landmarks: interosseous border (proximal), nutrient foramen, anterior border, longitudinal crest (proximal).

IV. Distal Diaphysis. Landmarks: medial surface, interosseous border (distal), pronator ridge, longitudinal crest (distal).

V. Distal Epiphysis. Landmarks: articular circumference, ulnar styloid process, groove for the *extensor carpi ulnaris*.

Carpal bones ossify after birth with occasional exceptions such as the capitate and hamate, that may be present perinatally in up to 8% of female individuals (4% for males). They mostly develop in a somewhat circular pattern starting from the capitate and moving laterally (Scheuer & Black, 2004), ending with the simultaneous appearance of the trapezium, trapezoid and scaphoid. Juvenile carpals are hard to differentiate up until they have obtained an adult's morphology, which will not happen until 12 to 13 years for females and 15 to 16 years for males. Sesamoid bones are the last group to ossify (the pisiform).

Considering the particularities of their ossification pattern and their relatively small size, sections chosen for the carpal bones were delimited based upon mature morphology and the location of fragile eminences or tubercles that may be lost postmortem. It is worth noting that some of these sections may be missing from pathologies related to abnormal ossification patterns, and when detected they were registered in along the pathological description (e.g., bipartite carpal, dislocations, etc.).

The **scaphoid** was divided into three sections: the tubercle, proximal, and distal (see **Figure 28**).

Figure 28. Sections chosen for the scaphoid (Original picture found in White & Folkens, 2005, p. 203, slightly modified).

Right Scaphoid (view from the capitate (right) and the radius (left))

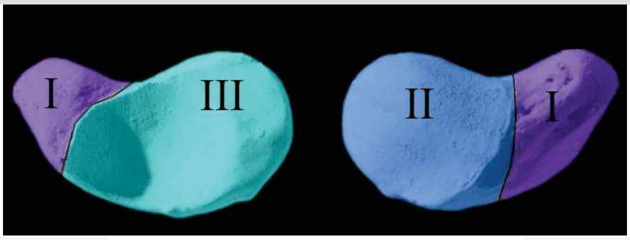

I. Olecranon. Landmarks: facet for the trapezium, tubercle, facet for the trapezoid.	**II. Proximal.** Landmarks: radial facet.	**III. Distal.** Landmarks: facet for the lunate and the head of the capitate.

The **lunate** was divided in two sections, proximal and distal (see **Figure 29**).

Figure 29. Sections chosen for the lunate (Original picture found in White & Folkens, 2005, p. 203, slightly modified).

Right Lunate (view from the scaphoid)

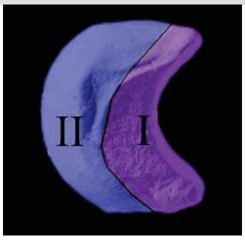

I. Proximal. Landmarks: facet for the head of the capitate, triquetral, hamate (inconstant) and scaphoid.

II. Distal. Landmarks: facet for the radius, facet for the triquetral.

The **triquetral** was subdivided into the volar and latero-inferior sections considering where it was most likely to fracture (see **Figure 30**).

Figure 30. Sections chosen for the triquetral (Original picture found in White & Folkens, 2005, p. 204, slightly modified).

Right Triquetral (palmar view)

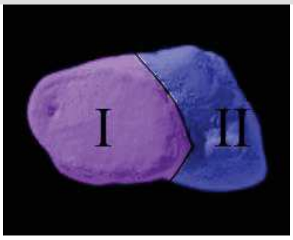

I. Volar. Landmarks: facet for the pisiform

II. Latero-inferior. Landmarks: facet for the lunate and the hamate.

The **pisiform** was divided into two morphological sections that comprise the articular facet for the triquetral and the body (see **Figure 31**). It is worth noting that the body of the pisiform was often found eroded, with the palmar surface missing or fragmented.

Figure 31 . Sections chosen for the pisiform (Original picture found in White & Folkens, 2005, p. 204, slightly modified).

Right Pisiform (view from the triquetral (left) and proximal view (right))

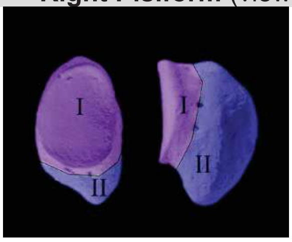

I. Facet for the Triquetral. Landmarks: facet for the triquetral, pisiform groove.

II. Pisiform Body. Landmarks: non articular body, attachment for *flexor retinaculum*.

The **trapezium**’s sections were chosen accordingly to breakage susceptibility, setting aside the trapezial ridge from the main body (see **Figure 32**).

Figure 32. Sections chosen for the trapezium (Original picture found in White & Folkens, 2005, p. 205, slightly modified).

Right Trapezium (view from the Second Metacarpal, palmar is up)

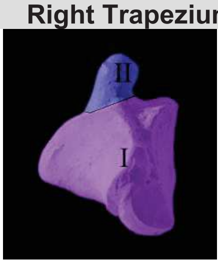

I. Ridge. Landmarks: trapezial ridge (or tubercle), anchor point for the *flexor retinaculum*.

II. Body. Landmarks: facets for MC1. MC2, trapezoid and scaphoid, trapezial groove for *carpis radialis*.

Although the **trapezoid** holds four articular facets (one for MC 2, the capitate, the trapezium, and the scaphoid respectively), its somewhat sturdy shape did not require a subdivision by sections. Erosion was only registered through the completeness score.

The **capitate**’s sections were considered morphologically as well, separating it into a proximal, a central and a distal portion (see **Figure 33**).

Figure 33. Sections chosen for the capitate (Original picture found in White & Folkens, 2005, p. 207, slightly modified).

Right Capitate (medial view)	
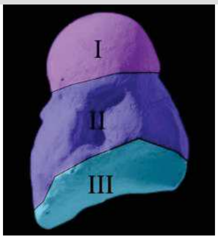	**I. Proximal Section.** Landmarks: head, facets for the lunate and scaphoid.
	II. Body. Landmarks: non articular dorsal and palmar surfaces, facet for the hamate.
	III. Distal Section. Landmarks: base, facet for MC2, Facet for MC3

The **hamate** was divided into the hamulus and body, considering that the former is prone to break-off during mechanical taphonomic processes (see **Figure 34**). It is also possible for the hamulus to separate from the main body during the lifetime of the individual, existing as a supernumerary bone.

Figure 34. Sections chosen for the hamate (Original picture found in White & Folkens, 2005, p. 208, slightly modified).

Right Hamate (lateral view)	
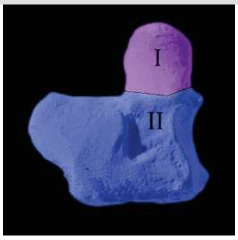	**I. Hamulus.** Landmarks: hamulus.
	II. Body. Landmarks: double facet for MC5, facets for MC4, the triquetral, the capitate, and the lunate (the latter is inconstant).

The **metacarpals**, **metatarsals**, and **phalanges** from hands and feet retain features that were deemed equivalent enough to create sections that are analogue among all of them. Most of these skeletal elements mature from a single ossification centre that develops before birth, although the middle phalanx for the fifth digit may present more than one centre. Long bones in the hand and foot develop differently to their counterparts in the limbs, as they do not possess differentiated epiphyses at both the proximal and distal poles, but only at one end. Epiphysis that are produced in secondary ossification centres are present either in the proximal end (phalanges and the 1st Metacarpal [MC1]/ metatarsal [MT1]) or the distal section (most metacarpals/ metatarsals, except for MC1/MT1) (Scheuer & Black, 2004). Pseudo-epiphyseal structures can be found in the epiphysis contrary to the one with a secondary ossification centre, leaving clefts on the corticoid bone. Multiple ossification centres have been recorded for the for the MC1/MT1, but they are rare and decrease in occurrence among the phalanges.

After considering the developmental stages for these skeletal elements and the location of postmortem breakages, all of them were divided into three sections that correspond to the proximal epiphysis, the diaphysis, and the distal epiphysis (see **Figure 35**). This division not only satisfies the ontogenetical process, but also represents the breakage patterns observed at GMS. Phalanges and metacarpals/metatarsals are one of the most abundant elements (25.8 %) in the collection, displaying a wide array of breakage patterns.

Figure 35. Sections chosen for the metacarpals and metatarsals (Original picture found in White & Folkens, 2005, p. 208 and 286, slightly modified).

Right Fifth Metacarpal (left) and Right Third Metacarpal (right) (dorsal view)

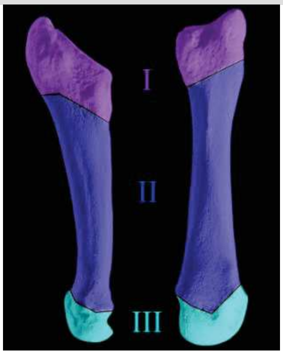

I. Proximal Epiphysis. Landmarks vary according to the skeletal element.

I. Diaphysis. Landmarks vary according to the skeletal element.

I. Distal Epiphysis. Landmarks vary according to the skeletal element.

The ***os coxae*** (i.e., innominate bone) is one of the most sexually dimorphic skeletal elements due to its role in locomotion and birthing demands. Bearing in mind its importance it was divided into five sections that correspond to its three developmental elements e.g., the ilium, ischium, and the pubis, and subdivides the first (Ilium) into three morphological units delimited by possible postmortem fragmentation patterns (see **Figure 37**).

Figure 36. Sections chosen for the *os coxae* (Original picture found in White & Folkens, 2005, p. 231, slightly modified).

Right *Os Coxae* (anterior view)

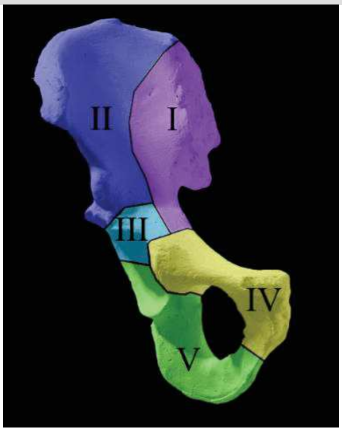

I. Body of Ilium. Landmarks: iliac tuberosity, posterior superior and inferior spine, articular surface, preauricular sulcus, greater sciatic notch, arcuate line.

II. Wing of Ilium. Landmarks: blade, iliac fossa, inner and outer lip, anterior superior and inferior iliac spine, iliac crest, anterior gluteal line.

III. Iliac Acetabular Region. Landmarks: acetabular fossa (shared among sections V and IV), lunate surface.

VI. Pubis. Landmarks: iliopubic eminence, pectineal line, iliopubic ramus, pubic tubercle, pubic crest, symphyseal surface, obturator groove.

V. Ischium. Landmarks: ischial spine, lesser sciatic notch, ischial body, ischial tuberosity, ischiopubic ramus, acetabular notch.

The Ilium, ischium and pubis are present prenatally and develop from a primary ossification centre, all located near the acetabulum. Secondary centres appear in all the skeletal elements, akin to the development of long bones in the limbs. Such behaviour produces a complex ossification and fusion pattern, when considering that at the same time they are merging with each other. The ilium acquires three secondary centres along the iliac crest and inferior spine that appear around adolescence and fuse in the early adulthood. The ischium acquires a secondary centre that develops and fuses at the same age range. The pubis develops a late secondary centre at young adulthood that fuses after 27 years old. The variability of secondary centres, coupled with the already tripartite nature of the *os coxae*, make it difficult to be segmented ontogenically.

Even though the *os coxae*'s morphology changes drastically depending on its developmental stage, the presence of the three main skeletal elements that compose it can be easily observed. Thus, special precautions were taken when recording it. In cases in which the skeletal element had not underwent complete fusion, **Major Classification** used the name of the bone before its fusion, filling the completeness score in the corresponding section of the mature bone.

Most osteology manuals introduce the **sacrum** either when approaching the vertebral column or when discussing the pelvic girdle, mainly because it is formed by the fusion of (usually) five vertebral bodies, but it is an essential component of the Ipelvis. The ossification pattern in the sacrum is complex, and includes approximately twenty-one separate primary centres of ossification divided into five sacral segments that behave similarly to other vertebral elements, diverging mostly in S1, S2, S3 (and sometimes S4), where additional paired lateral elements develop (Scheuer & Black, 2004).

The sacrum was subdivided into five sections, all corresponding to the sacral segments that fuse during its developmental stage (see **Figure 37**). The separation was constructed considering the possible presence of fragments that presented intervertebral foramens but no other landmarks to position them correctly within the sacrum, thus limiting accurate classification to clearly defined areas. If the observable landmarks were not enough to identify the section, the "**U/Undetermined**" category was used.

Figure 37. Sections chosen for the sacrum (Original picture found in White & Folkens, 2005, p. 220, slightly modified).

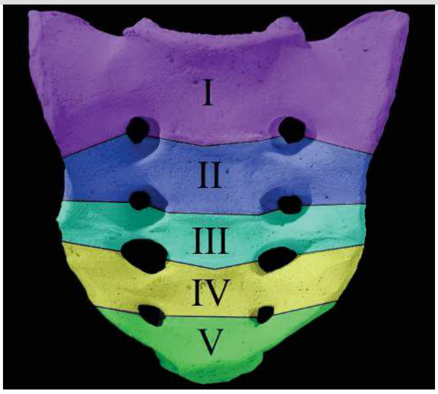

Sacrum (anterior view)
I. Sacral Segment 1 (S1). Landmarks: centrum, lateral part, ala, sacral promontory, anterior and posterior sacral foramina, intervertebral foramina, transverse ridge, medial sacral line, dorsal wall, sacral tuberosity, lateral sacral crest, superior articular facet, superior articular process, sacral plateau, articular surface for the *os coxae*.
I. Sacral Segment 2 (S2). Landmarks: centrum, lateral part, ala, anterior and posterior sacral foramina, intervertebral foramina, transverse ridge, medial sacral line, dorsal wall, lateral sacral crest, articular surface for the *os coxae*.
I. Sacral Segment 3 (S3). Landmarks: centrum, lateral part, anterior and posterior sacral foramina, intervertebral foramina, transverse ridge, medial sacral line, dorsal wall, lateral sacral crest.
I. Sacral Segment 4 (S4). Landmarks: centrum, lateral part, anterior and posterior sacral foramina, intervertebral foramina, sacral hiatus.
I. Sacral Segment 5 (S5). Landmarks: centrum, lateral part, anterior and posterior sacral foramina, intervertebral foramina, sacral hiatus, sacral cornu, facet for the coccyx, sacral apex.

The **femur** is the longest bone in the body and one of the easiest to recognize, even when fragmented. As most long bones, it develops from a bony collar in the centre of the shaft until it reaches the neck proximally and the lower epiphysis distally. At birth it is represented by two pieces (the shaft and the distal epiphysis) while cartilaginous sections represent the proximal epiphysis and the trochanters. The proximal epiphysis begins ossification after birth, while the whole bone fuses until young adulthood (Scheuer & Black, 2004).

Accordingly, the femur was subdivided into five sections that correspond to the head, the area of the distal epiphysis where the greater and lesser trochanter fuse, two sections for the shaft, and one for the distal epiphysis (see **Figure 38**).

Figure 38. Sections chosen for the femur (Original picture found in White & Folkens, 2005, p. 243, slightly modified).

Right Femur (posterior view)

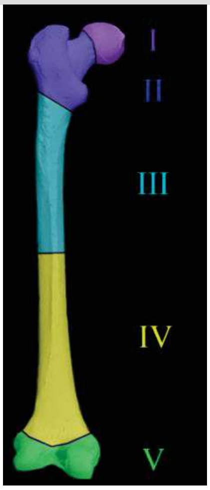

I. Femoral Head. Landmarks: fovea capitis.

II. Proximal Epiphysis. Landmarks: femoral neck, greater and lesser trochanter, third trochanter (inconstant), interotrochanteric crest, *obturator externus* groove, quadrate tubercle.

III. Proximal Diaphysis. Landmarks: pectineal line, spiral line, gluteal tuberosity, linea aspera (proximal).

IV. Distal Diaphysis. Landmarks: nutrient foramen, linea aspera (distal), lateral and medial lip of the linea aspera, medial and lateral supracondylar line, popliteal surface.

V. Distal Epiphysis. Landmarks: lateral and medial epicondyle, lateral and medial condyle, intercondylar fossa, adductor tubercle, patellar lip, impression for the lateral head of the *gastrocnemius*.

The **patella** is a sesamoid bone that ossifies after birth as early as eighteen months and as late as five years. Its morphology acquires adult contours only until puberty (Scheuer & Black, 2004). The sections chosen for this bone divide it morphologically, into its main body and its apex (see **Figure 39**).

Figure 39. Sections chosen for the patella (Original picture found in White & Folkens, 2005, p. 253, slightly modified).

Right Patella (anterior view)

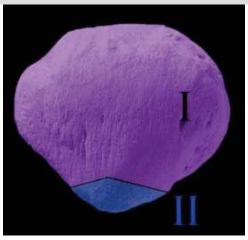

I. Body. Landmarks: base, medial and lateral articular facets, anterior patellar surface (proximal).

II. Apex. Landmarks: apex, anterior patellar surface (distal).

The **tibia** ossifies from a primary centre and its shaft is clearly recognizable at birth. Akin to the femur, the centre for the proximal epiphysis is present before birth being absent only in premature infants. The distal epiphysis starts ossification during the first year of life. A third secondary centre, responsible for the tibial tuberosity, undergoes a separate process of growth and fusion than the rest of the distal epiphysis (Scheuer & Black, 2004). Usually that the tuberosity is fully fused around twelve (males) or fourteen (females) years of age (Scheuer & Black, 2004).

Accordingly, the tibia was subdivided into five sections from which **Section I** and **II** correspond to the epiphyseal secondary ossification centres, **Section III** and IV divide the shaft in two, and **Section V** comprises the distal epiphysis. (see **Figure 40**). The seemingly arbitrary division of the tibial tuberosity was made so the region may be used alongside other age-diagnostic elements. The distal epiphysis of the tibia was one of the most common elements from juvenile individuals, along the proximal epiphysis of the tibia, femur, and humerus.

Figure 40. Sections chosen for the tibia (Original picture found in White & Folkens, 2005, p. 256, slightly modified).

Right Tibia (anterior view)	
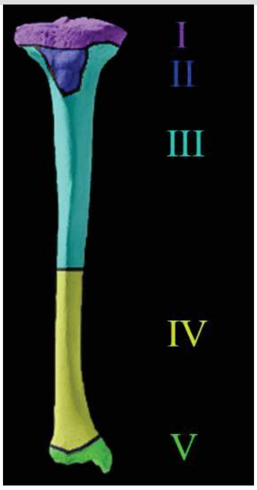	**I. Proximal Epiphysis.** Landmarks: anterior and posterior intercondylar area. Intercondylar eminence, medial and lateral intercondylar tubercle, lateral and medial condyle, groove for the *semimembranosus*, tibial plateau, superior fibular articular facet. **II. Tibial Tuberosity.** Landmarks: tibial tuberosity **III. Proximal Diaphysis.** Landmarks: interosseous surface, anterior crest, vertical line, and medial surface (proximal), popliteal surface, soleal line, nutrient foramen. **IV. Distal Diaphysis.** Landmarks: interosseous surface, anterior crest, vertical line, and medial surface (distal). **V. Distal Epiphysis.** Landmarks: anterior groove, talar facet, medial malleolus, posterior groove, intercollicular groove, groove for the *flexor hallucis longus*, fibular notch.

The ossification of the **fibula** starts later than any other long bone on the limbs. Its secondary centres begin to ossify until about one year (distal) and two years (proximal) (Scheuer & Black, 2004). The prenatal fibula presents a flat metaphyseal surface in its proximal end and a slightly sloped surface in its distal end. These characteristics can influence the shape of its epiphyses that, unlike those for the tibia and femur which present somehow concave shapes in the metaphyseal area, are somehow straight sections that follow the shaft's surfaces without overlapping or encasing one another. When found fragmented or isolated they seem to stretch further than their pairs on other long bones.

Another distinct morphological characteristic of the fibula is the presence of a quadrilateral or triangular cross section that is twisted onto itself. The degree of torsion has been related with strenuous physical activity. This proclivity makes the correct identification of sections of the within the shaft difficult when the bone is found fragmented. For this reason, the only diagnostic features to differentiate the superior and inferior sections of the shaft considered the location of the nutrient foramen and the rugosity in the distal portion. Otherwise, the bone was classified as undetermined.

The fibula was divided in four sections from which two represent the epiphyses and two the proximal and distal sections of the diaphysis (see **Figure 41**).

Figure 41. Sections chosen for the fibula (Original picture found in White & Folkens, 2005, p. 264, slightly modified).

Right Fibula (anterior view)

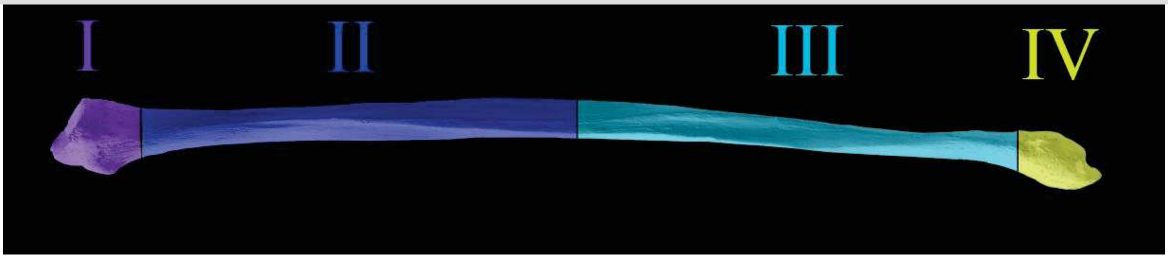

I. Proximal Epiphysis. Landmarks: styloid process, proximal fibular articular surface.	**II. Proximal Diaphysis.** Landmarks: neck, nutrient foramen, lateral, medial, and posterior surface, interosseous, anterior, and posterior border (proximal), posteromedial surface.	**III. Distal Diaphysis.** Landmarks: lateral, medial, and posterior surface, interosseous, anterior, and posterior border (distal), triangular subcutaneous area, surface for *interosseous membrane*.	**IV. Distal Epiphysis.** Landmarks: malleolar articular surface, malleolar fossa, lateral malleolus, fibular groove.

The **tarsals** behave similarly to the carpals in the sense that commonly most of them are not present at birth except for the talus and the calcaneus. On occasion, the cuboid can also be present perinatally. Most of them develop from single primary centres, although exceptions may occur. The calcaneus seems to be the only tarsal that consistently gains a secondary posterior ossification centre during childhood that fuses in late adolescence. However, individuals may present inconstant pedal epiphyses in various bones such as the talus, navicular, and fifth metatarsal.

Bearing this in mind, the sections chosen for most tarsals correspond to their morphology and fragmentation potential rather than to developmental stages (**Figure 42**, **Figure 43**, **Figure 44**, **Figure 45**, **Figure 46**, **Figure 47**, and **Figure 48**). The only exception made was for the calcaneus, to include the presence of the pedal epiphysis. The pattern of breakage displayed by the tarsals during the analysis was also considered during their delimitation.

Figure 42. Sections chosen for the talus (Original picture found in White & Folkens, 2005, p. 276, slightly modified).

Right Talus (medial view)

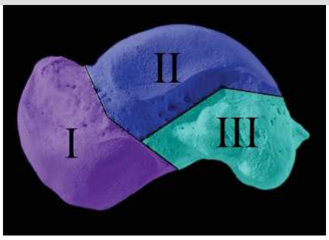

I. Head. Landmarks: head, neck, medial subtalar facet, anterior subtalar facet, facet for the navicular.

II. Body (superior). Landmarks: trochlea, medial and lateral malleolar articular surface, superior articular surface.

III. Body (inferior). Landmarks: posterior subtalar facet, lateral process, sulcus tali, groove for *flexor hallucis longus*, posterior process.

Figure 43. Sections chosen for the calcaneus (Original picture found in White & Folkens, 2005, p. 278, slightly modified).

Right Calcaneus (medial view)

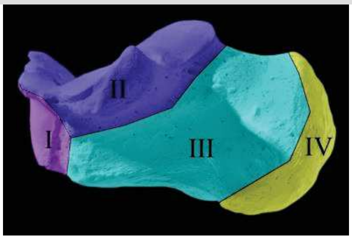

I. Anterior Facet. Landmarks: anterior talar facet, facet for the cuboid, anterior calcaneal process.

II. Superior Articular Surface. Landmarks: sustentaculum tali, sustentacular sulcus, anterior, medial, and posterior talar facet, sustentacular sulcus.

III. Body. Landmarks: lateral process of the calcaneal tuberosity, fibular tubercle, groove for *fibularis longus*.

IV. Calcaneal Epiphysis. Landmarks: calcaneal tuberosity, medial process of the calcaneal tuberosity.

Figure 44. Sections chosen for the cuboid (Original picture found in White & Folkens, 2005, p. 280, slightly modified).

Right Cuboid (dorsal view)

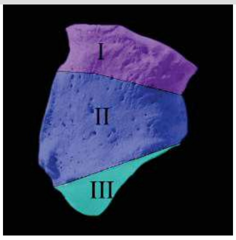

I. Distal Section. Landmarks: facets for MT4 and MT5, groove for the *fibularis longus*.

II. Body. Landmarks: Cuboid tuberosity, non-articular surface, facet for the lateral cuneiform.

III. Proximal Section. Landmarks: facet for the calcaneus.

Figure 45. Sections chosen for the navicular (Original picture found in White & Folkens, 2005, p. 281, slightly modified).

Right Navicular (*right* -proximal view, *left* – distal view)

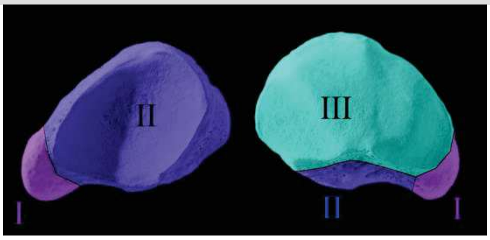

I Medial Section. Landmarks: tubercle of the navicular.

II. Proximal Section. Landmarks: facet for the talar head, non-articular dorsal surface.

III. Distal Section. Landmarks: facets for the lateral, intermediate, and medial cuneiform.

Figure 46. Sections chosen for the medial (first) cuneiform (Original picture found in White & Folkens, 2005, p. 282, slightly modified).

Right Medial (First) Cuneiform (medial view)

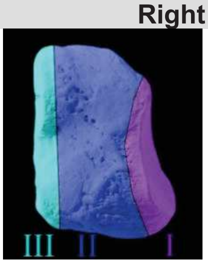

I. Proximal Section. Landmarks: facet for the navicular, facet for intermediate cuneiform.

II. Body. Landmarks: non-articular dorsal and plantar facets, facet for MT2.

III. Distal Section. Landmarks: Facet for MT1

Figure 47. Sections chosen for the intermediate (second) cuneiform (Original picture found in White & Folkens, 2005, p. 282, slightly modified).

Right Intermediate (Second) Cuneiform (medial view)

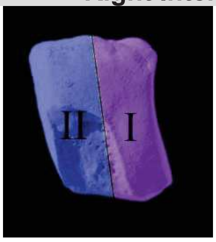

I. Proximal Section. Landmarks: facets for the navicular, lateral, and medial cuneiform, non-articular dorsal and plantar surfaces (proximal).

II. Distal Section. Landmarks: facet for MT2, non-articular dorsal and plantar surfaces (distal).

Figure 48. Sections chosen for the lateral (third) cuneiform (Original picture found in White & Folkens, 2005, p. 283, slightly modified).

Right Lateral (Third) Cuneiform (medial view)

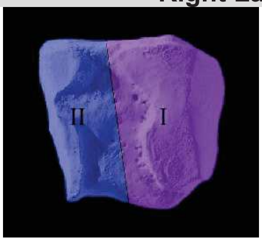

I. Proximal Section. Landmarks: facets for the navicular, the intermediate cuneiform, and the cuboid.

II. Distal Section. Landmarks: facets for MT2, MT3.

3.3.11. Number of Fragments

Finally, a complementary variable that counts the number of fragments per element registered was added to observe the level of fragmentation at an individual level. This variable had a maximum of seventy-two fragments in one entry, but the most common result was between one and three fragments per entry.

3.3.12. Anthropometric analysis – Measurements for sex allocation and stature estimation

The variables following completeness and fragmentation are the ones related to anthropometric measurements. A maximum of 10 measurements were taken from different skeletal elements, depending on the available methods for sex allocation and estimation of stature. The reasoning behind the amount of variables (10) was to fit all the measurements on the radius (Curate's research (2021b)), which had the highest number.

Depending on the conservation state of archaeological material, the paleodemographic techniques employed to allocate sex and estimate age at the time of death are usually chosen to suit the availability of information. Gruta do Morgado Superior required the implementation of methods that rely in probabilistic determination of paleodemographic and morphological traits, using a combination of standard and alternative measurements of bone features on skeletal elements that were suited for the analysis.

In recent decades, studies that rely on a strategic sampling methodology tilted towards favouring alternative statistical approach and meaningful combinations of reproducible anthropological measurements (Albanese, 2013). Although results obtained with said methodologies may have varying degrees of confidence when compared with more traditional -and morphological-methods-, they are particularly useful for fragmented contexts.

The measurements taken were aimed to the allocation of sex and the estimation of stature. Most of the methodologies suitable for Gruta do Morgado Superior will be presented next. Although most fragments allowed for the implementation of most techniques, some methods were ultimately not used in the results due to the lack of suitable material within square **K51**. However, the methodology may still be suitable for the remaining squares at Gruta do Morgado Superior.

3.3.12.1. Sex allocation

Sex allocation is a robust starting point for establishing the paleodemographic profile of a given individual or population in the past. Morphological and anthropometric characteristics that variate according to inherent patterns of sexual dimorphism are fairly accurate when allocating biological sex. Accuracy rates behave differentially as well, depending greatly on the analysed skeletal region and intra- and inter-populational variance.

Methods focused on sex allocation are generally separated into two broad categories: *morphoscopic* and *metric*. The *morphoscopic* or visual method is characterized by being observer-dependent and very sensitive to biases, since decision-making tends to be subjective.; The *metric* method is a more dependable approach, easier to assess and to interpret (Curate, 2022; Curate et al., 2021b). Both are likely to be influenced by population-specific parameters such as robusticity or average body size, which brings up the necessity of performing constant research on local historic and living populations. Locally obtained data may be linked with people in the past with more confidence than data extrapolated distant communities, regardless of whether the gap is genetic or geographic.

Additional methodologies such as molecular-based analysis, namely proteinic and genomic testing, have grown stronger in recent years. The results show high accuracy rates, with the only deterrence being its monetary cost and the challenging technical requirement of high-quality data (Curate, 2022). These techniques will not be contemplated due to budget constraints.

Techniques used in a bioarchaeological analysis are chosen mainly by assessing their accuracy rate, the provenance of the population used to hone the methodology, and the conservation status of the analysed material. Ideally, the first bone to be examined is the pelvis, as it is the most reliable when determining biological sex. Both *os coxae* are exposed to selective and ontogenetical pressures brought about by bipedal locomotion, hormonal mediation, and childbearing. Parturition influences dramatically the pelvic girdle sex-dimorphic features to the point that if the bone is sufficiently conserved, a simple observation of height and morphology may produce an accurate allocation of up to 100% (Curate, 2022). Second to the pelvis, morphological features present in cranial bones are often considered a highly reliable sex-allocation indicators. Up to twenty cranial markers and sex discriminant features have been proven to produce sex allocation accuracy rates over 84% (when analysed conjointly). Recently the multivariate analysis of cranial features has been recommended over examination of isolated markers; individually, their accuracy rates are lower: the glabella reaches an average of 57%, the nuchal crest 58%

and mastoid process 75% (Nikita, 2014). When variation between populations and individuals comes into play, some features' accuracy may dimmer even further.

Successful sex allocation depends greatly on the quantity and quality of preservation of the osteological remains, and some archaeological contexts may present poorly preserved pelvis or cranium bones, or both can be missing altogether. Other skeletal elements belonging to both the axial and appendicular skeleton have proven well suited for such studies (Amores-Ampuero & Viciano, 2020; Curate et al., 2017). One example is the femur, which generally tends to survive in good condition thanks to its overall resilience (Curate et al., 2017). High allocation rates have been found in other skeletal elements such as the clavicle (Albanese, 2013), humerus (Albanese et al., 2005), radius (Curate et al., 2021b), ulna (Albanese, 2013), tibia (Kieser et al., 1992), and fibula (Saunders & Hoppa, 1997). If the fragmentation level renders long bones unsuitable, other bone elements may be analysed such as ribs (Macaluso Jr. et al., 2012), vertebrae (Amores-Ampuero & Viciano, 2020), sternum (Macaluso Jr. & Lucena, 2014), patella (Peckmann et al., 2016), carpals (Mastrangelo et al., 2011; Sulzmann et al., 2008), and tarsals (Curate et al., 2021a; Navega et al., 2015). Tarsals have proven to convey robust results (Amores-Ampuero & Viciano, 2020; Curate et al., 2021a; Navega et al., 2015). Most of these methods are a direct result of the pressing need of obtaining reliable techniques for highly fragmented archaeological contexts analysis. Portuguese researchers have responded to this necessity enthusiastically from the 90's.

Portuguese researchers have a respectable number of historical collections available for anthropometric studies such as the Identified Collection of the *National Natural History and Science Museum of the University of Lisbon*, the *Coimbra Identified Skeletal Colelction*, the *Coimbra 21st Century Identified Skeletal Collection*, *Mendes Correira's Skeletal Collection*, *BoneMedLeg* (Porto), and the *Identified Skeleton Collection of Évora*, among others. Thanks to these collections, the decade of 1990 witnessed a surge of a several studies focused on sex allocation techniques utilizing metric parameters. Portuguese researchers directed their effort towards employing the use of Linear Discriminant Analysis (LDA). With time, new approaches introduced sectioning points meant to replace LDA analysis gradually. Yet, even in cases where the performance of machine-learning algorithms was better, the statistical difference was not overwhelming enough to achieve it (Curate, 2022).

Theoretical considerations for sex-allocation in Archaeology

Archaeological and historical perspectives have changed their notions of identity, gender, and social class over the last decades. New paradigms have started to question and challenge the western bias that taints much of scientific and social research in both disciplines. Deconstructionist arguments have brought up attention over the fact that that sex and gender can be fluid concepts, and the western binary partition of sex into males and females is a product of social discourse. These theoretical 'separate spheres' often are presented as dichotomous opposites or, in a cheap chivalrous way, as complements. In this sense, western (or namely Greco roman and Abrahamic) schools of thought have historically laid theoretical bases to reinforce and consolidate social misconceptions founded on a dichotomous relationship between masculine and feminine traits that extends to other social relationships such as domestic/public, natural/artificial, savage/civilized, etc. These biased conceptions do not allow any room for any mediation or categorical diversification between them. Archaeological thought often reproduces (and imposes) contemporary social bias onto the archaeological records through its interpretation (Spencer-Wood & Camp, 2013). Consequently, previous schools of thought imposed a strict and hierarchical relationship in which masculinity and femininity are terms mutually exclusive and constantly in conflict. Nowadays anthropologists and archaeologist are conscious about the possibility that the so-called binary rift was merely peripheral in many non-western societies, who recognized human variation in ways that did not fall into a precise two-sex system (Curate, 2022). Even chromosomal sex is diverse and does not map clearly onto two bodily morphologies (Curate, 2022). Understanding that even biologically there is sufficient data for the creation of at least a third category (1.8% of all births are considered intersexual), and that the use of these categories implicitly carry power dynamics that function as a detriment for certain social sectors (Spencer-Wood & Camp, 2013). Bearing this in mind is important to clarify that sex allocation is a marker of biological profile and thus it does not necessarily translate into the social fabric of the studied communities. This concept is, after all, a variable that has been conceived by modern researchers and, as everything does, it is bound to evolve with time.

Sex allocation analysis at GMS

Having said that, in Gruta do Morgado Superior, the metric approach will be favoured over the morphoscopic one given that the latter is more accurate in well-preserved archaeological contexts with clear funerary architecture. This decision has been taken considering each technique's reliability, as well as the possibility of producing biased results.

Morphoscopic analysis has been used for decades without any major modification or alteration, thanks mainly to the fact that they work. However, a robust metric frame for such analysis needs to be made. Just to name an example, Saskia and their team (2019) analysed the trustworthiness of a morphoscopic methodology applying it to the 21st Century Identified Skeletal Collection at the University of Coimbra. The methodological basis of the technique revolves around the fact that the differences in the shape of the trochlear constriction and olecranon fossa of the humerus can be used for sex allocation. Although their analysis used a robust methodology to examine dimorphic variability in shape, they concluded that the trochlear constriction did not present any reliable markers associated to sex. On the other hand, the olecranon fossa, although more reliable, only produced suitable results when observing matching patterns for triangularity/roundness or convexity/concavity. Testing morphoscopic methods using metric variables has become more of a necessity for current academic endeavours, as more trustworthy and tailor-made techniques are deemed more valuable in the field.

Portugal has a decent archive of studies focused on sex allocation using different skeletal regions, some which could be used in the analysis of a collection with the particularities of Gruta do Morgado Superior. The following sections will describe the methodologies that were reviewed for the elaboration of the biological profile and their requirements.

Measurements on Femora

The femur tends to be sturdier than most bones when exposed to taphonomic agents in archaeological contexts, which is why it has been frequently used in sex-allocation and stature estimation analysis (Curate et al., 2017). Nonetheless, the harsh conditions at GMS bested most of the specimens in the sample, rendering them into highly fragmented element. As stated before, alternative methodologies have been developed to ameliorate the data hiatus left by long bones in fragmentary contexts. In a research conducted by Francisco Curate, Anabela Albuquerque, Izilda Ferreira and Eugénia Cunha (2017) a method that utilized on the total area of the proximal femur using DXA and logistic regression was developed. The use of only a section of the femur has great advantages for Gruta do Morgado Superior, even when considering the need of additional equipment.

Curate and their team used data from living populations, extracted through non-invasive imaging techniques (e.g., computer tomography or protectional radiography). In clinical contexts Dual X-ray absorptiometry (DXA) (i.e., bone densitometry analysis) is used to evaluate a bone's mineral density (BMD) and diagnose pathologies such as osteoporosis. It uses a two-dimensional scan that cannot determine the real bone density by itself, so it measures bone mineral content (BMC – grams) in a specific projected area (cm^2). This technique has been used in studies that estimate sex, age at the time of death and ancestry (Wheatley, 2005- cited in Curate et al. (2017, p. 111)).

Curate's team generated and tested models for sex allocation based on the total area of the proximal femur (using DXA), applying logistic regression and Fisher's linear discriminant analysis. These methods were chosen as they are generally used for dichotomous dependent variables. Lastly, data was compared by using classification and regression trees and reducing error pruning trees, which are non-parametric decision tree learning techniques. The methodology tested the results in two Portuguese skeletal collections: the Coimbra Identified Skeletal Collection (CISC, University of Coimbra) with a sample of *n*=224, from which 112 individuals were female and 112 makes. Their age ranged between 20 to 96 years old at death. Most of them were born between 1910 to 1936; *and* the 21st Century Identified Skeletal Collection (ISC/XXI, University of Coimbra, Portugal) from which a sample of *n*=60 was selected (30 female and 30 male), with a range of 33 to 97 years old at death. Most of the individuals died between 1995 and 2001.

The Proximal femur's TA is composed by the femoral neck, trochanteric region, and intertrochanteric/proximal diaphysis region (femoral **Sections I** and **II** in the database). Every left femur from each specimen was subjected to a TA analysis in which the element was placed in anteroposterior position, with the femoral neck parallel to the plane of the scanner in a low-density box with dry rice acting as a soft-tissue surrogate. Measurements were performed with a Hologic QDR-4500A densitometer.

The logistic regression model was defined by the following equation (where females classified with negative values and males with positive values):

$$Sex = 0.800 * TA - 30.498$$

Linear discriminant analysis produced a single discriminant function with a cut-off point equal to zero (with the same behaviour as the logistic regression model):

$$Sex = 0.279 * TA - 10.738$$

In general, DXA TA values exhibited a slight variation with ancestry, but their sexually dimorphic features were strong enough to allocate sex. Results reflect the fact that once puberty arrives, females and males are exposed to it at different times (periosteal growth accelerates during puberty in males while earlier completion of longitudinal growth and inhibition of periosteal apposition produces smaller bones in females) (Curate et al., 2017). Genetic factors may influence the final shape of this area as well. Sex assessment with the total area of the proximal femur shows a high overall accuracy (of at least 90%). The accuracy in test collections suggest that it can be used in other populations with a somewhat high rate of confidence.

However, this methodology requires the use of additional equipment and the obtention of a complete femur's TA area. Although other squares may present fragments suitable for its application, the **K51** square did not provide a complete proximal femur, the closest element being the entry *K51-1173* with a completeness score of 3 and 4 for these Section I and II respectively (an average of 62.5%). In conclusion, future studies on other squares from Gruta de Morgado Superior may yield better results using this methodology, not only because it was elaborated using a Portuguese population, but also because it does not require a complete femur.

Measurements on bones of the Upper Limbs

The first explored method that employed sex allocation through upper-limb bones analysis was developed by John Albanese (2013). It relies in measurements of long bones such as the clavicle, humerus, radius, and ulna. Albanese's methodology was noticeable because it drew data from the Coimbra's skeletal collection, while the Lisbon's Skeletal Collection was used to test its accuracy.

Albanese argued that the use of *logistic regression*s should be considered as a more robust, and better performing approach, when extracted from fewer statistical assumptions, than a *discriminant function analysis*. His methodology employed a regular logistic regression that calculated a *p*-value that was first used to allocate an unknown individual, and then to make a probability statement about the likelihood of a correct allocation. The discriminant function was used for the post *hoc* calculation of posterior probability and/or typicality probability that is required to assess the likelihood of a correct datum. The collections selected for the construction of the equations presented were the Terry's Collection (From North America, with medium and large individuals that perished from 1830 to1930), the Collection of Coimbra (A Portuguese collection of small to medium sized individuals that died from 1830 to 1930), and the Grant's Collection (North American population with a very distinct pattern of sexual dimorphism).

Albanese's methodology produced a linear equation whose output is always between 0 and 1; in which a value under 0.5 is interpreted as a possible female, and one over 0.5 indicates a possible male (Albanese, 2013, P. 1413). A combination of standard and new measurements of the length, joints and midshaft for the clavicle, humerus, radius, and ulna was selected (see **Table 11**). and then combined in different arrangements to maximize the allocation accuracy under different scenarios. Possible settings included the recovery of *i*) one clavicle and one forearm bone; *ii*) one clavicle and one humerus; iii) one clavicle and one forearm bone; *iv*) one clavicle and both forearm bones; *v*) one humerus and one forearm bone; and *vi*) both forearm bones (Albanese, 2013, p. 1414).

The individual variables (measurements) that performed the best were: **MCL**, **CCDC**, **VHDH**, **EBH**, **APDU**. The most accurate value *Z* was calculated as a linear function:

$$Z = (0.043 * MCL) + (0.595 * CCDC) + (0.346 * VHDH) + (0.913 * EBH) + (0.825 * APDU) - 48.806)$$

Table 11. Variant and standard measurements (Albanese, 2013, p. 1414) [14].

Database ID	Bone	Measurement	Description
I	Clavicle	**(MCL) Maximum Length**	The maximum length from the sternal end of the clavicle to the scapular end of the clavicle. Measured using an osteometric board (measurement no. 35). Analog with measurements by Martin (1928, P.1005) and Buikstra & Ubelaker (1994, P. 79 - No.35)..
II		**(CCDC) Cranial-Caudal Diameter (Variant)**	The cranial-caudal diameter of the clavicle at midshaft. Measured using sliding callipers. The flat surface of the scapular end of the clavicle should be held parallel to the arms of the callipers (variant of measurement no. 37). Difference lies in the way the clavicle is held in standard position relative to the callipers. Analog with measurements by Martin (1928, P.1006) and Buikstra & Ubelaker (1994, P. 79 - No.36).
I	Humerus	**Vertical Head Diameter (VHDH)**	The maximum distance from the most superior point on the margin of the articular surface to the most inferior point on the margin of the articular surface on the head of the humerus. Measured using sliding callipers (measurement no. 42). **Measurement I** in Database.
II		**Epicondylar Breadth (EBH)**	The maximum distance between the medial epicondyle and the lateral epicondyle on the distal humerus. Measured using sliding callipers (measurement no. 41).
I	Ulna	**Anterior-Posterior Diameter (Variant) (APDU)**	The anterior-posterior diameter of the ulna perpendicular to the diameter at maximum crest pronouncement. Measured using sliding callipers (variant of measurement no. 49). Measurements were collected in reverse order when compared with traditional approach; for this paper the maximum diameter at the point of maximum crest pronouncement, which is only approximately medial-lateral, is collected first and the actual maximum diameter of the crest is collected.
II		**Diameter at Maximum Crest Pronouncement (Variant) (DMCP)**	The maximum diameter of the ulna at the point of maximum crest pronouncement. Measured using sliding callipers (variant of measurement no. 50).
I	Radius	**Maximum Length (ML)**	The maximum distance between the most proximal point on the head of the radius to the distal end of the styloid process of the radius. Measured using an osteometric board (Measurement no. 45).
VI		***Sagittal Diameter (SD)* (*)**	The anterior- posterior diameter at the midshaft of the radius. Measured using sliding callipers (measurement no 46).
VII		***Maximum Head Diameter (MHD)* (*)**	The maximum diameter of the head of the radius measured using sliding callipers.

(*) These measurements have analogue descriptions in Curate (2021b), that we considered clearer for this study. For these reasons they will be added to the database using Curate's methodology order.

[14] Most measurements were taken from Moore-Jansen P.H., Ousley S.D., Jantz R.L. (1994) (Data collection procedures for forensic skeletal material) except for the Maximum Head Diameter of the radius that followed the work of Berrizbeitia (1989). The GMS column states the name they were given on the database.

Additional combinations provided similar results (see **Annex 3**) when tested using four independent samples (*n* > 370) (including a forensic one). Although allocation accuracy varies depending on the sample used, the result of the remainder equations was considered reliable enough, with an accuracy rate range between 87.4% to 93.8%. Precision was hindered only when it was applied to males below the average size, which lived under extreme conditions of poverty and mortality. This may indicate that inter-population characteristics may affect the technique's performance.

Albanese argues that the method's sturdiness is a combined result of the use of *i*) new measures were developed to reliably capture patterns of sexual dimorphism; *ii*) a non-random approach used to construct a reference sample, that includes a wide range of human variation; *iii*) data drawn from a combination of biologically meaningful skeletal elements; *iv*) the use of a robust logistic regression instead of discriminant function analysis; and *v*) an independent question focused only on sec-allocation without any race-specific adjustments.

The greatest limitation for the application of this methodology, at least in Gruta do Morgado Superior's collection, is that Albanese concluded that equations which drew information from only one bone did not meet the minimum criteria of an overall accuracy of 90% and a sex bias of 5% or less. As such, only those bones that can be associated with one individual could be used to apply them.

Not only it is very difficult to infer with certainty that a clavicle, humerus, ulna, and radius belong to the same individual at GMS, but complete upper limb bones were a rare sight at **Square K51**. From the 4350 elements analysed, only one juvenile (complete) clavicle (under 16 years) was found (*K51-2479*), no humeri were found complete, only one adult ulna -complete, but highly fragmented- was registered (*K51-1245*), and only one adult radius -complete but highly fragmented- (*K51-1491A*) was recovered. Even so, the two complete elements were measured, considering the possible bias because of taphonomic alterations. Once the whole GMS collection is analysed, it is likely that at least two of these upper-limb elements could be successfully associated to the same individual.

Measurements on the Radius

An investigation led by Francisco Curate, Fernando Mestre and Susana J. Garcia (2021b) was able to construct a methodology for sex allocation based on the elaboration of univariable and multivariable models supported by measurements of the radius. The team used a Portuguese training sample from the Coimbra Identified Skeletal Collection (CISC). A total of *n*=364 individuals (166 Females and 198 Males) with a 17 to 96 years old range of age at the time of death were chosen to collect the raw data. The population was born between 1833 and 1918 and perished between 1910 and 1936.

This methodology relies on ten measurements that require only one complete radius, which makes it more appealing that Albanese's technique. Most of the measurements taken by the team followed Rudolf Martin's (Martin, 1928, pp. 1014-1016) guidelines and description, except for the Minimum Circumference in the Proximal Diaphysis (MCPDR-

Measurement III on the database) which was based on E. Fischer's (1906) descriptions (see **Table 12** and **Figure 49**).

Table 12. Measurements to allocate sex using the radius (Curate et al., 2021b, p. 101790(2) , Table 2).

Database ID	Original	Name	Description
I	**MLR**	**Maximum Length**	The distance from the most proximally positioned point of the head of the radius to apex of the styloid process (*osteometric board*).
II	**MCDDR**	**Minimum Circumference in the Distal Diaphysis**	The perimeter taken in the thinnest diaphyseal region located at the distal part of the bone (*measuring tape*) **Measurement II** in database.
III	**MCPDR**	**Minimum Circumference in the Proximal Diaphysis**	The perimeter taken immediately below the radial tuberosity (*measuring tape*).
IV	**TDSR**	**Transverse Diameter of the Shaft**	Maximum diameter of the diaphysis measured at the point where the interosseous crest shows the strongest development (*sliding calliper*).
V	**TDHR**	**Transverse Diameter of the Head**	Distance between the most medial and the most lateral points of the radial head surface, in the transversal plane (*sliding calliper*).
VI	**SDSR**	**Sagittal Diameter of the Shaft**	Diameter of the diaphysis measured at the level of the transverse diameter of the shaft and perpendicular to it (*sliding calliper*).
VII	**SDHR**	**Sagittal Diameter of the Head**	Distance from the most anterior to the most posterior points of the radial head surface, in the sagittal plane, and taken perpendicularly to TDHR (*sliding calliper*).
VIII	**HCR**	**Head Circumference**	Maximum perimeter of the radius head (*measuring tape*).
IX	**NCR**	**Neck Circumference**	Minimum perimeter of the neck, taken in the most strangled place of the neck (*measuring tape*).
X	**IEWR**	**Inferior Epiphysis Width**	Maximum projective distance from the ulnar notch to the lateral aspect of the styloid process (*sliding calliper*).

Figure 49. Visual representation of the measurements taken for the radius. Their number corresponds to that in the previous table. (Curate et al., 2021b, p. 101790(3), Figure 1, slightly modified).

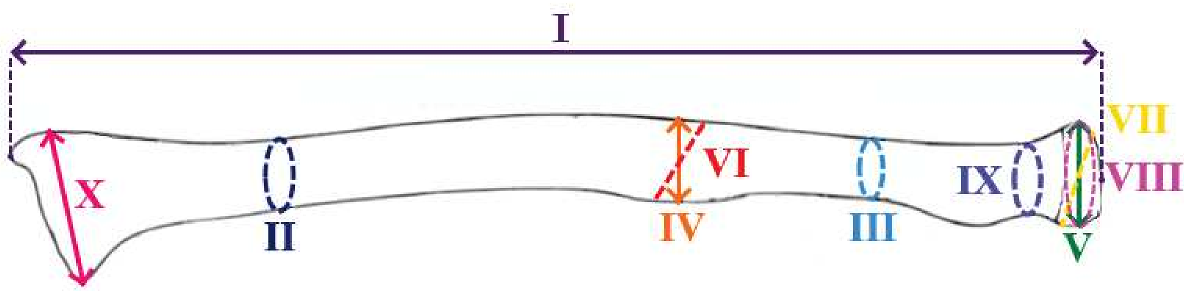

A classical Logistic Regression (LR) was used to model two mutually exclusive classes of a dichotomous dependent variable, implemented with stepwise variable selection and models that optimally separated sexes (negative values correspond to females, positive to males). Then two machine-learning (Support vector machines SVM and decision trees C4.5) algorithms were employed so that data was revaluated in cycles to increase accuracy levels.

Among the single measurements, **Measurement VII** obtained the highest overall accuracy rate (82 % to 93.7%) when used in the **SVM2** equation (see **Table 13**). Classification functions for the multivariable models with similar results were **LR** (89.3-93.4%) and **SVM** (88.7-93.7%)). Both equations were evaluated under cross-validation and presented low bias and high accuracy scores.

The most accurate classification functions employ the variables **MLR-Measurement I**, **HCR-Measurement VIII** and **MCDDR-Measurement II**. Accounting for accuracy and bias, the best classification functions are **LR3**, **LR4**, **LR6**, and **SVM4** (see **Table 13**). From these equations, **LR4** and **LR5** seem to be the most stable (since they do not need to be adjusted for inter- or intrapopulation patterns of sexual dimorphism).

Square K51 produced only one complete -but highly fragmented- radius (*K51-1491A*) belonging to a fully matured individual. This element allowed for the collection of most measurements, but results must consider the possible loss of bone tissue each postmortem fracture.

Table 13. Multivariate classification functions obtained for the radius. Each measurement is modified under its new nomenclature on GMS database (Curate et al., 2021b, p. 101790(4)).

Model	Classification Function
LR1	(0.157 × **MI**) + (0.424 × **MVIII**) - 61.899
LR2	(0.142 × **MI**) + (0.264 × **MVIII**) + (0.467 × **MII**) - 65.743
LR3	(0.133 × **MI**) + (0.237 × **MVIII**) + (0.409 × **MII**) + (0.275 × **MX**) - 68.280
LR4	(0.131 × **MI**) + (0.301 × **MVIII**) + (0.495 × **MII**) + (0.254 × **MX**) + (-0.136 × **MIX**) - 68.568
LR5	(0.559 × **MII**) + (0.700 × **MX**) - 42.223
LR6	(0.558 × **MVIII**) + (0.456 × **MVII**) + (-0.247 × **MV**) - 39.905
SVM1	(0.101 × **MI**) + (0.283 × **MVIII**)-40.526
SVM2	(0.094 × **MI**) + (0.178 × **MVIII**) + (0.270 × **MII**)-42.303
SVM3	(0.093 × **MI**) + (0.159 × **MVIII**) + (0.265 × **MII**) + (0.107 × **MX**) - 43.819
SVM4	(0.098 × **MI**) + (0.181 × **MVIII**) + (0.293 × **MII**) + (0.111 × **MX**) + (-0.053 × **MIX**) - 45.248
SVM5	(0.286 × **MII**) + (0.572 × **MX**) - 28.167
SVM6	(0.251 × **MVIII**) + (0.497 × **MVII**) + (-0.002 × **MV**) - 45.248

Measurements on Carpals

The dimorphic features of carpals, and their importance in sex allocation studies, started to be addressed recurrently over the last decade of the 1900, which catapulted a series of studies focused on their characterization and the creation of reliable and accurate methodologies (Sulzmann et al., 2008). While the use of discriminant function analysis has the advantage of creating a method that can be easily applied, reduces significantly any subjective judgement, and reduces the experience needed to allocate sex, it may only be applied in populations that are considered similar to the ones from which the original data was extracted (Mastrangelo et al., 2011).

Paola Mastrangelo and their team performed a discriminant function analysis for Mediterranean populations, starting with the Identified Collection of the University of

Granada (Spain). The population was comprised of 50 males and 50 females that died between 1962 and 1976. Their age at the time of death, sex, and provenience was well documented. Although this study was not performed directly on Portuguese populations, Spain is a close neighbour to Portugal. Although it is very likely that the geographic (and chronological) distance between Gruta do Morgado Superior's population and the one kept at the University of Granada affects the results, the methodology was still chosen since it bears similarities to previous 20th Century Portuguese collections that have been used in previous sections.

The measurements taken for each carpal followed Sulzman's and team description (2008), which in turn took after Martin and Saller (1957) parameters. The statistical analysis utilized SPSS v.15 software. Normality was tested using non-parametric Kolmogorov-Smirnov test, outliers identified and eliminated if corresponding to an error, and a final *t*-test for independent samples was used to establish the existence and direction of any asymmetry. A stepwise method was used for the selection of variables, and discriminant functions were created for the most statistically significant variables on each carpal. As Sulzmann did before, some measurements were kept in case the analysed element was fragmented or deteriorated, regardless of their dimorphic level (Mastrangelo et al., 2011).

The sex of an unknown specimen can be estimated by multiplying the value of each variable with its corresponding unstandardized coefficient, summing them, and adding the constant. If the score is greater than the demarking point (which is different for each bone), the individual was probably male, whereas if the score is lower it was probably a female (Mastrangelo et al., 2011). The main structure of the equation is as follows:

$$y = [\sum (x_1 \times UC_1) + (x_2 \times UC_2) \dots (x_n \times UC_n)] + K$$

Where x is the measurement, UC is the unstandardized coefficient and K is the constant (which varies with each equation). The comparison with the demarking point may result in less reliable results if the final number is too close to it.

A complete description of each carpal measurement and their visual guides can be seen in **Figure 50**, **Table 14**, **Table 15**, **Figure 51**, **Table 16**, **Table 17**, **Figure 52**, **Table 18**, **Table 19**, **Figure 53**, **Table 20**, and **Table 21**). It is worth noting that each measurement was renamed to fit Gruta do Morgado Superior's methodology. Whenever the measurement presented categorical differences between Sulzmann's and Mastrangelo's teams, the distinction was kept within a parenthesis "**()**".

Mastrangelo's team obtained several univariate equations with an accuracy over 80% for the lunate (5), scaphoid (3), triquetral (8), capitate (4), hamate (4), pisiform (2), trapezium (6) and trapezoid (5).

The lunate displayed the highest dimorphic features, considering all the measurements got a high accuracy score when allocating sex. Conversely, the scaphoid produced the lowest accuracies rates when analysing the length of its tubercle (Measurement IV), and the length and width of the capitate facet (**Measurement V** and **VI**) (Mastrangelo et al., 2011).

Figure 50. Visual guide for the measurements of the lunate (left) and scaphoid (right) (Sulzmann et al., 2008, pp. 253-254, slightly modified).

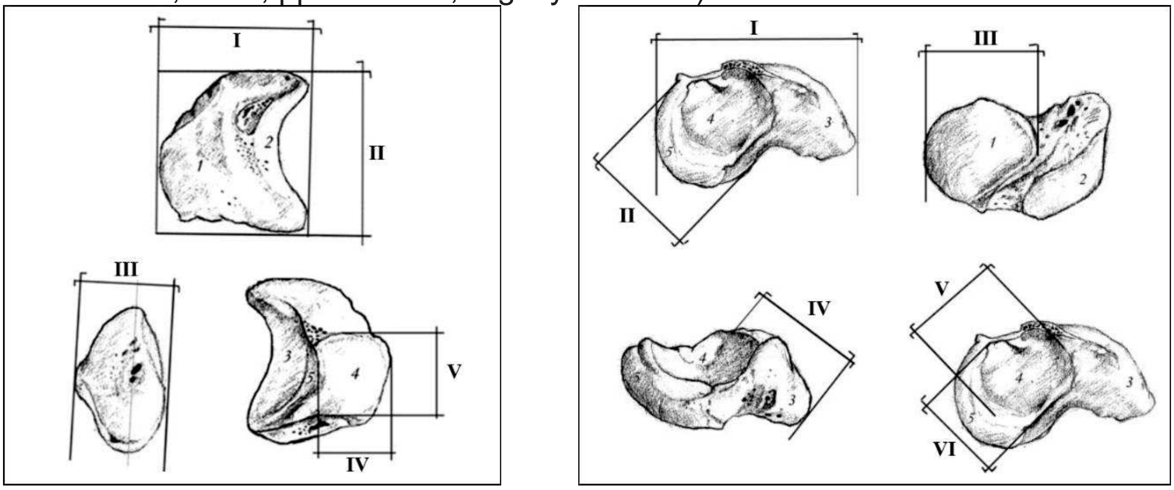

Table 14. Measurements taken for the lunate (Sulzmann et al., 2008, p. 253).

Database ID	Original ID	Description
I	A	**Maximum Length of the Lunate**: place the two eminences flat against one of the calliper arms and close the other arm on the most extended point on the rounded medial side.
II	B	**Maximum width**: Place the calliper arms on the projecting palmar and dorsal points of the horns. Move the calliper arms, pivoting on the most palmar and dorsal points of the carpal, until the maximum height is gained.
III	C	**Maximum width of the dorsal horn**: Hold the lunate in a dorsal view and place the calliper arms on the most projecting proximal and distal points either side of the dorsal horn, keeping the most lateral and medial points in a vertical plane with the calliper arms.
IV	D	**Maximum width of triquetral facet**: Place one calliper arm against the most projecting point of the triquetral facet on the medial rounded edge and then place the other horizontally across from that point laterally where the hamate facet meets the triquetral facet.
V	E	**Height of triquetral facet**: Orientate the callipers so that the maximum height of the facet is gained; from the base (palmar direction) to the top of the facet (dorsal direction).

Table 15. Measurements taken for the scaphoid (Sulzmann et al., 2008, p. 253).

Database ID	Original ID	Description
I	A	**Maximum length**: Place the tip of the tubercle against one calliper arm and the medial lunate facet against the other and then rotate the callipers until the maximum length is gained.
II	B	**Maximum width**: Place the calliper arms against the most projecting points either side of the scaphoid body and rotate the calliper arms until the maximum width is gained.
III	C	**Maximum length of radius facet:** Measured from the medial base of the body where the lunate articulates to the top of the radius facet laterally near the tubercle. Rotation is not usually required for this measurement.
IV	D	**Maximum length of scaphoid tubercle**: Place on calliper arm against the tip of the tubercle and the other against the ascending point of the tubercle, where it meets the capitate facet. The observer must turn the scaphoid on its side and measure from the crest of the tubercle near the capitate facet to the most projecting end of the tubercle.
V	E	**Maximum Length of capitate facet** Orientate the callipers so that they give the maximum length of the facet. Measured from the highest part of the rim of the facet at the medial base of the body to the highest part of the lateral rim near the tubercle. If the edge of the rim is not clear, then the observer should angle the scaphoid to increase the clarity of the landmarks.

Database ID	Original ID	Description
VI	F	**Maximum width of capitate facet**: place the calliper arms so that they are either side of the facet at the maximum points, perpendicular to the length of the scaphoid. This measurement is taken usually in the middle of the facet; however, individual variation can complicate the taking of this measurement. In most scaphoids, the widest point of the facet is in the middle, however in some cases, the widest point is at the base of the facet near the lunate facet. Regardless of the variation in the capitate facet

The triquetral's measurements had high accuracy rates for most of its variables except for the maximum width of the hamate facet (**Measurement IX**). The capitate had low accuracy rates when considering the maximum width of the head (alone) (measurement III), the maximum length and width of the distal base (**Measurement IV** and **V**) (Mastrangelo et al., 2011).

Figure 51. Visual guide for the measurements of the triquetral (left) and capitate (right) (Sulzmann et al., 2008, pp. 254-255, slightly modified).

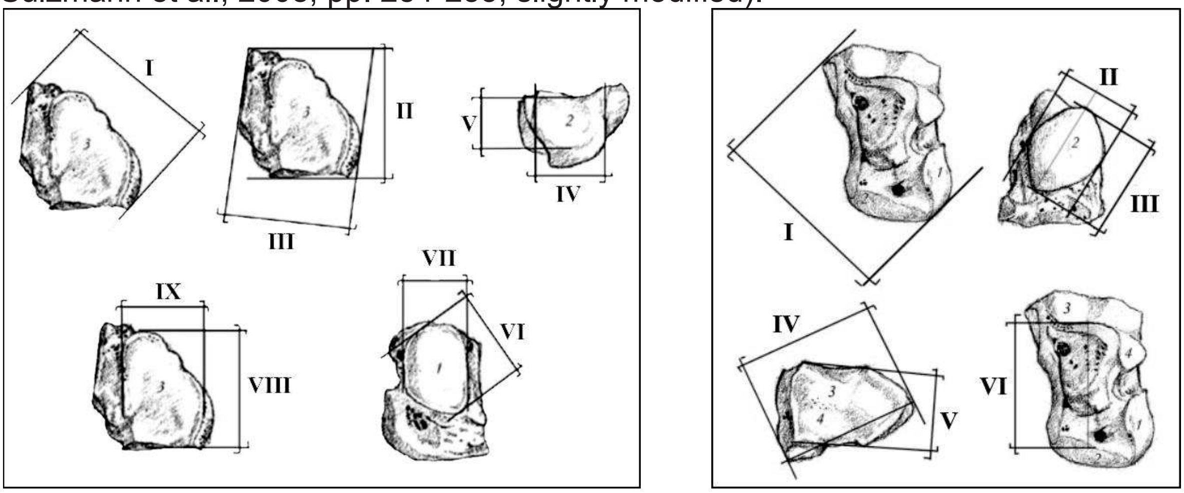

Table 16. Measurements taken for the triquetral (Sulzmann et al., 2008, pp. 253-254).

Database ID	Original ID	Description
I	A	**Maximum length**: Orientate the callipers so that the maximum length of the carpal is gained; place one calliper arm against the most projecting proximal point near the lunate facet and the other arm near the top of the pisiform facet distally. Rotation of the callipers may be required to gain the maximum length.
II	B	**Maximum heigh**t: Place the lunate facet flat against one arm of the callipers and the most projecting point thereafter against the other arm. No rotation of the calliper arms is required for this measurement.
III	C	**Maximum width**: Place the palmar pisiform facet flat against one calliper arm and the most projecting dorsal point thereafter against the other arm. Rotation of the calliper arms may be required to obtain the maximum width.
IV	D	**Maximum length of lunate facet**: Orientate the callipers so that the maximum length of the facet is obtained by placing calliper arms on the palmar to dorsal rims of the facet. Often, particularly in females, the facet border was not well defined, so the observer should angle the carpal to observe the rim of the facet to measure.
V	E	**Maximum width of lunate facet**: Orientate the callipers so that the maximum width of the facet is obtained by placing the calliper arms on the medial rim (which connects to the hamate facet) and the lateral rim of the facet. Like measurement (D-IV) the observer may have to angle the carpal to observe the rim of the facet if the border cannot be seen.

Database ID	Original ID	Description
VI	F	**Maximum length of pisiform facet**: Place the calliper arms on the most projecting points of the facet, normally in a diagonal plane.
VII	G	**Maximum width of pisiform facet**: Place the calliper arms on the most projecting points of the facet in a horizontal plane.
VIII	H	**Maximum height of hamate facet**: Orientate the callipers so that one arm is on the border between the lunate and hamate facets and the other is at the distal peak of the hamate facet to obtain maximum height.
IX	I	**Maximum width of hamate facet**: Place one calliper arm against the most projecting dorsal point of the facet and place the other arm against the point horizontal from the first arm, on the palmar side, where the facet ends.

Table 17. Measurements taken for the capitate (Sulzmann et al., 2008, pp. 254-255).

Database ID	Original ID	Description
I	A	**Maximum height**: Place the arms of the callipers on the most projecting point of the proximal capitate head and on the distal styloid process. Rotation of the calliper arms may be necessary to obtain the maximum height.
II	B	**Minimum width of head**: Hold the capitate in a proximal view and place one calliper arm against the projecting part of the head adjacent to the tuberosity, and the other calliper arm to the opposite side to give the minimum width. Rotation of the callipers will be necessary.
III	C	**Maximum width of head**: Place one calliper arm against the projecting point of the head that is above the styloid process and the other on the opposite side to give the maximum width. This should be perpendicular to measurement (B-II) and will require rotation of the calliper arms.
IV	D	**Maximum length of distal base**: Place one arm of the callipers against the base below the palmar tuberosity and the other arm against the most projecting dorsal point opposite. Rotation of the callipers may be necessary.
V	E	**Maximum width of distal base**: Place one arm of the callipers flat against the medial metacarpal III facet and the other against the lateral metacarpal II facet on opposite sides to give maximum width. Rotation of the calliper arms is usually not required.
VI	F	**Length of tuberosity**: Orientate the callipers to give the length of the tuberosity; measuring in the midline of the tuberosity from the proximal point of the lunate facet rim to the distal end of the tuberosity on the rim of the metacarpal III facet. Always measure with the tuberosity vertical to the callipers.

From the seven measurements from the hamate, equations that considered the maximum width (**Measurement II**), the height of the body (**Measurement III**), the maximum width of the hamulus (**Measurement IV**) and the maximum width of the distal facets (**Measurement V**) performed under 80% accuracy. The pisiform's maximum height (**Measurement I**) and maximum width (**Measurement II**) did not surpass the 80% success rate mark (Mastrangelo et al., 2011).

As previously mentioned (see numeral **3.3.10.1**), the pisiform is one of the last carpal bones to ossify, and it is considered a sesamoid bone along the ones that sprout on the thumb and the fifth digit. However, its late appearance predates the advent of puberty on both female and male individuals, which does not explain its low dimorphic score. Mastrangelo suggests that sexual dimorphism is directly linked the bone's biomechanical contribution on wrist movements, thus rendering the pisiform related only with a specific set, which would explain the results. Other approaches interpret the carpal region as the interaction between three columns: central (composed by the lunate, the capitate, and the hamate), lateral (the scaphoid), and medial (conformed by the triquetral and the pisiform). While the central column manages the wrist precision when controlling grip flexion and extension, the scaphoid and triquetral only move by rotating in central axis.

This effectively exempts the pisiform from a constant interaction with other carpals, making it less susceptible to morphological changes. In Gruta do Morgado Superior the pisiform was a common finding, more so in juvenile individuals where it presented faded contours.

Figure 52. Visual guide for the measurements of the hamate (left) and pisiform (right) (Sulzmann et al., 2008, pp. 255-256, slightly modified).

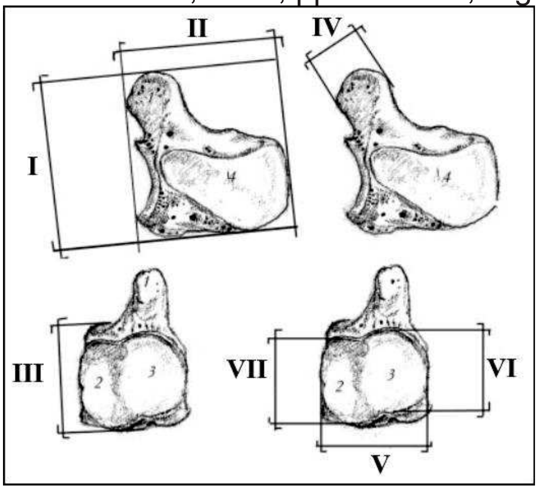

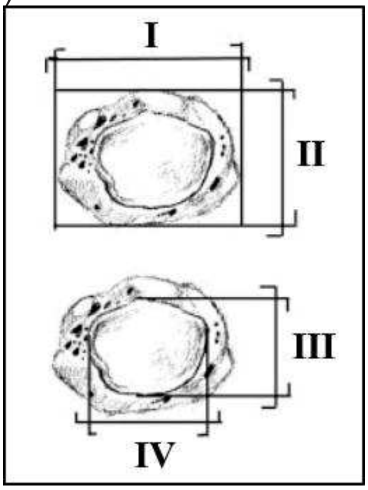

Table 18. Measurements taken for the hamate (Sulzmann et al., 2008, pp. 255-256).

Database ID	Original ID	Description
I	A	**Maximum height**: Place the dorsal base of the hamate flat against one arm of the callipers then place the other arm on the highest palmar point of the hamulus. The dorsal base of the hamate can often be undulating, however, by adjusting the placement of the callipers the observer can always measure the maximum height.
II	B	**Maximum width**: Place the most projecting point of the palmar hamulus and the dorsal base of the hamate against one arm of the callipers and place the other arm against the most projecting proximal point.
III	c	**Height of the body**: With the capitate facet facing towards you place one arm on the dorsal base of the hamate and the other arm on the highest point of the body excluding the hamulus. This measurement was designed to be used if the hamulus was missing and measurement (A-I) and (B-II) could no longer be taken.
IV	D	**Maximum width of the hamulus**: Place the calliper arms on either side of the widest points of the hamulus. Rotate the callipers to gain the maximum width.
V	E	**Maximum width of the distal facets**: Orientate the callipers from the medial rim of MC V facet to the lateral rim of MC IV facet so that the maxi- mum width of the two facets is obtained.
VI	F	**Height of metacarpal V facet**: Place one arm of the callipers at the top of the MC V facet nearest the palmar hamulus and the other arm at the bottom of the facet near the dorsal side.
VII	G	**Height of metacarpal IV facet**: Place one arm of the callipers at the top of the MC IV facet, at the top of the body (palmar side) and the other arm at the bottom of the facet (dorsal side).

Table 19. Measurements taken for the pisiform (Sulzmann et al., 2008, p. 256).

Database ID	Original ID	Description
I	A	**Maximum length (height in Mastrangelo (2011))**: Orientate callipers so that the maximum length is obtained.
II	B	**Maximum width**: Orientate callipers so that the maximum width perpendicular to measurement (A-I) is obtained.
III	C	**Height of triquetral facet**: Place one calliper arm against the base of the facet and the other at the highest point of the facet on the opposite side. This is the shorter of the two measurements of the facet.
IV	D	**Width of triquetral facet**: Place the calliper arms against the most projecting points of the sides of the facets to obtain the width. This is the longer of the two measurements of the facet and is made perpendicular to measurement (C-III).

The trapezium's maximum height (**Measurement II**) and the width of the scaphoid facet (**Measurement VII**) could not provide a univariable equation with an accuracy over 80%. The trapezoid's result was similar with univariable equations performed on the length of its dorsal surface (**Measurement II**) and its mid width (**Measurement V**).

Figure 53. Visual guide for the measurements of the trapezium (left) and trapezoid (right) (Sulzmann et al., 2008, pp. 256-257, slightly modified).

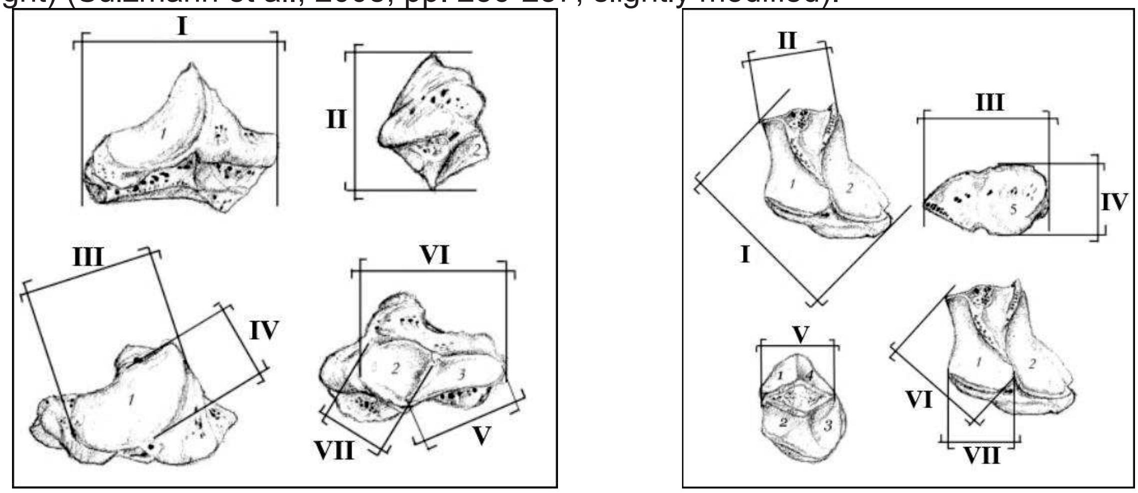

Table 20. Measurements taken for the trapezium (Sulzmann et al., 2008, p. 256).

Database ID	Original ID	Description
I	A	**Maximum length**: Place one calliper arm against the most projecting distal point of the MC II facet and the other against the projecting proximal point of the palmar ridge to obtain maximum length.
II	B	**(Maximum) Height**: Hold the trapezium so that the MC I facet is superior, then place one calliper arm on the most superior point at the top of the MCI facet and the other on the most inferior point where the trapezoid and scaphoid facets meet.
III	C	**Maximum length of MC I facet**: Orientate callipers so that the maximum length is obtained; place one arm on the edge of the facet near the distal MC II facet and the other arm on the opposite side on the most projecting point. Rotation of the trapezium may be necessary.
IV	D	**Maximum width of MC I facet**: Place the calliper arms against the widest points of the facet, which is normally at the proximal end of the trapezium.

Database ID	Original ID	Description
V	E	**Maximum length of trapezoid facet**: Place one calliper arm against the most projecting edge of the trapezoid facet near the distal MC II facet and the other at the furthest proximal palmar edge, on the border between the trapezoid and scaphoid facet.
VI	F	**Maximum length of trapezoid and scaphoid facets**: Place the calliper arms on the most projecting points of the trapezoid facet near the distal MC II facet and proximal edge of the scaphoid facets. Rotation of the trapezium may be required.
VII	G	**Width of scaphoid facet**: Place one calliper arm on the border between the trapezoid facet and the scaphoid facet and the other arm on the most projecting proximal point of the facet opposite.

Table 21. Measurements taken for the trapezoid (Sulzmann et al., 2008, p. 256).

Database ID	Original ID	Description
I	A	**Maximum height**: Place one calliper arm against the most projecting medial tip of the 'toe of the boot' and the other on the most projecting point away from that on the palmar 'neck of the boot.'
II	B	**Length of dorsal surface**: Place the carpal on the table with the trapezium and MC II facet facing superior and measure the 'neck of the boot,' which is the longest distance medial to lateral on the palmar surface.
III	C	**Length of palmar surface**: Place one calliper arm against the most projecting medial point 'the toe of the boot' and the other arm against the most projecting lateral point on the opposite side 'the heel of the boot.'
IV	D	**Width of the dorsal surface**: Place the calliper arms against the most projecting distal and proximal points of the dorsal surface to obtain the width. This is perpendicular to measurement (C-III).
V	E	**Mid width**: Place the calliper arms around the 'ankle of the boot' at the widest distal and proximal points.
VI	F	**Maximum length of trapezium facet**: Place one calliper arm at the highest point of the facet near the 'neck of the boot' and the other on the lowest border between the trapezium facet and the MC II facet.
VII	G	**Maximum width of trapezium facet**: Place one calliper arm against the top of the border of the MC II and trapezium facet and the other arm on the corner of the facet near the 'heel of the boot.'

Overall, the lunate achieved the best results when looking at isolated variables, with four of them having score rates over 90% (**Measurement II**, **III**, **IV**, and **V**). The triquetral achieved a similar result with **Measurement IV**, **V**, **VI** and **VII**. The pisiform obtained a similar success rate with measurement **IV**. Lastly, the trapezium performed similarly when measurements **III**, **IV** and **V**.

All the univariate equations present in Mastrangelo's paper were not chosen for the analysis of the material at Gruta do Morgado Superior, given the sheer amount of data that would have resulted from their application on each bone. However, the best performing univariate equation for each bone was used (**Sex_II**), as a control datum for comparison with the multivariate equations. Conversely, analysis on the hamate and pisiform used their second-best equation as control datum, because they did not yield a better multivariate equation.

Carpals provided the highest accuracy ranges when combining groups of measurements in multivariate equations: the lunate obtained a 98% success rate when using the *Maximum width of the dorsal horn* (**III**), the *Maximum width of the triquetral facet* (**IV**), and the *Height of the triquetral facet* (**V**); the scaphoid's best rate (90.1%) was achieved when combining its *Maximum length* (**I**) and the *Maximum length of its tubercle*

(**IV**); the triquetral displayed outstanding results (94.1% accuracy) when combining the *Maximum width of its facet for the lunate* (**V**), the *Maximum width of its pisiform facet* (**VII**), and the *Maximum height of its hamate facet* (**VIII**); the capitate performed at its best (88.3% accuracy) when combining the *Maximum width of the head* (**III**) and the *Length of its tuberosity* (**VI**); the hamate and pisiform achieved their best performance with only one variable (90.7 and 88.2% respectively), being the *Height of the MCV facet* (**VI**) for the former and the *Height of the triquetral facet* for the latter (**III**); the trapezium performed well when combining the *Maximum length of the MCI* facet (**III**) and the *Width of the scaphoid facet* (**VII**), reaching 97.1% accuracy; lastly, the trapezoid reached 93.7% accuracy when joining measurements for the *Length of the dorsal surface* (**II**), the *Width of the dorsal surface* (**IV**), and the *Maximum length of the trapezium facet* (**VI**) (Mastrangelo et al., 2011). The best results were achieved with the lunate and the trapezium, while most other carpals had a success rate above 90%. The only carpals that have lower values than 90% were the capitate and the pisiform, with accuracy rates of about 88% (see **Table 22**).

When compared to the univariate equations, multivariate equations provide more robust results utilising measurements on high dimorphic features, that raise the overall performance of carpal. For elements as the scaphoid and trapezoid a much better result was obtained through multivariate analysis. Other bones such as the capitate did not improve the accuracy rate much. For this reason, the main set of equations that were implemented in Gruta do Morgado Superior were the multivariate ones.

Table 22. Multivariant stepwise discriminant function with an accuracy over 80% (Mastrangelo et al., 2011, p. 216.e218, Table 5, slightly modified with new names for the measurements.).

Carpal	Var.	Unstandardized coefficient	Constant	Demarking point (mm)	Group centroid	Acc. (%)
Lunate	**III**	0.332	-12.515	p = -0.191	M = 1.696 F =-2.078	98.9
	IV	0.459				
	V	0.625				
Scaphoid	**I**	0.468	-15.008	p = -0.3415	M = 0.95 F = -1.217	90.1
	IV	0.202				
Triquetral	**V**	0.376	-14.279	p = -0.55	M = 1.49 F = -2.59	94.1
	VIII	0.519				
	VII	0.753				
Capitate	**III**	0.553	-15.090	p = -0.0665	M = 0.83 F = -0.963	88.3
	VI	0.524				
Hamate	**VI**	1.246	-12.514	p = -0.0185	M = 0.782 F =-0.819	90.7
Pisiform	**III**	1.214	-9.002	p = -0.281	M = 0.778 F = -1.34	88.2
Trapezium	**III**	0.643	-14.156	p = -0.335	M = 1.086 F = -2.553	97.1
	VII	0.615				
Trapezoid	**II**	0.486	-20.455	p = -0.3145	M = 1.147 F = -1.776	93.7
	IV	0.775				
	VI	0.534				

When the carpal bone did not display a topography consistent with a mature individual (probably juvenile), measurements were not considered for this study. Juvenile individuals display faint features which are too diluted or not developed enough to obtain reliable results. The fact that most sex allocation methods intrinsically imply that female features are by default smaller than those of males will inevitably result in a misclassification of juveniles as females.

Measurements on the Fibula

The fibula has not enjoyed the same attention than other skeletal elements among Portuguese researchers. The closest one was performed by Madeleine Lamer and their team (2021), who tested K.E. Stull research group's method for sex allocation in juvenile individuals (around 13 years old) utilizing bone measurements in diaphyseal length in long bones from upper and lower limbs, metaphyseal breadth of radius and tibia, distal metaphyseal breath of the humerus, radius, femur and tibia, and midshaft breadth of the ulna. The research's main objective was to evaluate the transportability of the formulas proposed by Stull using the collection curated at the National Museum of Natural History and Sciences in Lisbon. The results were underwhelming, and the authors concluded that new FDA equations must be drawn from local populations, so they can be properly used.

From the methodologies that use the fibula's measurements in a similar fashion to the ones exposed for upper limbs and carpals, only one foreign document stood out. Akin to Stull's population origin (Africa), the findings published by Akihiko Sacragi and Toshiko Ikeda for sex allocation using the the distal fibula were extracted from a Japanese collection. This methodology has not been tested in Portuguese (historical) populations, reason why the measurements were taken for Gruta do Morgado Superior in case such study is developed in the coming years. Their discriminant function was calculated as:

$$y = -40.54 + (0.478 \times \boldsymbol{MI}) - (0.41 \times \boldsymbol{MII}) + (0.377 \times \boldsymbol{MIII}) + (0.896 \times \boldsymbol{MIV}) + (0.923 \times \boldsymbol{MV})$$

All measurements are centred in the malleolar articular surface when assigning a letter to each apex: the anterosuperior one was denominated Apex A, the inferior's apex was designated as Apex B, while the posterosuperior apex was named Apex C. If the area is considered a triangle, its sides would be AB, BC, and AC. Thus, **MI** is the measurement from Apex A to the midpoint on side BC, **MII** is the measurement from Apex B to the midpoint of side AC, and **MIII** is the measurement from Apex C to the midpoint of side AB. Measurement IV (**MIV**) is the length of the lateral malleolus (LLM) and goes from Apex A to the apical point of the lateral malleolus. Measurement V (**MV**) is calculated by assessing the bilateral diameter of the lateral malleolar fossa (LMF) (see **Figure 54**).

Sacragi and Ikeda warn that the method performs better when all measurements are used in conjunction. In Gruta do Morgado superior, Square K51, the apical point of the malleolus was usually missing from the distal section of the fibula, with only one complete enough to carry out the method (*K51-2712*). Its measurements were 19, 23, 20, 9 and 29 (for each measurement) with a result using the discriminant function of 1.483. When comparing with the mean, minimum and maximum values for males in the study, the lengths were well within the ranges of a male individual. This outcome was not included in the results section due to the chronological, genetical, and geographical distances between Japanese and Portuguese populations, and the lack of explicit centroids for interpretation in Sacragi and Ikeda's paper.

Figure 54. Measurements taken for the distal fibula according to Sacragi and Ikeda (1995) (Original picture found in White & Folkens, 2005, p. 265 and 266, only the areas needed were taken, slightly modified).

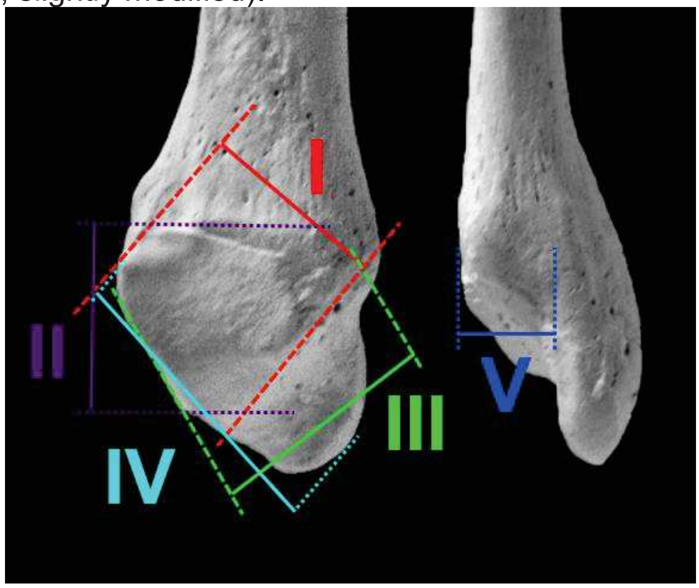

Measurements on Tarsals and Metatarsals

The use of metatarsals for sex allocation in incomplete or fragmentary archaeological collections has a high potential due to the elements' intrinsic trabecular strength, resistance to taphonomic alterations and inherent sexual dimorphism. Said potential has been recognized by several authors (Steele, 1976; Silva, 1995, Bidmos & Dayal, 2003; Gualdi-Russo, 2007; Robinson et al., 2008; DiMichele & Spradley, 2012; Harris & Case, 2012; Mahakkanukrauh et al., 2014, Navega et al., 2015; Peckmann et al., 2015; Alonso-Llamazares & Pablos, 2019; Scorrentino et al., 2020; cited in Curate et al. (2021a, P. 74)). Specific methodologies have been either tested or developed for Portuguese populations using the talus, calcaneus, cuboid, navicular, and the three cuneiforms.

Measurements on the Talus and the Calcaneus

Portuguese historical collections have been used before to construct sex allocation methodologies that are focused on the talus and the calcaneus. Two of the most outstanding works include the papers from Ana María Silva (1995) and David Navega and their team (2015). The latest work on the subject emerged in 2021 by Francisco Curate and their team, providing a specific methodology that used univariable and multivariable models for sex allocation and creating a free electronic tool for researchers (CalcTalus) (Curate et al., 2021a).

Curate and their team used anthropometric variables that followed Martin's (1928) guidelines for both bones, while adding some from Steele's (1976) own descriptions for the calcaneus. All the measurements described in this study were utilized and renamed in Gruta de Morgado Superior (see **Table 23**, **Table 24**, **Figure 55**, and **Figure 56**). Raw data was collected from a Portuguese historical sample (93 females and 87 males) that belongs to the Coimbra Identified Skeletal Collection (CISC). The population was born between1827 and 1913 and died from 1910 to 1936. It is very likely that the people within the collection lived in underprivileged economic conditions.

Table 23. Talus' measurements (Curate et al., 2021a, Annex I). The measurements taken for this study and their denomination are in bold, after the description.

Database ID	Measurement	Description
I	**Talus Maximum Length**	**TM1** From the *M. flexor hallucis* longus groove to the most anterior point on the head measured parallel to the sagittal axis of the trochlea (Martin, 1928). Analog to Talar Length in White et al.(2012, P.284). **Measurement I** in Database.
II	**Talus Width**	**TM2** Maximum projected line laterally/medially perpendicular to the sagittal plane. The lateral point is the most lateral point on the articular surface for the lateral malleolus and the line generally bisects the articular surface for the tibia slightly forward of the midpoint (Martin, 1928). **Measurement II** in Database.
III	**Talus Body Height**	**TM3** Height of the body along the sagittal plane, taking above the articular surface for the tibia. The measurement is taken by placing the talus on a flat surface (Martin, 1928). **Measurement III** in Database.
IV	**Talus Maximum Body Height**	**TM3a** Maximum height of the body in an inferior/medially perpendicular to the sagittal plane. The measurement is taken by placing the talus on a flat surface and then determining the most superior point of the articular surface for the tibia. The superior point is generally along the medial rim of the facet (Martin, 1928). **Measurement IV** in Database.
V	**Maximum Length of the Talar Trochlea**	**TM4** Maximum length of the trochlear articular surface on the midline measured parallel to the sagittal axis of the trochlea (Martin, 1928). **Measurement V** in Database.
VI	**Maximum Width of the Talar Trochlea**	**TM5** From the mid-lateral edge of the trochlea to its mid-medial edge measured perpendicular to the sagittal plane of the trochlea (Martin, 1928). **Measurement VI** in Database.

Figure 55. Variables measured in the talus: Superior view (*left*): talus maximum length (MI), talus width (MII), maximum length of the talar trochlea (MV), and maximum width of the talar trochlea (MVI); Anterior view (*right*): talus body height (MIII), and talus maximum body height (MIV) (Curate et al., 2021a, p. 74(2-3) Figures 1 and 2, slightly modified).

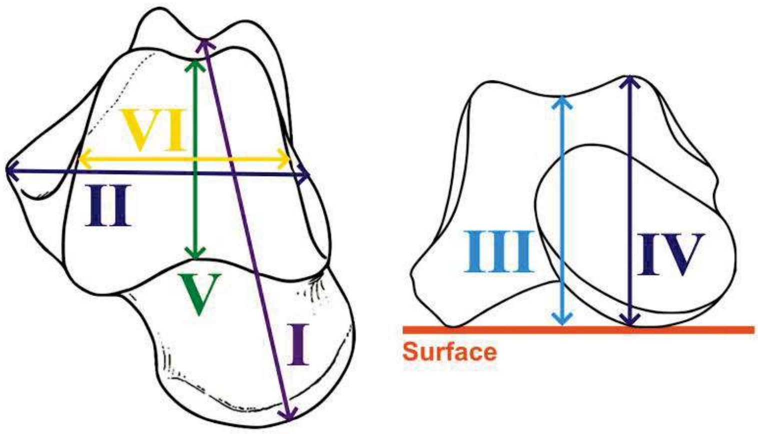

Table 24. Calcaneus' measurements (Curate et al., 2021a, P. 74). The measurements taken for this study and their denomination are in bold, after the description. The table was created with the information in the paper.

Abbr.	Measurement	Description
I	**Calcaneus Maximum Length**	**CM1** Projected line from the most posterior point of the tuberosity of the calcaneus to the most anterior/superior point of the cuboidal facet (Martin, 1928). Analog to White et al. Maximum Calcaneal Length (2012, P.283).
II	**Calcaneus Length**	**CM1a** Projected line from the most posterior point of the tuberosity of the calcaneus to the mid-point of the cuboidal facet (Martin, 1928).
III	**Calcaneus Load Arm Width**	**CM2** Transverse projected line perpendicular to the long axis from the most lateral point of the posterior articular surface to the most medial point of the *sustentaculum tali* (Martin, 1928).
IV	**Calcaneus Load Arm Length**	**CLAL** Projected line from the most posterior point of the posterior articular surface for the talus, to the most anterior/superior point of the cuboidal facet (Slal, according to Steele (1976).
V	**Calcaneus Body Height**	**CM4** Projected height from the most inferior point of the tuberosity of the calcaneus to the most inferior point of the body of the calcaneus (Martin, 1928).
VI	**Calcaneus Maximum Body Height**	**CMBH** Greatest projected height of the calcaneus and measured from the most inferior point of the tuberosity of the calcaneus to the most superior point of the posterior facet of the calcaneus (slightly modified from Steele (1976).
VII	**Calcaneus Body Length**	**CM5** Projected line from the most superior point of the tuber calcanei to the most distally point of the posterior facet of the calcaneus, measured parallel to the sagittal axis of the bone (Martin, 1928). Analog to White et al. Posterior Calcaneal Length (2012, P.283).
VIII	***Tuber calcanei* Height**	**CM7** Greatest projected height of the tuber calcanei, measured from the most superior point of the *tuber calcanei* to the most inferior point of the *Processus medialis tuberis calcanei* (Martin, 1928).
IX	***Tuber calcanei* Width**	**CM8** Projected line laterally/medially of the tuber calcanei, perpendicular to the sagittal plane (Martin, 1928).

Figure 56. Variables measured in the calcaneus: lateral view (*left*) and superior view (*right*) (Curate et al., 2021a, p. 74(73), Figure 3 and 4 slightly modified).

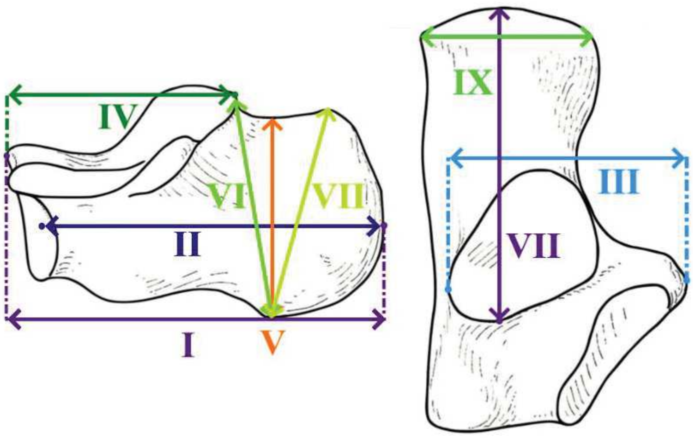

Curate's team deemed that differences in laterality were statistically negligible, although other authors have suggested that such differences must be considered (Harris & Case, 2012). Classical Logistic Regression (LR) modelling was performed on two mutually exclusive classes of a dichotomous dependent variable (male/female). They were implemented with stepwise variable selection and models that optimally separated sexes and two machine-learning.Then they projected a vector of predictors into a higher dimensional plane via linear or non-linear kernel functions, while the C4.5 algorithm generated decision trees. Their results concluded that all metric variables are normally distributed and all of them presented significant dimorphic traits. Accuracy under cross-validation varied from 78.3 to 82.2% (talus) and from 73.6 to 86.4% (calcaneus). The variables with the best overall performance were the talar maximum body height (**Measurement IV**) and the calcaneal load arm length (**Measurement IV**)

The resulting equations produced either negative values that associated with females or positive values that in turn are associated with males (see **Table 25**).

Table 25. Classification functions for univariate and multivariate models and their accuracy rates. LR functions are Logistic Regressions while SVM are support vector machines (Curate et al., 2021a, p. 74(6), Table 3).

Name	(%)	Classification Function
LR_T1	85	(1.005×T**MI**) - 50.925
LR_T2	87.8	(0.844×T**MI**) + (0.498× **TMV**) − 58.351
LR_T3	89.4	(0.665×**TMI**) + (0.494× **TMV**) + (0.471×**TMVI**) -61.487
LR_C1	85.9	(0.768×**CMVI**) −35.837
LR_C2	88.4	(0.562×**CMVI**) +(0.697×**CMIX**) -46.718
LR_TC1 (*)	89.6	(0.856× **TMI**) +(0.531×**CMIX**) − 58.846
LR_TC2 (*)	90.8	(0.741×**TMI**) +(0.374× **TMV**) + (0.443×**CMIX**) − 62.136
LR_TC3 (*)	91.3	(0.993× **TMI**) +(0.417× **TMV**) + (0.581× **CMIX**) − (0.328×**CMVII**) −62.676
LR_TC4 (*)	91.3	(0.863× **TMI**) +(0.577× **TMV**) + (0.824×**CMII**) + (0.533× **CMIX**) − (1.190×**CMVII**) −71.346
LR_TC5 (*)	92.4	(0.585× **MI**) + (0.660× **TMV**) + (0.753×**CMII**) + (0.403×**CMVI**) + (0.504× **CMIX**) − (1.209×**CMVII**) − 71.346
SVM_T1	85	(0.571× **TMI**) − 29.000
SVM_T2	87.8	(0.522× **TMI**) + (0.434× **TMV**) − 40.040
SVM_T3	87.8	(0.463× **TMI**) + (0.359× **TMV**) + (0.334×**MVI**) −43.360
SVM_C1	85.5	(0.571×**CMVI**) −26.714
SVM_C2	87.8	(0.290×**CMVI**) + (0.522×**CMIX**) − 28.955
SVM_TC1 (*)	89	(0.661× **TMI**) + (0.383×**CMIX**) − 44.654
SVM_TC 2 (*)	89	(0.475× **TMI**) + (0.276× **TMV**) + (0.259×**CMIX**) − 40.189
SVM_TC3 (*)	92.5	(0.648× **TMI**) + (0.195× **TMV**) + (0.413×**CMIX**) − (0.195×**CMVII**) −40.993
SVM_TC4 (*)	91.9	(0.495× **TMI**) + (0.296× **TMV**) + (0.519×**CMII**) + (0.259×**CMIX**) − (0.590×**CMVII**) − 46.721
SVM_TC5 (*)	91.9	(0.192× **TMI**) + (0.347× **TMV**) + (0.457×**CMII**) + (0.274×**CMVI**) + (0.396×**CMIX**) − (0.675×**CMVII**) − 40.829

(*) functions that require two bones from the same individual. Not applied at GMS in this study

Curate et al.'s methodology was implemented in Gruta do Morgado Superior similarly to Mastrangelo's: two equations for the variables **Sex_I** and **Sex_II**, both chosen by accuracy rate and type. The talus' chosen univariate equation was **LR_T3** (with accuracy rate of 89.4%) and the multivariate equation was **SMV_T3** (with accuracy rate of 87.8 %). The calcaneus' calculations used the equation **LR_C2** (with accuracy rate of 88.4 %) and the control equation was **SVM_C2** (with accuracy rate of 87.8 %). It is worth noting that multivariate functions with multiple bones have the highest success rate (over 90%), but they require both elements to belong to the same individual. These functions may be applied in the future to the foot bones found in anatomical position (Cruz, 2020). **Square K51's** did not bear any calcaneus or talus in anatomical position.

Measurements on the Cuboid, the Navicular, and the Cuneiforms

Sheena Harris and Troy Case (2012) presented a methodology using all tarsal bones and identifying sexually dimorphic characteristics in each of them. The study used a sample of 160 individuals from European-American males and females curated within the William M. Bass Donated Skeletal collection (Tennessee-Knoxville). These measurements have been praised as they were well documented and illustrated while easily reproducible thanks to the use of relatively accessible tools (osteometric board) (Navega et al., 2015). Harris and Case obtained high accuracy rates, ranging between 88 to 92%. By 2015 David Navega and their team would test this technique on a Portuguese Population (Coimbra Identified Skeletal Collection Sample) and obtain similar rates, achieving an accuracy of 88.3% by using tree-based algorithms. Contrary to Harris and Case, Navega's team would not provide linear regression equations, but instead demonstrate the applicability of statistical packages to create decision-based algorithms that were highly dependent on the presence of two or more tarsals to achieve a robust result.

Navega's team proved that the methodology assessed correctly sexual dimorphism patterns on Portuguese historical populations. Harris and Case's technique relies on measurements on the cuboid, the navicular, the first (medial) cuneiform, the second (intermediate) cuneiform, and the third (lateral) cuneiform. This method proposes additional measurements for the talus and calcaneus that were not considered for implementation. The measurements coincide only with the calcaneal maximum length (**Measurement I**) and talar height (**Measurement IV**), while the talar breadth and height are not consistent with Curate's team study. CalcTalus was chosen over Harris and Case's technique because it more recent, the method provides clear and easily appliable equations, has a more exhaustive approach, and it used Portuguese populations as its base. The measurement's ID in Gruta do Morgado Superior, their original name and descriptions may be seen in **Table 26**, **Table 27**, **Table 28**, **Table 29**, and **Table 30**. Their visual aids for each measurement can be seen in **Figure 57**, **Figure 58**, **Figure 59**, **Figure 60**, and **Figure 61**; all the images represent the osteometric board with purple bars to each side.

Table 26. Cuboid's measurements and their description (Harris & Case, 2012, p. 297).

Database ID	Name	Description
I	Cuboid Length (CubLg)	Place the cuboid on its medial side with the distal end resting against the stationary upright. The distal end should contact the stationary upright at two points. Measure to the most proximal point on the cuboid beak.
II	Cuboid Breadth (CubBrd)	Place the cuboid on its superior surface, with the medial side contacting the stationary upright at two points near the proximal and distal ends. The cuboid tuberosity should point upward. Measure to the most medial point on the medial side.
III	Cuboid Height (CubHt)	Place the cuboid on its lateral side with its long axis approximately perpendicular to the long axis of the board. The superior surface of the cuboid should contact the stationary upright at two points near the proximal and distal ends. Measure to the most inferior point on the beak

Figure 57. Cuboid's measurements visual guide (Harris & Case, 2012, pp. 298-299, modified). From left to right: lateral, superior, and lateral (distal up) views.

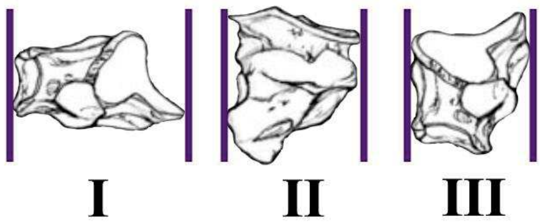

Table 27. Navicular measurements and their description (Harris & Case, 2012, p. 297).

Database ID	Name	Description
I	Navicular Length (NavLg)	Place the navicular with the proximal face against the stationary upright. It should contact the margins of the proximal facet at two points toward the medial and lateral ends. The medial tuberosity should contact the base of the board to the extent possible. Measure to the most distal point with the moveable upright.
II	Navicular Breadth (NavBrd)	Place the navicular on its proximal surface with the long axis of the bone approximately parallel to the long axis of the board. The lateral edge of the bone should contact the board at two points toward the inferior and superior ends. Measure to the navicular tuberosity.

Figure 58. Navicular's measurements visual guide (Harris & Case, 2012, p. 299, modified). From left to right: medial and distal views.

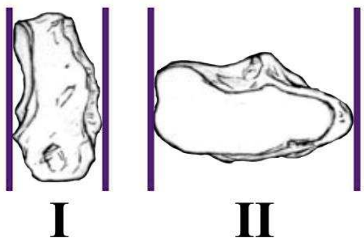

Table 28. First Cuneiform's measurements and their description (Harris & Case, 2012, p. 297).

Database ID	Name	Description
I	First Cuneiform Length (CF1Lg)	Place cuneiform I on its medial surface with the distal end resting against the stationary upright at two points toward the inferior and superior ends. Measure to the inferior edge of the proximal end.
II	First Cuneiform Breadth (CF1Brd)	Place cuneiform I on its distal surface with the medial side of the bone resting against the stationary upright at two points toward the superior and inferior ends. Measure to the most lateral point on the lateral side.
III	First Cuneiform Height (CF1Ht)	Place cuneiform I on its medial surface with the inferior edge resting against the stationary upright at two points toward the proximal and distal ends. Measure to the superior end with the moveable upright.

Figure 59. First Cuneiform's measurements visual guide. (Harris & Case, 2012, p. 299, modified). From left to right: medial, proximal, and medial (distal up) views.

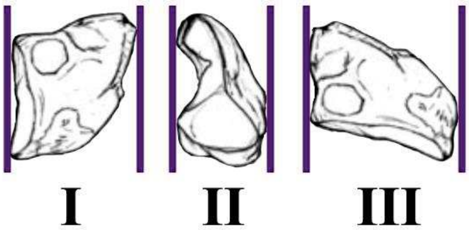

Table 29. Second Cuneiform's measurements and their description (Harris & Case, 2012, p. 297).

Database ID	Name	Description
I	Second Cuneiform Length (CF2Lg)	Place cuneiform II on its lateral side with the proximal end contacting the stationary upright at two points toward the superior and inferior ends. Measure to the distal end with the moveable upright.
II	Second Cuneiform Breadth (CF2Brd)	Place cuneiform II on its proximal end with the lateral edge contacting the stationary upright at two points toward the superior and inferior ends. Measure to the medial side with the moveable upright.
III	Second Cuneiform Height (CF2Ht)	Place cuneiform II on its proximal end with the superior edge contacting the stationary upright at two points toward the medial and lateral sides of the bone. Measure to the inferior edge with the moveable upright.

Figure 60. Second Cuneiform's measurements visual guide. (Harris & Case, 2012, p. 300, modified). From left to right: medial, distal (dorsal down), and distal views.

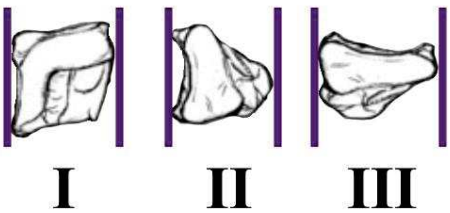

Table 30. Third Cuneiform's measurements and their description (Harris & Case, 2012, p. 297).

Database ID	Name	Description
I	Third Cuneiform Length (CF3Lg)	Place cuneiform III on its medial side with the distal end contacting the stationary upright at two points toward the superior and inferior ends. Measure to the most proximal point on the proximal end.
II	Third Cuneiform Breadth (CF3Brd)	Place cuneiform III on its distal end with the medial side contacting the stationary upright at two points toward the superior half of the bone. Measure to the most lateral point on the lateral side of the bone.
III	Third Cuneiform Height (CF3Ht)	Place cuneiform III on its medial side with the superior end contacting the stationary upright at two points toward the proximal and distal ends. Measure to the inferior edge.

Figure 61. Third Cuneiform's measurements visual guide. (Harris & Case, 2012, p. 300, modified). From left to right: lateral, and proximal (distal down) views.

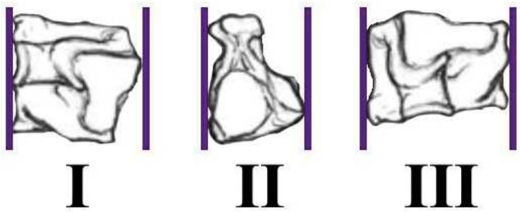

Harris and Case concluded that the highest mean dimorphism can be seen in the talus (13.3%), followed by the second (intermediate) cuneiform at 11.8%, and the cuboid and navicular at 11.3%. The first (medial) cuneiform and the third (lateral cuneiform showcased 11 and 10.5% respectively. Their findings on the calcaneus were modest (9.9%), but this skeletal element was only considered with a single measurement (Talar Maximum length – **MI**) which may have biased the results. Comparing with Curate's findings, this result may hold true as their best equations were obtained when analysing the body length and the *tuber calcanei*'s width.

Logistic regression analysis on complete skeletal elements suggested that bones in the right side tend to have a better accuracy rate than those from the left. Their results have slight variation when treating the original sample differentially according to sex. Univariate equations that performed over an 80% accuracy rate can be seen in **Table 31**. Multivariate equations performed better in most cases (see **Table 32**), except for Cuneiform II (-0.5%) on the left side and Cuneiform III (-0.3%) on the right side.

Harris and Case's study produced equations that include multiple bones of the same specimen, but they will not be showcased here, as Square K51 did not provide with any group of tarsal bones that could successfully be allocated to a single individual.

The multivariate equations were applied as the main sex allocation marker while univariate equations were kept for control.

Table 31. Univariate logistic regressions for one measurement (Harris & Case, 2012, p. 303, modified)

Skeletal Element	Accuracy rate (%)	Equation
Left		
Cuboid	81.7	-34.975 + (1.263***MII)**
Navicular	80.8	-26.248 + (0.655***MII)**
Cuneiform I	81.4	-25.583 + (0.962 ***MI**)
Cuneiform III	81.9	-33.905 + (1.369 ***MI**)
Right		
Cuboid	84.9	-31.695 + (1.137 ***MII**)
Navicular	80.3	-27.737 + (0.694***MII**)
Cuneiform I	86.1	-27.523 + (1.035 ***MI**)
Cuneiform II	82.4	-23.822 + (1.448 ***MII**)
Cuneiform III	85.9	-39.775 + (1.598 ***MI**)

Table 32. Multivariable logistic regression equations for single bones (Harris & Case, 2012, p. 304, modified).

Element	Accuracy rate (%)	Equation
Left		
Cuboid	84.7	-38.732 + 1.052(**MII**) + 0.399(**MIII**)
Navicular	84.1	-28.365 + 0.421(**MI**) + 0.492(**MII**)
Cuneiform I	83.0	-38.884 + 1.219(**MII**) + 0.504(**MIII**)
Cuneiform II	82.4	-36.046 + 1.018(**MI**) + 0.772(**MIII**)
Cuneiform III	82.3	-40.826 + 0.968(**MI**) + 0.702(**MIII**)
Right		
Cuboid	88.5	-36.676 + 1.006(**MII**) + 0.362(**MIII**)
Navicular	83.9	-28.313 + 0.710(**MII**)
Cuneiform I	88.6	-38.600 + 0.623(**MI**) + 1.191(**MII**)
Cuneiform II	86.6	-45.695 + 1.082(**MI**) + 0.623(**MII**) + 0.694(**MIII**)
Cuneiform III	85.6	-44.965 + 1.171(**MI**) + 0.660(**MIII**)

Regarding Portuguese populations, Navega and their team employed machine-learning algorithms that put to the test the inherent dimorphism of tarsal bones with similar allocation success. Their method found that, although the second cuneiform and the navicular present sexually dimorphic features, these were not considered relevant by statistical models when allocating sex. Their best algorithm was the BFT tree (decision) model, with a precision rate of 86.7% for females and 90.8% for males (see **Figure 62**).

Figure 62. BFTree model for sex estimation using tarsal bones. (Navega et al., 2015, p. 657)

```
CalcLg < 77.5
|       TalHt < 29.5: Female : P(Female|X)=0.961
|       TalHt >= 29.5
|       |       CF1Lg < 23.5: Female : P(Male|x)=0.800
|       |       CF1Lg >= 23.5
|       |       |       CF3Brd < 16.5
|       |       |       |       TalBrd < 41.5:Female : P(Female|X)=0.850
|       |       |       |       TalBrd >= 41.5: Male : P(Male|x)=0.600
|       |       |       CF3Brd >= 16.5
|       |       |       |       CalcLg < 74.0:Female : P(Female|X)=1.000
|       |       |       |       CalcLg >= 74.0: Male : P(Male|x)=1.000
CalcLg >=77.5
|       TalLg < 56.5
|       |       CF1Lg < 24.5: Female : P(Female|X)=1.000
|       |       CF1Lg >= 24.5
|       |       |       CubHt < 23.5
|       |       |       |       TalLg < 55.5: P(Male|x)=0.666
|       |       |       |       TalLg >= 55.5: P(Female|X)=1.000
|       |       |       CubHt >= 23.5: Male : P(Male|x)=0.883
|       TalLg >= 56.5:Male P(Male|x)=1.000
```

However, their methodology requires the use of various skeletal pieces and their measurements, making it hard to implement for contexts such as Gruta do Morgado Superior. Navega and their team did not produce any equations that could be directly applied to isolated bones, nor did they modify the ones presented by Harris and Case. The best first decision tree did show differences in analysis for demarking points for the first cuneiform (MI-Longitude:23.5mm and 24.5mm), the third cuneiform (MII-Breadth: 16.5mm), and the cuboid (MIII-Height: 23.5mm) (see **Figure 62**). These values would be useful after applying Harris and Case's functions, as the genetic, spatial, and chronological distances between the Euro-American population used and GMS' own seem to play a significant role in the result.

Measurements on vertebrae

A. Amores-Ampuero and J. Viciano (2020) developed a method for sex allocation that utilizes anthropometric data extracted from four specific vertebral elements, selected thanks to their outstanding morphological characteristics. Four vertebrae can be identified without the need of comparison with adjacent bones: the first cervical vertebra (C1) or atlas, has a characteristic ring-shape and lacks the spinous process; the second cervical vertebra (C2) or axis, that is easily identified by its odontoid process; the seventh cervical vertebra (C7) which possesses a distinctively long and prominent spinous process; and the twelfth thoracic vertebra (T12) that presents convex inferior articular surfaces (Amores-Ampuero & Viciano, 2020). The vertebral measurements can be seen in **Table 33** and **Figure 63**.

Table 33. Vertebral measurements selected for sex allocation logistic regression equations (Amores-Ampuero & Viciano, 2020, p. 4).

Element	Database ID	Description
All vertebrae	I	**LFV** Length of vertebral foramen: the internal length of the vertebral foramen, measured at the inferior edge of the foramen in the median plane
	II	**WFV** Width of vertebral foramen: the maximum internal width of the vertebral foramen, wherever it may occur, measured perpendicular to the median plane
	III	**SFS** Superior facet sagittal diameter: the maximum sagittal diameter of the superior articular facet
	IV	**SFT** Superior facet transverse diameter: the maximum transverse diameter of the superior articular facet measured perpendicular to the sagittal diameter
	V	**IFS** Inferior facet sagittal diameter: the maximum sagittal diameter of the inferior articular facet
	VI	**IFT** Inferior facet transverse diameter: the maximum transverse diameter of the inferior articular facet measured perpendicular to the sagittal diameter
Only for C2	VII	**SFB** Maximum width across the superior facets: the maximum width between the superior articular facets measured from the most lateral edges of the superior facets
	VIII	**DTD** Dens transverse diameter: the maximum transverse (latero-lateral) diameter of the dens
Only for C7 and T12	VII**	**SVB** Vertebral body sagittal diameter: the maximum sagittal diameter of the vertebral body
	VIII**	**TVB** Vertebral body transverse diameter: the maximum transverse diameter of the vertebral body

*All measurements were previously defined by either Marino, Wescott or Martin and Saller, though exact terminology and abbreviations may differ slightly.

**These measurements are in the same slot as the ones for C2, only varying in C7 and T12. It was not deemed necessary to create additional (IX and X) categories.

Figure 63. Visual guide for measurements taken on vertebrae (Based on a similar figure found in Amores-Ampuero & Viciano, 2020, P. 3). From left to right: Thoracic vertebra 1 (superior view, Thoracic vertebra 12 (lateral view), Cervical vertebra 2/Axis (anterior view), and Thoracic vertebra 12 (superior view). Featured pictures can be found in White et al. (2012, pp. 140 ,142, 138, and 141 respectively), slightly modified and resized.

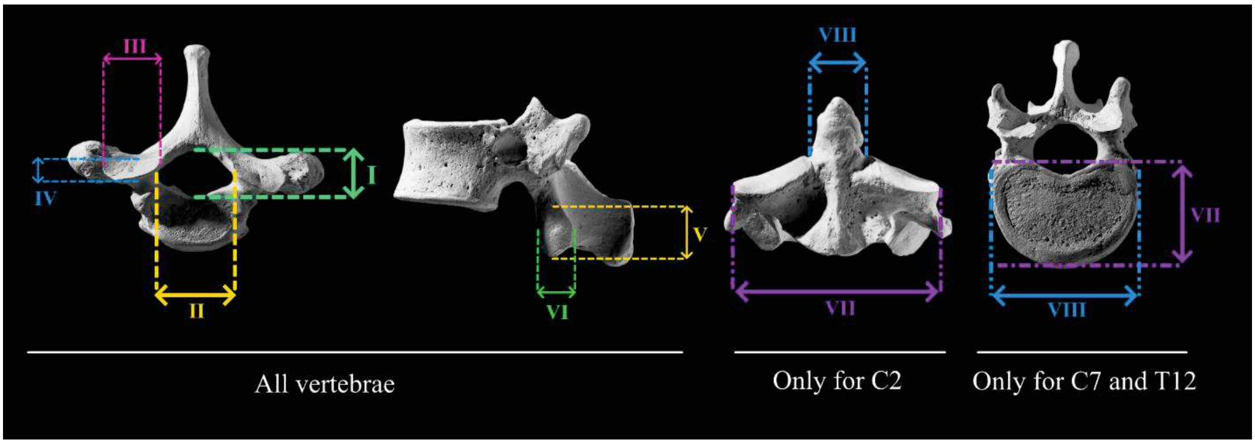

The methodology requires that all measurements should be obtained with sliding callipers rounded to the nearest 0.01 mm Sexual diagnosis using vertebral bones has had accuracy rates of up to 100% when used correctly.

Raw data was extracted from the Skeletal Collection of the University of Coimbra (Portugal), on a sample included 73 individuals (38 males and 35 females) and had a mean of 50.10 ± 18.34 years at the time of death. Amores-Ampuero and Viciano concluded that males present a general higher mean value for vertebral measurements than females. From these, 66.7% of the vertebral measurements displayed significant differences between the sexes, emphasizing traits of sexual dimorphism (Amores-Ampuero & Viciano, 2020).

Their results highlight the utility of articular surfaces and vertebral foramen measurements (**MI** and **MII**) for estimating sex using C1; **Measurement VI** was the variable that performed the best using C2, and **Measurement I** was the most efficient for sex estimation when using C7. **Measurement VII** behaves similarly for T12. Akin to previous studies, the more measurements are included the more accurate is the allocation rate. Each bone had differentiated performance (C1: 77-85%; C2: 78-100%; 80-90%; 80-94%) which may indicate that genetic, environmental, and socio-economic factors can influence the degree of sexual dimorphism and size of each vertebra.

Additionally, a suitable preservation degree of the skeletal element may influence these results, given the fact that thoracic vertebrae tend to be more affected by taphonomic factors, followed by lumbar and cervical pieces. Overall, results obtained using this technique are reliable, especially when using C1 (Up to 92.5% when all measurements are taken) (Amores-Ampuero & Viciano, 2020).

Eleven equations had had a performance that exceeded 80% of success, distributed as follows: six equations for C1, from which **L6** and **L5** were chosen for Gruta do Morgado Superior; one equation for C2 (**L7**), two equations for C7 (**L8** and **L9**) and two for T12

(**L10** and **L11**) (see **Table 34**). The best results (over 90% accuracy) were obtained when using C1.

Table 34. Sex allocation equations that exceeded an 80% success rate using vertebrae (Amores-Ampuero & Viciano, 2020, P. 8).

Element	Accuracy (%)	Logit Equation
C1	80.9	L1 = 31.760–0.749(**MI**) – 0.449(**MIII**)
	80.9	L2 = 36.971–0.683(**MI**) – 1.035(**MVI**)
	80	L3 = 23.520–0.505(**MII**) – 0.461(**MIII**) *
	82.1	L4 = 38.885–0.944(**MI**) + 0.714(**MIV**) – 1.176(**MVI**)
	86.6	L5 = 48.510–1.128(**MI**) – 0.536(**MIII**) + 1.052(**MIV**) – 0.957(**MVI**)
	92.5	L6 = 56.929–0.773(**MI**) – 0.635(**MII**) – 0.677(**MIII**) + 1.290(**MIV**) + 0.817(**MV**) – 1.847(**MVI**)*
C2	80	L7 = 29.893–0.073(**MI**) – 0.305(**MII**) – 0.071(**MIII**) – 0.110(**MIV**) + 0.194(**MV**) + 0.004(**MVI**) – 0.294(**MVII**) – 0.759(**MVIII**)*
C7	80	L8 = 33.574–1.573(**MI**) – 0.748(**MVII**)
	83.6	L9 = 54.005–1.664(**MI**) – 0.452(**MII**) + 0.287(**MIII**) + 0.014(**MIV**) – 0.412(**MV**) – 0.102(**MVI**) – 0.972(**MVII**) – 0.079(**MVIII**)*
T12	82	L10 = 17.479–0.513(**MIII**) – 0.437(**MVII**)
	81.8	L11 = 31.093–0.455(**MII**) – 0.598(**MIV**) – 0.595(**MVII**)*

(*) MFV (Measurement II) presented on original as WFV. It may be a typo.

Usage of spinal elements to allocate sex is wildly debated among supporters and detractors. Nevertheless, evidence found in sexual markers from C1 and C2 indicate that in fragmented or secondary contexts the success rate is high enough to be considered as a robust methodology. Moreover, these elements are easily recognizable and do not require adscription to a single individual, which makes them appliable to Gruta do Morgado Superior’s collection.

Sex allocation by Mental Eminence’s Morphology

The analysis of cranial morphology has been used as an indicator of sexual dimorphism based on the premise that males tend to “have larger, more robust skulls than females” (Buikstra & Ubelaker, 1994, p. 19). Sex allocation using markers on the skull morphology (i.e., size of the mastoid process, sharpness of the supraorbital margin, prominence of glabella, and projection of the mental eminence) is often used with caution as its reliability depends greatly on the experience of the researcher and the particularities of the population being analysed; some communities may present more gracile males while displaying robust females, and older individuals may become more robust as part of the aging process (Nikita, 2014). Several authors have tried to strengthen the reliability of the scoring system of sexually dimorphic skull markers by eliminating some of the bias related to the observer and the description on manuals, resulting in various attempts to used discriminant functions and statistical data. These attempts have resulted in mixed results, some displaying similar accuracy rates, while others require the pondering of many features’ score to obtain better results (Nikita, 2014). Classification trees have also been developed, in which several markers are combined and assign different probabilities depending on the combined score of two or more markers (White et al., 2012).

Although during the revision of material some skulls in a relatively good conservation state were observed, most of the cranial elements on **Square K51** were limited to fragmentary and incomplete skull bones. The only recurrent, and observable, feature was the mental eminence. Buikstra and Ubelaker's method for scoring the mental eminence relies on holding the mandible between the thumbs and the index fingers while placing the latter at either side of the lateral eminence. Then the observer should move the thumbs medially until each has reached the limits of the eminence. The grading score goes as follows: 0= undetermined sex; 1= female; 2=probable female; 3= ambiguous sex; 4=probably male; and 5= male. Decision trees have tilted results towards male classification, understanding a value of 3 as a male individual, depending on other markers. Efthymia Nikita (2017) has taken this approach even further, stating that a robust result can be obtained only when using a wide array of cranial markers (up to 20), given that observers may under- or overscore certain features without taking into consideration the whole dimension of the cranium.

Since all the mandibles found in **K51** were not associated to other skull fragments decision trees could not be implemented. However, for future analysis in other squares it is recommended that decision trees are prioritized over Buikstra and Ubelaker's scoring system. An example of a decision-based approach can be found in **Figure 65**.

Figure 64. Sex allocation score by examining the mental eminence. *Up*: Original visual guide found in Buikstra and Ubelaker (1994, p. 20). Down: Examples of decision tree analysis (only for mandibles) (2012, p. 413, extracted from Stevenson et al. 2019)

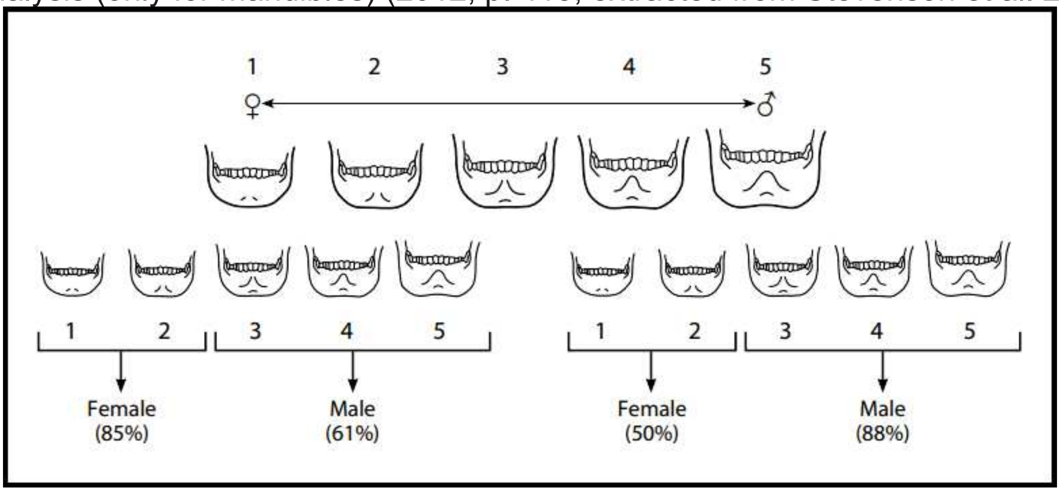

3.3.12.2. Morphological traits: Stature prediction

Estimating the probable stature in past populations is fundamental for the reconstruction of patterns of sexual dimorphism, paleodiets and inter- or intracommunity patterns (Cordeiro et al., 2009). Even though this marker relies heavily on measurements on the long bones, such as the femur and tibia, the absence of these elements on certain contexts requires the application of techniques that are focused on the pieces that were complete when excavated.

Previous campaign reports in Gruta do Morgado Superior preferred using a method developed by T.D: Holland (1995) using the talus and the calcaneus. Although Holland states that stature is not that influenced by race or biological sex, the method is almost thirty years old at the time, and the skeletal collection from which it drew its data is American. Nevertheless, for comparison's sake, it will be retained as an academic exercise.

Measures on metatarsals

A methodology developed by Cristina Cordeiro, Jose Munoz-Barus, Sofia Wasterlain, Eugénia Cunha and Duarte Vieira (2009) was elaborated to reconstruct approximate stature from metatarsal measurements. This technique was developed in a forensic setting, using a collection from the National Institute of Legal Medicine of Portugal, from which 110 cadavers (20 female and 90 male) from 2001 were analysed.

The authors decided to exclude skeletons that presented deformities, pathologies or fractures that could bias the result. The study was conducted only in individuals from 20 to 75 years old at the time of death. Bones were measured with and without cartilage, which resulted in the lack of any statistically significant difference, so all the measurements were taken with the cartilage. Four measurements were used in both metatarsal 1 and 2 (M1 and M2 from now on) (see **Table 35** and **Figure 65**).

Table 35. Measurements taken in Cordeiro et al.'s team (2020, P. 131.e2).

Database ID	Abbreviation	Measurement	Description
I	**F1**	Physiological length of 1st metatarsal	The distance between the deepest point of the proximal articular surface and the most distal point of the head.
I	**F2**	Physiological length of 2nd metatarsal	The distance between the deepest point of the proximal articular surface and the most distal point of the head.
II	**M1**	Maximum length of 1st metatarsal	The distance between the tip of the tuberosity and the most distal point of the head.
II	**M2**	Maximum length of 2nd metatarsal	The distance between the proximal tip and the most distal point of the head.

Figure 65. Visual guide for measurements taken on metatarsals (Based on similar figures found inCordeiro et al., 2009, p. 132.e2). From left to right: first and second metatarsals (medial view) (Original pictures of the bones taken a resized fromWhite et al., 2012, p. 289).

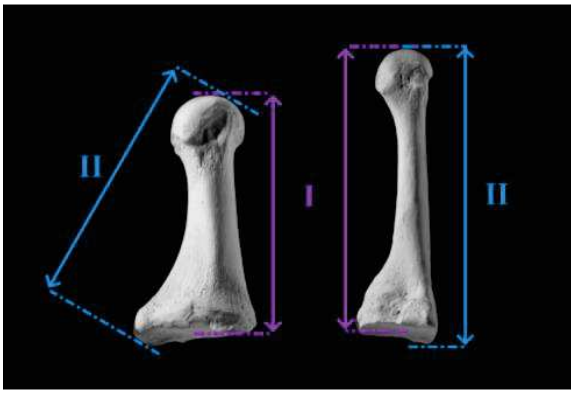

Using a series of logistic regressions, a total of four equations were extracted. The correlation between the metatarsal lengths and the true stature were always positive and statistically significant. When the value was applied to the whole sample (‘unknown sex’), its effectiveness ranged from 0.7 to 0.8, but once they were separated by sex the correlations were slightly lower. Whatever the value, the highest correlation was obtained with **Measurement II** (2nd metatarsal maximum length):

$$S = 790.294 \pm 11.69\boldsymbol{MII}$$

Contrary to previous studies, *R* figures do not increase when a combination of the four equations is performed. The results were tested using Byers et al. formula on material from the collection of the Museum of Anthropology of Coimbra University, where they yielded better results. Although the correlation coefficient was higher on MT2, in archaeological and fragmentary contexts MT1 tends to preserve better, and since the *R* value has a difference of around ≅ 0.07, equations using this skeletal element may be used with confidence. Gruta do Morgado Superior’s collection fits the conditions for the application of equations labelled under ‘unknown sex’, given its greater accuracy rate (see **Table 36**).

Table 36. Regression formulae for estimating stature from metatarsal measurements. (unknown sex) (Cordeiro et al., 2009, p. 131.e3).

Element	Database ID	Equation	R
MT1	Stature II	S=887.530+(12.826***MI**)	0.702
	Stature I	S=871.260+(13.007***MII**)	0.721
MT2	Stature II	S=798.894+(11.990***MI**)	0.792
	Stature I	S=790.041+(11.689***MII**)	0.793

Cordeiro and their team argue that this method is more robust than those that use total foot length to determine stature (footprints), because weight has a strong and positive correlation that may result in an overestimation. Therefore, methodologies using metatarsals’ measurements are thus free from such bias. The results were very close to Byers and may be used with confidence. Byers and Bidmos’ formula should not be rejected, since it may be useful when the ethnicity of the sample is unknown; however, the formula developed in this study may be applied to present-day Portuguese populations.

From the archaeological point of view, given that the collection used was Portuguese, and that one of the equations performed particularly well, the technique was applied to GMS’ context with a robust degree of confidence.

Measurements on the Talus and Calcaneus

Bioanthropological analysis during most of the campaigns in Gruta do Morgado Superior employed T.D. Holland’s (1995) methodology to estimate stature from tarsal bones, namely the talus and the calcaneus. Results obtained with said methodology were the base upon which affirmations about sexual dimorphism were woven by Tomé (2012; 2013), Curto (2015; 2019), Relvado & Anselmo (2016), and Ribeiro (2018). Holland’s method was constructed using elements from the Hamann Todd Collection at the Cleveland Museum of Natural History, heavily focused on racial traits, with an age at the time of death from 16 to 81 years.

Holland's measurements coincided with some measurements explained before for sex allocation in the calcaneus, while the talus required a variation of its first measurement (see **Table 37** and **Figure 66**).

Table 37. Measurements needed to predict stature according to Holland (1995, p. 316).

Database ID	Name (Holland)	Description
MI	MCLAL	Maximum Length (Calcaneus): maximum length taken parallel to the long axis.
MVII	PCLAL	Posterior Length (Calcaneus): maximum length between the most anterior point of the posterior talar articular surface and the most posterior point of the calcaneus (on the tuberosity).
MVII	MTAL	Maximum Length (Talus): maximum length between the most anterior point of the head and the posterior tubercle It differs from other measurements in the sense that it takes the tubercle as a landmark instead of the sulcus for the f*lexor hallucis* longus muscle.

Figure 66. Maximum Length of the Talus according to Holland (Original image on Curate et al., 2021a, p. 74, modified).

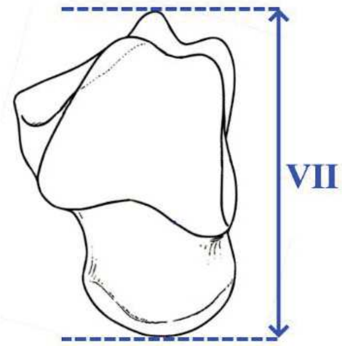

Holland's results using race and sex-specific formulas did not yield lower standard errors than when using unspecified ones. He concludes that both skeletal elements are linearly linked with stature and that allometric, racial or sexual proportional relations that affect long bones are seemingly less impactful on the talus and the calcaneus. Although Holland has multivariate equations with two measurements on the calcaneus, or mixing both bones, their performance was lower than those with only one variable. From all the equations presented by the author, only three were not adjusted for race or sex, and were deemed appropriate for their use in Gruta do Morgado Superior (see **Table 38**).

Table 38. Formulas to predict stature according to Holland (1995, p. 318).

Skeletal Element	Type	Accuracy	Formula
Calcaneus	Main	95	(1.150***MI**)+77.37
	Support	86.25	(1.617***MVII**)+76.91
Talus	Main	91.5	(1.411***MVII**)+85.95

Unfortunately, previous field reports do not specify which specific equations were used when estimating stature, but if Holland's statement is considered, it is likely that previous researchers used general formulas without adjusting them for sex. A comparison between Holland's raw data and Gruta do Morgado Superior's material will be presented in further sections. Although Holland's data is the farthest away from historical Portuguese populations, it has the advantage of linking the variables of sex allocation and stature estimation. Nonetheless, results must be cautiously interpreted.

3.3.13. Age estimation

Determining the age at the time of death in past populations is understood as an estimate of the biological age of an individual that is inferred from variables that are related with chronological aging (Kemkes-Grottenthaler, 2002). Chronological and biological age are uninterchangeable terms, and one cannot be substituted the other. Palaeodemographic studies can usually only assess the biological age of a specimen while inferring possible age groups that coincide with the former. Consequently, age-determining technique's applicability and/or precision will inevitably vary depending on the chronological, cultural, and genetical makeup of past populations.

Variation may occur at different levels, including within the body itself (different skeletal regions develop dissimilarly), among individuals in the same age group (sexually dimorphic development), within the same population (cultural and epigenetic factors), and between populations (genetic makeup and environmental constrictions) (Kemkes-Grottenthaler, 2002). Ontogenesis follows sexually dimorphic rhythms that are influenced by the strength and duration of growth hormones' exposure, environmental constraints, diet, and pathological conditions.

To further complicate matters, most ontogenetical studies derive from revisions performed on contemporary populations, which inevitably serve as paleodemographic reference points for Prehistoric populations. Aging patterns in prehistoric societies may have been different, and that age estimation techniques could under- or overrepresent some age groups (Bocquet-Appel & Masset, 1982). Additionally, mortality patterns are easier to analyse in contexts where data about the specific age at the time of death can be counter examined, but when dealing with prehistoric from age groups results tend to dilute.

Further concerns arise from the methodological point of view. Intra and inter-observer bias play an important role in the result. As A. Miles (2001) states, the lack of sturdy methodologies to assess the most difficult age groups (such as mid-twenties to mid-thirties, or all those that follow the 50+ mark) ends up skewing the distribution of the whole sample. When replacing numerical age groups by nominal variables another problem arises: due to the lack of well-defined ranges among researchers, data cannot ultimately be compared among each other.

Overall, caution is advised when approaching populations in the past, as methods used on historical collections may not perform well on prehistoric ones. Techniques using dental wear analysis on historic populations may perform poorly on communities with coarser diets or specific behavioural patterns -such as Gruta do Morgado Superior- (White et al., 2012).

Most manuals advise performing a complete skeletal evaluation in which all the markers related to biological age are thoroughly examined. The probability of accurately estimate the age of an individual from bioarchaeological material increases diametrically the more skeletal regions are suitable for analysis. Multifactorial analysis should be prioritized and implemented whenever possible, always considering the patterns of dental development and eruption, and epiphyseal appearance and fusion (White et al., 2012). The use of isolated indicators of age will always be hampered by several factors that negatively affect its accuracy.

Fragmentation, coupled with material redeposition, weighs down the process of retrieving multifactorial data in fragmentary and/or secondary funerary contexts. Gruta do Morgado Superior's material lacks some of the most popular markers for age estimation that (akin to those used for sex allocation) are found in skeletal regions that were highly fragmented, eroded, or missing altogether. Thus, most of the methods for age allocation were applied to GMS depending on the bone. Whenever possible, analysis of the pubic symphysis and the iliac articular surface were included, using the summarized guidelines on White et al. (2012).

Dental development and eruption stages have been thoroughly described in several publications (Herrmann et al., 1990; Schaefer et al., 2009). In Gruta do Morgado Superior, the base classifying system developed by Moorees et al. was used for preliminary descriptions (see **Table 39** and **Figure 67**), mainly because this method has been employed by previous field reports. Data regarding specific age ranges for each developmental stage was extracted from Smith's compilation (1991). Considerations by Hillson (2014) were used as control information for missing data. It is worth noting that most age tables provide a mean value for most teeth, presenting sturdy data for molars and variable for incisors and canines. Data for certain stages was not presented in male or female subcategories (mainly incisors) which led to less specific ranges in anterior dentition than in posterior elements.

Table 39. Tooth formation stages according to Moorrees et al. (1963) (Schaefer et al., 2009, p. 81).

Database ID	Description
C_i	Initial cusp formation
C_{co}	Coalescence of cusps
C_{oc}	Cusp outline complete
$CR_{1/2}$	Crown half complete
$CR_{3/4}$	Crown three-quarters complete
CR_c	Crown complete
R_i	Initial root formation
Ci_i	Initial cleft formation
$R_{1/4}$	Root length quarter
$R_{1/2}$	Root length half
$R_{3/4}$	Root length three-quarters
R_c	Root length complete
$A_{1/2}$	Apex half closed
A_c	Apical closure complete

Figure 67. Visual guide for tooth formation stages according to Moorrees et al. (1963) (Schaefer et al., 2009, p. 80).

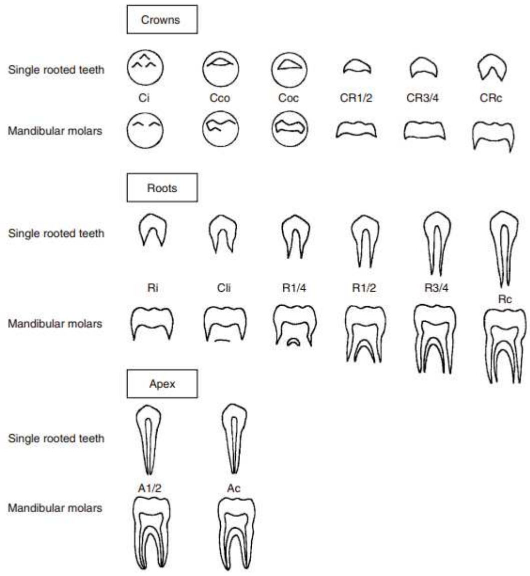

Epiphyseal appearance and fusion patterns behave similarly to tooth formation and can be easily tracked down. A general summary of the ontogenetical process for each skeletal element was thoroughly discussed in previous sections (**3.3.10.1**), while the age groups that can be drawn from each state can be found in Scheuer et al. (2004). Each element at Gruta do Morgado Superior (**Square K51**) was given an age range according to the time of appearance and fusion of each primary and secondary ossification centres following Scheuer textbook's guidelines.

This methodology is focused on obtaining the biological age ranges between important ontogenetical events that could be linked to a chronological age profile. However, the data collected is not to be interpreted as the latter. The columns dedicated to age estimation provide a category for tooth formation stages, a class for an age interval that is usually constructed according to the minimum or maximum age of appearance and/or disappearance of the trait (considering both male and female development), an estimated age for males, an estimated age for females, an age class, and a juvenile/mature variable.

Although the use of nominal categories for age groups comes inevitably with comparison-wise disadvantages, it can be used as an additional (and independent) variable to generate general descriptions of different age ranges. If one considers the ontogenetical development of an individual as a non-linear process, several developmental landmarks can be placed along significant growth-related events to divide an individual's life into various age classes. Different authors have various interpretations of which landmarks should be taken into consideration, but the most useful ones are those that consider the biological variability in frequency and speed of such events, over their chronological weight (see **Table 40**).

Table 40. Age classes for different ontogenetical milestones (White et al., 2012, p. 385).

Age Class	Perinatal	Infant	Child	Adolescent	Young Adult	Mature Adult	Old Adult
Milestone	Embryonic and fetal development	Birth	Eruption of the second milk molar	Eruption of the second molar	Epiphyseal fusion	Closure of basilar suture	Onset of gross skeletal degeneration
Associated chronological age	8 to 9 months	0-year-old	2 years old	10 years old (female), 12 years old (male)	18 years old (female) 20 years old (male)	25 years old	50 years old or more+

Other methodologies for age estimation such as dental measurements applied to logistic regressions (White et al., 2012), histological analysis of bone structure and composition, quantification by numerical imagery, radiography, and aspartic acid racemization (Kemkes-Grottenthaler, 2002) were not used due to time and funding constraints, but they could be considered in the future.

3.3.14. Identified Individuals

Although most of the bones in GMS were rarely associated to the same individual, there were isolated cases in which articulated elements were found and assigned a consecutive. The most common elements were mandibles and maxillae, juvenile long bones, and vertebrae. Identification of single individuals was pursued to avoid overcounting the final Minimal Number of Individuals, as well as locate spatially the distribution of surviving articulated elements.

The individuals were assigned an alphabetic character, and an additional (i) was used when the probability of the elements belonging to the same specimen was dubious. At least seventeen (17) individuals were identified within the collection, with an additional entry [A(i)] that presented a possible connection that could not be checked.

3.3.15. Palaeopathology and Stress

Most abnormalities present in the skeleton are caused by imbalanced activity between osteoblasts and osteoclasts. Pathogenic agents that alter these patterns include external living organisms (e.g., viruses, fungi, bacteria, protozoa, and multicellular parasites) and internal homeostatic alterations (influenced by diet, daily activities, and the normal aging process)(Hillson, 2014). Bone architecture is ultimately modelled by the constant interaction between these two types of cells and their response to stress (Ortner, 2003).

However, defining what is consider ‘abnormal’ is a difficult task when considering skeletal variation on size, shape, and physiology. The matter complicates even further by morphological and genetical differences among individuals and populations. Additionally, markers associated with deteriorating conditions and endemic diseases become so common to the point that almost all individuals in a sample display it at various stages; effectively transforming an abnormal characteristic into a population trait.

Bearing this in mind, a disease should be understood as the confluence of abnormal factors that lead to a state in which the body cannot operate efficiently (Hillson, 2005).

Hence, variation should be put in a scale that allows for the registration of certain markers without tilting the interpretation of data towards a rushed and unfavourable conclusion.

An ideal approach for palaeopathological description should focus on a descriptive method that allows for comparison among variables and differentiation between pathological and taphonomical processes. This system must *i*) elaborate clear and unambiguous definitions for each abnormality, *ii*) efficiently locate and measure the spread pattern of each marker, and *iii*) be able to produce a descriptive summary of all the identified features once all the skeletal pieces have been analysed (Ortner, 2003).

When analysing a sample, researchers must ponder if the skeletal element has an abnormal rate of bone formation, an abnormal rate of bone destruction, or inexistent bone formation/bone destruction. Once the individual description is finished, patterns of occurrance are described (weather the markers present themselves in isolation or throughout specific skeletal regions).

Gruta do Morgado Superior (Square K51) was analysed using a series of variables that serve as the foundation to perform pathological descriptions and the subsequent the identification of well-known ailments. These variables were constructed to register the location of **abnormalities**, **bone forming lesions**, **musculoskeletal markers**, **dental wear**, **dental lesions**, and **non-metric traits** on most bones.

3.3.15.1. Abnormalities on skeletal elements

Identification of pathological conditions through the analysis of bioarchaeological material, even when the skeleton's conservation state is optimal, can only be achieved in broader terminology. Some abnormality markers may be a direct result of several pathologies with different aetiologies, resulting in a wide range of probable causes for a single lesion. Methodologically, the key to a successful palaeopathological analysis relies on a sturdy description and a flexible interpretation. This allows for a certain degree of error while preserving the collected data for future studies. Furthermore, markers described this way may be used as by other researchers in a variety of studies, such intra- and intercommunity comparisons of pathological conditions (Ortner, 2003).

Just as sexual allocation and age determination analysis, palaeopathological examination is more accurate in complete skeletons. Fragmentary contexts do not allow for the observation of abnormal markers in conjunction, which makes difficult to produce a reliable diagnosis.

Gruta do Morgado Superior's collection did not produce enough identified bodies to accurately diagnose certain pathologies, as abnormalities can only be associated to the skeletal elements in which they were originally observed, without correlation to adjacent bones or associated lesions in other regions. Diagnosis drawn from comparisons between markers located in specific skeletal regions may overstretch this study's reach. At any rate, the value of a robust descriptive analysis of the lesions was not deterred in the slightest, and each step of Ortner's methodology was implemented.

The first set of variables to be defined was the location of observed abnormalities/lesions on bones. Categories described by Ortner (2003) were used without major modifications, but as the analysis advanced, new classes were added. The inclusion was focused on short and irregular bones that could not be described using only the parameters for long bones and the cranium (see **Table 41**). Location categories were useful to describe both, abnormalities, and lesions.

Table 41. Classification of a lesion according to its location (within a single skeletal element) (Ortner, 2003, p. 50, slightly modified).

Skeletal Element		Location (Database*)
Long Bones	Longitudinal Axis	Proximal Joint Surface
		Proximal Epiphysis
		Proximal Apophyses
		Proximal Metaphysis
		Diaphysis
		Diaphysis (Lateral and Medial) (*)
		Diaphysis (Lateral) (*)
		Diaphysis (Medial) (*)
		Medullary
		Distal Metaphysis
		Distal Apophyses
		Distal Epiphysis
		Distal Joint Surface
	Cross-sectional axis	Extra cortical
		Periosteal
		Cortical
		Endosteal
		Medullary
Skull/Mandible		Outer cortex
		Diploe
		Inner cortex
Hands/Feet (*)		Body (*)
		Medial Articular Surface (*)
		Lateral Articular Surface (*)
		Non-articular Surface (*)
		Palmar (*)
		Dorsal (*)

(*) Added to Ortner's list for GMS database.

Abnormalities include most general markers that are associated with a wide arrange of ailments and degenerative processes. Generally, abnormalities referring to osteological quality and density are called *osteolysis* (localized bone resorption that alters the typical anatomy), *osteopenia* (loss of bone quality without a clear cause), and *osteoporosis* (below average density without deformation). When these concepts are brought to specific context, a wide array of categories arise (see **Table 42**). These categories were used to describe the anomalies on the GMS collection without any modification to Ortner's method.

Table 42. Variables for describing types of bone abnormalities (Ortner, 2003, p. 50, slightly modified).

Abnormality	Location	Abnormality (Database ID)
Size		Abnormally small for age and sex Abnormally large for age and sex
Shape		Abnormal shape resulting from defects in growth and development Abnormal shape resulting from biomechanical stress on poorly mineralized bone Abnormal shape resulting from poor alignment following a fracture
Formation	On woven (fibre) bone	General woven bone Porous bone Striated bone Spiculated bone
	On compact bone	Smooth compact bone Porous compact bone Striated compact bone Spiculated compact bone Plaque Lesions on spongy bone
Destruction		No margin or clear border Clear border but no sclerosis Clear border with sclerosis Central destruction with marginal formation Repair of central destruction with marginal formation Focal porous destruction Destructive remodelling General porous destruction Osteopenia (Osteoporosis) Trauma (Fracture)

3.3.15.2. Bone forming lesions.

Bone forming lesions are the second group of categories that refer to specific abnormalities. These were divided into abnormal growths that alter the bone's typical topography (see **Table 43**) and abnormal loss/addition of bone mass while retaining the element's regular topography (see **Table 44**). These variables allow for a more specific description that retains inherent information about location and aetiology.

Table 43. Variables for describing types of bone forming lesions (Ortner, 2003, p. 51, slightly modified).

Lesion (Database ID)	Description
Osteophyte	A small, abnormal bony outgrowth often found at the margins of articular surfaces that usually indicates the presence of osteoarthritis (White et al., 2012, p. 587).
Syndesmophyte	A small, abnormal bony outgrowth that starts at the fibrous cartilage within a joint. It is considered to be diagnostic for ankylosing spondylitis (White & Folkens, 2005, p. 590).
Enthesophyte	Bony spurs that develop alongside an enthesis (a ligament attachment to a bone). They are response to repetitive mechanical stress and are found oriented in the direction of the muscle(Arjmandi et al., 2021).
Spicule formation on subchondral bone	Bony spurs that sprout from subchondral bone into the limit for calcified cartilage. They tend to increase in number when the cartilage is damaged and are associated with mechanical stress and osteoarthritis (Arjmandi et al., 2021).
Fusion of joint	It is usually preceded by joint destruction.

Table 44. Variables for describing types of bone destroying lesions (Ortner, 2003, p. 51, slightly modified).

Type	Lesion (Database ID)	Description
Subchondral surface breakdown (general retention of anatomical contours).	**Pores_A**	Small openings on the cortical bone (White & Folkens, 2005, p. 588).
	Cavities_A	Holes within the surface of the bone that are the result of demineralization processes that started long before their appearance (Hillson, 2005).
	Eburnation_A	Worn, polished, ivory-like appearance of bone resulting from exposure and wear of adjacent subchondral bone at a joint. (White et al., 2012, p. 582)
Subchondral surface breakdown (retention of some anatomical contours).	**Pores_B**	q.v.
	Cavities_B	q.v.
	Eburnation_B	q.v.
Complete breakdown of subchondral surface (no retention of anatomical contours or features)	**No sclerosis**	Reactive bone formation, without any thickening.
	Sclerosis	Thickening and hardening of the subchondral plate that result from chondrocytes' failure to repair the cartilage matrix (Hilal et al., 1998).
Juxta-articular erosion	**Pores_C**	q.v.
	Cavities_C	q.v.

3.3.15.3. Dental wear

The study of dental attrition has prioritized the state and condition of the enamel, mainly on occlusal surfaces (Scott, 1979). Dental wear is usually attributed to two main activities (mastication and cutting of objects), which wear down the outer enamel layer changing the topography of the dental crown. Most approaches specialize in one of two types of modifications, the first being small lesions (microwear analysis) and the second pertaining the exposure of the dentine (microwear analysis). Although microwear analysis was not explored in Gruta do Morgado Superior's collection due to time constraints, it should be considered on future studies using a smaller sample.

Methods used to assess the different degrees of dental wear through visual inspection have converged in the use of scoring systems within ordinal scales, thanks to the pioneer work developed by E.C. Scott (1979). More recently, Emma Lagan and Daniel Ehrlich (2021) developed an updated scoring method based on the amount of dentine exposed rather than the lost enamel, that is comparable with the most recognized dental wear techniques (i.e., Scott's and Todd's). This technique divides molars into four quadrants to which a specific value is assigned and then pondered. Molwear, as they called it, allows for the observation of wear patterns on different tooth sections that provide additional information about the angle of the attrition, the intensity by area, and distribution of the lesions. Dental wear is more than a score, as they put it, hence collecting additional data may illustrate better cultural practices and behaviour in prehistoric communities.

The analysis of Gruta do Morgado Superior utilized Lagan and Ehrlich scoring system without any modification to its description. Time and equivalence constraints did not allow for the division in quadrants for all dental elements. Instead, the angle of attrition was registered to supplement the score.

Anterior teeth do not present a similar set of scores that accounts for teeth with one or two cusps. An attempt to register similar information for these elements was added, based solely on the morphology of the tooth and the overall missing percentage. This scoring worked by using general landmarks such as the mamelons/cusps, the mesiodistal crown diameter and the cervical buccolingual crown diameter (see **Table 45** and **Figure 68**).

Table 45. Scores of dental wear and their descriptions (Lagan & Ehrlich, 2021, p. 834).

Score	Description (MolWear)	Description I/C/P	ED (%)
0	Little to no wear, tooth just in occlusion	Little to no wear, tooth just in occlusion	0
1	Enamel worn; no dentine exposed	Enamel worn; no dentine exposed	0
2	Pinprick to small dot	Mamelons no longer visible	<1
3	Moderate dentine patch	N/A	1-24
4	Large dentine patch, likely still surrounded by on all sides by enamel	distance between the enamel patch and the mesiodistal crown diameter is half to the original	25-50
5	Some inter-cuspal coalescence	N/A	45-60
6	Extreme inter-cuspal coalescence	It has reached the maximum mesiodistal crown diameter, turning it into a triangular shape	50-75
7	Thick enamel ring	It has eroded until reaching half the distance between the mesiodistal crown diameter and the cervical buccolingual diameter	60-85
8	Thin enamel Ring	It has reached the buccolingual diameter	85-99
9	Full dentine exposure	It has surpassed the buccolingual diameter	100

The orientation of the lesion was recorded in three categories: **transverse** (evenly distributed attrition), **oblique** (tangential attrition), and **concave** (u-shaped attrition with the deepest point in the medial section of the dental element). The latter was added during the laboratory phase, as it was not expected to be present.

Figure 68. Dental scores according to dentine exposure(left). (Lagan & Ehrlich, 2021, p. 834), and dental scores according to crown loss (right).

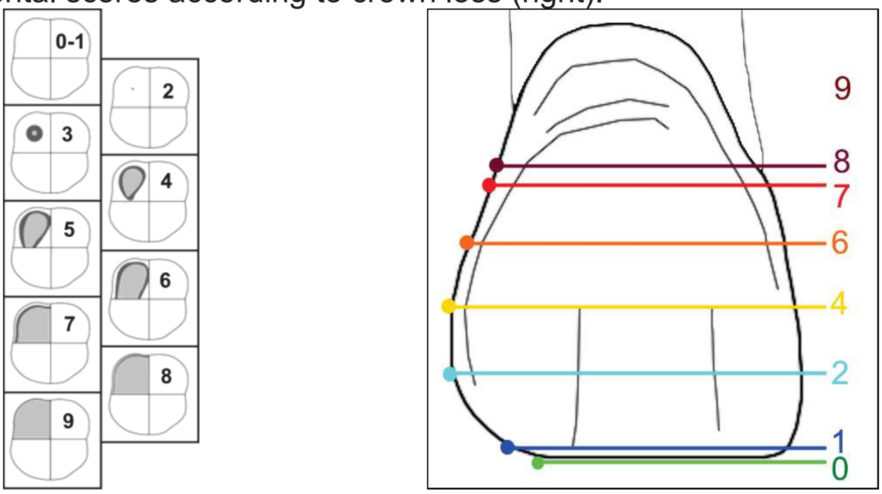

3.3.15.4. Dental lesions

Despite the innate resilience of dental structures, they are prone to various abnormal modifications at different ontogenetic stages. The analysis of these alterations attempts to describe them thoroughly by identifying the type of lesion and its location. Once identified, the next step is to propose a possible diagnosis. Some authors reckon that the former step is far more important than the latter in palaeopathological studies, because even if the diagnosis is incorrect the first time around, future researchers can revise and adjust the results (if the description was elaborated properly) (Smith, 1991; White et al., 2012).

To understand better any abnormality in dental tissues, investigators often reconstruct how they come to happen. The aetiology of a lesion is a methodological tool that helps to understand the relation between it and the events that led to its appearance; after all, a lesion represents the impact of the environment on an individual (or community) and their physiological response to it. Since dental pieces are one of the most resistant skeletal elements, most of their pathological conditions can be well documented in archaeological contexts. Common ailments include tartar, cavities, periodontal diseases, trauma, eruption anomalies, and different types of hypoplasia (see **Table 46**).

Table 46. List of selected dental disorders for analysis and their aetiology.

Database ID	Aetiology
Tartar	Bacteria, viruses, yeasts, and protozoa.
Coronal Caries Root Caries Caries of Worn Tooth surfaces Gross Caries	Bacteria, viruses, yeasts, and protozoa. Dental wear and aging process.
Periodontitis	Infection, homeostatic imbalances.
Apical Periodontitis	Infection
Abscess	Infection.
Trauma Impaction Retention Resorption Tumour (Carcinogenic)	Mechanical force Genetic/Epigenetic factors
Hypoplasia	Metabolic stress

Dental calculus (or *tartar*) grows from the lifeless remains of large communities of buccal fauna and flora that built up over dental pieces (i.e., plaque) and from which the deepest layers begin to mineralise and consolidate. It tends to be found in supragingival regions, although when coupled with periodontic diseases it may colonize the roots. Calculus tends to accumulate in areas that are far from the salivary ducts such as upper molars or the buccal area.

Caries is a progressive disease that results from tooth demineralisation under its surface due to the accumulation of organic acids. These byproducts are expelled by bacteria living on the plaque while they ferment carbohydrates. Sugars and starches have been directly linked to its prevalence rate, while sone milk products seem to counter the effect. This disease may occur initially on coronal and root surfaces, and it can rapidly involve the dentine and undermine the enamel, ending in pulp exposure.

In prehistoric communities the aetiology of cavities tends to be related with the aging process; worn tooth surfaces give way to dentine exposure which inevitably turns into gross caries with discernible starting point (Hillson, 2005). Larsen (2004) argues that the cultural shift towards agricultural-based socioeconomic systems increases the frequency of carious lesions. The analysis of its prevalence may even provide differences on diet within the same community, which can be extrapolated to hierarchic or differentiated behaviour. Conversely, other authors have concluded that the frequency of cariogenic lesions does not vary, but the location and depth does (Lanfranco & Eggers, 2010).

Most methodologies rely on scoring systems to count cavities and their prevalence per individual, but in fragmentary archaeological contexts these methods are not so easily implemented (Hillson, 2005). GMS collection allowed only for the registration of lesions on isolated teeth according to their location (see **Table 47**). In cases where individuals were identified, abnormalities were registered by maintaining the same consecutive and dividing the number of entries into the number of observable teeth plus the location of the alveolar region in which they were embedded into.

Table 47. Classification of cariogenic lesions by their location.

Location	Types
Occlusal	Pit and fissure, Approximal
Lingual	Pit and fissure, Approximal
Labial/Buccal	Used for Incisors and Canines/ Premolars and Molars. Pit and fissure, Approximal
Cervical	Any smooth area adjacent to an edentulous space.
Root	

Periodontal disease is an inflammatory process that results from an immune response to imbalances between foreign organisms and the overall homeostatic state of the body. A sharp increase in foreign organisms' number may trigger an overreactive lymphatic response (even if they are not particularly hostile) that ends up being more hurtful to body tissues than to the pathogens that it tries to eliminate. In bone surfaces, periodontal disease tends to be observable after it has reached an advanced stage, involving alveolar matter when it turns chronic. Depending on the seriousness of the lesion, abscesses may result in severe bone loss as well as deformation.

Periapical periodontitis has a different aetiology than gingival lesions, resulting from freshly opened pathways from the mouth to a dental apex (where the tooth receives its blood supply), causing an infection that, if acute, may result in bone loss. In archaeological material it can be observed directly in alveolar tissue.

Trauma (fracture) on roots and/or crown is a type of bone damage caused by the application of force to the jaw by an external agent. It is more common on the anterior elements and usually is accompanied by mandibular and maxillary fractures. Trauma can even be observed in developing teeth; tooth germs that are damaged in jaw fractures can halt tooth development completely.

Eruption Anomalies include conditions such as impaction (presence of deciduous teeth after their normal shedding age), retention (halt or delay of a tooth's eruption), and resorption (fusion of the element with the alveolar bone). These anomalies are not that uncommon and can be a combined result of converging genetic and epigenetic traits.

Enamel Hypoplasia is a structural anomaly that occurs during the amelogenesis process and manifests in the form of transverse lines, pits, and grooves on the surface of tooth crowns. Its aetiology has been linked to high levels of stress (metabolic insults) during tooth formation, where each event creates one set of marls (Larsen, 2010). Generally, lesions can have a furrow-form, a pit-form, a plane-form, or all combined. Furrow-form defects are the most common, and more complex (Hillson, 2014). Hypoplasia scoring methods are prone to a high level of interobserver variability on archaeological material (White et al., 2012), as differences between microscopic and macroscopic analysis are considerable. GMS's analysis was performed at a macroscopic level, so this category did not include its variants.

3.3.15.5. Musculoskeletal Stress Markers

Skeletal elements serve as anchor points of various muscles and ligaments. The interaction between these tissues creates a series of ridges, edges, eminences, and processes on the bone's topography. These features are usually called Musculoskeletal Stress Markers (MSM). Some authors prefer to refer to them as enthesopathies to reflect a pathological condition. In some instances, they have been named markers of occupational stress, thus including a wide array of variables such as robusticity and cultural behaviour. In older texts they have been interpreted as signs osteoarthritis, defined as pressure facets, or related to syndesmoses. Cashmor and Zakrzewski (2013) prefer the term MSM, as reflects a methodological focus on the markers themselves and the scoring methods, rather than their aetiology (physical causes) and morphology (Cashmore & Zakrzewski, 2013). In this study MSM were considered different indicators from abnormalities, as only the latter may be linked directly to pathological conditions. Abnormalities were already described and assigned categories in previous segments (see sections **3.3.15.1** and **3.3.15.2**) Considering that one of the objectives of the present study is the construction of a general biological profile, Musculoskeletal Stress Markers are defined only as a bone's response to repetitive physical activity. Whether or not the marker is linked to a particular pathology would require the convergence of other abnormalities or deformities on the same element.

MSM have been used to determine occupational patterns and sociocultural divisions of activity, based on the understanding that strenuous muscle activity may result in bone remodelling. This response usually takes place at locations where the muscles and tendons are attached to the bone (Cashmore & Zakrzewski, 2013). Increased activity at these sites leads to a surge in the intensity of vascular irrigation that supplies the periosteum. If exposed long enough, repeated exposure to this process over stimulates osteon remodelling that leads to the appearance of bone forming processes. These processes can be observed through macroanalysis by identifying the rugose appearance of the surface of the bone at the location where the muscle attachment lies. If the bone is stressed beyond its capabilities for a large amount of time, the osteolytic process can appear, resulting in pitting of the cortical surface of the bone.

The methodology proposed by L.A. Cashmore and Sonia R. Zakrzewski (2013) assumes that “the degree and type of marker are related directly to the amount and duration of habitual stress placed on a specific muscle” (Cashmore & Zakrzewski, 2013, P. 335). This system tries to recognize the features (usually *marginal osteophytes*) and register their location. Variability in size and the possible correlation with pathological conditions are not included. On the database MSM were recorded as **present**, and their location used Ortner’s categories as previous variables.

One of the most interesting features of MSM is their apparent independence according to the skeletal region in which they develop. Cashmore and Zakrzewski observed that MSM on the hand do not necessarily imply MSM in the arm and vice versa. For once, the level of fragmentation in GMS collection may not have a severe impact on a bioarchaeological method, as each MSM responds to a specific muscle attachment that can be traced down with a single skeletal element.

3.3.15.6. Non-metric traits

Non matric traits and minor variances in the human skeleton are generally associated to a specimen genetic makeup, that on occasion can be influenced or modified by epigenetic factors. These traits can take the form of tubercles, bony bridges, spines, accessory ossicles, foramina, vessel and nerve grooves, and sutural variations (Mann & Hunt, 2019). When found in archaeological (and forensic) contexts, such traits are often confused with lesions associated with trauma or pathologies. Bearing this in mind, recording non-metric traits can help to avoid such mistakes. Furthermore, their presence may provide epigenetic profiles of these markers’ prevalence on prehistoric populations for future comparison. A provisional list was taken from Mann and Hunt’s paper on non-metric traits (see **Table 48**) as the base for this category. It was necessary to add the *Cusp of Carabelli* and the *Bipartite Navicular* after performing the GMS’s collection analysis.

Table 48. List of some non-metric traits and variances in the human skeleton (Mann & Hunt, 2019).

Non-Metric trait	Prevalence	Non-Metric trait	Incidence
Cusp of Carabelli		Stafne defect	Uncommon
Accessory frontal groove	Common	Torus palatinus	Uncommon
Accessory nasal suture	Rare	Tympanic dehiscence	Common
Bipartite zygomatic bone	Rare	Enlarged parietal foramen	Rare
Buccal and lingual exostosis	Common (age related)	Inca bone	Uncommon
Deviated nasal septum	Common	Inion spike/hook	Common
Infraorbital suture	Common	Lambdoidal ossicle	Common
Metopic inter-frontal suture	common	Trace Mendosal suture	Common
Metopic fissure/ossicle	Uncommon	Supra-inion depression	Uncommon
Supranasal suture	Common	Parietal foramen	Common

Non-Metric trait	Prevalence	Non-Metric trait	Incidence
Supraorbital foramen and notch	Common	Bifid C1 (atlas)	Uncommon in adults
Torus mandibularis	Common	Bifurcated rib	Uncommon
Bipartite parietal bone	Unknown	Bifid spinous process	Uncommon in thoracic and lumbar vertebrae
Coronal ossicle	Common	Cervical rib	Rare
Epipteric ossicle/bone	Common	Bifid costal cartilage	Rare
Lateral extension of the sagittal suture	Uncommon	Manubrial aperture	Rare
Mastoid notch bone	Common	Os acromiale	Uncommon
Parietal extension of the squamous	Common	Sternal aperture (*fenestrato sterni*)	Common
Parietal notch bone	Common	Xiphoid aperture	Common
Petrosquamous suture	Common	Spina bifida	Uncommon
Squamosal ossicle	Common	Sacral hiatus	Common
Auditory exostosis	Common	Triradite scar	Common (aging process related)
Arachnoid pit	Common	Supracondylar process (humerus)	Rare
Segmented, elongated, crooked temporal syloid process	Common	Septal aperture	Common
Basilar fissure	Uncommon	Accessory ossicles (hand and feet)	Common
Bregmatic bone	Uncommon	Bipartite hamate	Rare
Parietal thinning	Common	Bipartite patella	Uncommon
Post bregmatic depression	Common	Thid trochanter	Uncommon
Atlanto-occipital fusion	Uncommon	Cervical fossa of Allen	Uncommon
Bifurcated mandibular condyle	Rare	Calcaneus secundarius	Common
Unfused hyoid	Common	Os subfibulare	Uncommon – Pathological
Paracondylar process	Common	Os trigonum	Common – Repeated trauma
Paracondylar tubercle	Uncommon	Os vesalianum	Rare
Pterygoalar bridging	Common	Unfused apophysis of the fifth metatarsal	Rare
Pterygospinous bridging	Common (aging process related)	Bipartite Navicular	Rare

3.3.16. Taphonomy

Yolanda Fernández-Jalvo and Peter Andrews define taphonomy as the study of all the processes involved in the transition of the remains of past living organisms into the lithosphere. The transition ends as soon as the material is found and extracted for analysis. These processes are the action of one or more taphonomic agent, that can be recognized as the “immediate cause of modification” (Fernández-Jalvo & Andrews, 2016, P. 1).

Regardless of its organic or inorganic origin, chemical and physical modifications to archaeological material can act independently or in conjunction. As soon as an organism perishes, it is exposed to decay (perimortem occurrences), exposure (erosion), burial (deposition and/or displacement), and diagenetic processes (mineral substitution). Although not all the stages may be present on the same element, a methodology that correctly and identifies some of them can produce a complete sequential reconstruction (Fernández-Jalvo & Andrews, 2016).

In the past, taphonomic modifications were often regarded as mere destructive processes that affect the archaeological record negatively, a view that relegates them to be considered methodological nuisances. Current research has understood that these modifications bear additional information about post-depositional processes that ultimately become an archaeological record by themselves (Fernández-Jalvo & Andrews, 2016). The study of taphonomy aims to obtain data about events in the past to obtain quantitative estimation of the degree of bias added by taphonomic processes to archaeological material, so that it may suggest corrections that can clear said bias before they are used for further analysis (Fernández-Jalvo & Andrews, 2016, P. 4).

Consequently, taphonomic studies are a medullar pillar in any prehistoric study, and their correct identification and quantification can help understand how the material came to be the way it was found. To perform this analysis data collection and classification must be sorted in a way that allows for comparison to other databases while producing valuable data.

Among the thorough description of taphonomic modifications and agents associated with them, Fernández and Andrews (2016) created a matrix that was considered very useful for the present study (see **Table 49**). The database included two possible modifications and their suspected agent. Although the anthropological material at GMS has not shown any evidence of human, carnivore, bird, or digestive activity on the bioarchaeological material, the categories were left just in case they are present, as it is the case with faunal remains (Almeida et al., 2023).

Table 49. Taphonomic modifications and probable agents related to them (slightly modified) (Fernández-Jalvo & Andrews, 2016, P. 4).

Modification	Agent I	Agent II	Agent III	Agent IV	Agent V
Abrasion	Sediment + Water	Wind	Bioturbation	Trampling	Carnivores
Breakage	Human	Carnivores	Sediment pressure	Trampling	Bioturbation
Cave corrosion	High humidity				
Chop marks	Human	Falling blocks			
Corrosion	Humic acids	Organic acids	Dense low plant cover	Cave humidity	Moss and lichen
Flaking/ Cracking	Weathering	Digestion	Organic acids	Humic acids	Plant roots
Curved ends	Human	Falling blocks			
Deformation/Bending	Human	Sediment pressure			
Digestion	Carnivores	Birds	Crocodiles		
Disarticulation	Carnivores	Humans	Trampling	Bioturbation	Weathering
Discoloration: black	Burning	Manganese	Carbon stain	Fungi	
Discoloration: Brown	Burning	Humic Acids			
Discoloration: Light	Burning	Gleysol	Leaching		
Discoloration	Burning	Oxidized Soil		Oxidation (Copper) (*=	
Double arch punctures	Human Molars				

Modification	Agent I	Agent II	Agent III	Agent IV	Agent V
Enamel Loss	Digestion	Corrosion			
Gouges	Carnivores	Birds			
Linear Mark U-Shape	Carnivore Chewing	Plant Roots	Insects	Beak Marks	Herbivore and Rodent Gnawing
Linear Mark V-Shape	Human Cut Marks	Trampling	Bone Tool Preparation		
Multiple Scrapes	Human	Trampling	Gnawing		
Notches	Human Percussion Marks	Carnivores			
Peeling	Human				
Pits	Carnivore	Birds	Insects	Trampling	Plant roots
Polishing	Wind + Sand	Water + Gravels	Licking	Digestion	
Punctures	Carnivore	Birds	Insects	Plants	Human
Rounding	Sediment + Water	Wind	Digestion	Carnivores	Trampling
Solution Marks	Diatoms	Lichen	Algae		
Splitting	Weathering	Digestion			

Taphonomic techniques for data collection include microscopic analysis, DNA collection and thin sectioning. This study was not conceived to achieve such depth level, and by its sheer size, only a handful of fragments could have been chosen for these types of techniques. Thus, the modifications were recorded macroscopically, sometimes with the help of magnifying lenses. Additionally, this methodology does not include changes in the chemical composition (organic or inorganic) during fossilization; but considering the chronological adscription of the material recovered at GMS it was not deemed necessary. The modifications can be classified according to their nature: surface modifications, shape modifications, colour modifications, and structural modifications. Surface modifications may present in the form of linear marks, pits, perforations, discoloration, and staining. Shape modifications presents in the form of abrasion and rounding. Alterations that penetrate bone tissue include flaking, cracking, corrosion, and digestion. Changes brought about by the loss of bone tissue or skeletal elements are seen in breakage and deformation, disarticulation, and completeness of the fragment.

Linear marks are defined as marks with lengths four times their breadths and longer. They may be classified depending on their shape into two categories: “v” shaped or “u” shaped cross-section. V-shaped cross-sections on bone are usually produced by a material harder than the bone (such a stone tool, a rock involved in abrasion, or trampling). These marks penetrate the outer surfaces of bones or teeth and remove some tissue while displacing adjacent material. Stress patterns accumulate in front of the cutting edge and this tissue is periodically displaced to form Hertzian fracture cones along both sides of the striation. They are usually evident in one side of the cut but may occur at both. The cut is asymmetrical, with one side steeper than the other. They may be present in animal (skinning) and human (occupational stress) teeth. In hominoids they are present with a recurrent orientation and frequently in anterior teeth on their exterior facets. They have been related with the identification of handedness and indirect evidence of brain lateralization (Fernández-Jalvo & Andrews, 2016). Linear marks with U-shaped cross-sections are usually left by gnawing processes, made either by incisors (scraping) or canines and premolars/molars (deeper penetration). Since the cutting edges from teeth are less sharp than tools or stones, the resulting U-shape is caused by abrasion. They may as well be left by birds (beak lines) or insects (termites) (Fernández-Jalvo & Andrews, 2016).

Pits are superficial marks left on the bone's surface; they differ from perforations as the latter penetrates deeply into the underlying layers of the bone. They have lengths that are less than four times their breadth. Inorganic agents involved in the process include erosional elements (air and water), anthropogenic agents (accompanied by percussion marks), and gravity and fluid dynamics (trampling). Organic agents include chewing by carnivores, raptors, or termites. Plants may leave pits and perforations as well (root marks). Although pits normally have an irregular form, perforations may be classified according to their shape and dimensions, since they allow to identify specific agents (Fernández-Jalvo & Andrews, 2016). This specification was not used in this study.

Changes in colour could be result of the speed of exposure to environmental factors (i.e., exposition to humic acids, oxygenated environments, fire, water, etc.). These modifications can be misleading because skeletal tissue is prone to quickly change colour within and between sedimentary horizons. Changes in hue can result from ontogenetic processes as well (e.g., the age at the time of death). Nevertheless, the most important information that can be extracted from colour are variations on single elements, indicating changes in microstratigraphy or alterations. Among the inorganic processes that may affect colour the most important ones are water (which may cause leaching), staining minerals (metal and oxidation), or wildfires (charring). Biological agents include organic acids that may already be part of the surrounding soil or result from root growth, microbial attack, or decomposition. Finally, chemical changes brought about by fire may be caused by natural events (wildfires) or human activity (e.g., hearths) (Fernández-Jalvo & Andrews, 2016).

Processes of abrasion are characterized by any degree of rounding and/or polishing on a bone. The inorganic agents involved include physical weathering and displacement by water, air, and sediment flows. Organic agents are represented by carnivores (digestive processes), large animals (trampling), plant roots, and aquatic bioerosion/corrosion. Occasionally, abrasion and polishing are direct result from intentional anthropogenic activity.

Cracking is defined as the opening of splits and cracks penetrating beneath the surface of the bone, but without any apparent loss of surface tissue. On teeth it may present as shrinkage of dentine at first, but once the dehydration level reaches a critical level it may present cracks. Flaking is associated with cracking processes, but it includes loss of surface tissue along the cracks. Inorganic processes associated with cracking and flaking are weathering, exposition to heat, sediment pressure or exposure to alkaline environments. Organic agents may induce this phenomenon by digestion or solution marks (e.g., plant roots) (Fernández-Jalvo & Andrews, 2016). The most probable cause of cracking and flacking is weathering, as exposure to dry conditions favours their appearance. Cracking and flaking were the most common taphonomic process on Gruta do Morgado Superior and therefore were classified using a scoring system that uses records only their presence (see **Table 50**).

Table 50. Recommended categories for the classification of flaking and cracking by Fernández-Jalvo and Andrews (2016, P. 203)).

Score (*)	Database ID	Description
0	**-**	No modification – Not used on database.
1	**Flacking/Cracking I**	Cracking parallel to fibre structure.
2	**Flacking/Cracking II**	Concentric flacking associated with cracks and loss of moist.
3	**Flacking/Cracking III**	Bone surface with patches of rough compact bone resulting in fibrous structure extending to cover the entire surface. Penetration up to 1.5mm.
4	**Flacking/Cracking IV**	Bone surface is coarsely fibrous and rough, splinters falling away, cracks open and rounded edges.
5	**Flacking/Cracking V**	Bone falling apart in situ, with splinters around the remaining bone core which is fragile and easily broken.

(*)Behrensmeyer's score.

Corrosion is understood as a surface modification that results from inorganic and organic chemical reactions acting in conjunction. The inorganic agents involved are generally chemical dissolution processes typical in caves and the presence of corrosive material on soils. Organic agents can be fungi, algae, moss, lichen, and bacteria. Digestion, although closely related, has a broader area of effect on the element that includes the surface and the interior of the bone. This penetration is possible thanks to the stomach's highly acidic environment and the digestive enzymes involved (Fernández-Jalvo & Andrews, 2016).

Breakage of skeletal elements is understood as a bone's integral dissolution. Methodological approaches to breakage usually employ the definition and classification of fracture patterns. Fracture patterns can be classified by morphology of the outline, angle, and edge. In Gruta do Morgado Superior, these categories were included for further description on broken elements (see **Table 51**).

Table 51. Types of fracture as described in Fernández-Jalvo and Andrews (2016).

Type	Description	
Fracture Outline	Curved or pointed	angle oblique to the long axis of the bone ending in a sharp point.
	Transverse	Perpendicular to the bone.
	Mixed	On dry bone.
Fracture angle	Oblique	Either acute or obtuse, associated with green bone fractures.
	Perpendicular	Perpendicular to the .to the long axis.
	Transverse	Typical on buried bones.
	Perpendicular and Transverse	
Fracture edge	Smooth	Usually found on green bone-; perimortem.
	Jagged	Usually found on dry bone; postmortem
	Peeled	Heavily jagged material (*),
Shaft Circumference of limb bones	Complete shaft More than half of the shaft Less than Half of the shaft	The extent to which the circumference is complete or split.

(*) Peeling definition and extent was extracted from Blasco et al. (2020), as they are clearer and include other taphonomic agents such as carnivores.

Organic agents involved in bone breakage include large animals (trampling), carnivores and herbivore activity (chewing), raptors (scavenging), and humans (dislocation and butchery). Fractures that present peeling (i.e., heavily jagged material, with a parallel fracture on the periosteum) are usually associated with human activity, but recent studies have noticed that carnivore activity (such as the one produced by bears) bear a striking similarity (Blasco et al., 2020). Inorganic agents are usually confined to sediment pressure and/or movement, although the weakening process may be catalysed by other factors.

Breakage has plenty of application in funerary contexts. Indexes obtained through these patterns are used often to assess the fragmentation degree of a sample, by analysing the breadth/length ratios of fragments. However, in extreme breakages (such as GMS) it may be impossible to reconstruct the generation pathway. Dental breakage analysis usually compares the number of isolated teeth against the ones still in mandibles/jaws to estimate the lost percentage of material.

When approaching fragmentation, some methodological tools have been suggested to obtain ratios useful for analysis. The Anatomic Preservation Index (API) is a score that assess the quantity of osseous material present. It was proposed by Dutour (1989) and presents the ratio between the score of preservation and the total anatomical number of bones in the skeleton. The score of preservation is a number between 1 and 10, each representing 10%. The Bone Representation Index (BRO) measures the frequency of each bone in the sample. It is the ratio between the actual number of bones removed during excavation and the total number of elements that should be present (vertebral column, costal cage, hands and feet are counted as one) (BRI= 100 x $\sum Nb\ observed / Nb\ theoretical$) (Fernández-Jalvo & Andrews, 2016, P.315). These indexes present methodological difficulties for their correct application in Gruta do Morgado Superior, as most of the material is fragmented and the ones complete or most abundant belong to areas that are diminished by the scoring system.

3.3.17. Coordinated Elements

As previously stated, (**see section 3.2.5**), most of the coordinates were transformed into a new system that accurately represented the site's morphology. The original **UTM** coordinates for point **0** (the intersection of x and y axes) were: **Quadrant 29 UTM – M 549741 / P 4390127**;(Cruz & Oosterbeek, 2012, p. 1). Thanks to the location of this point, the entirety of the coordinated entries was extrapolated to UTM (Portugal-29) coordinates. These coordinates were later used to plot most of the maps and graphs in the results section.

4. Results

Paleontological and archaeological contexts are often composed by disarticulated skeletal elements (understood as the separation and dispersal of these from their anatomical position). A handful of inorganic and organic agents may be responsible for such depositions. Thus, activities like scavenging, transport, trampling, and human disturbance are common agents responsible for the deposition patterns. Although the sequence in which a living organism is disarticulated depends heavily on the species, its size and environmental factors, some patterns are exclusive to certain taphonomic processes (Fernández-Jalvo & Andrews, 2016).

Generally, the first elements to separate from a body are the scapula and the mandible. The shoulder and neck articulations separate next, followed by the hindlimbs. The forelimbs and hindlimbs follow a similar pattern afterwards, disarticulating from the distal elements towards the proximal ones. The vertebral column remains bound together longer than the rest, and once it begins the process it does so starting with the cervical section towards the sacrum. This pattern applies to a body that has been left relatively untouched by most of the agents previously mentioned. Butchery patterns result in very different patterns of disarticulation, as well as hunting, scavenging, and flooding events.

Additionally, some skeletal elements tend to be more susceptible to transport and dispersal than others. Hydrodynamic dispersion may be responsible for transport, deposition, and final orientation of some bones. Flat bones, such as the scapula, may be especially prone to be swayed away by water streams. Carpals, tarsals, and phalanges require a somehow small amount of energy to be relocated, while teeth, mandibles, and some skull sections provide the most resistance, requiring a rate of energy of approximately 152 cm/s. Gravitational dispersion is also responsible for disarticulation, although its effects differ depending on the landscape (degrees and type of slopes) as well as the shape and weight of the skeletal element (Fernández-Jalvo & Andrews, 2016).

Funerary contexts complicate the matter further, as anthropic activity couples with other inorganic and organic forces to complexify the pattern of deposition. One of, if not the most important question, is what caused the pattern of material distribution found at Gruta do Morgado Superior? Several theories have been proposed (see **2.3.3**), mainly attributing the site's configuration to a continuous anthropogenic use from the Neolithic until the Early Bronze Age, in which new burials were placed on top of the old ones, altering the sediment during each inhumation. In this scenario, anthropogenic modifications acted in conjunction with numerous (and secondary) taphonomic agents such as soil alkalinity, the cave's natural remodeling process, and weathering (e.g., air water, and bioturbation). Although the academic consensus points to the presence of a primary burial context (given the proliferous presence of sesamoid bones), many questions are left unanswered.

For starters, the bulk of the archaeological material is confined to a slither of sediment which thickness barely surpasses 3.2 cm (the minimum value was 76.9 while the maximum 80.1 msl). Either the original level of the soil during the Neolithic was much higher, eroding away gradually (which would explain why most of the elements were scattered without any apparent pattern), or the Chalcolithic and Early Bronze Age communities were aware of the site's usage in ancient times, enticing them to perform similar burials on top of the ones already on place. The second theory would imply that (given the small range of movement) new inhumations would have needed some clearing of soil old bones towards the sides to make space for new burials.

To prove either theory, it was first necessary to perform a bioarchaeological analysis (see section **3**) to be able to differentiate and compare the location of the material by chronological, biological, and taphonomical adscription.

This section is subdivided into two large portions. The first one's main objective is to convey the results obtained when applying the multivariate analysis exposed in Materials and Methods. The second one will provide cross-related data among the variables.

4.1. Minor changes to Database Information

Once the analysis was finished, some changes were made to correct issues related to missing information or incongruencies.

First, there was a group of variables that recorded material orientation and size (inclination, C_cm, L_cm, E_cm, A_cm, D_cm), mostly used on pottery fragments. These variables would have been useful if not for the fact that from the 18636 records only 160 records were filled. Their prevalence was too poor to consider them as a global variable, so the group was not included in the results.

A second group of modifications was done regarding the chronological adscriptions of Stratigraphic Units that were left unclassified. Material recovered in fringe zones (e.g., SU [002-003], SU [002-004], etc.) was given all periods associated with each parent SU. SU [009] was separated into the material belonging to historic times and material without chronological allocation. SU [011] was registered as an archaeologically sterile layer on field reports, but due to the existence of an arrowhead and four skeletal elements fragments, it was allocated to the Chalcolithic, considering that the contiguous layers belong to that period. SU [024], classified as archaeologically sterile, yielded 47 records of human remains, and was chronologically ascribed to the Neolithic/ Chalcolithic/ Early Bronze Age as it is contiguous to layers bearing all three chronologies.

Although SU [030] yielded 62 records, lack of information about adjacent layers impeded any inference of its chronological allocation. The material includes a considerable amount of malacological samples, an arrowhead, lithic and human remains. The same holds true for SU [048] (47 human skeletal elements fragments, 1 anthracological sample, 1 mineral sample) , SU [049] (41 human skeletal elements fragments), SU [050] (6 human skeletal elements fragments), SU [051] (9 human skeletal elements fragments, one diagnostic sherd, and 2 faunal bones), SU [052] (13 human skeletal elements fragments and two mineral samples), SU [053] (one skeletal element), SU [057] (11 skeletal elements), SU [058] (2 skeletal elements), and SU [060] (6 skeletal elements).

It is worth noting that these changes are subject to revision in the future, as these fringe locations may belong to different chronological periods. The most reliable way of finding out would be through absolute or relative dating. This process is highly recommended once the material (including all categories) is analysed in conjunction.

4.2. Ecofact and Artifact distribution in Gruta do Morgado Superior

Ecofact and artifact distribution provided a general overview of the patterns already described during previous campaigns. The bulk of human remains was found along the southern wall, creating a cluster that comprises squares I51, I52, J50, J51, J52, J53, K50, K51, K52, K53, L51, L52, and F53. The cluster is limited to the North by blocks resulting from the rock shelter's ceiling collapse, effectively dividing the cave into northern and southern sections. Small clusters of human remains are visible towards the western side of the cave and correspond to Sepulchral Pit 1 (see **Figure 1**).

Figure 69. Spatial distribution patterns of artifacts: (Ceramic ware (red square), lithics (green diamond), tools (purple circle), adornments (yellow square), figurines (green circle), metal tools (orange circle), portable rock art (brown circle); and ecofacts: human remains (light-blue circle), fauna (dark-blue circle). Elaborated with *ArcGIS Pro 3.0.0*.

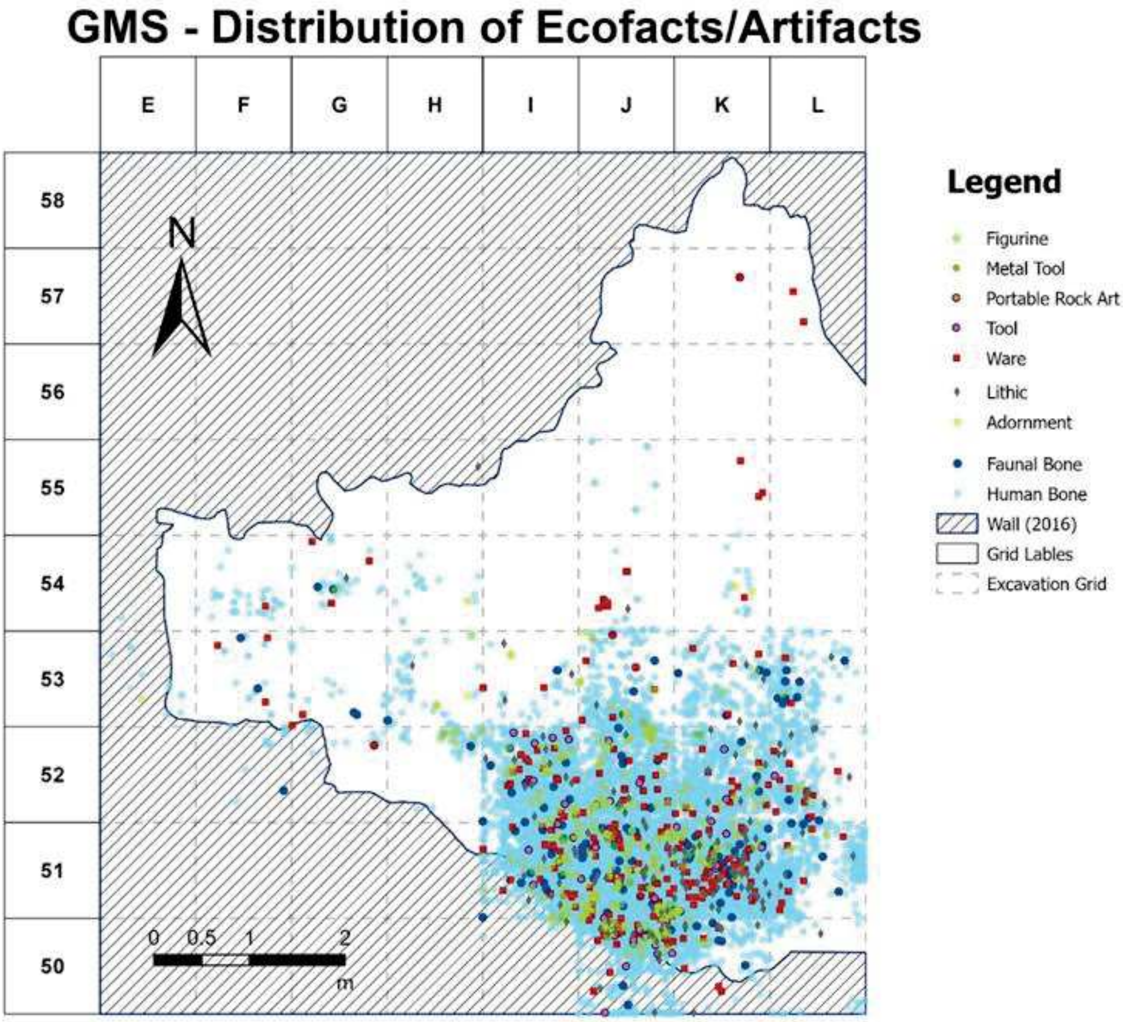

The remainder of the material follows a similar pattern, except for ceramic ware that is found in the northern section of the cave as well.

Even though the cave's exposed floor (sterile contours) has not been fully mapped yet, an alternative solution was implemented to see the microtopography of the excavation, taking the recorded material as the reference point. The minimum altitude (height) of each coordinated item on the cave was utilized to produce a small extrapolation to the surrounding area, thus creating two schematics that represent the lowest altitude at which elements were found (see **Figure 70** and **Figure 71**). The results showcase a southern basin, where most of the records concentrate, with a few smooth plateaus at the south-west section and at the centre. There is an abnormally elevated area that encloses the main cluster at the south-east section of the entrance.

Figure 70. Altitude recorded for the lowest values coordinated at Gruta do Morgado superior. These values are extrapolated to an area of 0.1 m. Elaborated with *ArcGIS Pro 3.0.0*.

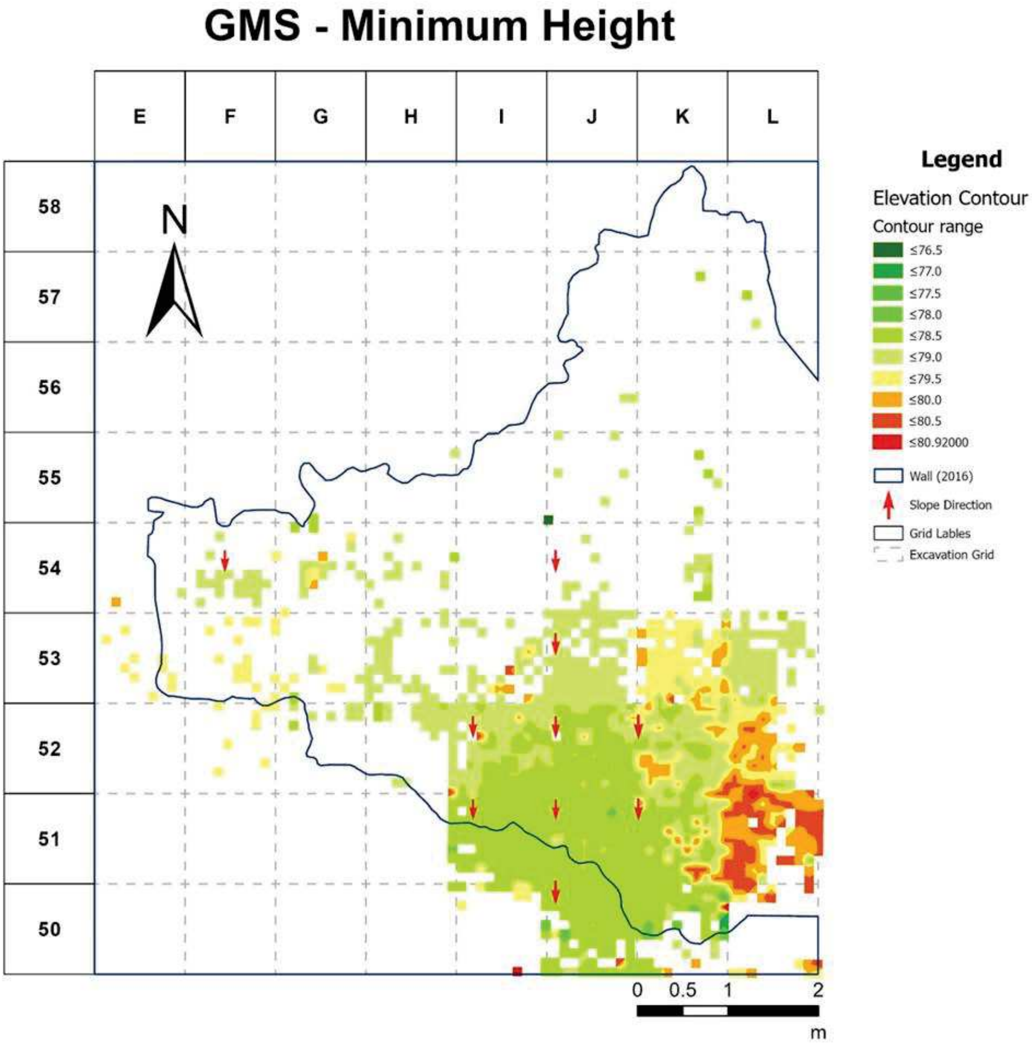

Figure 71. Altitude recorded for the lowest values coordinated at Gruta do Morgado superior. These values are interpolated to create a continuous surface area. Elaborated with *ArcGIS Pro 3.0.0*.

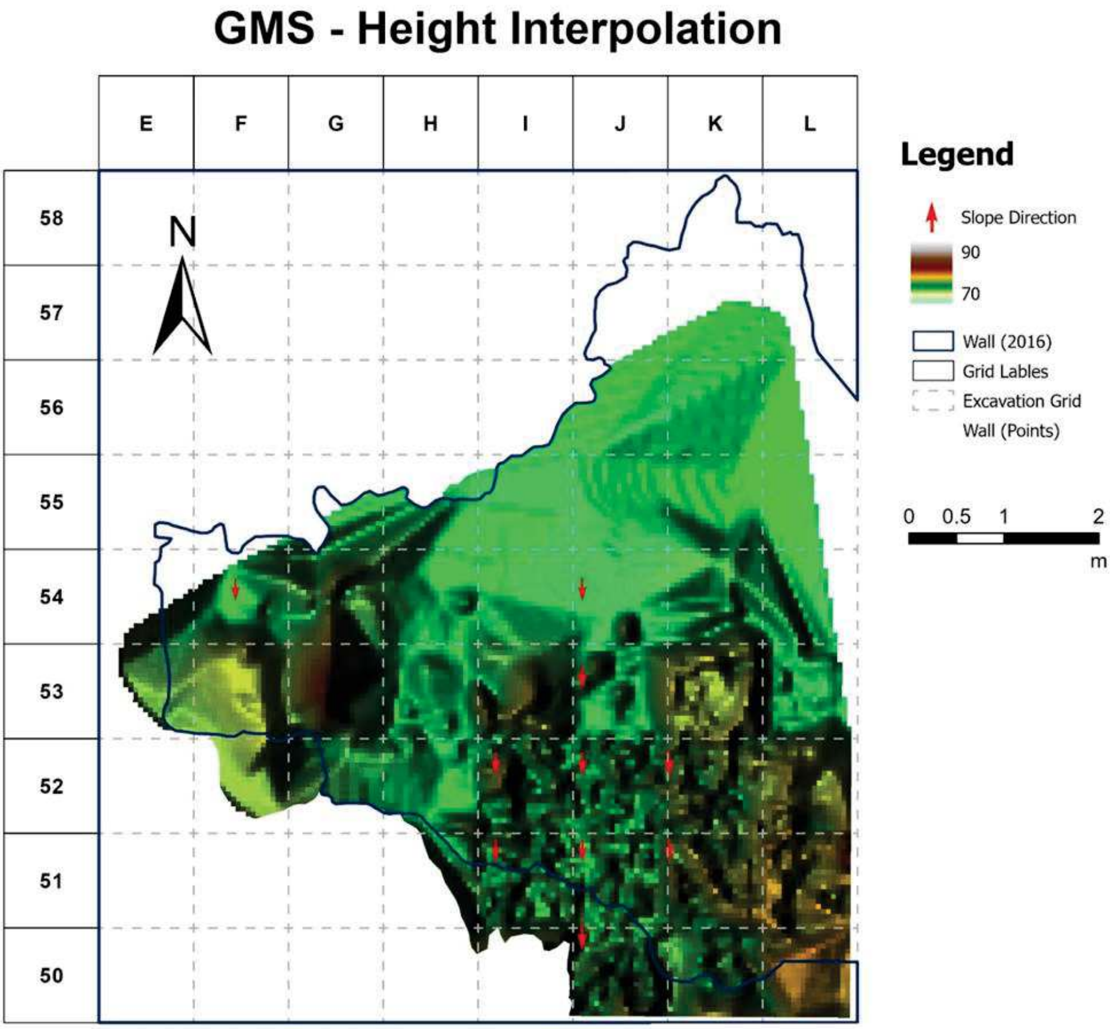

Its counterpart (Figure 71) displays a similar layout, in which two areas represent relatively high values (around 80 msl) at the west and south-east corners. Two zones present mean values of around 75 msl at the northern and southern margins. The last figure is an interpolation, which means that the topography's complexity does not represent the actual topography of the cave; a rather clumped layout symbolizes a high density of material, which is why the northern section seems to be flatter than its southern counterpart. However, darker maroon colours represent the halt of archaeological material appearance in the soil, which happened relatively sooner than in the brighter green areas. These coincide with the highest concentration of blocks. The same can be said about the smooth sections that represent a similar landscape, located at a slight lower elevation and more homogeneous. The eastern maroon elevation represents several boulders that span from Square G53 to G54, while the middle maroon spots represent the block barrier that divides the site. Another remarkable feature is the fact that material in the southern wall may indicate that the archaeological layers subducts towards the subsoil at the base of the cave, effectively creating pockets of sediment that had to be reached by excavating the under the visible southern wall. The presence of materials under the cave's original limits may indicate that the whole structure has a different layout, obscured by sediment fillings. The irregular lapiés-like (Lapiaz) surface that emerged once Cruz arrived at the archaeological sterile horizons (see **Map 3**) may have served as a south-oriented slope that concentrated most of the ecofacts and artifacts in the greatest cluster.

4.3. Chrono-cultural distribution and overall density: Kernel density plot

Kernel density estimation is a statistical tool that, when applied to spatial data, is able to smooth the visual representation of a variable (Duong, 2007). Other density estimators are informative, but they are not usually smooth nor sensitive enough to local variability of the variable (f). The estimation is calculated as follows:

$$f(x) = \frac{1}{nh}\sum_{i=1}^{n} K\left(\frac{x-x_i}{h}\right), \text{ where } K(u) = \begin{cases} \frac{1}{2}, if \ -1 < u \leq 1, \\ 0, \text{otherwise} \end{cases}$$

Kernel's estimation is a uniform density function that works on a specific range $(-1,1]$. The depiction of data will ultimately depend on the smoothness of the kernel function (Simonoff, 1996). Generally, the equation uses a Gaussian density for *K* (*h* = 08), as it seems to perform better than others (e.g., Epanechnikov, Biweight, Triweight, Uniform, etc.) (Carbon et al., 1996; Simonoff, 1996). The resulting plot is a representation of an average of the Gaussian densities centred at each observation. Kernel's density may be applied to non-parametric data without the need of refining it, while having the potential of being used to test spatial interaction (Hallin et al., 2004).

In Gruta do Morgado Superior the kernel density plot was applied the *Categories* variable and a Gaussian density fork, using **ArcGIS Pro 3.0.0**. The software package calculated a magnitude per unit area from a single point, assigning a visual value. This exercise's main objective was to determine the mean dispersion of the material and eliminate possible confusion when observing many individual points. It is worth noting that this plot may eliminate isolated (outlier) points that behave erratically. The categories analysed were *Metal Tools*, *Ideotechnic Elements*, *Lithic Tools*, *Ceramic Ware*, *Faunal Remains*, and *Human Remains*.

4.3.1. Metal tools

Density analysis of metal tools provided two small clusters in the southern wall of the rock shelter. Both represent two out of three elements found on squares I51, J51, and K51 (see **Figure 72**).

Figure 72. Kernel density plots for different categories. Elaborated with *ArcGIS Pro 3.0.0*.

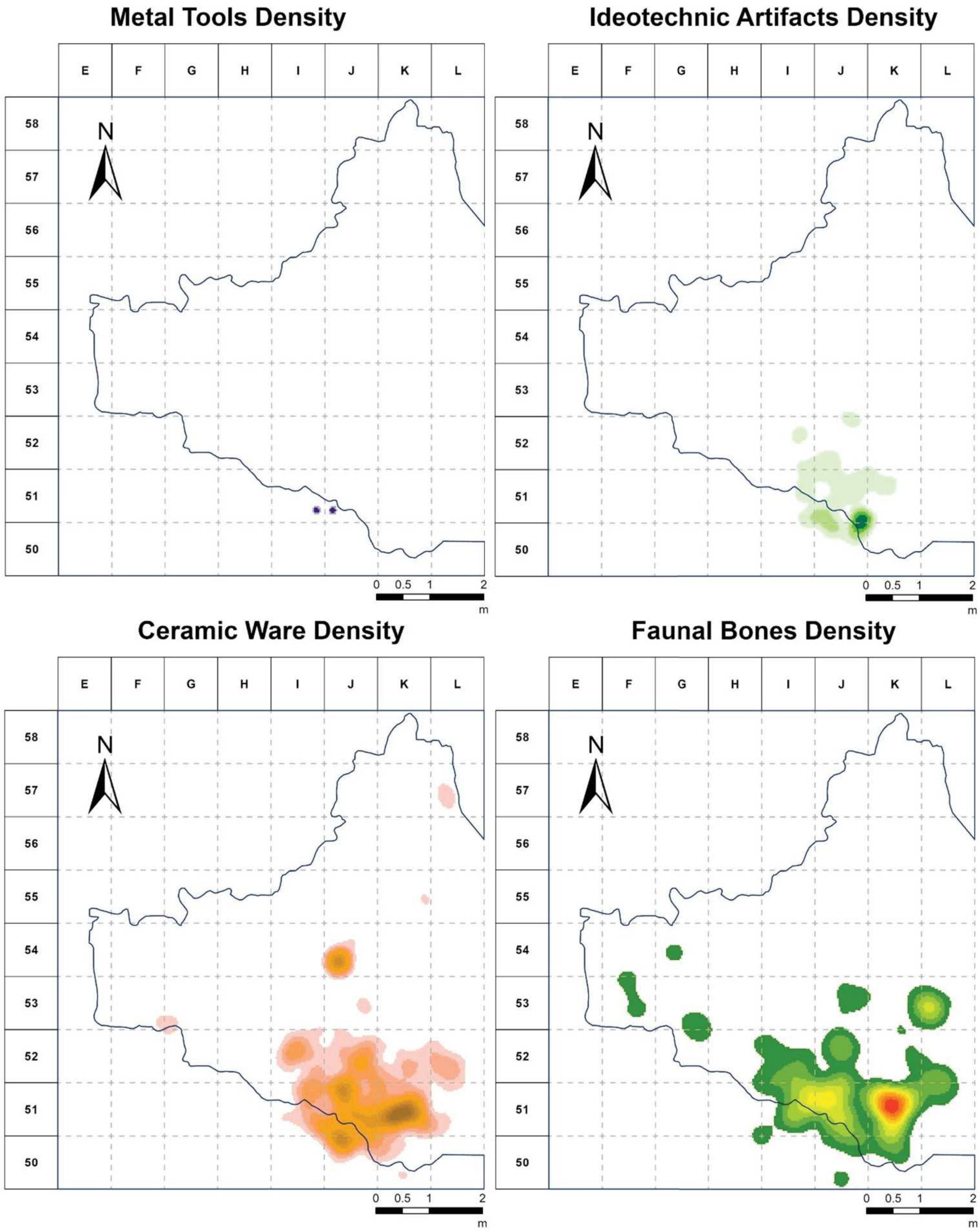

Previous campaign reports mentioned one barbed arrowhead on copper (J51-0119 - found in 2012), a casting drop on bronze (found in 2013) and a diamond-shaped perforator (*punção losânguico*) on bronze (I51-1173 - found in 2015) (Cruz, 2020). The database differs from the reports slightly, as the casting drop record was not found, but an additional copper arrowhead was registered as K51-0392. It is possible that they may refer to the same item. All these elements were found within Stratigraphic Units (SU) associated chronologically to the Chalcolithic (i.e., [001],[002], and [002i4i]) at an average height of 78 msl.

4.3.2. Ideotechnic material

Material associated with symbolic behaviour, here referred to as ideotechnic, showcased an amorphous cluster located at the southern wall. Categories such as *Adornments*, *Bone Tools*, *Figurines* and *Portable Rock art* were included. Field repots described adornments such as earring (made on a boar's tusk), five earrings without any specifications, a portable rock art slate (carved on schist), one hundred eighty-eight beads (mostly carved on muscovite), four perforated shells, one polished ring, and forty-three hair pins. Tools carved on bone included seventy-one burins and thirty spatulas. A few items exhibited anthropomorphic features: a zoomorphic statue, three anthropomorphic figurines, one *Almeria*-type figure, two decorated plaques (carved in schist and bone respectively), and four spatulas. (Cruz, 2020).

A discrepancy was found between field reports and elements within the database. The steepest difference was observed on the number of bone tools and their specific classification, as most burins are missing from the database (see **Table 52**). It may be possible that the missing material is a result of miscount. Further spatialized research is recommended.

Table 52. Representation by category of ideotechnic artifacts.

Period	Adornment	Bone Tool	Figurine	Portable Rock Art	Total
Neolithic	18		2		20
Late Neolithic/ Early Chalcolithic	1				1
Neolithic/ Chalcolithic	6	2	1		9
Chalcolithic	226	38	8		272
Chalcolithic/ Early Bronze Age	54	8		2	64
Early Bronze Age	7		1		8
Undetermined	1				1
Total	**313**	**48**	**12**	**2**	**375**

The spatial dispersion pattern of ideotechnic material was concentrated along the southern wall, presenting a main cluster surrounded by two small concentrations that diminish in intensity the farther away they are from the south. Figurines seem to be contained within contiguous squares; one was found on square I51, five on square J51, one in square J53, two in square K51, and two on square K52. Nine figurines were associated to Stratigraphic Units (SU) from the Chalcolithic, while the remaining three were distributed into the Neolithic (J51 – SU [004]), the Neolithic / Chalcolithic (K51 - SU [032]), and the Early Bronze Age (J51 - [003]).

Chronologically, there is an apparent lack of diversity when comparing material from both the Neolithic and the Early Bronze Age to the Chalcolithic. Rock art elements are confined to the transitional phase between the Chalcolithic and the Bronze Age, while most bone elements tend to concentrate in the Chalcolithic and its peripheric sub-categories (see **Chart 1**).

Chart 4. Distribution of ideotechnic artifacts by chrono-cultural period.

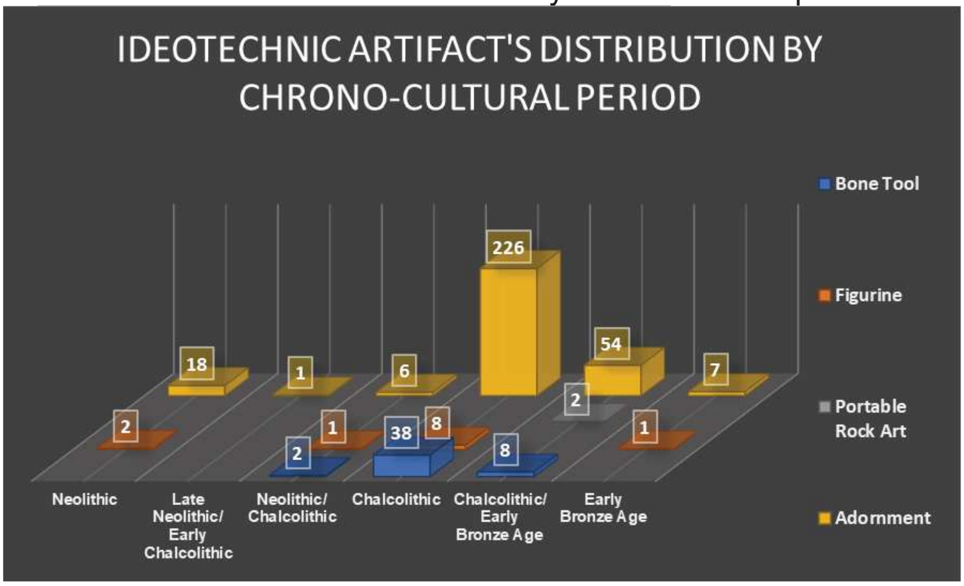

This pattern is analogous to the adornment's subcategories chrono-cultural distribution. As previously stated in **section 3.3.5**, adornments included five subcategories that include rings, trinkets, earrings, hairpins, and beads. A closer evaluation (see Figure **73**) reveals that the presence of beads is ubiquitous in all squares, with different degrees of density.

Figure 73. Spatial distribution of adornments contrasted with kernel's density plot (light green) (figurines and plaques included). Elaborated with *ArcGIS Pro 3.0.0*.

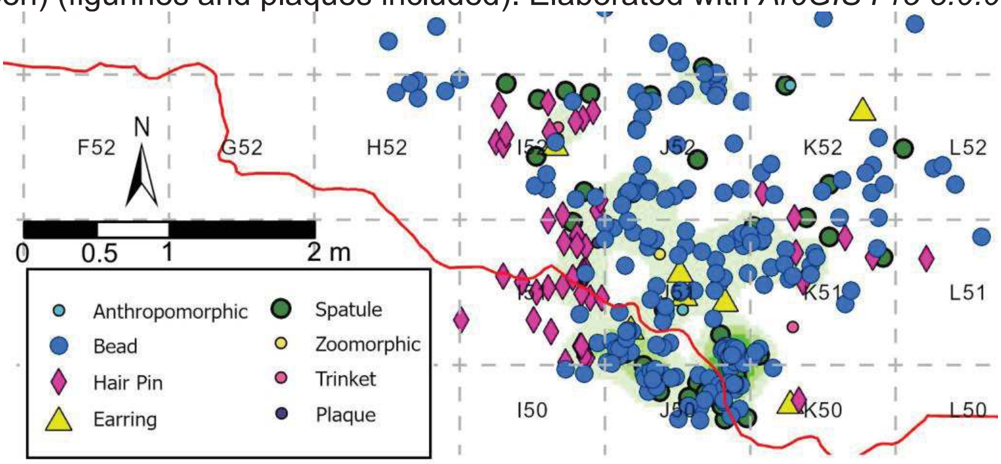

Hair pins seem to form two distinct clusters to the east (squares K50, K51, and K52) and to the west (squares I51 and I52), spatulas revolve in three distinct clusters around square J51, each placed in squares K52, I52 and J50 respectively. Idols, rings, earrings, and trinkets don't seem to follow a specific pattern but are confined within the same area from columns I, J and K at the rows 50, 51 and 52.

The gap observed within the ideotechnic material Kernel's plot (see **Figure 72**) represents the apparent lack of material from this category at Square J51. It is worth noting that from this point some elements appear to follow radial distribution towards adjacent squares. The densest point between J50 and K50 is mostly a result of an accumulation of beads, following the same southern inclination.

Diversity at the chrono-cultural level behaves similarly, as beads and hair pins are found in most of the chrono-cultural periods. The distribution of both subcategories' mirrors that of the general ideotechnic spread: a small quantity of objects ascribed to the Neolithic, a surge in size of Chalcolithic elements, and an overall decline in the Bronze Age. Furthermore, material associated to the Chalcolithic is more diverse than the other two, containing earrings, trinkets, and rings (if one includes the transition to the Early Bronze Age) (see **Chart 1**).

Chart 5. Distribution by Adornment's subcategory in different Chrono-cultural periods.

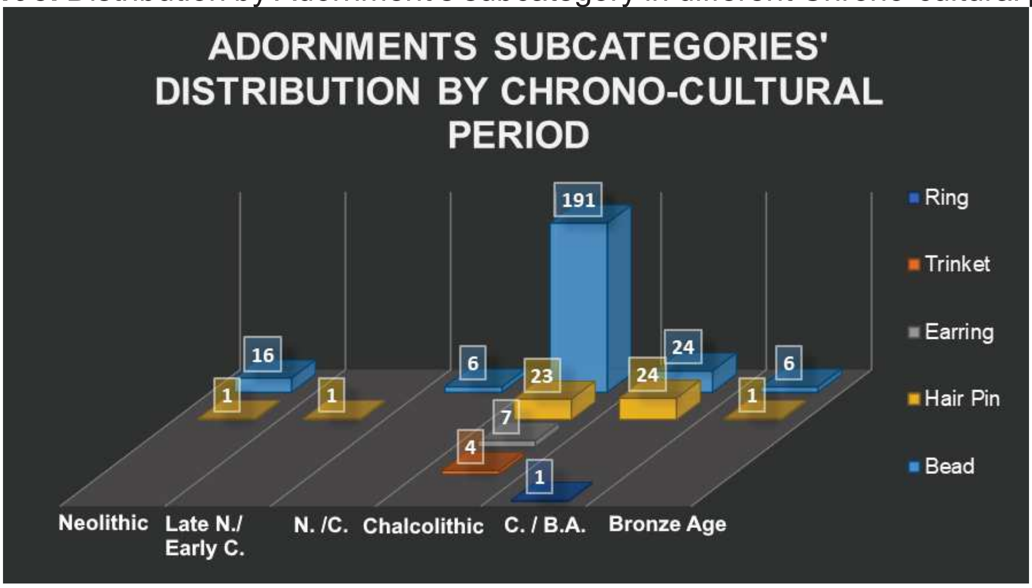

The distribution of ideotechnic material could be interpreted as an indicative of funerary patterns that grow in complexity through time. The advent of grave woods during the Neolithic was wildly popularized in the Chalcolithic, and eventually started to decline during the Bronze Age. On the other hand, it could also indicate that Gruta do Morgado Superior was used as a burial site by Chalcolithic-associated communities more frequently than Neolithic or Bronze-Age communities.

4.3.3. Ceramic ware

Pottery fragments included two hundred and two sherds (unclassified), five bases, thirty-nine rims and nine complete profiles (Cruz, 2020). Although ceramic description regarding its overall characteristics was detailed on the field reports, the information on the database was not as specific, hampering any comparison between them in terms of style. Ceramic ware follows a similar pattern to previous categories (when observed through time) reaching its peak during Chalcolithic and the Chalcolithic/Early Bronze Age. Variance in fragmentation and identification was the most important feature, as the Neolithic, Chalcolithic, and Chalcolithic/Early Bronze Age contained well-preserved vessels and profiles (see **Table 53** and **Chart 6**). In contrast, sherds or partially complete elements were found in the transition from Chalcolithic to Neolithic, or within the Early Bronze Age sediment. Its spatial distribution (see **Figure 72**), forms one main cluster to the south, and two small ones at the centre/North. Interestingly, the minor cluster on J54 is mostly shared with lithic artifacts, as the rest of materials seem to have lesser densities at this square, including human remains.

Table 53. Chrono-cultural distribution of ceramic ware at GMS.

Period	Diagnostic	Sherd	Vessel	Total
Neolithic	5	54	1	60
Late Neolithic/ Early Chalcolithic		2		2
Neolithic/ Chalcolithic	3	12		15
Chalcolithic	47	124	11	182
Chalcolithic/ Early Bronze Age	17	137	4	158
Early Bronze Age	3	9		12
Total	**75**	**338**	**16**	**429**

Chart 6. Chrono-cultural distribution of ceramic ware at GMS.

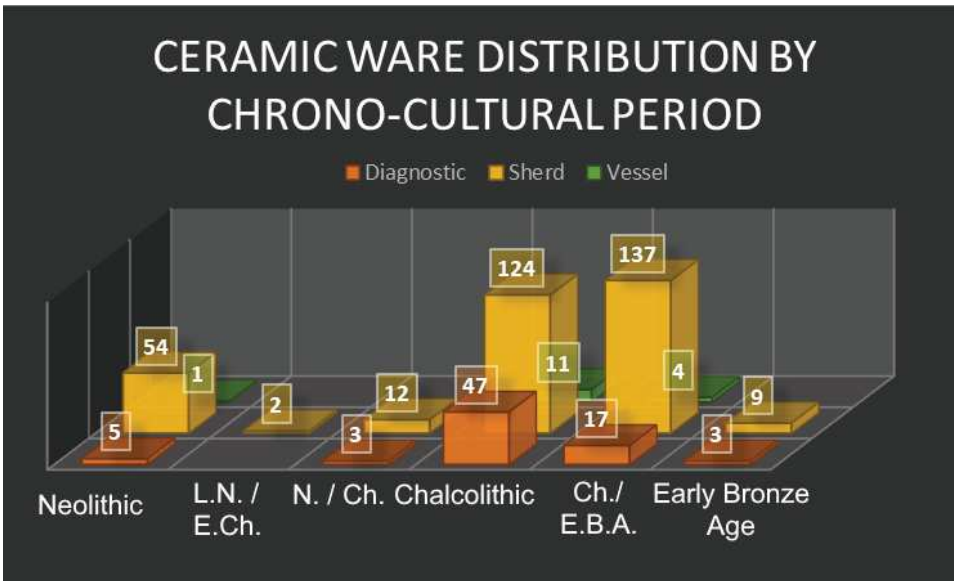

It is not clear if the material was subdivided between historic and prehistoric typologies. Cruz (2013) already stated the fact that some of the fragments found within the context have characteristics linked with Republican periods (late 1980's). If the material was indeed separated, it is expected that all the fragments in prehistoric SUs are, in fact, prehistoric ceramic ware.

The only subcategory with enough data for analysis was the manufacture process (**Chart 7**). Manufacture was divided between manual (possibly a coiling technique) and mechanical (using a potter's wheel). Both methods were apparently employed simultaneously throughout all three chrono-cultural periods. Variance in usage between one or the other seemed steeper during the Neolithic, where the manual technique is hardly represented. The potter's wheel remained as the most popular technique until the Bronze Age, never fully replacing the manual procedure. Further spatialized analysis is required.

Chart 7. Chrono-cultural distribution of ceramic manufacture at GMS.

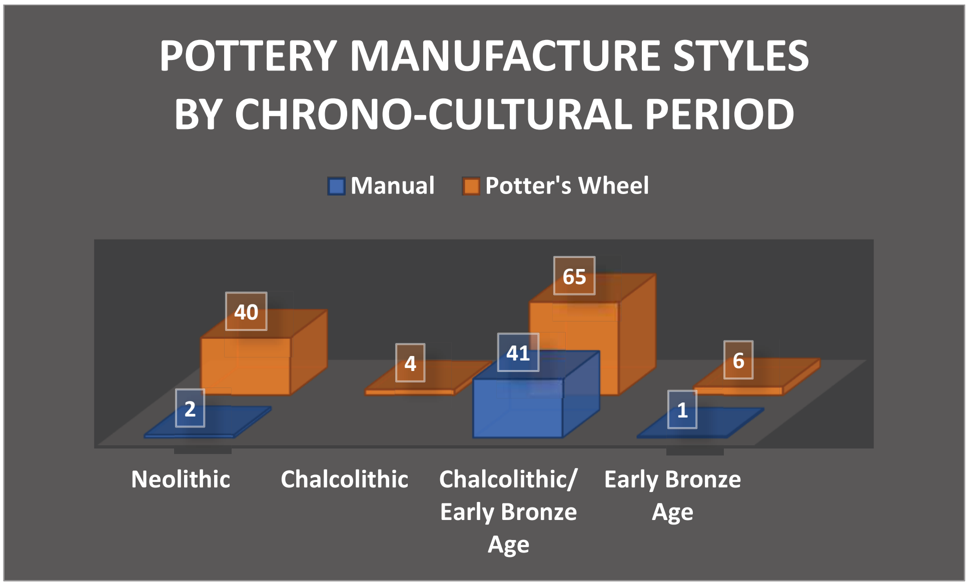

The variable of Minor classification yielded a few notable results such as plastic decorations (2 elements), glazed surfaces (1 element), and incised decorations (1 element). All characteristics belong to pottery sherds associated to SUs linked to the Chalcolithic. Hemispherical vessels (2 elements) were ascribed to the same chrono-cultural period. The apparent lack on ceramic ware motifs and decoration may result of the level of fragmentation of the material, or the absence of systematic information on the type of ware found at the rock shelter. If the information recorded on the previous database is accurate, this would indicate that ceramic ware in the Chalcolithic was also more diverse than its Neolithic and Bronze Age counterparts.

4.3.4. Faunal remains

According to the balance presented in 2020, the total number of fragments belonging to faunal remains corresponds to 57 elements (*peças*) including teeth (Cruz, 2020, p. 47). Conversely, the database yielded 181 elements (see **Table 54**). Recent studies have raised amount to over 800 fragments. It is important to bear in mind that the field reports and database refer mostly to coordinated elements. As mentioned before, records without coordinates are composed of bags filled with material recovered from sieved sediment. These bags contain dozens of pieces that only have a square designation as main point of reference. It remains unclear if the missing data in the reports corresponds to entries that were added later.

Table 54. Distribution of the faunal assemblage into chrono-cultural periods.

Chrono-cultural period	Faunal Bone	Total
Neolithic	26	26
Neolithic/ Chalcolithic	11	11
Chalcolithic	60	60
Chalcolithic/ Early Bronze Age	79	79
Early Bronze Age	4	4
Neolithic/ Chalcolithic/ Early Bronze Age	1	1
Grand Total	**181**	**181**

A study, mainly focused on leporids from Gruta do Morgado Superior, was published recently by Nelson Almeida et al. The publication has an inventory with most of the identified taxa, in which at least 851 elements were analysed (see **Table 55**).

Table 55. Absolute (NISP) and Relative (NISP%) number of Identified Specimens and Minimum Number of Elements (MNE) at GMS (Almeida et al., 2023, p. 4, modified).

Taxa	NISP	NISP%	MNE
Bos taurus	1	0.2	1
Ovis aries	11	2.5	6
Ovis/Capra	20	4.5	13
Cervus elaphus	2	0.5	2
Capreolus capreolus	2	0.5	2
Sus sp.	4	0.9	4
Vulpes vulpes	2	0.5	2
Meles meles	7	1.6	7
Felis silvestris	1	0.2	1
Carnivora ind.	4	0.9	4
Lepus sp.	2	0.5	2
Oryctolagus cuniculus	196	43.8	150
Leporidae	187	41.7	124
Aves ind.	9	2	8
Indeterminate	403	-	
Total	**851**	**100**	**326**

The kernel density plot of faunal remains showcases several clusters, with the densest being situated at K51. When compared with Almeida's team results, the highest density point (for leporids, carnivores, and carnivore activity) is not the same; for them Square F53 would have the most leporids and carnivores, with squares 51, J52 and J53 being secondary assemblages. The publication is focused on fragments without dividing any chrono-cultural description, because the faunal material on the cave could be contaminated by taphonomic and erosive processes. Although they found evidence of heat exposition, they concluded that the leporid accumulation's main depositional agent were carnivores (namely *vulpes vulpes*), and that human alteration was unlikely or sporadic.

When comparing Almeida's team results with both the Kernel's density plot and the location of coordinated faunal elements by chrono-cultural adscription, Square F53 seems to contain bones from the Early Bronze Age while Square K51 and its adjacent squares have a higher composition of Chalcolithic material. The clusters to the North-East (Squares K53 and L53) are dominated by Early Bronze Age assemblages. Chalcolithic-associated material is located south-east from F53 and northwest from K51 (see **Figure 74**). However, when analysing fringe chrono-cultural associations, the southern cluster appears to bear material from all periods.

Figure 74. Comparison between the location of the material (database), kernel's density plot (green area), and squares with the most density of leporid and carnivore remains described by Almeida et al. (2023, p. 10).

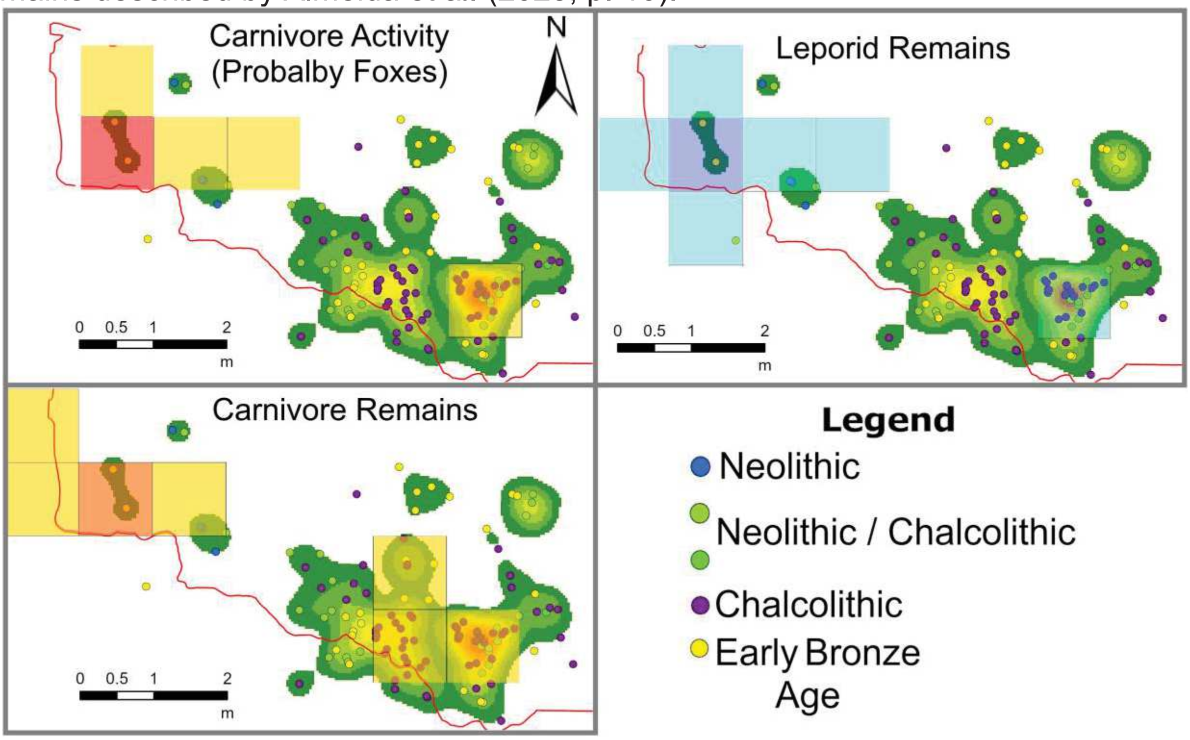

It is recommended that in future analysis Almeida et al.'s inventory is added to the general database of the site.

4.3.5. Lithic technology

On previous field reports, lithic materials included one polished adze, one polished axe, five scrappers, sixty-nine arrowheads, one core, seventeen flakes, twenty blades, twelve bladelets and three hammerstones (Cruz, 2020). After the database consolidation the number of cores increased by one while the bladelets lost one, and flakes and arrowheads increased their presence significantly (see **Table 56**).

The distribution of elements presents only one oddity, the presence of a chopper (I51-1559) that usually is found in older chronologies (Mode I), however it may be part of macrolithic traditions associated to the Mesolithic/Early Neolithic. The rest of the assemblage behaves as expected, indicating a continuous process of specialization towards an agricultural socio-economic system that is supported by hunting activities (or the other way around if one compares quantities of each).

Table 56. Distribution of the lithic material by chrono-cultural period at GMS.

Lithic element	Neolithic	L. N./ E. C.	Neolithic/ Chalcolithic	Chalcolithic	Chalcolithic/ E. Bronze Age	Early Bronze Age	Total
Adze			1				**1**
Axe			1				**1**
Chip				1			**1**
Chopper			1				**1**
Core	1				1		**2**
Scrapper	1	1		1			**3**
Sickle					1		**1**
Composite				2			**2**
Debitage				2	1		**3**
Hammerstone				3	2		**5**
Bladelet	3			12	3	1	**19**
Flake	2		1	18	9		**30**
Blade	1			14	1	1	**17**
Arrowhead	1	1	6	63	9	3	**83**
Total	**9**	**2**	**10**	**116**	**27**	**5**	**169**

Berruti and Daffara (Berruti & Daffara, 2014) performed micro-wear an analysis on well-preserved arrowheads (*n*=38) concluding that most of them were used or broken intentionally before the being deposited. The absence of distal portions of the lithic elements indicates intentionality, as even in highly disturbed contexts it is expected that at least some arrowheads are found complete. The material also presented white patina, suggesting chemical taphonomic alterations after deposition or recycling. By comparing the weight of each element and the kind of hafting, they concluded that two hunting methods were widespread within the assemblage. Unfortunately, this analysis was not focused according to SUs or chrono-cultural adscriptions, so it remains unclear if each hunting method belongs to a specific period or if they both coexisted at different points in time. It is recommended that Berruti and Daffara's database be included and translated into the new corpus of information.

The Neolithic and Chalcolithic assemblages display inherent characteristics that separate both groups, with the former including tools often associated with hunting and processing, while the latter diversifies into tools that combine agriculture and hunting. The process culminates in the Bronze Age with the presence of specialized processing and hunting material as blades, bladelets and arrowpoints (see **Chart 8**).

Chart 8. Distribution of lithic material by Chrono-cultural period.

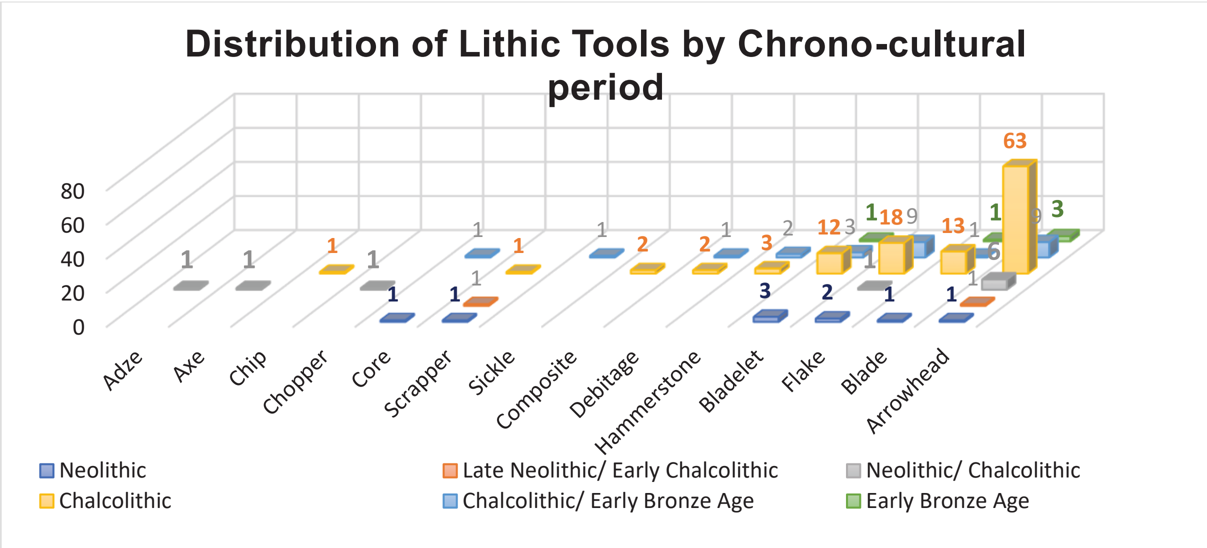

Finally, the spatial distribution locates the highest cluster of lithic material at Square K51, with some peripheral accumulations (see **Figure 75**)

Figure 75. Kernel density plot for lithic artifacts. Elaborated with *ArcGIS Pro 3.0.0*.

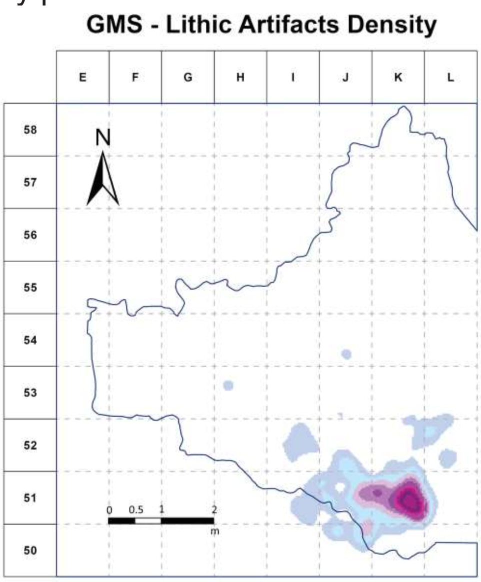

Small clusters can be seen at H52, K52, and L52. The assemblage behaves as the other categories, with a small gap in J51 that bears a striking resemblance to a similar feature on the density plot for ideotechnic material.

4.3.6. Human Remains

The final category of analysis corresponds to human remains. Kernel's density plot presents two main groups of clusters, one in the centre-south area of the assemblage, and another composed by four distinct groups towards the west. The smaller clusters correspond to the excavations from 1988 to 2013, which pale in comparison to the ones performed on the southern wall (see **Figure 76**).

Figure 76. Kernel's density plot for human remains. Elaborated with *ArcGIS Pro 3.0.0*.

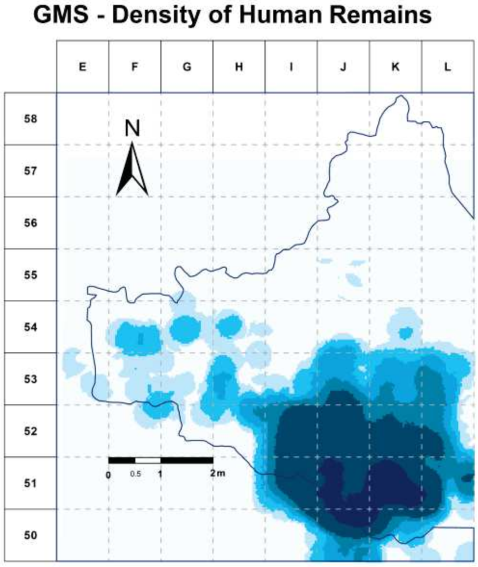

Although theoretically, the western clusters should correspond to the Sepulchral Pit I, and the one to the south to Sepulchral Pit II, these labels were dropped after the 2016's campaign, rendering a full comparison difficult as they were intrinsically linked to the original archaeological layers that would later be revamped into the Stratigraphic Units.

The only subcategory that can be analysed globally is the presence of dental elements (see **Figure 77**). Teeth tend to be concentrated in the biggest cluster, towards the southern wall and the lowest points on the altitude plot. Elements outside this section are isolated and do not seem to form big concentrations.

Material distribution by chrono-cultural period of human remains presents a similar pattern to previously analysed categories, with most of it found within Chalcolithic SUs. Groups that follow in size are those closely bounded to the Chalcolithic, followed by the Neolithic. Lastly, the lowest values belong to SUs linked to the Bronze Age, as expected (see **Table 57** and **Chart 9**).

Figure 77. Location of teeth (purple dots). Elaborated with *ArcGIS Pro 3.0.0*.

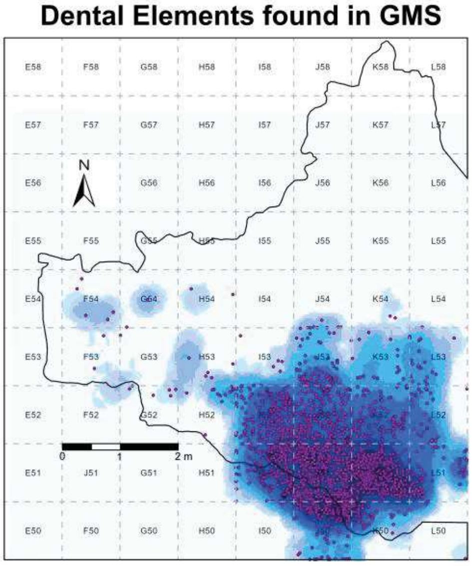

Table 57. Distribution of human remains by Chrono-cultural period.

Period	Bone	Dentine/Enamel	Total
Neolithic	642	127	**769**
Late Neolithic/ Early Chalcolithic	34	4	**38**
Neolithic/ Chalcolithic	1103	148	**1251**
Chalcolithic	9982	2431	**12413**
Chalcolithic/ Early Bronze Age	1799	475	**2274**
Early Bronze Age	226	36	**262**
Neolithic/ Chalcolithic/ Early Bronze Age	37	8	**45**
Total	**13823**	**3229**	**17052**

Chart 9. Distribution of human remains by Chrono-cultural period.

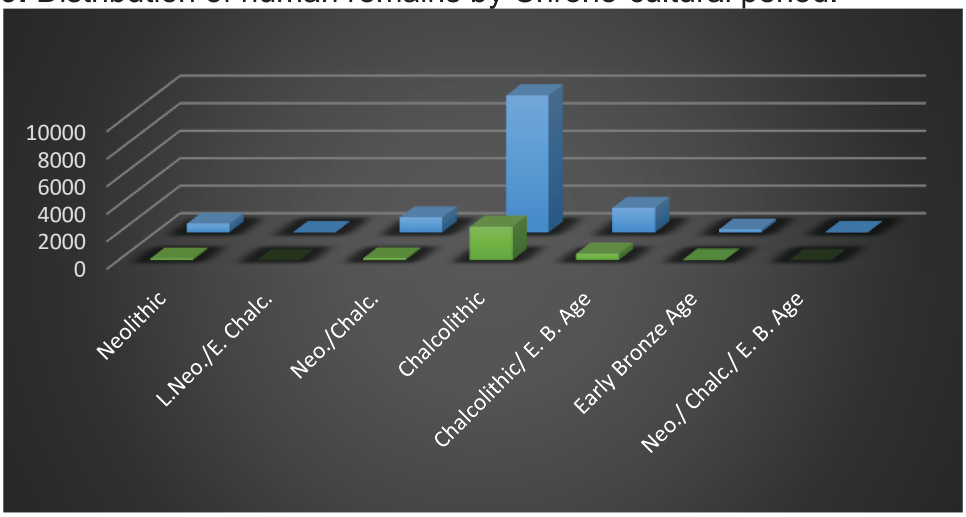

4.3.7. Conclusion

Gruta do Morgado superior presents a clear spatial pattern of distribution that seems to be concentrated in the southern wall. The secondary groupings towards the inner section of the rock shelter, to the east, coincides with the first excavation campaigns on the site. The high-density may also be a result of the excavation's methodology, which started focusing on the southern wall after 2012's campaign.

The distribution of the material also seems to create small pockets of missing elements such as square J51, and great concentrations towards K51. Most chrono-cultural periods are found in conjunction in the densest squares, which was interpreted in the past as the area where the earliest inhumations were placed.

Chrono-cultural period distribution follows the same pattern in all the categories, with the lowest concentration at the Bronze Age, the second highest concentration for the Neolithic, and the greatest belonging to the Chalcolithic. The latter also displays the highest rates of diversity and abundance in all categories and subcategories. Major and minor classifications derived from the previous database, especially ceramic ware and lithic technology are especially varied in this period.

4.4. Inventory and Minimal Number of Individuals

In the forthcoming sections, all the information exposed will be restricted to analysed bioarchaeological material on **Square K51**. First, an inventory of the observed skeletal regions by chronological ascription was made to observe the distribution of the human remains at its lowest level of depth (see **Table 58**). The inventory includes the number of elements that exhibited recognizable features to be catalogued into one of the skeletal regions, regardless of specific missing information such as ray (in phalanges), zone (in vertebrae), or side (for paired elements). The methodology used for the calculation of the Minimal Number of Individuals (MNI) carries inherently bias of proportions, as a considerable amount of elements will inevitably lose visibility, even more so in highly fragmented contexts where most fragments will not be used for the final count (Casteel, 1977; Domínguez-Rodrigo, 2012).

Table 58. Distribution of human remains by skeletal region and chrono-cultural asctiption.

Skeletal Region	Neolithic	Neo. / Chalc.	Chalcolithic	Chalc. / Early B.A.	Early Bronze Age	Und.	Total
Cranium and Mandible	7	28	105	2		2	144
Dentition (Und.)	2	22	96	10	2		132
Upper Dentition	10	50	228	20	1	1	310
Lower Dentition	11	42	226	20	1	3	303
Hyoid and Vertebrae	20	80	209	14			323
Thorax	15	59	198	9	1		282
Shoulder Girdle	3	8	32	2			45
Upper Limb	6	15	70	3			94
Hand	45	187	606	52	6	6	902
Pelvic Girdle	3	9	28	3	1		44
Lower Limb	11	25	107	11			154
Foot	56	125	568	42	4	7	802
Undetermined	26	235	530	23	1	1	816
Total	**215**	**885**	**3003**	**211**	**17**	**20**	**4351**

The most prominent skeletal regions are the hand (902 entries), the feet (802 entries), and teeth (745 entries) (see **Chart 10**). Elements from the intersection between the Neolithic and the Chalcolithic, as well as those from the Early Bronze Age behave differently to the general trend (See **Chart 11**). Material found within Neolithic SUs had the highest count value when observing elements in the *Foot* category, followed closely by the *Pelvic Girdle*, the *Shoulder Girdle*, the *Upper limb* and the *Hyoid and Vertebrae*. The Neolithic/Chalcolithic's associated material has its higher representation per bone on *Hyoid and Vertebrae*, followed closely by the *Hand* and the *Pelvic Girdle*. This chrono-cultural period presents a noticeable difference between the percentages of *Upper* and *Lower Dentition* (0.9%), while the others have lesser differences under 0.5% (the Neolithic has a difference of 0.46%, the Chalcolithic of 0.06%, and the rest have equal distributions).

Chart 10. Distribution of material by skeletal region and chrono-cultural period.

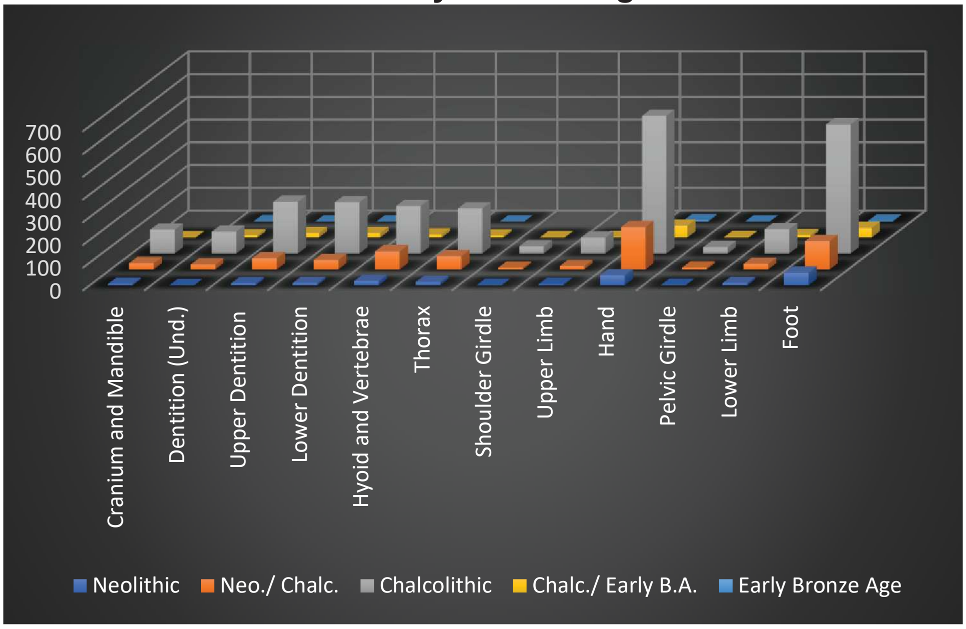

Chart 11. Distribution of material by percentage of participation in each chrono-cultural period.

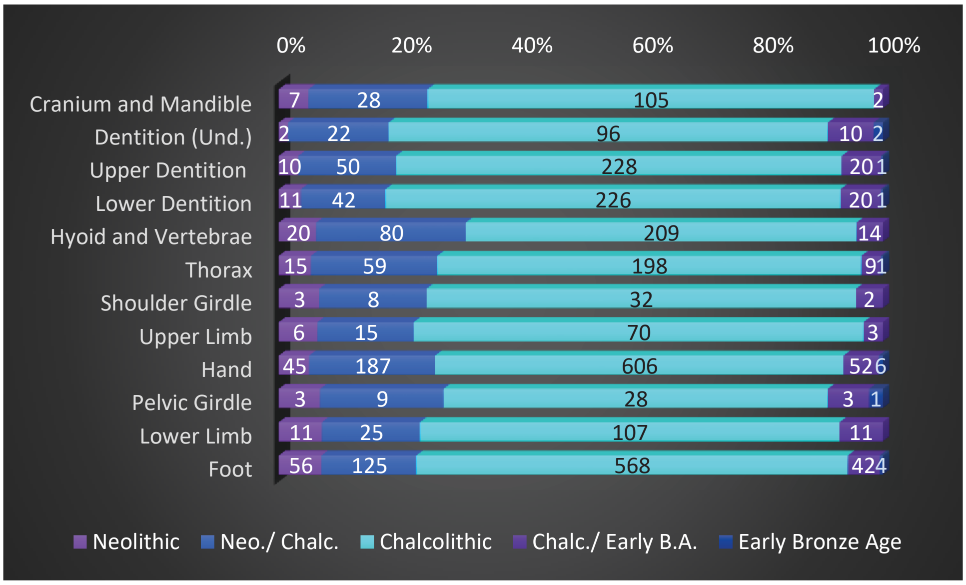

Material associated to the Chalcolithic represents around 67.5% of the total count by skeletal region, being the most abundant among all chrono-cultural periods. Its values only plumet when observing the count of *Hyoid and Vertebrae* (64.7%) and the *Pelvic Girdle* (63.6%). In both cases material associated with the Neolithic was more abundant. Internally, the most abundant categories are *Hand*, *Foot*, and *Dentition*.

The Chalcolithic/Early Bronze Age is composed mostly by bones in the *Hand* followed by the *Foot*. The remaining categories have smaller compositions (about two thirds less than the previous ones), from which the most outstanding are the categories of *Dentition* and *Hyoid and Vertebrae*.

Lastly material from the Early Bronze Age was devoid of any skeletal element associated to the *Cranium and Mandible*, *Hyoid and Vertebrae*, the *Shoulder Girdle*, the *Upper* and the *Lower Limb*.

Overall, the Neolithic assemblage as well as its related SUs present a pattern in which the axial and proximal appendicular skeleton is more usual than other elements. This trend can differentiate it from other periods, where distal elements are more common. The Chalcolithic-related material, given its size, represents the general trend that was pointed out in previous field reports, exhibiting mostly elements on the distal appendicular skeleton as well as dentition. The Early Bronze Age Material behaves likewise, displaying high counts of bones in the Hand and Foot regions, albeit the overall presence of dental pieces diminishes greatly.

4.4.1. Distribution by skeletal element

Skeletal elements presented in this section were identified satisfactorily (e.g., ray, side, region, etc.). leaving aside categories for splinters and undetermined skeletal elements. An inventory of skeletal elements by Major Skeletal Element group can be seen on **Annex 4**.

The distribution by skeletal element showcases the biggest tributaries for each skeletal region (see **Chart 12.** Distribution of skeletal elements by chrono-cultural ascription. The order of each period was tweaked so the highest values appear on the back.): dentition is represented mostly by molars, incisors, and premolars; the cranial region is represented mostly by mandibles and maxilla; unclassified vertebrae compose most of the spinal elements while unclassified ribs do the same in the thorax. metacarpals and hand phalanges (from all types) comprise the bulk of bones in the hand, while metatarsals and proximal hand phalanges do the same on the foot. Conversely, skeletal region distribution does not follow a recognizable pattern spatially. When observed by complete elements, the result is the same (see **Map 4**).

Map 4. Spatial distribution of complete elements by skeletal region.

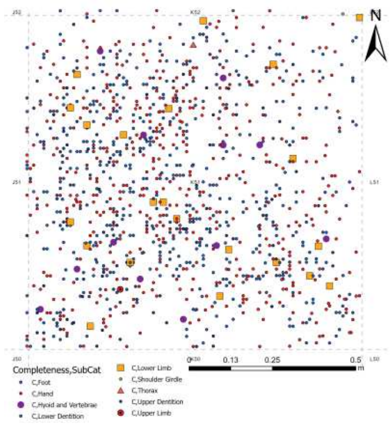

Chart 12. Distribution of skeletal elements by chrono-cultural ascription. The order of each period was tweaked so the highest values appear on the back.

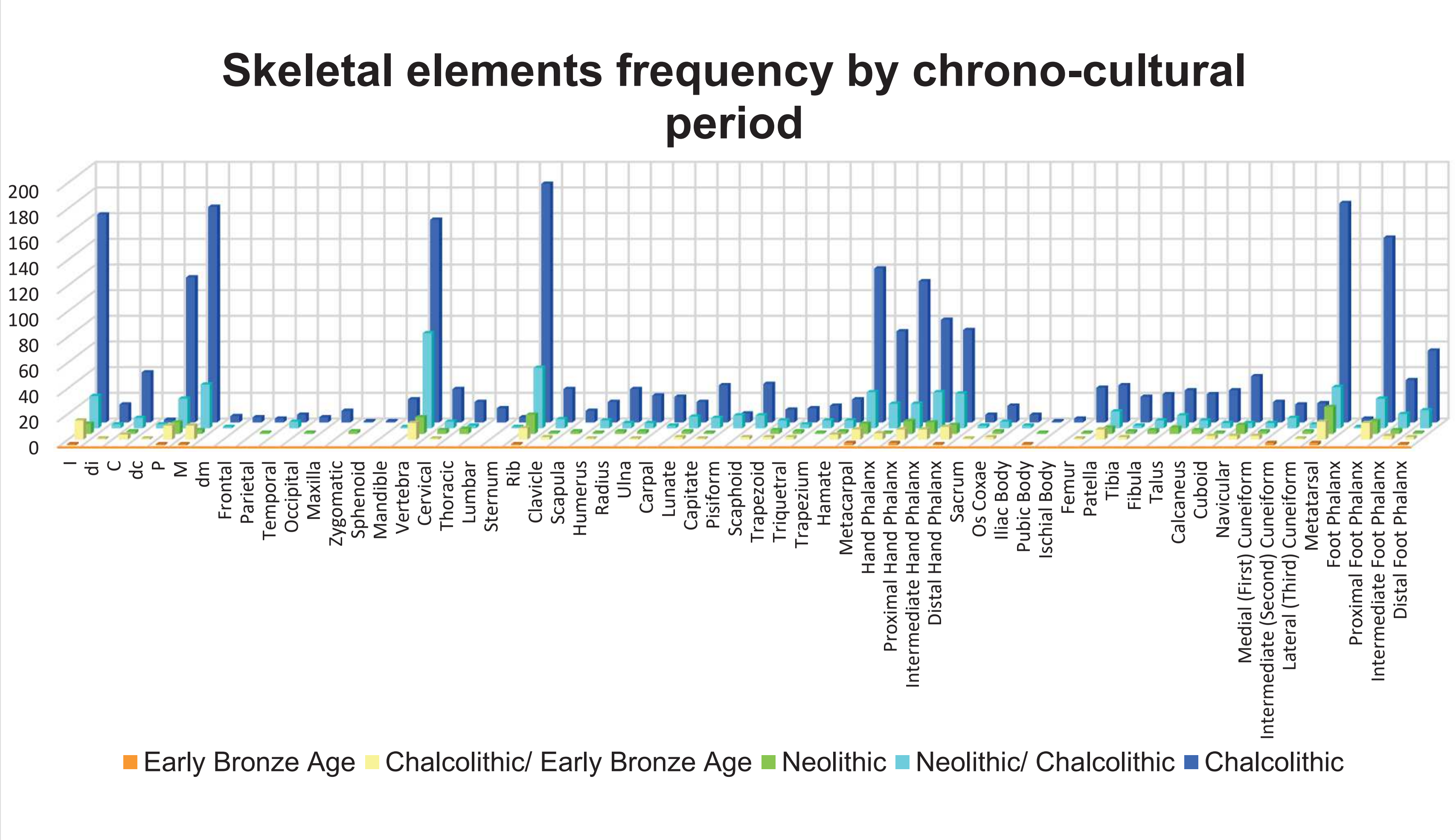

Dental elements had similar proportions between the Neolithic/Chalcolithic, the Chalcolithic and the Chalcolithic/Early Bronze age, encompassing permanent and deciduous teeth, all with a greater participation of molars and incisors, followed by premolars and canines. The Neolithic did not contain any deciduous elements, as well as the Early Bronze Age.

Cranium and Mandible bone fragments were only registered in the Neolithic (presence of parietal, occipital and zygomatic bones), the Neolithic/Chalcolithic (presence of temporal and mandible bones), and the Chalcolithic (presence of all types of registered cranial bones). The general trend for the whole Square K51 is corresponds almost entirely to the Chalcolithic associated SUs.

Vertebrae are present in all chrono-cultural periods, with the cervical being most abundant, while those belonging to the thoracic section were only recognized in the Neolithic and Chalcolithic, and the lumbar were only differentiated in the Chalcolithic. Although the pattern of variability and proportion is akin to the general trend, the high level of fragmentation of these elements may have skewed the result. The difference may lie in preservation conditions.

The thorax presented and ubiquitous presence of ribs, with a volume that diminishes the further away is the period from the Chalcolithic. The Neolithic/Chalcolithic and Chalcolithic assemblages were the only ones in which the sternum was identified.

The shoulder girdle was mostly represented by clavicles that followed the same trend, being absent in SUs from the Early Bronze Age. Scapular elements were only found in the Chalcolithic and, to a lesser extent, the Neolithic.

The upper limbs behaved as the previous region, being absent from the Early Bronze Age, and with minimal representation in the intermediate period between it and the Chalcolithic. The Chalcolithic had a higher presence of radii, followed by humeri and ulnae respectively. The transitional period between the Neolithic/Chalcolithic presented an inverse behaviour, where ulnae were the most abundant skeletal element. The Neolithic had the same pattern of the Chalcolithic with far fewer elements.

The bones in the hand are divided in three sections: carpals, metacarpals, and phalanges. Carpals were absent from Early Bronze Age SUs, while the pisiform and trapezium were missing from the Chalcolithic/Early Bronze Age period. The Neolithic SUs did not bear any pisiform or scaphoid. Metacarpals were found in all SUs within Square K51. Phalanges were more common proximally in most of the SUs, with the exceptions of the Neolithic/Chalcolithic (where intermediate phalanges were more common) and the Early Bronze Age (where the intermediate phalanges were missing).

The pelvic girdle had a differentiated prevalence depending on its fusion patterns. The sacrum was observed in all Chalcolithic-related SUs, while the *os coxae* was only missing from the Early Bronze Age. Juvenile elements were found mostly on the Chalcolithic, while the Neolithic and Early Bronze Age contained just pubic bones.

The lower limbs were well represented in the Chalcolithic, where all four bones have a similar distribution. Neolithic Stratigraphic Units present the same patter with a lower prevalence of femoral fragment. The Chalcolithic/Early Bronze Age lack any records for fibulae, while the Early Bronze Age has no entries at all.

Bones in the foot were analysed in three categories as well. The tarsals were present in the Chalcolithic-ascribed SUs, with a higher prevalence of naviculars and tali. The

Neolithic and the Chalcolithic/Early Bronze Age lacked records of the second cuneiform, while the latter also was missing any for tali or calcanei. Early Bronze Age units only bore second cuneiform bones. Next, metatarsals were present in all periods with different volumes in the same pattern. Foot phalanges were present in most SUs, displaying a higher prevalence of proximal and distal elements. The SUs associated with the Bronze Age only contained distal phalanges.

The analysis by skeletal element draws together the pattern displayed Neolithic/Chalcolithic and the Chalcolithic as a cohesive unit. Such resemblance may respond as well to the amount of material, as both periods encompass most of the skeletal elements (89.4%). The Neolithic and Early Bronze Age have two distinct patterns that essentially respond to variety. While the Neolithic presents most types of skeletal elements, the Early Bronze Age is missing a considerable amount. If the size of the assemblages was the direct cause of the differences in variability, one would expect the Neolithic material to behave similarly to the Early Bronze Age, so the answer may lie in the intensity of the occupation. The Chalcolithic/Early Bronze Age behaves as expected by its denomination, sharing more in common with the Early Bronze Age than with the Chalcolithic.

4.4.2. Identified Individuals

Some skeletal elements were either found articulated to adjacent pieces or in proximity from elements of the same skeletal region in a single record. All bones belonging to these individuals were taken out of the general count, as their inclusion would have resulted in an overrepresentation of their presence in Gruta do Morgado Superior. The material was seriated with alphanumerical consecutive. A total of eighteen individuals were identified, seventeen adults and one juvenile, all found within Stratigraphic Units linked to the Chalcolithic (see **Table 59**). Individuals **A** and **C** were found in anatomical position, both being represented by two cervical vertebrae and one cranial suture respectively. Individual **B** was paired because the elements were found in a separate bag (both belonging to the left foot), thus indicating an excavation decision taken on the field. Individual **I** was a juvenile in their early childhood, and had approximately 5 to 5.3 years at the time of death according Smith's method based on dental eruption(1991). The remaining individuals were represented by either mandibular or maxillary elements with teeth *in situ*. Individual A(i) was separated tentatively, as the incisor was not found along the alveolar tissue on the same day, but it had the same consecutive.

Table 59. Identified individuals in Square K51.

ID	SU	Chron	Bone	Serial	Siding	Complet.	Consecutive	Maturity
K51-2700	[013]	Chalcolithic	Cervical	U		C	A	Adult
K51-2700'	[013]	Chalcolithic	Cervical	U		F	A	Adult
K51-3317	[013]	Chalcolithic	Distal Foot Phalanx	1	Left	C	B	Adult
K51-3317'	[013]	Chalcolithic	Talus		Left	F	B	Adult
K51-2690	[022]	Undetermined	Parietal		Right	F	C	Adult
K51-2690A'	[022]	Undetermined	Sphenoid		Right	F	C	Adult
K51-0259'	[002]	Chalcolithic	Mandible			F	D	Adult

K51-0259"	[002]	Chalcolithic	M	3	Left	C	D	Adult
K51-1463A	[002i4i]	Chalcolithic	Mandible			F	E	Adult
K51-1463A'	[002i4i]	Chalcolithic	M	1	Left	F	E	Adult
K51-1463A"	[002i4i]	Chalcolithic	M	2	Left	C	E	Adult
K51-1463A"'	[002i4i]	Chalcolithic	M	3	Left	C	E	Adult
K51-1365A	[002i4i]	Chalcolithic	Maxilla		Right	F	F	Adult
K51-1365A'	[002i4i]	Chalcolithic	P	3	Right	C	F	Adult
K51-1365A"	[002i4i]	Chalcolithic	P	4	Right	C	F	Adult
K51-3700	[013]	Chalcolithic	Mandible			F	G	Adult
K51-3700'	[013]	Chalcolithic	P	4	Right	F	G	Adult
K51-3700"	[013]	Chalcolithic	M	1	Right	F	G	Adult
K51-3700"'	[013]	Chalcolithic	M	2	Right	F	G	Adult
K51-3700""	[013]	Chalcolithic	M	3	Right	F	G	Adult
K51-0578	[002]	Chalcolithic	Maxilla		Right	F	H	Adult
K51-0578'	[002]	Chalcolithic	Maxilla		Left	F	H	Adult
K51-0578"	[002]	Chalcolithic	I	1	Right	F	H	Adult
K51-0578"'	[002]	Chalcolithic	I	2	Right	C	H	Adult
K51-0578""	[002]	Chalcolithic	C		Right	C	H	Adult
K51-0578""	[002]	Chalcolithic	C		Left	F	H	Adult
K51-0762'	[002]	Chalcolithic	Mandible			F	I	Juvenile
K51-0762"	[002]	Chalcolithic	dm	1	Right	C	I	Juvenile
K51-0762"'	[002]	Chalcolithic	dm	2	Right	C	I	Juvenile
K51-0762""	[002]	Chalcolithic	dm	1	Left	C	I	Juvenile
K51-0762""'	[002]	Chalcolithic	dm	2	Left	C	I	Juvenile
K51-0762"""'	[002]	Chalcolithic	M	1	Left	C	I	Juvenile
K51-0661'	[002]	Chalcolithic	Maxilla		Left	F	J	Adult
K51-0661"	[002]	Chalcolithic	C		Left	C	J	Adult
K51-0661"'	[002]	Chalcolithic	P	4	Left	C	J	Adult
K51-0492	[002]	Chalcolithic	Mandible			F	K	Adult
K51-0492'	[002]	Chalcolithic	M	1	Left	C	K	Adult
K51-0492"	[002]	Chalcolithic	M	2	Left	C	K	Adult
K51-2664	[013]	Chalcolithic	Mandible			F	L	Adult
K51-2664'	[013]	Chalcolithic	I	2	Right	C	L	Adult
K51-2664"	[013]	Chalcolithic	C		Right	C	L	Adult
K51-2664"'	[013]	Chalcolithic	P	3	Right	C	L	Adult
K51-2664""	[013]	Chalcolithic	P	4	Right	C	L	Adult
K51-2664""'	[013]	Chalcolithic	M	1	Right	C	L	Adult
K51-2656	[013]	Chalcolithic	Mandible			F	M	Adult
K51-2656'	[013]	Chalcolithic	M	1	Right	C	M	Adult
K51-2656"	[013]	Chalcolithic	M	2	Right	C	M	Adult
K51-2656"'	[013]	Chalcolithic	M	3	Right	C	M	Adult
K51-2509'	[013]	Chalcolithic	Maxilla		Left	F	N	Adult
K51-2509"	[013]	Chalcolithic	M	2	Left	C	N	Adult
K51-2619	[013]	Chalcolithic	Mandible			F	O	Adult
K51-2619'	[013]	Chalcolithic	M	1	Left	C	O	Adult
K51-1935	[002]	Chalcolithic	Mandible			F	P	Adult
K51-1935'	[002]	Chalcolithic	M	1	Left	C	P	Adult
K51-1935"	[002]	Chalcolithic	M	2	Left	C	P	Adult
K51-1935"'	[002]	Chalcolithic	M	3	Left	C	P	Adult
K51-3731	[013]	Chalcolithic	Mandible			F	Q	Adult
K51-3731'	[013]	Chalcolithic	M	1	Left	F	Q	Adult
K51-0473	[002]	Chalcolithic	Maxilla		Right	F	A (i)	Adult
K51-0473	[002]	Chalcolithic	I	2	Right	C	A (i)	Adult

It is worth noting that all the individuals are not in perfect condition but represent the best-preserved elements in terms of articulation. Vertebrae, maxillae, and mandibles are usually elements that decay later than appendicular ones (Fernández-Jalvo & Andrews, 2016), and this would indicate that the conditions of preservation could have been better during the Chalcolithic.

4.4.3. Minimal Number of Individuals

The count of elements chosen for the calculation of Minimal Number of Individuals was performed once all the available material was analysed. This was done by adding new variables that accounted for the most repeated section on each bone when observing groups by age (only skeletal maturity) and side on paired elements. Then the results were analysed using a chrono-cultural approach in which each period was treated as a separate assemblage. For an overview of the calculation without the chronological subdivisions see Annex 5 and Annex 6 The global MNI obtained was 45 mature individuals (lateral right incisor), 10 juvenile individuals (right 1st molar), and 1 undetermined individual (right pisiform). The total values when differentiated by chrono-cultural adscription is 52 adults, 14 juveniles, and one undetermined individual. The differentiated treatment of data may assess a more accurate number, although the difference among them is not that overwhelming (see **Table 60**, **Table 61**, **Table 62**, and **Chart 13**).

Table 60. Inventory and Minimal Number of Individuals per chrono-cultural period of unpaired elements (both mature and juvenile).

Row Labels Mature	Neolithic	Neolithic/ Chalcolithic	Chalcolithic
Frontal			**3**
Occipital	0		**4**
Mandible		1	5
Sphenoid			**1**
C1	**1**	**2**	3
C2		1	7
C7			**1**
Sternum			**0**
MNI	1	**2**	**4**
Juvenile			
Sternum	**1**	N/A	**2**
Sacrum	**1**	N/A	1
MNI	**1**	N/A	**2**

Table 61. Inventory and Minimal Number of mature Individuals per chrono-cultural period of paired elements. A value of 0 represents a skeletal section that obtained a null global value (see section3.3.10.1).

Row Labels	Neolithic		Neo./Chalc.		Chalcolithic		C/E.B. Age		E. Bronze Age		Und.	
	R	**L**	**R**	**L**	**R**	**L**	**R**	**L**	**R**	**L**	**R**	**L**
I1 (*)		**3**	**6**	4	21	**31**	**4**	2				**1**

Row Labels	Neolithic		Neo./Chalc.		Chalcolithic		C/E.B. Age		E. Bronze Age		Und.	
I2	**3**	2	**6**	6	**33**	29	2	**3**	**1**			**2**
C			**4**	1	1	**12**		**2**				
P3	3		**2**	2	**17**	13	**2**	1				
P4	1		**4**		**10**	4		**2**				
M1			**3**	2	**13**	12	**1**					
M2			**3**		**10**	8						
M3					**2**			**1**				
Maxilla					**1**	1						
Temporal				2	**2**	2						
Zygomatic					**1**							
1st Rib		**1**		1	**3**	2						
Clavicle				3	7	**8**	**1**					
Scapula					**1**	1						
Humerus	0		**1**		**5**	2						
Radius	0	**1**	**0**		**7**	4						
Ulna	1		**1**	1	**6**	1		**1**				
Lunate		**2**	**6**		**9**	7	**1**	1				
Hamate	**1**	1	2	**3**	5	**8**	**3**	1				
Pisiform			**5**	2	**3**	2						
Capitate	**1**		3	**5**	**15**	11		**1**				
Scaphoid			4	**5**	7	**22**		**1**			**1**	
Triquetral		**2**	1	1	4	**7**	**1**	1				
Trapezoid	**3**			4	**5**	5	**1**	1				
Trapezium		**1**		**5**	**8**	4						
MC1 (*)					**1**							
MC2			1		**3**	3	**0**					
MC3			1	1	3	**4**						
MC4			1		**2**	1						
MC5			1									
Os Coxae	**0**			2	1	**2**	**1**					
Femur					**6**	3						
Patella	**2**	**2**	**4**	**7**	**17**	9	**4**	**4**				
Tibia			**1**		**1**	1						
Fibula		**2**	**1**	1	2	**4**						
Talus	**1**	**2**	2	**5**	**13**	6						
Calcaneus	**2**		1	**3**	7	**8**					**1**	
Cuboid	**1**		**2**	2	**12**	10	**3**					
Navicular	**4**	2	**2**	1	11	**22**		**2**				
1st Cun.	**1**	1	1	**3**	7	**9**	1	**2**				
2nd Cun.			**5**	2	**9**	2			**1**			**1**
3rd Cun.	**1**	1	**2**	1	**10**	3		**1**				
MT1 (*)	**2**		**1**	1	7	**11**	**1**	1		**1**		
MT2	**2**	1	**3**	1	10	**15**						
MT3			1	**2**	**8**	7	**2**		**1**			
MT4	**2**	1	**1**	1	**14**	14						
MT5	**3**	1	1	**2**	**7**	4	**2**	1				
MNI	**4**	3	6	**7**	**33**	31	**4**	**4**	**1**	1	1	**2**

(*) The abbreviations are ***I*** for Incisor, ***C*** for canine, ***P*** for Premolar, ***M*** for Molar, ***MC*** for Metacarpal, ***MT*** for Metatarsal, ***Cun***. for cuneiform,

Table 62. Inventory and Minimal Number of juvenile Individuals per chrono-cultural period of paired elements. A value of 0 represents a skeletal section that obtained a null global value (see section3.3.10.1).

Element	Neolithic		Neo./Chalc.		Chalcolithic		Chalc./E.B. Age		E. Bronze Age	
	R	L	R	L	R	L	R	L	R	L
I1				1	2					
I2				1	1					
di1			1		1	2				
di2				2	5	2	1			
C		1			1	1				
dc			1	2	1			1		
P3			1	1	1	1				
P4			1		1	1				
M1	1		1		7	7	1			
M2			3	1	5	5	1	2		
M3					1					
dm			1		1					
Iliac Body					1					
Ischial Body						2				
Pubic Body		1								1
Clavicle			1	3	1	1				
Humerus			0	0	2	1				
Radius						1				
Ulna						2				
Lunate				1						
Trapezium			1							
MC2						1				
MC5		1				1				
Femur					2	1				
Tibia					4	1				
Fibula				1		2				
Talus				1		1				
2nd Cun.						1				
MT5				1						
Grand Total	1	1	3	3	5	5	1	2	N/A	1

Table 63. Inventory undetermined individuals. A value of 0 represents that the sections observed are not the most common.

Row Labels	Right	Unpaired	Total
Pisiform (Neolithic/Chalcolithic)	1		1
Sacrum (Chalcolithic)		0	0
MNI	1	0	1

Chart 13. Comparison between the maximum value obtained per side and maturity stage in each chrono-cultural period.

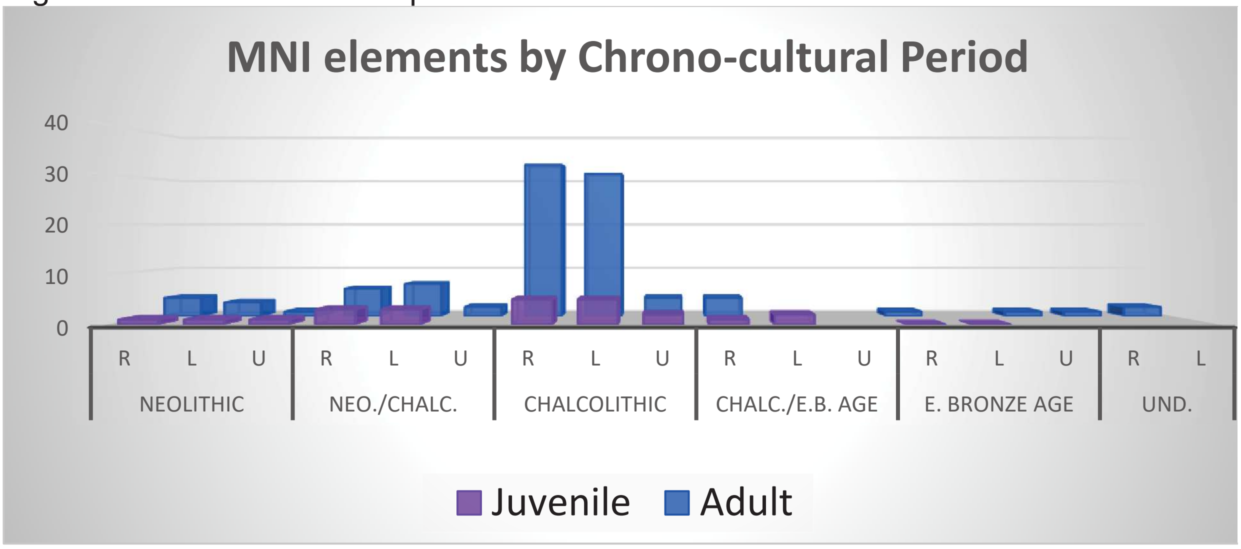

The minimal number of individuals was counted considering the most repeated section by element and assigning it a value of 1 for each time it was present. Bones that were identified through other sections were assigned a value of 0. The latter was left on the tables to showcase the possible existence of more individuals that did not make it to the final count.

The Neolithic burials had estimate of at least 5 adults and 2 juveniles. The Neolithic/Chalcolithic units bore 9 adults and 3 juveniles. The Chalcolithic, once again the most abundant, showcased 37 (+17) adults and 7 juveniles (+1). The Chalcolithic/Early Bronze Age presented 4 adults and 2 juveniles. Finally, the Early Bronze age bore 2 adults. Undetermined chronological Stratigraphic Units bore 2 individuals.

4.5. Paleodemographic description

Biological age assessment was performed using epiphyseal fusion patterns to determine if the individual was either juvenile or mature. Specific chronological ranges (based on modern dental eruption patterns) were also utilized following Smith (1991) (see **Photograph 5**).

The neolithic has a population that with a high composition of adolescents (5), followed by early children (2), mature adults (2), and a late child. The Neolithic/Chalcolithic has mostly adolescent individuals (50), followed by early children (54), late children (12), young adults (4), and one perinatal (1). The Chalcolithic follows a similar trend with a great number of adolescents (166), early children (54), late children (26), young adults (22), infants (7), one mature adult and one perinatal juvenile. The transition between the Chalcolithic and the Early Bronze Age was composed as well by of adolescents (11), late children (5), young adults (2), one early child and one infant. The Early Bronze Age only presented one late child (see **Table 64**, **Chart 14, Chart 15**).

Photograph 5. K51-2665b (*left)*: Fragment of pubic symphysis, 35.2 to 38.2 years old (depending on their sex) K51-1243, unfused femoral distal epiphysis (*Right*): Juvenile (8 to 12 years).

Table 64. Age group distribution by period.

Age Group	Neo.	Neo. / Chalc.	Chalc.	Chalc./ E. Bronze A.	E. Bronze A.
Perinatal		1	1		
Infant			7	1	
Early Child	2	14	54	1	
Late Child	1	12	26	5	1
Adolescent	5	50	166	11	
Young Adult		4	22	2	
Mature Adult	2		1		
Grand Total	**10**	**81**	**277**	**20**	**1**

When analysed by spatial dispersion, bones with specific age-ranges present no discernible pattern **Map 5**.

Map 5. Spatial distribution of skeletal elements with specific age ranges

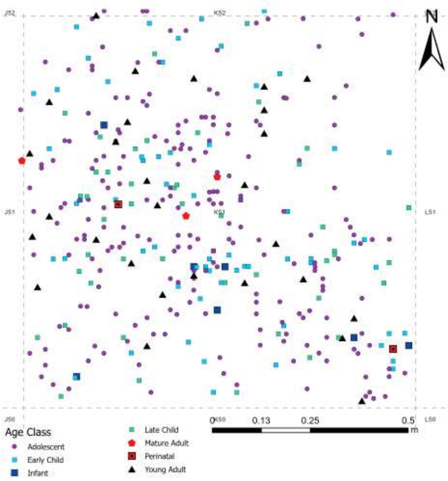

Chart 14. Composition of the mortality spectrum by chrono-cultural period.

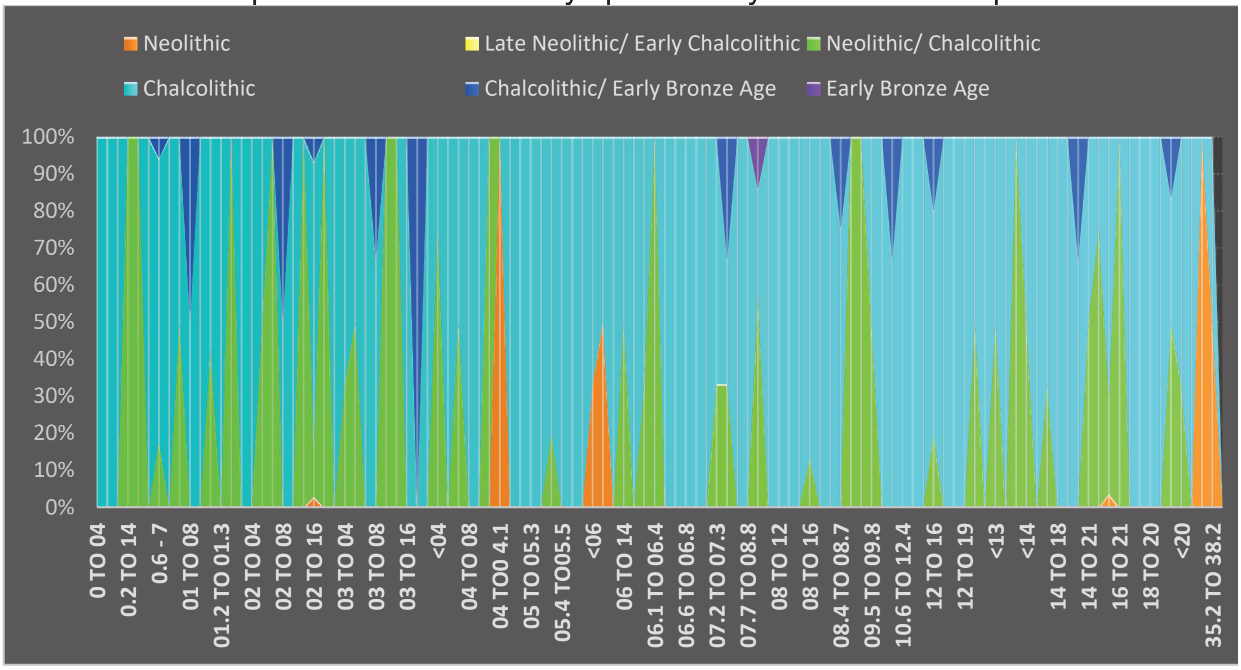

Chart 15. Specific age groups' distribution by chrono-cultural period.

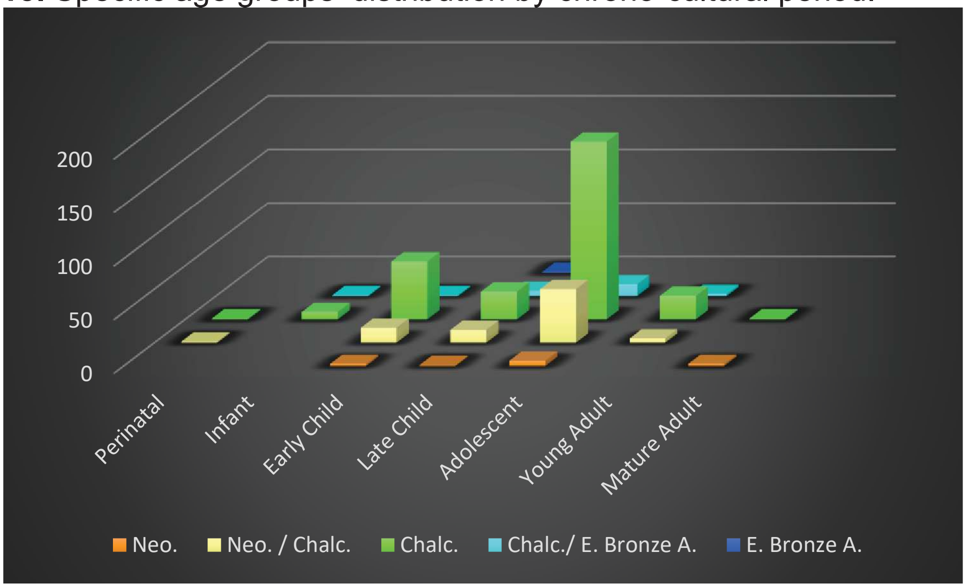

Age distribution presents a similar pattern for every chrono-cultural period, with the ones missing possibly responding to the overall size of the sample. Nevertheless, considering the Chalcolithic as a reliable source of information, the mortality pattern is more severe on early children and adolescents (4 to 18 years, taking both sexes ranges) (see **Annex 7**). When assessing the overall weight of juvenile (fragments) on the population it returns a 0.18% value for the Neolithic, 1.85% in the Neolithic/Chalcolithic, 6.37% in the chalcolithic, 0.46% in the Chalcolithic/Early Bronze Age, and 0.02% in the Early Bronze Age (see **Table 1** and **Chart 16**).

Table 65. Juvenile and mature elements by chrono-cultural period.

Period	Neolithic	Neo. / Chalc.	Chalc.	Chalc./ E. Bronze A.	E. Bronze A.
Mature	169	441	2065	174	12
Juvenile	8	80	276	20	1
Total	**177**	**521**	**2341**	**194**	**13**

Chart 16. Distribution of Mature and Juvenile individuals (by fragments) by chrono-cultural period.

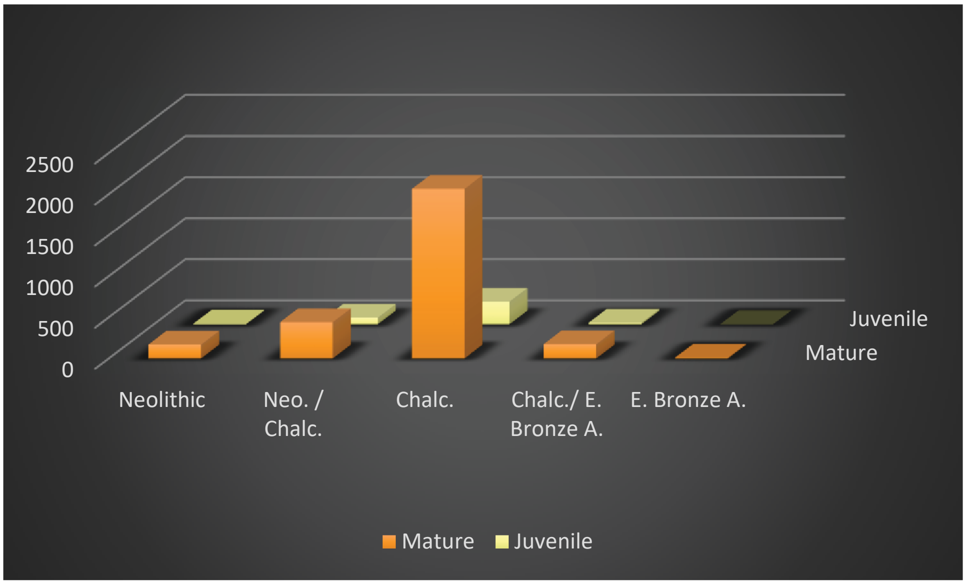

Given the difficulty of comparing percentages by fragment and associating them to the actual mortality patterns on a population, it is possible to conclude at least that adolescents and early children are the most vulnerable age groups (before reaching full maturity), but they do not represent more than a fifth of the population buried in the site. As for its pattern, it is likely skewed because the skeletal elements that give specific age-ranges are also the most resistant.

4.5.1. Sex allocation

Sex allocation utilized various methods with different bones (see **above**), from which the most reliable were the talus, calcaneus, radius, and vertebrae. Measurements on carpals had varied results, favouring one category over the other, or producing different allocations to their control equations. Carpal measurements were the only ones that used a Spanish population as the principal source of information, which could explain the high variability. Globally, females were more frequent than males in all chrono-cultural periods, and males were not registered during the Early Bronze Age. Similarly to the results with juvenile and mature fragments, sex allocation has produced values higher than the MNI (see **Table 66** and **Chart 17**). Intraobserver error was calculated with White et al. (2012) 's formula to 0.2.

Table 66. Sex distribution by chrono-cultural period.

Sex	Neo.	Neo. / Chalc.	Chalc.	Chalc./ E. Bronze A.	N/C/EBA
Female	15	36	119	10	1
Male	6	17	51	5	
Undetermined		4	6		
Grand Total	**21**	**57**	**176**	**15**	**1**

Chart 17. Sex distribution by chrono-cultural period.

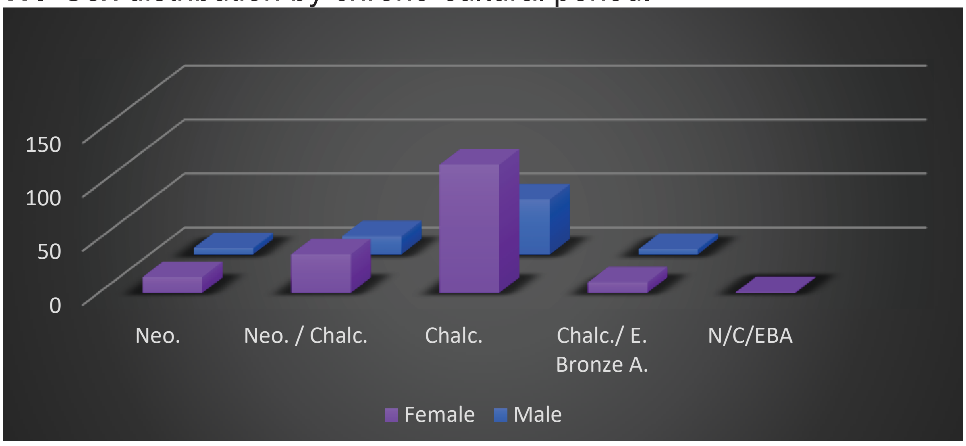

4.5.1.1. **Radius**

Only one complete radius was recovered. **K51-1491A** belongs to SU [002i4i] – Chalcolithic. It was fragmented into 6 pieces (see **Photograph 1**), with multiple cracking and flaking of the periosteum (postmortem), thus measurements **I** and **X** may be off because of this. Nevertheless the equations **LR4** and **LR5** developed by Curate (2021b), and deemed by his team as the most stable, were applied to the skeletal element using Excel software (**LR4**=(0.131*AA12938) + (0.301*AH12938) + (0.495 *AB12938) + (0.254 *AJ12938) + (-0.136 * AI12938)-(68.568); **LR5**=(0.559 *AB12938) + (0.7*AJ12938)-42.223). The results were6.402 and 4.768 respectively, which indicate that the bone probably belonged to an adult male.

Photograph 6. Radius K51-1491A (left). Probably an adult male.

4.5.1.2. **Carpals**

Lunate

Sex allocation results that employed measurements on the lunate relied on a main multivariate equation [= (MIII*0.332) + (MIV*0.495) + (MV*0.625) + (-12.515)] and a control univariate equation [=(MV*1.161)-9.501]. The accuracy rates for each equation are 98.9% and 97.8 % respectively. No juvenile elements were used to perform the analysis (see **Table 67**).

Table 67. Sex allocation results obtained by discriminant function using the lunate.

Consecutive	SU	Chronology	Siding	Result (m)	Sex (m)	Result (u)	Sex (u)
K51-2150	[004]	Neolithic	Left	1.549	Male	0.948	Male
K51-2246	[004]	Neolithic	Left	4.903	Male	4.431	Male
K51-2313	[004-013]	Neolithic/ Chalcolithic	Right	2.337	Male	2.109	Male
K51-4022	[025]	Neolithic/ Chalcolithic	Right	6.062	Male	4.431	Male
K51-4150	[025]	Neolithic/ Chalcolithic	Right	6.264	Male	3.27	Male
K51-4322	[026]	Neolithic/ Chalcolithic	Right	2.539	Male	0.948	Male
K51-4477	[033]	Neolithic/ Chalcolithic	Right	1.803	Male	3.27	Male
K51-4639	[041]	Neolithic/ Chalcolithic	Right	**1.081**	**Male**	**-0.213**	**Female**
K51-0127	[001]	Chalcolithic/ Early Bronze Age	Left	3.197	Male	0.948	Male
K51-0131A	[001]	Chalcolithic/ Early Bronze Age	Right	2.174	Male	2.109	Male
K51-0198G	[002]	Chalcolithic	Left	1.51	Male	2.109	Male
K51-0220	[002]	Chalcolithic	Left	1.145	Male	3.27	Male
K51-0277	[002]	Chalcolithic	Left	-0.105	Male	0.948	Male
K51-0342	[002]	Chalcolithic	Right	2.174	Male	2.109	Male
K51-0395	[002]	Chalcolithic	Left	0.885	Male	0.948	Male
K51-0436E	[002]	Chalcolithic	Right	2.337	Male	2.109	Male
K51-0446	[002]	Chalcolithic	Right	1.015	Male	2.109	Male
K51-0560	[002]	Chalcolithic	Right	2.135	Male	3.27	Male
K51-1141	[002]	Chalcolithic	Right	0.722	Male	0.948	Male
K51-1233	[002]	Chalcolithic	Right	2.298	Male	3.27	Male
K51-1938	[002]	Chalcolithic	Right	1.712	Male	0.948	Male
K51-2513	[013]	Chalcolithic	Right	3.659	Male	2.109	Male
K51-2701E	[013]	Chalcolithic	Right	-3.178	Female	-1.374	Female
K51-2931	[013]	Chalcolithic	Left	1.51	Male	2.109	Male
K51-2985	[013]	Chalcolithic	Left	2.467	Male	3.27	Male

Scaphoid

Sex allocation results that employed measurements on the scaphoid relied on a main multivariate equation [=((MI*0.468) +(MIV*0.202) -(15.008))] and a control univariate equation [=((MII*0.958)-13.774)] were utilized. The accuracy rates are 90.1% and 85.4 % respectively. No juvenile elements were used to perform the analysis (see **Table 68**).

Table 68. Sex allocation results obtained by discriminant function using the scaphoid.

ID	SU	Chronology	Siding	Result (m)	Sex (m)	Result (u)	Sex (u)
K51-2339	[004-013]	Neolithic/ Chalcolithic	Left	-1.214	Female	-0.362	Female
K51-2354	[004-013]	Neolithic/ Chalcolithic	Right	-3.022	Female	-2.278	Female
K51-2384	[004-013]	Neolithic/ Chalcolithic	Right	-1.884	Female	-0.362	Female
K51-4263	[025]	Neolithic/ Chalcolithic	**Left**	**-0.682**	**Female**	**0.596**	**Male**
K51-4382	[032]	Neolithic/ Chalcolithic	Left	-2.288	Female	-0.362	Female
K51-4561	[033]	Neolithic/ Chalcolithic	Left	-0.948	Female	-0.362	Female
K51-4701F	[035]	Neolithic/ Chalcolithic	Right	-2.756	Female	-1.32	Female
K51-0198	[002]	Chalcolithic	**Left**	**-0.746**	**Female**	**0.596**	**Male**
K51-0212'	[002]	Chalcolithic	**Left**	**-0.48**	**Female**	**1.554**	**Male**
K51-0242	[002]	Chalcolithic	**Left**	**-3.426**	**Female**	**4.428**	**Male**
K51-0355	[002]	Chalcolithic	Left	-2.756	Female	-1.32	Female
K51-0369	[002]	Chalcolithic	Left	**-1.416**	**Female**	**0.596**	**Male**
K51-0436C	[002]	Chalcolithic	Left	-4.362	Female	-2.278	Female
K51-0594	[002]	Chalcolithic	Right	**-2.086**	**Female**	**1.554**	**Male**
K51-0914	[002]	Chalcolithic	Right	-2.288	Female	-0.362	Female
K51-1045	[002]	Chalcolithic	Left	-2.756	Female	-0.362	Female
K51-1198'	[002]	Chalcolithic	Right	**-1.15**	**Female**	**1.554**	**Male**
K51-1262	[002]	Chalcolithic	Left	-2.756	Female	-0.362	Female
K51-1310	[002]	Chalcolithic	Left	**0.988**	**Male**	**-2.278**	**Female**
K51-1348A	[002]	Chalcolithic	Right	-1.416	Female	-0.362	Female
K51-2432	[013]	Chalcolithic	Right	0.19	Male	1.554	Male

ID	SU	Chronology	Siding	Result (m)	Sex (m)	Result (u)	Sex (u)
K51-2434	[013]	Chalcolithic	Left	-1.884	Female	-0.362	Female
K51-2504	[013]	Chalcolithic	Left	-3.692	Female	-1.32	Female
K51-2625A	[013]	Chalcolithic	Right	-0.48	Undetermined	-1.32	Female
K51-2638B	[013]	Chalcolithic	Right	-0.012	Male	0.596	Male
K51-2798	[013]	Chalcolithic	Left	-3.894	Female	-3.236	Female
K51-3184	[013]	Chalcolithic	Left	-2.352	Female	-1.32	Female
K51-3308	[013]	Chalcolithic	Left	-3.894	Female	-3.236	Female
K51-0167	[001]	Chalcolithic/ Early Bronze Age	Left	-1.884	Female	-3.236	Female
K51-2698	[024]	Neolithic/ Chalcolithic/ Early Bronze Age	Right	-3.692	Female	-2.278	Female

Triquetral

Sex allocation results that employed measurements on the triquetral relied on a main multivariate equation [=(V*0.376) +(IX*0.519) +(VII*0.753) -14.279] and a control univariate equation [=(IV*0.942)-8.339]. The accuracy rates are 94.1% and 93.6 % respectively. No juvenile elements were used to perform the analysis (see **Table 69**).

Table 69. Sex allocation results obtained by discriminant function using the triquetral.

ID	SU	Chronology	Siding	Result (m)	Sex (m)	Result (u)	Sex (u)
K51-2093	[002-004]	Neolithic/ Chalcolithic	Left	1.591	Male	1.081	Male
K51-2209	[004]	Neolithic	Left	-1.043	Female	-1.745	Female
K51-2290	[004]	Neolithic	Left	-3.729	Female	-2.687	Female
K51-0814	[002]	Chalcolithic	**Left**	**-0.576**	**Undetermined**	**1.081**	**Male**
K51-0944	[002]	Chalcolithic	Left	1.734	Male	2.965	Male
K51-0983	[002]	Chalcolithic	Right	0.695	Male	2.023	Male
K51-1035	[002]	Chalcolithic	**Right**	**-0.576**	**Undetermined**	**0.139**	**Male**
K51-1064	[002]	Chalcolithic	**Right**	**-0.291**	**Undetermined**	**0.139**	**Male**
K51-1427A'	[002i4i]	Chalcolithic	Left	1.591	Male	2.023	Male
K51-2600	[013]	Chalcolithic	Right	1.448	Male	1.081	Male

ID	SU	Chronology	Siding	Result (m)	Sex (m)	Result (u)	Sex (u)
K51-2701U	[013]	Chalcolithic	Left	-1.848	Female	-0.803	Female
K51-2876	[013]	Chalcolithic	Left	-3.118	Female	-2.687	Female

Capitate

Sex allocation results that employed measurements on the capitate relied on a main multivariate equation [=(MIII*0.553) +(MVI*0.524) -15.09] and a control univariate equation [=(I*0.771)-19.502]. The accuracy rate for both equations is 88.3%. No juvenile elements were used to perform the analysis (see **Table 70**).

Table 70. Sex allocation results obtained by discriminant function using the capitate.

ID	SU	Chronology	Siding	Result (m)	Sex (m)	Result (u)	Sex (u)
K51-2176	[004]	Neolithic	Right	-2.224	Female	-1.769	Female
K51-2380	[004-013]	Neolithic/ Chalcolithic	Right	-0.07	**Undetermined**	**-0.998**	**Female**
K51-4026	[025]	Neolithic/ Chalcolithic	**Right**	**1.007**	**Male**	**-0.227**	**Female**
K51-4074	[025]	Neolithic/ Chalcolithic	**Left**	**0.512**	**Male**	**-0.227**	**Female**
K51-4287	[026]	Neolithic/ Chalcolithic	**Left**	**2.579**	**Male**	**-3.311**	**Female**
K51-4548	[033]	Neolithic/ Chalcolithic	Left	-0.565	Female	-1.769	Female
K51-0231'	[002]	Chalcolithic	Right	-1.147	Female	-0.998	Female
K51-0319	[002]	Chalcolithic	**Right**	**-0.565**	**Female**	**1.315**	**Male**
K51-0405	[002]	Chalcolithic	Left	-1.118	Female	-1.769	Female
K51-0436A	[002]	Chalcolithic	Left	-0.565	Female	-0.227	Female
K51-0436B	[002]	Chalcolithic	Left	-2.748	Female	-2.54	Female
K51-0871	[002]	Chalcolithic	Right	-2.166	Female	-2.54	Female
K51-0943	[002]	Chalcolithic	Right	-1.613	Female	-0.998	Female
K51-0958	[002]	Chalcolithic	Right	-0.565	Female	-0.998	Female
K51-1055	[002]	Chalcolithic	Right	-1.089	Female	-0.227	Female
K51-1414A	[002i4i]	Chalcolithic	Right	2.608	Male	1.315	Male
K51-2026	[011]	Chalcolithic	Right	2.608	Male	0.544	Male
K51-2418	[013]	Chalcolithic	Right	0.483	Male	0.544	Male

ID	SU	Chronology	Siding	Result (m)	Sex (m)	Result (u)	Sex (u)
K51-2574B	[013]	Chalcolithic	Left	-1.671	Female	-2.54	Female
K51-2723B	[013]	Chalcolithic	Right	-1.118	Female	-0.998	Female
K51-2730B	[013]	Chalcolithic	Right	-1.118	Female	-2.54	Female
K51-2761	[013]	Chalcolithic	Left	-2.719	Female	-3.311	Female
K51-2818	[013]	Chalcolithic	Left	-3.272	Female	-7.166	Female
K51-3191	[013]	Chalcolithic	Left	1.007	Male	0.544	Male
K51-3373	[013]	Chalcolithic	Right	-1.642	Female	-3.311	Female
K51-3876	[013]	Chalcolithic	Left	-2.253	Female	-2.54	Female
K51-0053	[001]	Chalcolithic/ Early Bronze Age	Left	2.084	Male	2.086	Male

Hamate

Sex allocation results that employed measurements on the hamate relied on a main multivariate equation [=(MVI*1.246) -12.514] and a control univariate equation [=(MVII*1.431)-15.492]. The accuracy rates are 90.7% and 88% respectively. No juvenile elements were used to perform the analysis. This is the only case in which the multivariate equation performs worse than the univariate among carpals (see **Table 71**).

Table 71. Sex allocation results obtained by discriminant function using the hamate.

ID	SU	Chronology	Siding	Result (m)	Sex (m)	Result (u)	Sex (u)
K51-2092	[002-004]	Neolithic/ Chalcolithic	Left	-0.054	Female	-2.613	Female
K51-2251	[004]	Neolithic	Left	-0.054	Female	-2.613	Female
K51-2293	[004]	Neolithic	Right	-2.546	Female	-5.475	Female
K51-4020	[025]	Neolithic/ Chalcolithic	**Left**	**-0.054**	**Female**	**0.249**	**Undetermined**
K51-4139	[025]	Neolithic/ Chalcolithic	Right	-0.054	Female	-4.044	Female
K51-4312	[026]	Neolithic/ Chalcolithic	Left	-1.3	Female	-1.182	Female
K51-0609	[002]	Chalcolithic	Right	-0.054	Female	-2.613	Female
K51-0669	[002]	Chalcolithic	Left	-0.054	Female	-1.182	Female
K51-0685	[002]	Chalcolithic	Left	-0.054	Female	-2.613	Female
K51-1129'	[002]	Chalcolithic	Right	-1.3	Female	-1.182	Female
K51-1231	[002]	Chalcolithic	**Left**	**-0.054**	**Female**	**0.249**	**Male**
K51-1403A	[002i4i]	Chalcolithic	Left	-1.3	Female	-1.182	Female
K51-1458A	[002i4i]	Chalcolithic	Right	-0.054	Female	-2.613	Female
K51-2447	[013]	Chalcolithic	Left	1.192	Male	1.68	Male
K51-2539	[013]	Chalcolithic	Right	-0.054	Female	-2.613	Female
K51-2679	[013]	Chalcolithic	**Left**	**-0.054**	**Female**	**0.249**	**Undetermined**

ID	SU	Chronology		Siding	Result (m)	Sex (m)	Result (u)	Sex (u)
K51-1993	[002-003]	Chalcolithic/ Bronze Age	Early	Right	-0.054	Female	-1.182	Female
K51-1998	[002-003]	Chalcolithic/ Bronze Age	Early	**Right**	**-0.054**	**Female**	**0.249**	**Male**

Pisiform

Sex allocation results that employed measurements on the pisiform relied on a main multivariate equation [=(III*1.214) -9.002] and one control univariate equation [=(IV*0.896)-7.951]. The accuracy rates are 88.2% and 90.4 % respectively. No juvenile elements were used to perform the analysis. This is the only case in which the multivariate equation performs worse than the univariate (see **Table 72**).

Table 72. Sex allocation results obtained by discriminant function using the pisiform.

ID	SU	Chronology	Siding	Result (m)	Sex (m)	Result (u)	Sex (u)
K51-2390	[004-013]	Neolithic/ Chalcolithic	Left	0.71	Male	1.009	Male
K51-4143	[025]	Neolithic/ Chalcolithic	Right	0.71	Male	1.905	Male
K51-4317	[026]	Neolithic/ Chalcolithic	Left	1.924	Male	0.113	Male
K51-4343	[026]	Neolithic/ Chalcolithic	**Right**	**-0.504**	**Female**	**0.113**	**Male**
K51-4447	[033]	Neolithic/ Chalcolithic	**Right**	**-0.504**	**Female**	**0.113**	**Male**
K51-4479	[033]	Neolithic/ Chalcolithic	**Right**	**0.71**	**Male**	**-1.679**	**Female**
K51-4544	[033]	Neolithic/ Chalcolithic	Right	0.71	Male	1.905	Male
K51-4608	[035]	Neolithic/ Chalcolithic	Right	-1.718	Female	-0.783	Female
K51-0834	[002]	Chalcolithic	**Right**	**0.71**	**Male**	**-0.783**	**Female**
K51-0868	[002]	Chalcolithic	**Right**	**1.924**	**Male**	**-0.783**	**Female**
K51-0984	[002]	Chalcolithic	Left	0.71	Male	1.905	Male
K51-3290	[013]	Chalcolithic	**Left**	**-0.504**	**Female**	**1.009**	**Male**

Trapezium

Sex allocation results that employed measurements on the trapezium relied on a main multivariate equation [=(MII*0.486) +(MIV*0.775) +(MVI*0.534) -20.455] and one control multivariate equation [=(MI*0.933)-17.393]. The accuracy rate for the first equation is 97.1% and for the second 92.8%. No juvenile elements were used to perform the analysis (see **Table 73**).

Table 73. Sex allocation results obtained by discriminant function using the trapezium.

ID	SU	Chronology	Siding	Result (m)	Sex (m)	Result (u)	Sex (u)
K51-1984	[004]	Neolithic	Left	0.381	Male	-0.018	Male
K51-2084	[002-004]	Neolithic/ Chalcolithic	Left	2.981	Male	4.552	Male

ID	SU	Chronology	Siding	Result (m)	Sex (m)	Result (u)	Sex (u)
K51-2399	[004-013]	Neolithic/ Chalcolithic	Left	-1.52	Female	-1.846	Female
K51-2409	[004-013]	Neolithic/ Chalcolithic	Left	-1.52	Female	-1.846	Female
K51-4108	[025]	Neolithic/ Chalcolithic	Left	-0.262	Undetermined	-0.932	Undetermined
K51-4542	[033]	Neolithic/ Chalcolithic	**Left**	**-0.234**	**Undetermined**	**-0.018**	**Male**
K51-0187C	[002]	Chalcolithic	**Left**	**-0.262**	**Undetermined**	**-0.932**	**Female**
K51-0418	[002]	Chalcolithic	Left	-2.806	Female	-3.674	Female
K51-0470	[002]	Chalcolithic	Left	-3.421	Female	-3.674	Female
K51-1000	[002]	Chalcolithic	Right	-0.877	Female	-0.932	Female
K51-1151	[002]	Chalcolithic	Right	-1.52	Female	-1.846	Female
K51-1170	[002]	Chalcolithic	Right	1.024	Male	0.896	Male
K51-1229	[002]	Chalcolithic	Right	0.996	Male	-0.018	Male
K51-1275	[002]	Chalcolithic	**Right**	**-0.262**	**Undetermined**	**-0.932**	**Female**
K51-2960	[013]	Chalcolithic	**Left**	**0.912**	**Male**	**-2.76**	**Female**
K51-2987	[013]	Chalcolithic	Right	0.996	Male	-0.018	Male

Trapezoid

Sex allocation results that employed measurements on the trapezoid relied on a main multivariate equation [=(MII*0.486) +(MIV*0.775) +(MVI*0.534) -20.455] and one control univariate equation [=(MI*0.933)-17.393. The accuracy rate for the first equation is 93.7% and for the second 85.5%. There was another univariate equation with the same success rate as the latter but only one was picked. No juvenile elements were used to perform the analysis.

Table 74. Sex allocation results obtained by discriminant function using the trapezium.

ID	SU	Chronology	Siding	Result (m)	Sex (m)	Result (u)	Sex (u)
K51-2105	[004]	Neolithic	Right	0.94	Male	0.334	Male
K51-2123	[004]	Neolithic	Right	-1.63	Female	-5.264	Female
K51-2164	[004]	Neolithic	**Right**	**-1.196**	**Female**	**0.334**	**Male**
K51-2389	[004-013]	Neolithic/ Chalcolithic	Left	-2.891	Female	-1.532	Female
K51-4182	[025]	Neolithic/ Chalcolithic	Left	-3.377	Female	-6.197	Female
K51-4216	[025]	Neolithic/ Chalcolithic	Left	-2.65	Female	-1.532	Female
K51-4633	[041]	Neolithic/ Chalcolithic	Left	0.165	Male	1.267	Male
K51-0231''	[002]	Chalcolithic	Right	-0.855	Female	-0.599	Female
K51-1022	[002]	Chalcolithic	Right	-0.855	Female	-0.599	Female
K51-1293	[002]	Chalcolithic	**Right**	**-0.807**	**Female**	**0.334**	**Male**
K51-1296	[002]	Chalcolithic	Left	-0.855	Female	-6.197	Female
K51-2020	[011]	Chalcolithic	Left	0.94	Male	0.334	Male

ID	SU	Chronology	Siding	Result (m)	Sex (m)	Result (u)	Sex (u)
K51-2459	[013]	Chalcolithic	Right	-2.602	Female	-0.599	Female
K51-2589	[013]	Chalcolithic	Left	-3.136	Female	-3.398	Female
K51-3093	[013]	Chalcolithic	Right	-4.204	Female	-2.465	Female
K51-3934	[013]	Chalcolithic	Left	-2.068	Female	-0.599	Female
K51-0137	[001]	Chalcolithic/ Early Bronze Age	Right	-3.425	Female	-2.465	Female
K51-2002	[002-003]	Chalcolithic/ Early Bronze Age	Left	0.699	Male	1.267	Male

4.5.1.3. **Tarsals**

Talus

Sex allocation results that employed measurements on the talus relied on a main multivariate equation [=((0.665***MI**) + (0.494***MV**) + (0.471***MVI**) -61.487)] and one control multivariate equation [=((0.463* **MI**) + (0.359***MV**) + (0.334***MVI**)-43.36)]. The accuracy rate for the first equation is 88.4% and for the second 87.8%. There were two other equations with a success rate of 87.8%, but the former was picked as it used the same variables as the main equation. No juvenile elements were used to perform the analysis (see **Table 75**).

Table 75. Sex allocation by results obtained multivariate functions using the calcaneus.

ID	SU	Chronology	Siding	Result (m)	Sex (m)	Result (u)	Sex (u)
K51-2696	[022]	Undetermined	Right	2.157	Male	0.973	Male
K51-2328	[004-013]	Neolithic/ Chalcolithic	Left	-1.62	Female	-1.463	Female
K51-0484	[002]	Chalcolithic	Right	4.81	Male	2.829	Male
K51-0826	[002]	Chalcolithic	Left	-0.788	Female	-0.709	Female
K51-0945	[002]	Chalcolithic	Left	-1.485	Female	-1.231	Female
K51-1125	[002]	Chalcolithic	Right	4.54	Male	2.365	Male
K51-2461	[013]	Chalcolithic	Left	-0.361	Female	-0.651	Female
K51-3044	[013]	Chalcolithic	Left	1.752	Male	0.277	Male

Calcaneus

Sex allocation results that employ measurements on the calcaneus relied on a main multivariate equation [=((0.562***MVII**)+(0.697***MIX**)-46.718)] and one control multivariate equation [=((0.29***MVII**)+(0.522***MIX**)-28.955)]. The accuracy rate for the first equation is 89.4% and for the second 87.8%. No juvenile elements were used to perform the analysis (**Table 76**).

Table 76. Sex allocation results obtained by multivariate functions using the calcaneus.

ID	SU	Chronology	Siding	Result (m)	Sex (m)	Result (u)	Sex (u)
K51-2192	[004]	Neolithic	Right	1.682	Male	1.345	Male
K51-2226	[004]	Neolithic	Left	-2.866	Female	-1.915	Female
K51-2275	[004]	Neolithic	Left	-3.231	Female	-2.148	Female
K51-2340	[004-013]	Neolithic/ Chalcolithic	Left	-5.207	Female	-3.584	Female
K51-3646'''''	[013-013a]	Neolithic/ Chalcolithic	Left	-3.083	Female	-2.069	Female
K51-4647	[041]	Neolithic/ Chalcolithic	Left	-5.013	Female	-3.455	Female
K51-0234	[002]	Chalcolithic	Right	0.519	Male	0.451	Male
K51-0655	[002]	Chalcolithic	Left	-1.282	Female	-0.809	Female
K51-0807	[002]	Chalcolithic	Right	0.371	Male	0.372	Male
K51-0905	[002]	Chalcolithic	Left	4.342	Male	3.197	Male
K51-2415	[013]	Chalcolithic	Left	-1.947	Female	-1.272	Female
K51-2518	[013]	Chalcolithic	Right	-1.434	Female	-0.96	Female
K51-2549	[013]	Chalcolithic	Right	-11.062	Female	-7.745	Female
K51-2768	[013]	Chalcolithic	Right	-3.041	Female	-2.091	Female
K51-3940	[013]	Chalcolithic	Left	1.53	Male	1.194	Male

Cuboid

The methodology used to allocate sex on the cuboid relies on different equations depending on the side the bone belongs to. If the skeletal element is left, the main multivariate equation used was [=(-38.732+(1.052***MII**)+(0.399***MIII**))] and the control univariate equation was [=(-34.975+(1.263***MII**))]. The accuracy rate for the first equation is 84.7% and for the second 81.8%. If the bone belongs to the right side, the main multivariate equation used was [=(-36.676+(1.006***MII**)+(0.362***MIII**))] and the control univariate equation was [=(-31.695+(1.137 ***MII**))]. The accuracy rate for the first equation is 88.5% and for the second 84.9%. No juvenile elements were used to perform the analysis (see **Table 77**).

The best first decision tree did show differences in analysis for demarking points for the first cuneiform (MI-Longitude:23.5mm and 24.5mm), the third cuneiform (MII-Breadth: 16.5mm), and the cuboid (MIII-Height: 23.5mm)

Table 77. Sex allocation results obtained by multivariate and univariate functions using the cuboid.

ID	SU	Chronology	Siding	Result (m)	Sex (m)	Result (u)	Sex (u)
K51-3646'	[013-013a]	Neolithic/ Chalcolithic	Right	-3.924	Female	-3.27	Female
K51-3982	[025]	Neolithic/ Chalcolithic	Left	-0.752	Female	-0.874	Female
K51-2152	[004]	Neolithic	Right	-2.556	Female	-2.133	Female
K51-0171	[001]	Chalcolithic/ Early Bronze Age	Right	2.554	Male	2.415	Male

ID	SU	Chronology	Siding	Result (m)	Sex (m)	Result (u)	Sex (u)
K51-0177	[001]	Chalcolithic/ Early Bronze Age	Right	-4.93	Female	-4.407	Female
K51-0877	[002]	Chalcolithic	Right	-6.298	Female	-5.544	Female
K51-0885	[002]	Chalcolithic	**Right**	**-0.544**	**Female**	**0.141**	**Male**
K51-1174	[002]	Chalcolithic	Left	0.554	Male	1.652	Male
K51-1225	[002]	Chalcolithic	Right	-8.672	Female	-7.818	Female
K51-1226	[002]	Chalcolithic	Left	-2.203	Female	-2.137	Female
K51-1376A	[002i4i]	Chalcolithic	Right	-6.942	Female	-6.681	Female
K51-2437	[013]	Chalcolithic	Right	-4.286	Female	-3.27	Female
K51-2640	[013]	Chalcolithic	Right	-2.556	Female	-2.133	Female
K51-2709A	[013]	Chalcolithic	Right	-5.292	Female	-4.407	Female
K51-2723	[013]	Chalcolithic	Left	-1.804	Female	-2.137	Female
K51-2861	[013]	Chalcolithic	Left	-1.55	Female	-0.874	Female
K51-3739	[013]	Chalcolithic	Right	-1.832	Female	-2.133	Female
K51-3940'	[013]	Chalcolithic	Left	-2.602	Female	-2.137	Female

Navicular

The methodology used to allocate sex on the navicular relies on different equations depending on the side the bone belongs to. If the skeletal element is left, the main multivariate equation used was [=(-28.365+(0.421***MI**)+(0.492***MII**))] and the control univariate equation was [=(-26.248+(0.655***MII**))]. The accuracy rate for the first equation is 84.1% and for the second 80.8%. If the bone belongs to the right side, the main univariate equation used was [=(-28.313+(0.710***MII**))] and the control univariate equation was [=(-27.737+(0.694***MII**))]. The accuracy rate for the first equation is 83.9% and for the second 80.3%. No juvenile elements were used to perform the analysis (see **Table 78**).

Table 78. Sex allocation results obtained by multivariate and univariate functions using the navicular.

ID	SU	Chronology	Siding	Result (m)	Sex (m)	Result (u)	Sex (u)
K51-2351	[004-013]	Neolithic/ Chalcolithic	Right	-4.173	Female	-4.141	Female
K51-3985	[025]	Neolithic/ Chalcolithic	Right	-1.333	Female	-1.365	Female
K51-4418	[033]	Neolithic/ Chalcolithic	Left	-2.162	Female	-2.013	Female
K51-1979	[004]	Neolithic	Right	-4.883	Female	-4.835	Female
K51-1991	[004]	Neolithic	Left	-4.551	Female	-4.633	Female
K51-2158	[004]	Neolithic	Right	-0.623	Female	-0.671	Female
K51-2274	[004]	Neolithic	**Left**	**0.156**	**Male**	**-0.048**	**Undetermined**
K51-0612	[002]	Chalcolithic	Left	-5.322	Female	-3.978	Female
K51-0692'	[002]	Chalcolithic	Left	-5.885	Female	-5.288	Female
K51-1058	[002]	Chalcolithic	Left	-6.306	Female	-5.288	Female
K51-1060'	[002]	Chalcolithic	Left	-5.043	Female	-5.288	Female

ID	SU	Chronology	Siding	Result (m)	Sex (m)	Result (u)	Sex (u)
K51-1206	[002]	Chalcolithic	Left	-2.583	Female	-2.013	Female
K51-1213	[002]	Chalcolithic	Right	-2.753	Female	-2.753	Female
K51-1343A	[002]	Chalcolithic	Left	-4.901	Female	-3.978	Female
K51-2014	[011]	Chalcolithic	Left	-4.972	Female	-4.633	Female
K51-2455	[013]	Chalcolithic	Left	-4.059	Female	-3.978	Female
K51-2468	[013]	Chalcolithic	Left	-5.114	Female	-5.943	Female
K51-2506	[013]	Chalcolithic	Right	-3.463	Female	-3.447	Female
K51-2535	[013]	Chalcolithic	Right	-6.303	Female	-6.223	Female
K51-2607	[013]	Chalcolithic	Left	-4.551	Female	-4.633	Female
K51-2612A	[013]	Chalcolithic	Right	-2.753	Female	-2.753	Female
K51-2721	[013]	Chalcolithic	Left	-4.059	Female	-3.978	Female
K51-2866	[013]	Chalcolithic	Left	-3.567	Female	-3.323	Female
K51-3412	[013]	Chalcolithic	Right	-6.303	Female	-6.223	Female
K51-3435	[013]	Chalcolithic	Left	-4.059	Female	-3.978	Female
K51-3504	[013]	Chalcolithic	Right	-0.623	Female	-0.671	Female
K51-0057	[001]	Chalcolithic/ Early Bronze Age	Left	-2.091	Female	-1.358	Female

First (medial) Cuneiform

The methodology used to allocate sex on the first cuneiform relies on different equations depending on the side the bone belongs to. If the skeletal element is left, the main multivariate equation used was [=(-38.884+(1.219***MII**)+(0.504***MIII**))] and the control univariate equation was [=(-25.583+(0.962 ***MI**))]. The accuracy rate for the first equation is 83% and for the second 81.4%. If the bone belongs to the right side, the main multivariate equation used was [=(-38.600+(0.623***MI**)+(1.191***MII**))] and the control univariate equation was [=(-27.523+(1.035 ***MI**))]. The accuracy rate for the first equation is 88.6% and for the second 86.1%. No juvenile elements were used to perform the analysis. The gap between Harris and Case and Navega et al. is visible here, as the limit of 23.5mm for MI in Portuguese populations seems to have tilted the results toward female individuals (see **Table 79**).

Table 79. Sex allocation results obtained by multivariate and univariate functions using the first cuneiform.

ID	SU	Chronology	Siding	Result (m)	Sex (m)	Result (u)	Sex (u)
K51-1986	[004]	Neolithic	Left	-4.764	Female	-5.381	Female
K51-2346	[004-013]	Neolithic/ Chalcolithic	Right	-3.401	Female	-2.683	Female
K51-4499	[033]	Neolithic/ Chalcolithic	Left	-1.318	Female	-0.571	Female
K51-0190	[002]	Chalcolithic	Right	-2.155	Female	-0.613	Female
K51-0370	[002]	Chalcolithic	Right	-5.838	Female	-4.753	Female
K51-0430'	[002]	Chalcolithic	Left	-3.545	Female	-4.419	Female

ID	SU	Chronology	Siding	Result (m)	Sex (m)	Result (u)	Sex (u)
K51-0516'	[002]	Chalcolithic	**Left**	**0.405**	**Male**	**-2.495**	**Female**
K51-0639'	[002]	Chalcolithic	Left	1.413	Male	1.353	Male
K51-0739	[002]	Chalcolithic	Left	-3.838	Female	-3.457	Female
K51-0849	[002]	Chalcolithic	**Right**	**1.418**	**Male**	**-0.613**	**Female**
K51-1155	[002]	Chalcolithic	Right	-5.215	Female	-3.718	Female
K51-2023	[011]	Chalcolithic	Left	-3.041	Female	-2.495	Female
K51-2440	[013]	Chalcolithic	Left	-4.764	Female	-1.533	Female
K51-2510	[013]	Chalcolithic	Left	-2.748	Female	-4.419	Female
K51-2547	[013]	Chalcolithic	Right	-5.215	Female	-3.718	Female
K51-2716	[013]	Chalcolithic	Left	4.566	Male	0.391	Male
K51-0042	[001]	Chalcolithic/ Early Bronze Age	Right	-2.778	Female	-1.648	Female
K51-0123	[001]	Chalcolithic/ Early Bronze Age	Left	-2.326	Female	-5.381	Female
K51-2001	[002-003]	Chalcolithic/ Early Bronze Age	Left	-8.21	Female	-3.457	Female

Second (intermediate) Cuneiform

The methodology used to allocate sex on the second cuneiform relies on different equations depending on the side the bone belongs to. If the skeletal element is left, the main multivariate equation used was [=(-36.046+(1.018***MI**)+(0.772***MIII**))], with an accuracy rate of 82.4%. If the bone belongs to the right side, the main multivariate equation used was [=(-45.695+1.082***MI**)+(0.623***MII**)+(0.694***MIII**))] and the control univariate equation was [=(-23.822+(1.448 ***MII**))]. The accuracy rate for the first equation is 86.6% and for the second 82.4%. No juvenile elements were used to perform the analysis (see **Table 80**).

Table 80. Sex allocation results obtained by multivariate and univariate functions using the second cuneiform.

ID	SU	Chronology	Siding	Result (m)	Sex (m)	Result (u)	Sex (u)
K51-4676	[048]	Undetermined	Left	-5.09	Female		
K51-2310	[004-013]	Neolithic/ Chalcolithic	Right	-9.333	Female	-3.55	Female
K51-3641	[013-13a]	Neolithic/ Chalcolithic	Right	-2.371	Female	-0.654	Female
K51-4489	[033]	Neolithic/ Chalcolithic	**Right**	**0.394**	**Undetermined**	**-4.998**	**Female**
K51-4576	[035]	Neolithic/ Chalcolithic	Left	-5.09	Female		
K51-4583	[035]	Neolithic/ Chalcolithic	Right	-8.874	Female	-4.998	Female
K51-0425	[002]	Chalcolithic	Right	-8.251	Female	-3.55	Female
K51-0777	[002]	Chalcolithic	Left	-1.756	Female		
K51-2624	[013]	Chalcolithic	Right	1.498	Male	0.794	Male
K51-2839	[013]	Chalcolithic	Left	-12.776	Female		
K51-3041	[013]	Chalcolithic	Right	-6.546	Female	-2.102	Female

ID	SU	Chronology	Siding	Result (m)	Sex (m)	Result (u)	Sex (u)
K51-3884	[013]	Chalcolithic	Left	2.562	Male		

Third (lateral) Cuneiform

The methodology used to allocate sex on the third cuneiform relies on different equations depending on the side the bone belongs to. If the skeletal element is left, the main multivariate equation used was [=(-40.826+(0.968***MI**)+(0.702***MIII**))] and the control univariate equation was [=(-33.905+(1.369 ***MI**))]. The accuracy rate for the first equation is 82.3% and for the second 81.9%. If the bone belongs to the right side, the main multivariate equation used was [=(-44.965+(1.171***MI**)+(0.660***MIII**))] and the control univariate equation was [=(-39.775+(1.598 ***MI**))]. The accuracy rate for the first equation is 85.6% and for the second 85.9%, in this case the univariate performs a little better than the multivariate equation (+0.3%), though it is a very slight variation. No juvenile elements were used to perform the analysis (see **Table 81**).

Table 81. Sex allocation results obtained by multivariate and univariate functions using the third cuneiform.

ID	SU	Chronology	Siding	Result (m)	Sex (m)	Result (u)	Sex (u)
K51-2203	[004]	Neolithic	Right	-6.003	Female	-4.619	Female
K51-4158	[025]	Neolithic/ Chalcolithic	Right	-5.854	Female	-6.217	Female
K51-0197	[002]	Chalcolithic	Right	-4.172	Female	-3.021	Female
K51-0648	[002]	Chalcolithic	Right	-6.514	Female	-6.217	Female
K51-1054	[002]	Chalcolithic	Right	-8.494	Female	-6.217	Female
K51-1093	[002]	Chalcolithic	Right	-13.838	Female	-12.609	Female
K51-1319	[002i4i]	Chalcolithic	Right	-0.723	Female	-4.619	Female
K51-3318	[013]	Chalcolithic	Right	-6.514	Female	-6.217	Female
K51-3508	[013]	Chalcolithic	Right	-12.518	Female	-12.609	Female
K51-0151	[001]	Chalcolithic/ Early Bronze Age	Left	-5.49	Female	-3.787	Female

Cervical

The methodology used for sex allocation using vertebrae was applied only to Cervical vertebra 2, as those were the elements found in good conditions. Although C1 and C7 were identified, these elements did not provide a well conservated specimen. The equation used was [=29.893-(0.073***MI**)-(0.305***MII**)-(0.071***MIII**)-(0.110***MIV**)+(0.194***MV**)+(0.004***MVI**)-(0.294***MVII**)-(0.759***MVIII**)], with an 80% accuracy rate (see **Table 82**).

Table 82. Sex allocation results obtained by multivariate and univariate functions using the axis.

ID	SU	Chronology	Result (m)	Sex (m)
K51-1091	[002]	Chalcolithic	1.169	Male
K51-1341A	[002]	Chalcolithic	-1.965	Female
K51-3937	[013]	Chalcolithic	-1.714	Female

Mental eminence

Morphological analysis by the examination of the mental eminence provided mixed results. The analysed mandibles were tested under Buikstra and Ubelaker (1994) scoring system, which treats score 3 as undetermined. As previously (p. 86) stated, decision trees would treat said score as a probably male individual, but since other skull markers are missing the interpretation was left as undetermined (see **Table 83**).

Table 83. Sex allocation results obtained by morphoscopic examination of the mental eminence.

ID	SU	Chronology	ME Score	Result
K51-0349	[002]	Chalcolithic	4	Male
K51-0456	[002]	Chalcolithic	2	Female
K51-3700	[013]	Chalcolithic	3	Undetermined
K51-3774	[013]	Chalcolithic	3	Undetermined

Finally, spatial distribution for sex allocated elements provided no recognizable pattern once again (see **Map 6**).

Map 6. Spatial distribution of sexed elements.

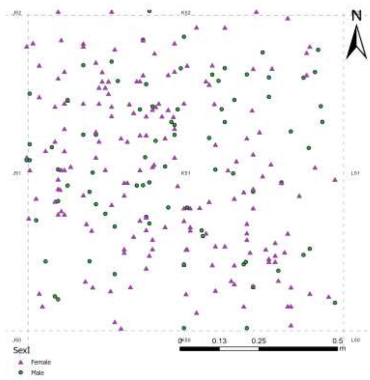

4.6. Morphological description

4.6.1. Stature prediction

Equations for stature were applied to the first and second metatarsals. The order of application depended primarily on their *R* value. Thus, for MT1 the equations were [871.260+(13.007***MII**)] with an R value of 0.721 and [887.530+(12.826***MI**)] with an R value of 0.702. In MT2's case the main equation was [790.041+(11.689***MII**)] with an R value of 0.793, while the secondary equation was [798.894+(11.990***MI**)] with an *R* value of 0.792 (see **Table 84**).

Table 84. Stature estimates based on metatarsal (MT) measurements. The average was obtained using the first two values.

ID	SU	Chronology	MT	Side	Stat. I	Stat. II	Average
K51-2188	[004]	Neolithic	1	Right	1664.69	1631.44	1648.06
K51-2213	[004]	Neolithic	1	Right	1638.67	1580.13	1609.40
K51-4138	[025]	Neolithic/ Chalcolithic	1	Right	1625.67	1580.13	1602.90
K51-0513	[002]	Chalcolithic	1	Right	1638.67	1605.79	1622.23
K51-0957	[002]	Chalcolithic	1	Right	1664.69	1631.44	1648.06
K51-1184	[002]	Chalcolithic	1	Right	1742.73	1682.74	1712.74
K51-1422A	[002i4i]	Chalcolithic	1	Right	1703.71	1657.09	1680.40
K51-2481	[013]	Chalcolithic	1	Right	1573.64	1541.66	1557.65
K51-2725	[013]	Chalcolithic	1	Right	1534.62	1503.18	1518.90
K51-0489	[002]	Chalcolithic	1	Left	1560.63	1541.66	1551.14
K51-0568	[002]	Chalcolithic	1	Left	1677.69	1580.13	1628.91
K51-1013	[002]	Chalcolithic	1	Left	1690.70	1657.09	1673.90
K51-1242	[002]	Chalcolithic	1	Left	1612.66	1580.13	1596.40
K51-1248	[002]	Chalcolithic	1	Left	1625.67	1580.13	1602.90
K51-2990	[013]	Chalcolithic	1	Left	1651.68	1592.96	1622.32
K51-3745	[013]	Chalcolithic	1	Left	1599.65	1567.31	1583.48
K51-1999	[002-003]	Chalcolithic/ Early Bronze Age	1	Right	1625.67	1554.48	1590.07
K51-0096	[001]	Chalcolithic/ Early Bronze Age	1	Left	1625.67	1580.13	1602.90
K51-1963A	[003]	Early Bronze Age	1	Left	1612.66	1580.13	1596.40
K51-2183	[004]	Neolithic	2	Left	1596.58	1590.23	1593.41
K51-2372	[004-013]	Neolithic/ Chalcolithic	2	Right	1514.76	1494.31	1504.54
K51-3637	[013-013a]	Neolithic/ Chalcolithic	2	Right	1619.96	1638.19	1629.08
K51-4211	[025]	Neolithic/ Chalcolithic	2	Right	1596.58	1614.21	1605.40
K51-4404	[032]	Neolithic/ Chalcolithic	2	Left	1549.83	1554.26	1552.05
K51-0505	[002]	Chalcolithic	2	Right	1655.03	1650.18	1652.61
K51-0867	[002]	Chalcolithic	2	Right	1573.20	1566.25	1569.73
K51-2453	[013]	Chalcolithic	2	Right	1549.83	1554.26	1552.05
K51-2528	[013]	Chalcolithic	2	Right	1549.83	1542.27	1546.05
K51-3018	[013]	Chalcolithic	2	Right	1608.27	1590.23	1599.25
K51-2458	[013]	Chalcolithic	2	Left	1666.72	1662.17	1664.45
K51-2620	[013]	Chalcolithic	2	Left	1596.58	1542.27	1569.43
K51-2648	[013]	Chalcolithic	2	Left	1608.27	1614.21	1611.24
K51-3497	[013]	Chalcolithic	2	Left	1608.27	1614.21	1611.24

Stature and sex allocation

T.D. Holland analysed 119 paired calcaneus and talus (and one unpaired) to elaborate his methodology. In GMS's case, the number of pieces that could be measured to obtain a value for sex allocation was only 23. However, a brief comparison between the means for each sample was made, to assess how far away was Morgado Superior from the data provided by Holland.

The mean value for **Measurement VII** (MTAL in Holland's method) for female individuals was 46.9 mm (*n*=10, from which 3 were eroded in the distal portion) in GMS, while the analogous number for white females was 56.02 in Holland's paper. In males the mean at GMS was 51.4 (*n*=5) against Holland's mean of 61.44.

The calcaneus's **Measurement I** (PCAL in Holland's method) presented a mean value of 75 (*n*=4) in GMS males, while its equivalent in Holland's sample was 81.66. Females had a mean value of 69.5 (*n*=4) in GMS, while their counterpart in Holland's sample presented a value of 75.38.

The calcaneus **Measurement VII** (PCAL in Holland's method) had a mean value of 52.75 for males in GMS and 58.64 in Holland's sample. In the case of females, the mean value of this measurement was 47.75, while Holland's sample reached 53.5.

Each compared mean value was lower than those found Holland's paper. The application of the first equation for the calcaneus (using maximum length) was the one that stood out the most, presenting statures over 170 cm, which when compared with data obtained through metatarsal analysis or the second equation (using the calcaneal body length) were over the mean.

The measurements on the calcaneus were utilized in two equations, the main one was [1.150***MI**)+77.37] with a pooled accuracy rate of 95%, while the second one was [(1.617***MVII**)+76.91] with a pooled accuracy of 86.3%. The latter had values that were similar to the results found with the metatarsals. The first equation had outlier values over 1.7 m that had not been obtained with any other methods (see **Table 85**).

Table 85. Stature prediction using Holland's equations on the calcaneus.

ID	SU	Chronology	Side	Sex	Stature 1	Stature II	Average
K51-2696	[022]	Undetermined	Right	Male	159.02	159.377	159.1985
K51-2328	[004-013]	Neolithic/ Chalcolithic	Left	Female	157.87	154.526	156.198
K51-0484	[002]	Chalcolithic	Right	Male	170.52	160.994	165.757
K51-0826	[002]	Chalcolithic	Left	Female	156.72	152.909	154.8145
K51-0945	[002]	Chalcolithic	Left	Female	154.42	152.909	153.6645
K51-1125	[002]	Chalcolithic	Right	Male	164.77	164.228	164.499
K51-2461	[013]	Chalcolithic	Left	Female	160.17	156.143	158.1565
K51-3044	[013]	Chalcolithic	Left	Male	160.17	164.228	162.199

The talus only used one variable and one equation [((1.411***MVII**)+85.95] with a 91.5% of accuracy. The talus' stature estimation results had similar ranges to those obtained using the metatarsals (see **Table 86**).

Table 86. Stature prediction using Hollands equations on the talus.

ID	SU	Chronology	Side	Sex	Stature
K51-2192	[004]	Neolithic	Right	Male	156.5
K51-2226	[004]	Neolithic	Left	Female	153.678
K51-2275	[004]	Neolithic	Left	Female	149.445
K51-2340	[004-013]	Neolithic/ Chalcolithic	Left	Female	150.856
K51-3646""""	[013-013a]	Neolithic/ Chalcolithic	Left	Female	150.856
K51-4647	[041]	Neolithic/ Chalcolithic	Left	Female	152.267
K51-0234	[002]	Chalcolithic	Right	Male	159.322
K51-0655	[002]	Chalcolithic	Left	Female	153.678
K51-0807	[002]	Chalcolithic	Right	Male	157.911
K51-0905	[002]	Chalcolithic	Left	Male	160.733
K51-2415	[013]	Chalcolithic	Left	Female	152.267
K51-2518	[013]	Chalcolithic	Right	Female	156.5
K51-2549	[013]	Chalcolithic	Right	Female	145.212
K51-2768	[013]	Chalcolithic	Right	Female	156.5
K51-3940	[013]	Chalcolithic	Left	Male	159.322

There is a big difference when using one method or the other, Metatarsal measurements produce higher values in their outputs. Unfortunately, averages for periods other than the Chalcolithic could not be obtained. The difference between the average stature of males and females during the Chalcolithic was of 8.05 cm, while the global difference was 7.085 cm (see **Table 87**). The differences between periods are not as expected, with a value that decreases over time. It is likely that the reason behind it is the use of different methodologies, as it was heavily influenced by average heights on undetermined individuals (metatarsal).

Table 87. Average stature distributed by sex and chrono-cultural region.

Sex	Neo.	Neo. / Chalc.	Chalc.	Chalc./ E. Bronze A.	E. B. A.	Global
Female		157.87	157.1033333			157.295
Male			165.1533333			165.1533333
Undet. (Metat.)	169.0701	171.6715	169.3065909	162.5666	161.2659	168.9912697
Average (Tot.)	**169.0701**	**169.37125**	**167.5541071**	**162.5666**	**161.2659**	**167.5337975**

4.6.2. Pathological conditions

For a full inventory of bone abnormalities please see **Annex 8**. Abnormal features seem to be far more common during the Chalcolithic, including abnormalities in shape (mechanical, generical, and traumatic), sclerosis, porotic destruction, plaque, and trauma. It is followed by its sister category, Neolithic/Chalcolithic, at a much lower prevalence of shape abnormalities and trauma. Although it lacks the remaining features, it contains lesion on spongy bones and loss of contours. The Neolithic only presents abnormalities on shape and trauma, while the Chalcolithic/ Early Bronze Age only presents shape abnormalities (see **Chart 18**, **Photograph 7** ,and **Photograph 8**).

Chart 18. Distribution of bone abnormalities by chrono-cultural period.

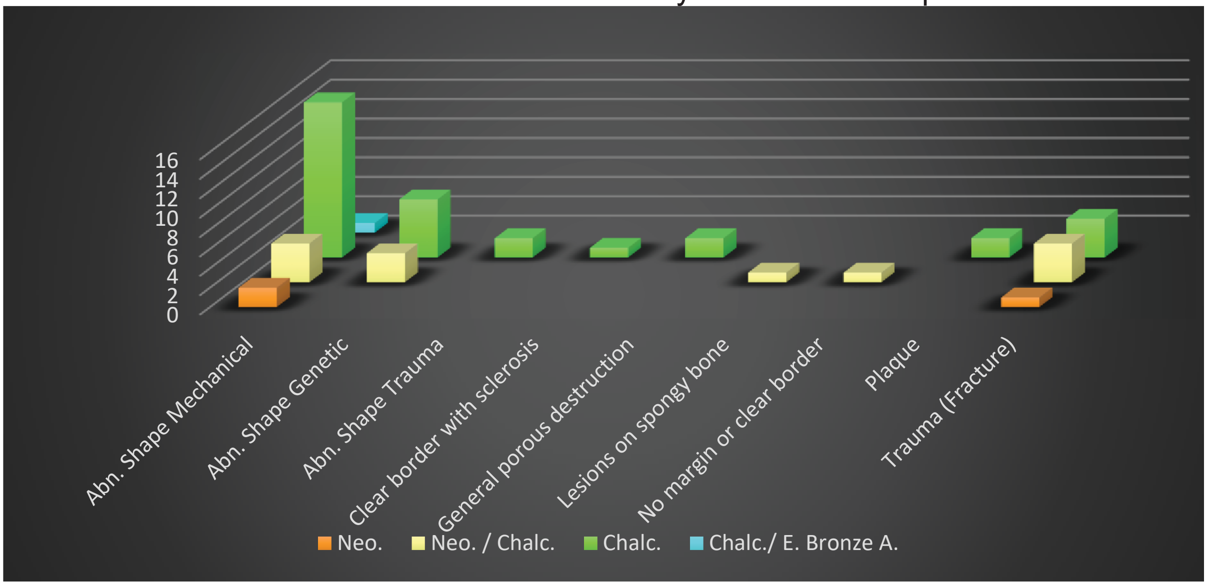

Photograph 7. Ankylosing and fusion of a proximal and intermediate hand phalanx (*Left*) (*Right)* K51-0580. First distal phalanx with marginal osteophytes.

Photograph 8. K51-0215' Undetermined metacarpal with trauma -badly consolidated (*Left*); K51-3135- Fused intermediate and distal foot phalanges (*Right*)

Although results may reflect the abundance of material during the Chalcolithic, the overwhelming absence from the Neolithic and Early Bronze Age are noticeable. Without more data to compare it is difficult to propose a theory as to what the cause for these patterns were.

Abnormal bone lesions followed a similar pattern, mostly presenting marginal osteophytes in articular regions. The prevalence of enthesophytes and joint fusion was also elevated. Only one case of eburnation was detected within the interphase of the Chalcolithic and the Bronze Age. In essence, most abnormal lesions are related with articular degenerative processes. These are not to be confused with musculoskeletal markers, as they are in areas without muscle/tendon insertions (see **Chart 19** and **Photograph 9**).

Chart 19. Distribution of abnormal lesions by chrono-cultural period.

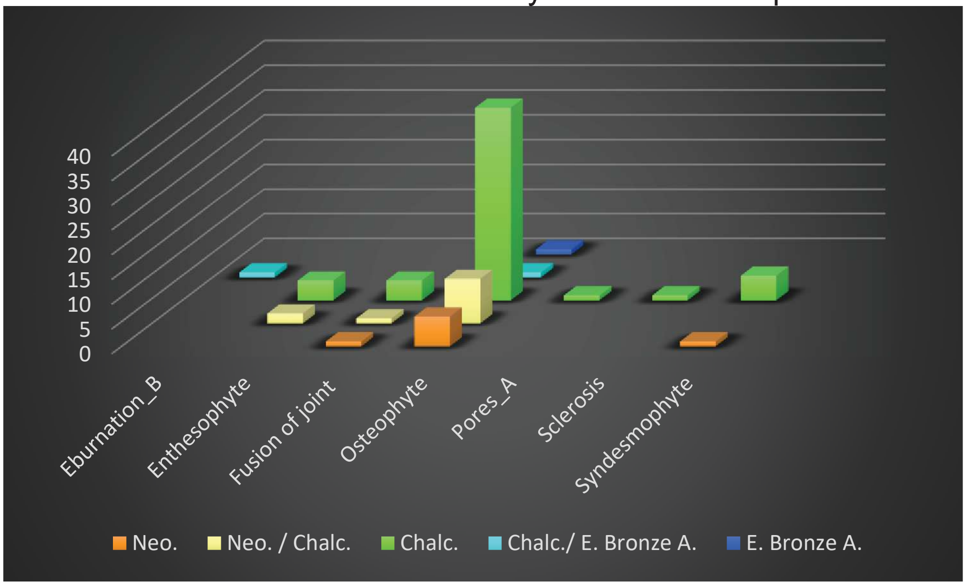

Only three non-metric traits were identified: cusp of Carabelli (K51-0678), a bipartite navicular (K51-1464A) (see **Photograph 9**), and a septal aperture (K51-2668).

Photograph 9. K51- 4164A- A bipartite left navicular (*Left*); K51-0131A – a right lunate with eburnation at the non-articular portion of the radial portion (probably a dislocation) (*Right*).

4.6.2.1. **Dental wear**

Dental wear patterns had a distinctive behaviour in each chrono-cultural period. The lowest scores were relatively prevalent in all of them, but the Neolithic tended to mild scores (2), while the Chalcolithic and its associated periods were prone to have severe scores. The Early Bronze Age did not have enough material to recognize a trend. The higher values on scores 2, 3, 5, 5, 7 and 9 are highly influenced by the peculiar wear of incisors, that not only have several contributors, but most of them seem to be caused by non-masticatory activities. It is likely that the hypothesis presented by previous researchers of anterior teeth used as tools (see **Table 88**, **Chart 20**, and **Photograph 11**)

Table 88. Dental wear scores by chrono-cultural period.

Score	Neo.	Neo. / Chalc.	L. Neo. / E. Chalc.	Chalc.	Chalc./ E. Bronze A.	E. Bronze A.
0	2	21		84	8	
1	1	9		60	12	1
2	8	12		76	8	
3		3		9		
4	3	21		61	7	
5	1	2		5		1
6	3	9		63	4	
7	2	11		27	1	1
8	2	8		54	6	1
9	1	3		21	2	

Chart 20. Dental wear scores distributed by chrono-cultural period.

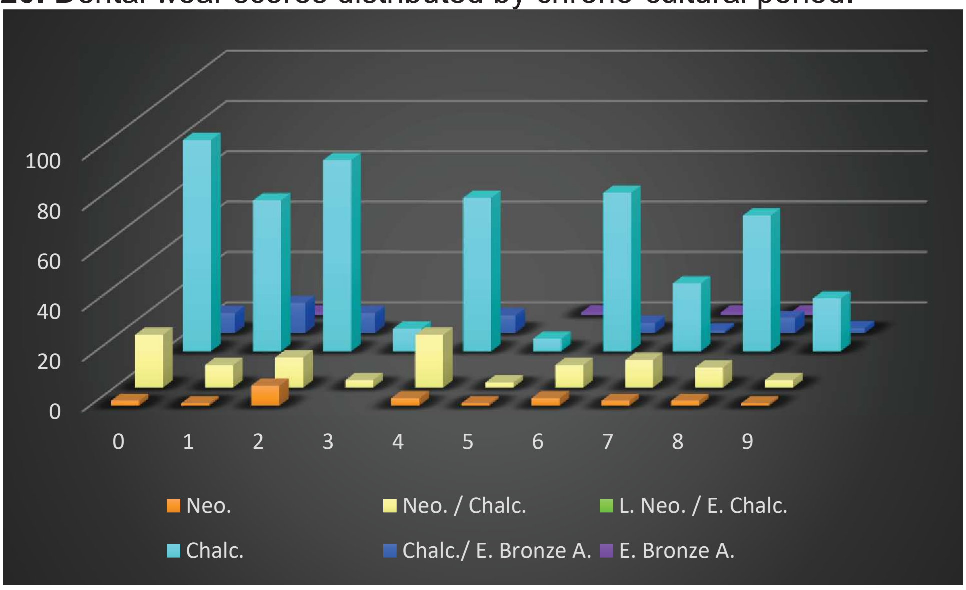

Photograph 10. K51-2292 – premolar (undetermined) with a concave dental wear pattern (*Left*); K51-393 - premolar (undetermined) with a concave dental wear pattern (*Right*)

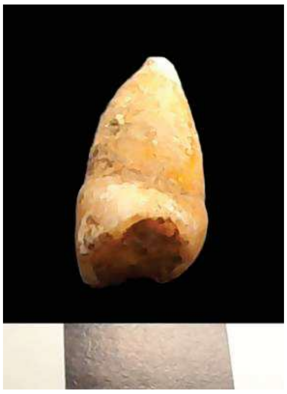

Commonly, the interpretation of dental wear is that foragers tend to display flatter angles while agriculturists have oblique ones (see **Table 89**).

Table 89. Dental wear by location

Row Labels	Occlusal	Incisal
Concave	**8**	**3**
5	1	1
6	1	1
7	3	1
8	3	
Oblique	**87**	**155**
1		40
2	32	72
3	10	
4	44	43
5		
6		
7		
8		
9	1	
Transverse	**191**	**42**
0		
1	34	10
5	5	
6	48	24
7	35	2
8	51	5
9	18	1
Total	**286**	**200**

The transverse and oblique pattern are almost identical in proportion during most chrono-cultural periods, except for the Chalcolithic, where their prevalence is 35 (transverse) to 75% (oblique). This would support the subdivision between Chalcolithic and Neolithic communities, as farming takes a bigger role in economy. When observing cariogenic lesions (see **Table 90**) the shift to agriculture may be more evident, as Chalcolithic communities present dental lesions much more frequently. Unfortunately, material related to the Early Bronze Age did not provide enough data to support a complete change. Tartar presented a methodological problem during analysis, as teeth were also subject to typical cave taphonomic processes, and unless they present cases that grow from the root, the pieces must be cleaned completely before making any assumptions.

Table 90. Dental lesions by chronology.

Ro	Neolithic	Neolithic/ Chalcolithic	Chalcolithic
Abscess			1
Coronal Caries	1		13
Hypoplasia			1
Root Caries		1	1
Tartar			1

Photograph 11. K51- 2846 **-** musculoskeletal markers on a proximal hand phalanx.

4.6.2.2. *Musculoskeletal markers*

The analysis of musculoskeletal markers resulted in the identification of strenuous activities, mostly in the hands and feet. The count might differentiate populations as, even though the Early Bronze Age had a high representation of phalanges from both areas, it did not present the same frequencies as the Chalcolithic. The Chalcolithic also dwarfs the Neolithic in terms of prevalence (see **Table 91**). The markers did not present a pattern regarding their location, but the highest counts were found on palmar sections.

Table 91. Musculoskeletal markers by chronology

Location	Neo.	Neo. / Chalc.	Chalc.	Chalc./ E. Bronze A.	E. Bronze A.
Diaphysis (Lateral and Medial)			2		
Diaphysis (Medial)			1		
Distal Epiphysis			2		
Distal Joint Surface			1		
Dorsal			1		
Palmar			4		
Proximal Epiphysis		1	2		1
Proximal Joint Surface	2		1	1	
Total	**2**	**1**	**14**	**1**	**1**

4.6.2.3. *Taphonomic alterations*

Taphonomic alterations were mostly present in the form of flaking and cracking, followed by breakage, surface pits, and discoloration. None of them were attributed to carnivore activity (see **Photograph 12**). It is likely that the agents behind the alterations were mostly mechanical forces, cave humidity and chemical composition (alkaline soils), and bioturbation by plant roots (see **Table 92**).

Table 92. Taphonomic alterations by chrono-cultural period.

Alteration	Neo.	Neo. / Chalc.	L. Neo. / E. Chalc.	Chalc.	Chalc./ E. Bronze A.	E. Bronze A.
Abrasion			2	3		
Breakage	89	483		1417	87	6
Cave Corrosion		1		1	1	
Corrosion		1		1	1	
Deform. / Bending				1	1	
Burned		1				
Discol.	2	3		4		
Discol. Black	1	4				
Discol. Light				4		
Flaking/ Cracking 1	31	128		484	20	7
Flaking/ Cracking 2	40	145		605	68	3
Flaking/ Cracking 3	23	230		425	23	1
Flaking/ Cracking 4	28	152		479	27	1
Flaking/ Cracking 5	3	10		30		
Notches				1		
Peeling	1			11		
Pits		1		12		
Rounding	2		1	1		
Total	**125**	**667**		**2027**	**138**	**12**

Photograph 12. K51-2562 – Highly fragmented left radius.

4.7. Absolute dates

Four samples were chosen for absolute dating, financed by the Geoscience Centre (CGeo) from the Instituto Politécnico de Tomar. The laboratory used a single stage accelerator mass spectrometer (SSAMS, NEC, USA), specifically a Low-Energy Accelerator (LEA, Ionplus AG, Zürich) Automated Graphitization Equipment AGE-3 (Ionplus AG, Zürich). The samples were pretreated utilizing acid-base-acid and collagen extraction protocol. NIST-OXII and phthalic anhydride were used as reference materials.

UE [013] was interpreted a disturbed grave from the Neolithic, it contained a foot in anatomical position that unfortunately we were not able to locate for this study. The new dates place it in the Chalcolithic. SU [006] had no absolute dates, but was ascribed to the Neolithic before, which was confirmed by the analysis. Regarding SU [002] and SU [002i4i], both had been already classified as units from the Chalcolithic, which was also confirmed.

It seems that the methodology followed during the excavation was able to classify each SU accurately by relative dates.

ID	SU	Period	Laboratory	Radiocarbon	Calibrated 2σ	Sample
F53-0013	[006]]	Neolithic	FTMC-HC63-3	6142±33	5210-4995 calBC	A.M.S. – *bone - homo*
I52-1165	[002i4i]	Chalcolithic	FTMC-HC63-3	4400±31	3104-2912 calBC	A.M.S. – *bone - homo*
K51-0980	[002]	Chalcolithic	FTMC-HC63-3	4326±31	3017-2891 calBC	A.M.S. – *bone - homo*
K51-2820	[013]	Chalcolithic	FTMC-HC63-3	4496±31	3354-3092 calBC	A.M.S. – *bone - homo*

Graph 2. Results of radiocarbon analysis. Radiocarbon date (Red), part of the calibration curve (blue) and the calibrated probability density function (grey) calculated in OxCAl.

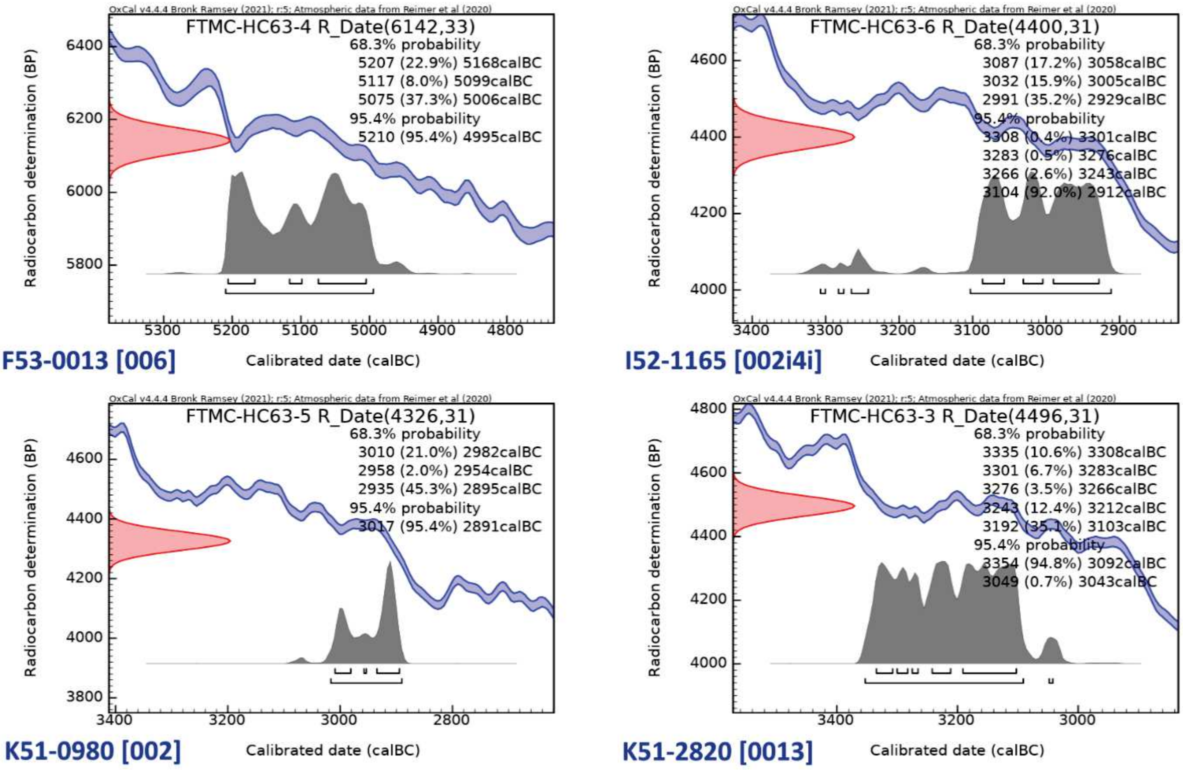

5. Discussion

Square K51 is just a snapshot of Gruta do Morgado Superior; at only 28% of its full capacity. The analysis of 4352 fragments led to the partial characterization of its assemblage. Although comparing a partial result to sites in the Canteirões region is premature, it needs find its place among its neighbours.

5.1. Bioanthropological comparison

As previously stated, the assemblage was analysed by chrono-cultural affiliation of the material to i) determine if there were paleodemographic differences among different periods, and ii) characterize each population accordingly (see **Table 93**)..

The Neolithic community was comprised by 9 adults and 2 juveniles. Most of the population was mature, and the juvenile individuals were mainly adolescents and children. It is an assemblage dominated by female individuals, and the overall height was 169 m.

The transition period between the Neolithic and the Chalcolithic is akin to the Neolithic community, with a MNI of 9 adults and 3 juveniles. Most of the population was mature, and the juveniles were represented by adolescents and children. Inhumated people was dominantly female, with an average height of 157 cm.

The Chalcolithic was the most populous and diverse assemblage, not only in artifacts but in kinds of people. It presented a MNI of 54 adults and 8 juveniles. Early development stages are well represented with a crushing majority of adolescents. It had a predominance of female individuals with an average height of 157 cm, while males reached a value of 165 cm. The overall population was about 170 cm tall.

The transition period between the Chalcolithic and the Early Bronze Age dwindles in comparison to the previous one, with only 4 adults and 2 juvenile individuals. It has a similar paleodemographic profile as the ones before.

The Early Bronze Age assemblage is the smallest, with a MNI of 2. None of its skeletal elements provided enough data for sex allocation, and only has one value recorded for stature estimation.

Table 93. General results obtained during the analysis of Square K51.

Results	**Neo.**	**Neo./Chalc.**	**Chalc.**	**Chalc./E.B.A.**	**E.B.A.**
MNI - Adults	5	9	54	4	2
MNI- Juveniles	2	3	8	2	
Perinatal			1		
Infant			7	1	
Early Child	2	14	54	1	
Late Child	1	12	26	5	1
Adolescent	5	50	166	11	
Young Adult		4	22	2	
Mature Adult	2		1		
Mature	169	441	2065	174	12
Juvenile	8	80	276	20	1

Results	Neo.	Neo./Chalc.	Chalc.	Chalc./E.B.A.	E.B.A.
Female	15	36	119	10	
Male	6	17	51	5	
Undetermined		4	6		
St. Female		157.87	157.1033333		
St. Male			165.1533333	162.5666	
St. Und.	169.0701		169.3065909		161.2659

Regarding neighbouring caves, GMS stands out for many reasons. Its assemblage during the Chalcolithic is greater than the one at GRO. The Neolithic counterpart is lower (bearing in mind that the result is partial) than the MNI registered at CDV for the same period (see **Table 95**).

The mortality pattern in CDV was only analysed for juvenile specimens since adult individuals had no observable markers that could be linked to specific age groups after 25 (see **Table 94**). The pattern reaches expected values for early and late children, and adolescents, while it had lower scores for infants. This may respond to either inherent characteristics of the osteological record that hampers the state of preservation of the material, or a cultural predilection based on age (Tomé et al., 2013). GMS has an outstanding prevalence of adolescents in its mortality pattern, but as mentioned before, it may be caused by the overrepresentation of unfused elements that tilt the balance. Be that as it may, the numbers at GMS are far greater for juveniles than for GRO, CDV, and NSL, even including perinatal individuals. The comparison must be approached cautiously, as Tomé's age groups are divided chronologically and not biologically.

Table 94. Age-Group distribution, extracted from Table 4 (Oosterbeek & Tomé, 2012; Tomé & Oosterbeek, 2011, p. 47)

Age group	GRO	CDV	NSL
Infant	2	1	1
Child	3	2	1
Teenager	2	4	2
Young Adult	2	1	2
Middle Adult	4	2	2

If one considers each site globally, Tomé's palaeodemographic results seem to be akin to those at the littoral. Underrepresentation of younger individuals, higher mortality rates for individuals between 5 and 9 years old, that goes down slightly in the 10 to 14 year old group and rises again in the 15 to 19 year old group (Tomé, 2010). GMS seems to have a similar pattern if the information is indirectly compared, having spikes in early childhood, that decrease during late childhood, and skyrocket in adolescence. Tomé does not provide a theory as to why is it that this pattern repeats in Portuguese collections.

Tomé and Oosterbeek (2011) present a summary with results of sex distribution for Gruta do Cadaval differentiated by Layer (see **Table 95**). Most sites present an equal ratio for both sexes, except for NSL that has a 1:2 ratio for females-males. In this sense, all chrono-cultural periods in GRO differ from the neighbouring sites.

Table 95. Canteirões do Nabão general overview, updated. Various sources: Oosterbeek et al. (2020), Tomé et al. (2013; 2013), Tomé and Oosterbeek (2011) Tomé (2010)., Cruz (1997), Oosterbeek (1993a)

CD	**CDV**	**CDV**	**NSL**		**GRO**		**GMS (Tomé, 2010)**
	Layer C	Layer D	Layer B	Layer A	Layer 1 to 3	Layer 4	
Period	Middle Neolithic		Early Neolithic	Early Bronze Age	Late Neolithic		
Absolute Date calBC 2σ	4354-3732	4350-4045 4212-3817	5230-4847	N/D	3628-3100 3400-2880 2954-2217 3020-2890		
MNI (Adult)	16 (14 (2010))		4	1	20		3
MNI (juvenile)	17		5		11		
Probable Males	1		6	-	9		
Probable Females	3		3	1	10		
Context	Individual/ Collective		Collective	Individual	Collective	Individual	
Av. Height Men					1.65 to 1.73		
Av. Height Women					1.48 to 1.54		
Mortality 1-4	100 –				50 -		
Mortality 5-9	160+				180 +		
Mortality 10-14	150+				80		
Mortality 15-19	190				40		
Young Adult							
Adult							

Cavities	5.58		9.26[15]		11.63	
Dental Wear	2.92		3.48		3.64	
Antemortem Dental loss	0		0		5.6	
Trauma	2 (MC)		1 (cranium) [16]		5 (cranium)	
Pathologies	Infection ear canal				2 MC infection	
Porotic Hyperostosis			2		8	
Cribra supr. Orb.			3		26	
Hypoplasia	12.02		14.81		13.7	14.29
Notes			Arthritis on metatarsals[17]		Low iron content, overdevelopment of arm muscles, hypoplasias (30%), Oblique dental wear, lowet cavity frequency	
Lithic	Points, blades, notches, bladelets, burins, microliths, scrappers, polished stone, macrolithic cores	Trapezes, blades, bladelets, burins, scrappers, polished stones.	End-scrapers, burins, points, blades, bladelets, macrolithic cores	Disturbed contexts	Points, blades, notches, bladelets, burins, microliths, scrappers, polished stones, occasional microlithic cores	
Ceramic	Grooved ware	Incised and Impressed.	Impressed	Bell Beaker	Grooved ware	

[15] It is unclear to which layer/stratigraphic unit do these percentages refer to.
[16] It is unclear to which layer/stratigraphic unit do these percentages refer to.
[17] It is unclear to which layer/stratigraphic unit do these percentages refer to.

The fact that most sex allocation methods imply intrinsically that female features are by default smaller than those of males, could result the misclassification of juveniles as females. This could be the case when allocating sex by some of the methodologies employed at GMS:

Articular degenerative pathologies are ubiquitous to most of the sites in the region, including GMS. Some markers such as cribra orbitalia, which is a marker that was not observed at GMS (mostly because of the scarcity of skulls). It is not clarified if there was a methodological distinction for its observation between postmortem erosion, osteitis, anaemia, or other pathologic conditions. The presence of the marker without the registration of other palaeodemographic and morphological characteristics make it difficult to include it with other insult events such as hypoplasia (Wapler et al., 2004).

The methodology used for abnormalities in form and lesions allows for a deep description, but unfortunately cannot be compared directly to other sites, as they are usually registered as percentages.

Regarding lesions associated with trauma, GMS presents a regular profile with fully consolidated fractures. Their location could also be related to aging processes, or skeletal regions prone to accidents. Evidence of trauma in cranial elements is not that common in the area, the except for GRO, where at least 5 individuals (4 male) present traumas in the parietal (4), frontal (1), and occipital (1). Only one individual from NSL presents a similar lesion on the left parietal (Oosterbeek & Tomé, 2012). The lesions appear to be caused by blunt elements, and even though the European Neolithic/Chalcolithic communities are no strange to inter and intracommunity violence, evidence of such is sparce in Portugal. Even when considering the frequency of arrowheads at GMS, there is no evidence of injury that could be associated directly to them.

The faunal assemblage has a higher concentration of ovicaprids than NSL and CDV, but an outstanding presence of leporids, carnivores (in general), and European Badgers. The absence of *Bos Taurus* is notable, and even though *Sus scrofa* is not on the list, one of the polished bone adornments may belong to one.

Table 96. Number of Identified species by taxa for different sites Based on information published by Tomé et al. (2013) and Almeida et al. (2023)

Taxa	NSL	CDV (Layer C)	CDV (Layer D)	GMS
***Bos* sp.**	5			1
Bos taurus	5	4	1	
Cervus elaphus		3		2
***S. scrofa* ssp.**	2	8	3	
Capreolus capreolus		1	2	2
C. hircus		5	5	
Ovis*. *aries	13	7	1	11
Ovis/ Capra				20
***Sus* sp.**				4
O/C	44	29	21	

Taxa	NSL	CDV (Layer C)	CDV (Layer D)	GMS
C. ef. *lupus*		2		
***Canis* sp.**	3			
Vulpes vulpes	9			2
Felis sylvestris	2	1		1
Meles meles	1		2	7
C. *fiber*		1		
***Lepus* sp.**	2			2
Oryctolagus cuniculus	77			196
Leporidae	9			187
Carnivora ind.				4
Aves ind.	5		2	9
Chelonioids		2		
Indeterminate	217	132	87	403
Total	394	201	133	851

Chart 21. Faunal assemblage in NSL, CDV (layers C and D) and GMS. Based on information published by Tomé et al. (2013) and Almeida et al. (2023)

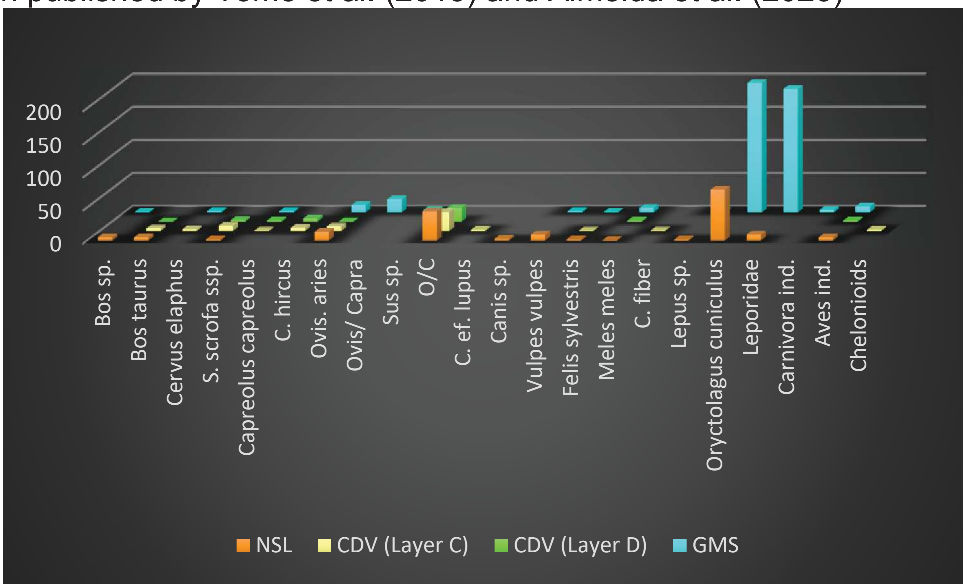

Regarding the assemblage, adornment distribution can be interpreted as a surge in grave goods in the Chalcolithic, trend that starts in the Neolithic and disappears in the Bronze Age. Spatially the gap at J50 and radial diffusion is noticeable, but without any further analysis it is impossible to determine its cause. The Chalcolithic diversification of adornments has already been described in other works (Cruz, 1997).

If one considers the (micro) topographic layout of the site, and the fact that metallic (and heavy) elements were dragged to the seemingly subduction zone, it is likely that the material was transported thanks to gravitational forces (either by water or sediment).

Lithic technology is usually related to the occurrence of macrolithic elements and the Neolithic (pottery in particular). The association has been reinforced by the artefactual context in Anta 1 (Layer C), and megalithic necropolises from Vale Chãos and Jogada. Technologic and morphologic studies registered a generalized resemblance among lithic industries from the Lower Palaeolithic to the Chalcolithic. However, some elements may be grouped within two operational sequences, both supported by quartzite pebbles, one aimed to the production of flakes and another to the use of pebbles as tools. Macrolithic industries dominate lithic assemblages from the Early Neolithic to the Zêzere's Megalithic period, diminishing in usage during the Chalcolithic (Cruz et al., 2000). The existence of a highly specialized ensemble during the Chalcolithic that showcases both, a toolkit that seems to be used for agropastoral activities and another that seems to be focused on hunting (or warfare) can be interpreted as the implementation of a large spectrum economy that used economic models associated to the hunter-gatherer communities (Middle Palaeolithic) and the farming ones (Neolithic). If both systems survived until the Chalcolithic, even developing two distinct hunting methods (Berruti & Daffara, 2014), it is possible that the adoption of typical Neolithic traits took longer than expected (Cruz, 1997). The Chalcolithic is marked by a growing sense of importance and diversification of tools, which reflects the growing complexity of the economic activities.

There is no evidence of large or small mammal activity as well as carnivores on human remains. The high level of fragmentation and bone loss could have altered the skeletal element's topography enough to wash away the evidence, though. However, the cave's humidity, coupled with plant-root expansion and possible exposure to air and water (weather it was seasonal or spaced) seem to be responsible for the shape of the deposition. Alkaline soils are linked as well with the cracking and peeling. Human agents may have contributed by trampling, but there is no evidence of percussion or any other sign of intentional breaking.

Funerary architecture is akin to nearby sites. GRO and NSL present similar patterns in occupation, with disturbed (and probably individual) burials at their bases, and collective inhumations on top. Patterns in grave goods indicate a Chalcolithic explosion of material that comes from the Neolithic. The Bronze Age marks a decline of diversity and quantity. Comparison must be done through frequency and location (Lanfranco & Eggers, 2010)

Gruta dos Ossos also presents a concentration of material in the Southwest sector while Anta 1 displayed thin layers of sediment as well. Caves and dolmens seem to reflect two different occupation moments, one with individual inhumations and another with collective burials, the latter usually on top of the other. Other Neolithic sites present similar patterns (e.g., Bom Santo in Lisbon (Carvalho et al., 2016)). The Estremadura region presents two main non-megalithic cycles of funerary activity during the Neolithic, the first being characterized by individual burials and the second by collective inhumations. Collective inhumations started appearing around 3800 BC, that according to most experts on the area is related to the beginning of the Middle Neolithic. This period would also witness the advent of arrowheads, large flint blades, carinated vessels, and engraved slate plaques (Almeida et al., 2019).

Silva and Tomé concluded that there are two different architectural moments, one that uses caves and another that uses monuments (dolmens) in the intermediate chronologies between the Neolithic and the Early Bronze Age. The latter would culminate in the use of megalithic structures and the introduction of practices like cremation, which probably would have been a direct result of the emergency and consolidation of metallurgic societies. Regarding this hypothesis, the cave seems to be used mostly during the Chalcolithic, following a tradition that started in the Neolithic. The Early Bronze Age main characteristic is the lack of material overall. When compared to Tomé's argument it seems that the process of "death's collectivization" did occur in Morgado, with a seemingly predilection for individual burials during the Neolithic, collective burials during the Chalcolithic, and the subsequent abandonment of the site during the dawn of the Bronze Age.

Some megalithic sites emplaced in the Upper Nabão, relatively close to Canteirões, have been linked local and regional funerary patterns during the transition between the Chalcolithic and the Neolithic. The burials, dubbed Megalithic Monuments of Rego da Murta, include sites such as Anta 1, Anta 2 (Alviázere), and Tumulus 1 do Souto (Abrantes).

Anta 1 is an archaeological site that consists of a dolmen with a subpolygonal chamber with a descending entrance hall that levels once it reaches the main entrance. Up to 50 individuals were inhumated in the site, and the number may increase as the excavations are still ongoing. Absolute dating suggests two occupation moments, the first being in the late 4th millennium BC., and the second between the 3rd and the 2nd millennium BC. Although the analysis has not been focused on funerary practices, preliminary reports suggest that the site is a primary inhumation (Tomé & Silva, 2013).

Anta 2 is located 500m North of Anta 1, and it has a similar structure supported by eight limestone pillars. Differences between sites are evident mostly on the shape of the corridor, since in this case it has a diffused shape. Anta 2 also presents two moments of occupation, one ascribed to the Middle/Late Neolithic by indirect dating, and other attributed to the Early/Middle Chalcolithic by absolute dating (first half of the 3rd millennium BC). Preliminary analysis situates the MNI at around 69 individuals inhumated in a primary context, but a global study is required.

Tumulus 1 do Soto is a funerary structure characterized by small barrows. It is recognized as one of the first with evidence of intentional cremation, which includes chromatic alterations in one juvenile individual kept within two urns filled with ashes.

6. Conclusion

The main objective of this study was the bioanthropological characterization of the chrono-cultural periods as defined by Ana Rosa Cruz (1997) and found within Gruta do Morgado Superior and identify the differences between the communities that produced them. The assemblage has proven that, regardless of the level of fragmentation and remixing of its soils, the chronologies identified during the excavation seem to be accurate.

Spatially, the cave presents a southern slope that influenced the location of the material, accumulating small elements in the meridional wall. Sediment pressure, the cave's humidity, and soil composition seem to have joined efforts with local aeolian and water erosion processes that culminated into the disarticulation and dislocation of the material in the cave. The lapiés-llike underlying layout (Oosterbeek, 2023) may have served as a pathway for small bones to accumulate into. Gravitational dispersion analysis (Fernández-Jalvo & Andrews, 2016) is recommended for future analysis

Taphonomically, although human activity could easily be the main reason for the examples of breakage and flaking, there is no discernible pattern in the funerary context that seem to suggest intentionality behind its internal organization. The only traces of such occurrence are the primary *in situ* burials from the Neolithic, all of which have been heavily disturbed. There is no evidence of postdepositional anthropogenic intervention of the soil, as even excavating a grave would necessarily imply clearing the way for new ones. If the ritual included opening pathways for new bodies, at least the last one deposited in the soil should have shown any type of anatomical connection on top of the others.

The Stratigraphic Units, albeit thinner than expected and convoluted, maintained a level of cohesion high enough as to retain grave goods that later would serve as the cornerstone for the elucidation of relative dates. This theory is further supported by the absolute dates taken during this study, which confirmed that the site was occupied at least from 5210 calBC.

The assemblage of grave goods coincides with elements described in several sites that are in the vicinity of GMS, and some others at the regional, or even peninsular, level. The most interesting conclusions drawn from them is the existence of long-trading routes that reflect cultural ties all over the region, and the survival of pre-Neolithic practices until the Chalcolithic, as well as different types of specialization (for hunting).

The Neolithic assemblage as well as its related SUs present a pattern in which the axial and proximal appendicular skeleton is more usual than other elements. This trend can differentiate it from other periods, where distal elements are more common. The Chalcolithic-related material, given its size, represents the general trend that was pointed out in previous field reports. The Chalcolithic behaviour focuses on the distal appendicular skeleton as well as dentition.

From the bioarchaeological point of view, the main difference between Neolithic, Chalcolithic and Early Bronze Age communities relies on their demography and on their dental elements. Mortality patterns tend to be greater in early children and adolescents, a pattern that links them to other caves in Portugal with similar Chronologies. The prevalence of oblique dental wear patterns in the Neolithic/ Chalcolithic, although diminished, coupled with the amount of arrowpoints may suggest that farming was not the only economic activity, and that it was supplemented with hunting through the Chalcolithic. Cariogenic lesions' surge during the Chalcolithic support this claim. The concave wear patterns on the anterior dentition (including premolars) suggest that whatever the activity that caused them, it started in the Chalcolithic. The presence of oblique and transverse dental wear patterns in the Chalcolithic also suggests a mixed diet.

Although sister caves have depicted almost equivalent sex ratios, GMS seems to display higher female counts, in all three periods. However, carpal analysis might have resulted in an overestimation of females, given that the source population was not Portuguese. Methodologies on the carpals need to be tested on Portuguese prehistoric populations.

Another methodological difference was the estimation of stature with the metatarsals and the tarsals (talus and calcaneus). It seems that the result from the former tends to produce higher values, and when used in conjunction the overall average seems affected.

Musculoskeletal markers had a higher prevalence in Chalcolithic communities when compared to the Neolithic or the Early Bronze Age.

Finally, given the fact that the burials may have been left with thin layers of soil instead of buried for long periods of time before they are reoccupied, the area of Canteirões may correspond to a series of passage graves, as their location was kept in the cultural library of Neolithic, Chalcolithic, and Early Bronze Age communities long enough for each remembering possible associated funerary practices (Stojanovski et al., 2020). Ethnogenetic routes must also increase in complexity in rougher landscapes, such as the Alto Ribatejo, which may help understand the location of the burials in relation to the settlements.

7. References

Albanese, J. (2013). A Method for Estimating Sex Using the Clavicle, Humerus, Radius, and Ulna. *Journal of Forensic Sciences*, *58*(6), 1413-1419. https://doi.org/10.1111/1556-4029.12188

Albanese, J., Cardoso, H. F. V., & Saunders, S. R. (2005). Universal methodology for developing univariate sample-specific sex determination methods: an example using the epicondylar breadth of the humerus. *Journal of Archaeological Science*, *32*(1), 143-152. https://doi.org/10.1016/j.jas.2004.08.003

Allué, E. (2000). Pollen and Charcoal Analysis from Archaeological Sites from the Alto Ribatejo (Portugal). *ARKEOS*, *9*, 37-57.

Almeida, N., Costa, L., & Oosterbeek, L. (2019). Contemporary non-megalithic interments. In L. Oosterbeek & C. Scarre (Eds.), *Megalithic tombs in Western Iberia: excavations at the Anta da Lajinha* (pp. 120-126). Oxbow. https://doi.org/10.2307/j.ctv138wsbz

Almeida, N. J., Saladié, P., Cerrillo-Cuenca, E., & Oosterbeek, L. (2023). Another non-anthropic leporid accumulation in Southwestern Iberia? The case of a leporid sample from Morgado superior (Tomar, Portugal). *Historical Biology*, 1-14. https://doi.org/10.1080/08912963.2023.2204328

Ammer, S., d'Oliveira Coelho, J., & Cunha, E. M. (2019). Outline Shape Analysis on the Trochlear Constriction and Olecranon Fossa of the Humerus: Insights for sex Estimation and a New Computational Tool. *Journal of Forensic Sciences*, *64*(6), 1788-1795. https://doi.org/10.1111/1556-4029.14096

Ammerman, A. J., & Cavalli-Sforza, L. L. (1971). Measuring the Rate of Spread of Early Farming in Europe. *Man. Royal Anthropological Institute of Great Britain and Ireland*, *6*(4), 674-688. https://www.jstor.org/stable/2799190

Ammerman, A. J., & Cavalli-Sforza, L. L. (1984). *The Neolithic Transition and the Genetics of Populations in Europe* (1 ed.). Princeton University Press. https://doi.org/10.1515/9781400853113

Amores-Ampuero, A., & Viciano, J. (2020). Sexual Dimorphism from Vertebrae: Its Potential Use for Sex Estimation in an Identified Osteological Sample. *Australian Journal of Forensic Sciences*, 1-13. https://doi.org/10.1080/00450618.2020.1840629

Arjmandi, M., Kelly, P., & Thambyah, A. (2021). The mechanical influence of bone spicules in the osteochondral junction: A finite element modelling study. *Biomechanics and Modeling in Mechanobiology*, *20*(6), 2335-2351. https://doi.org/10.1007/s10237-021-01510-z

Berruti, G. L. F., & Daffara, S. (2014). Theory and methods of the use wear analysis of lithic tools and the example of the arrowheads from the Morgado Superior cave (Tomar, PT). *Antrope. Metodologias de Trabalho Arqueológico, Campo, Laboratório, Divulgação.*, *220*(1), 220-242.

Blasco, R., Arilla, M., Domínguez-Rodrigo, M., Andrés, M., Ramírez-Pedraza, I., Rufa, A., Rivals, F., & Rosell, J. (2020). Who peeled the bones? An actualistic and taphonomic study of axial elements from the Toll Cave Level 4, Barcelona, Spain. *Quaternary Science Reviews*, *250*, 106661(106661-106621). https://doi.org/10.1016/j.quascirev.2020.106661

Bocquet-Appel, J.-P., & Masset, C. (1982). Farewell to paleodemography. *Journal of Human Evolution*, *11*(4), 321-333.
Buikstra, J. E., & Ubelaker, D. H. (1994). *Standards for Data Collection from Human Skeletal Remains* (Vol. 44). Arkansas Archaeological Survey. https://doi.org/10.1002/ajhb.1310070519
Carbon, M., Hallin, M., & Tat Tran, L. (1996). Kernel density estimation for random fields: the L 1 theory. *Journal of nonparametric Statistics*, *6*(2-3), 157-170. https://doi.org/10.1080/10485259608832669
Carvalho, A. F., Alves-Cardoso, F., Gonçalves, D., Granja, R., Cardoso, J. L., Dean, R. M., Gibaja, J. F., Masucci, M. A., Arroyo-Pardo, E., & Fernández-Domínguez, E. (2016). The Bom Santo Cave (Lisbon, Portugal): catchment, diet, and patterns of mobility of a Middle Neolithic population. *European Journal of Archaeology*, *19*(2), 187-214. https://doi.org/10.1179/1461957115Y.0000000014
Cashmore, L. A., & Zakrzewski, S. R. (2013). Assessment of musculoskeletal stress marker development in the hand. *International Journal of Osteoarchaeology*, *23*(3), 334-347. https://doi.org/10.1002/oa.1254
Casteel, R. W. (1977). Characterization of faunal assemblages and the minimum number of individuals determined from paired elements: Continuing problem in archaeology. *Journal of Archaeological Science*, *4*(2), 125-134. https://doi.org/https://doi.org/10.1016/0305-4403(77)90059-0
Christensen, A. M. (2009). Techniques for siding manual phalanges. *Forensic science international*, *193*(1-3), 84-87. https://doi.org/10.1016/j.forsciint.2009.09.012
Cordeiro, C., Munoz-Barus, J. I., Wasterlain, S., Cunha, E., & Vieira, D. N. (2009). Predicting Adult Stature from Metatarsal Length in a Portuguese Population. *Forensic science international*, *193*(1-3), 131. e131-131. e134. https://doi.org/10.1016/j.forsciint.2009.09.017
Cruz, A. (2015). *Relatório Técnico da Campanha de Trabalhos Arqueológicos da Gruta do Morgado Superior*
Cruz, A. (2017). *Relatório Técnico da Campanha de Trabalhos Arqueológicos da Gruta do Morgado Superior (2016)*.
Cruz, A. (2020). *Balanço do PIPA “Meandro_CVR”: O PACTO ESTABELECIDO ENTRE AS PRÁTICAS FUNERÁRIAS E A PAISAGEM: O EXEMPLO DO MEANDRO ALTO DA CORVINA - MOINHO VELHO - FONTE DA ROMÃ NA PRÉ-HISTÓRIA RECENTE (TOMAR, PORTUGAL) – 2016 – 2019*.
Cruz, A., de Senna-Martinez, J. C., Santos, L., Relvado, C., Ribeiro, C., Fernandes, T., & Curto, A. (2018). Upper Morgado Shelter, still a peripheral funeral context, or perhaps not?(Tomar, Central Portugal). In A. Cruz & J. F. Gibaja (Eds.), *Interchange in Pre-and Protohistory: Case Studies in Iberia, Romania, Turkey and Israel* (Vol. 2891, pp. 91-105). British Archaeological Reports Oxford Ltd.
Cruz, A., Graça, A., Oosterbeek, L., Almeida, F., & Delfino, D. (2013). Gruta do Morgado Superior. Um Estudo de Caso Funerário no Alto Ribatejo (Tomar, Portugal). *Vínculos de Historia*(2), 143-168. http://hdl.handle.net/10578/3127
Cruz, A., & Oosterbeek, L. (2012). *Relatório da Campanha de Trabalhos Arqueológicos em 2012*.
Cruz, A., & Oosterbeek, L. (2013). *Relatório da Campanha de Trabalhos Arqueológicos da Gruta do Morgado Superior em 2013*.

Cruz, A. R. (1997). *Vale do Nabão: do Neolítico à Idade do Bronze*. Arkeos.

Cruz, A. R., Grimaldi, S., Oosterbeek, L., & Rosina, P. (2000). Indústrias Macrolíticas do Pós-Glaciar no Alto Ribatejo. *ARKEOS*, *9*, 9-21.

Curate, F. (2022). The Estimation of Sex of Human Skeletal Remains in the Portuguese Identified Collections: History and Prospects. *Forensic Sciences*, *2*(1), 272-286. https://doi.org/10.3390/forensicsci2010021

Curate, F., Albuquerque, A., Ferreira, I., & Cunha, E. (2017). Sex estimation with the Total Area of the Proximal Femur: A Densitometric Approach. *Forensic science international*, *275*, 110-116. https://doi.org/10.1016/j.forsciint.2017.02.035

Curate, F., d'Oliveira Coelho, J., & Silva, A. M. (2021a). CalcTalus: An online decision support system for the estimation of sex with the calcaneus and talus. *Archaeological and Anthropological Sciences*, *13*(5), 74 (71-10). https://doi.org/10.1007/s12520-021-01327-y

Curate, F., Mestre, F., & Garcia, S. J. (2021b). Sex assessment with the radius in Portuguese skeletal populations (late 19th–early to mid 20th centuries). *Legal Medicine*, *48*, 101790. https://doi.org/10.1016/j.legalmed.2020.101790

Curto, A. (2015). *Gruta do Morgado Superior: Relatório Antropológico da campanha de escavação de 2015*.

Curto, A., & Ribeiro, C. (2019). *Abrigo do Morgado Superior: Relatório Antropológico da Campanha de Escavação de 2018*.

Domínguez-Rodrigo, M. (2012). Critical review of the MNI (minimum number of individuals) as a zooarchaeological unit of quantification. *Archaeological and Anthropological Sciences*, *4*, 47-59. https://doi.org/10.1007/s12520-011-0082-z

Drennan, R. D. (2010). *Statistics for Archaeologists: A Common Sense Approach* (Second ed.). Springer. https://doi.org/https://doi.org/10.1007/978-1-4419-0413-3

Duong, T. (2007). ks: Kernel density estimation and kernel discriminant analysis for multivariate data in R. *Journal of statistical software*, *21*, 1-16.

Fernández-Jalvo, Y., & Andrews, P. (2016). *Atlas of Taphonomic Identifications: 1001+ Images of Fossil and Recent Mammal Bone Modification*. Springer. https://doi.org/10.1007/978-94-017-7432-1

Ferreira, C., Allué, E., Burjachs, F., Rosina, P., & Oosterbeek, L. (2013). Dados Arqueobotânicos do Alto Ribatejo - Perspectivas Futuras. *ARKEOS*, *34*(1° Congresso de Arqueologia do Alto Ribatejo), 153-159.

Fischer, E. (1906). Die Variationen an Radius und Ulna des Menschen. Eine anthropologische Studie. *Zeitschrift für Morphologie und Anthropologie*(H. 2), 147-247. http://www.jstor.org/stable/25747245

Frye, C., Sayre, R., Murphy, A. B., Karagülle, D., Pippi, M., Gilbert, M., & Richards, J. W. (2023). Named Landforms of the World: A Geomorphological and Physiographic Compilation. *Annals of the American Association of Geographers*, 1-19. https://doi.org/10.1080/24694452.2023.2200548

Guiry, E. J., Hillier, M., Boaventura, R., Silva, A. M., Oosterbeek, L., Tomé, T., Valera, A., Cardoso, J. L., Hepburn, J. C., & Richards, M. P. (2016). The transition to agriculture in south-western Europe: new isotopic insights from Portugal's Atlantic coast. *Antiquity*, *90*(351), 604-616. https://doi.org/10.15184/aqy.2016.34

Hallin, M., Lu, Z., & Tran, L. T. (2004). Kernel density estimation for spatial processes: the L1 theory. *Journal of Multivariate Analysis*, *88*(1), 61-75. https://doi.org/10.1016/S0047-259X(03)00060-5
Harris, S. M., & Case, D. T. (2012). Sexual Dimorphism in the Tarsal Bones: Implications for Sex Determination. *Journal of Forensic Sciences*, *57*(2), 295-305. https://doi.org/10.1111/j.1556-4029.2011.02004.x
Herrmann, B., Grupe, G., Hummel, S., Piepenbrink, H., & Schutkowski, H. (1990). *Prähistorische Anthropologie: Leitfaden der Feld-und Labormethoden*. Springer-Verlag.
Hilal, G., Martel-Pelletier, J., Pelletier, J. P., Ranger, P., & Lajeunesse, D. (1998). Osteoblast-like cells from human subchondral osteoarthritic bone demonstrate an altered phenotype in vitro: possible role in subchondral bone sclerosis. *Arthritis & Rheumatism: Official Journal of the American College of Rheumatology*, *41*(5), 891-899.
Hillson, S. (2005). *Teeth* (2nd ed.). Cambridge university press.
Hillson, S. (2014). *Tooth development in human evolution and bioarchaeology*. Cambridge University Press. https://doi.org/https://doi.org/10.1017/CBO9780511894916
Holland, T. D. (1995). Estimation of Adult Stature From the Calcaneus and Talus. *American Journal of Physical Anthropology*, *96*(3), 315-320.
Kemkes-Grottenthaler, A. (2002). Aging through the ages: historical perspectives on age indicator methods. In R. D. Hoppa & J. W. Vaupel (Eds.), *Paleodemography, Age Distribution from Skeletal Samples* (pp. 48-72). Cambridge.
Kieser, J. A., Moggi-Cecchi, J., & Groeneveld, H. T. (1992). Sex allocation of Skeletal Material by Analysis of the Proximal Tibia. *Forensic science international*, *56*(1), 29-36. https://doi.org/10.1016/0379-0738(92)90143-K
Lagan, E. M., & Ehrlich, D. E. (2021). An improved method for measuring molar wear. *American Journal of Physical Anthropology*, *174*(4), 832-838. https://doi.org/10.1002/ajpa.24238
Lamer, M., Spake, L., & Cardoso, H. F. (2021). Testing the cross-applicability of juvenile sex estimation from diaphyseal dimensions. *Forensic science international*, *321*, 110739.
Lanfranco, L. P., & Eggers, S. (2010). The Usefulness of Caries Frequency, Depth, and Location in Determining Cariogenicity and Past Subsistence: A Test on Early and Later Agriculturalists From the Peruvian Coast. *American Journal of Physical Anthropology*, *143*(1), 75-91. https://doi.org/10.1002/ajpa.21296
Larsen, C. S. (2004). *Bioarchaeology: Interpreting behavior from the human skeleton*. Cambridge University Press. (1997)
Larsen, C. S. (2010). *A Companion to Biological Anthropology* (C. S. Larsen, Ed.).
Macaluso Jr., P. J., & Lucena, J. (2014). Estimation of sex from sternal dimensions derived from chest plate radiographs in contemporary Spaniards. *International Journal of Legal Medicine*, *128*(2), 389-395. https://doi.org/10.1007/s00414-013-0910-z
Macaluso Jr., P. J., Rico, A., Santos, M., & Lucena, J. (2012). Osteometric sex discrimination from the sternal extremity of the fourth rib in a recent forensic

sample from Southwestern Spain. *Forensic science international*, *223*(1-3), 375. e371-375. e375. https://doi.org/10.1016/j.forsciint.2012.09.007
Mann, R. W. (2017). *The Bone Book: A Photographic Lab Manual for Identifying and Siding Human Bones*. Charles C. Thomas.
Mann, R. W., & Hunt, D. R. (2019). Non-metric traits and anatomical variants that can mimic trauma in the human skeleton. *Forensic science international*, *301*, 202-224. https://doi.org/10.1016/j.forsciint.2019.05.039
Martin, R. (1928). *Lehrbuch der Anthropologie: In Systematischer Darstellung. Mit Besonderer Berücksichtigung der Anthropologischen Methoden. Für Studierende Ärzte und Forschungsreisende.* (Vol. 2nd). Jena, Gustav Fischer.
Martin, R., & Saller, K. (1957). *Lehrbuch der Anthropologie. In Systematischer Darstellung mit Besonderer Berücksichtigung der Anthropologischen Methoden* (Vol. 4th). Gustav Fischer Verlag.
Mastrangelo, P., De Luca, S., Alemán, I., & Botella, M. C. (2011). Sex assessment from carpals bones: Discriminant function analysis in a 20th Century Spanish Sample. *Forensic science international*, *206*(1-3), 216.e211-216.e210. https://doi.org/10.1016/j.forsciint.2011.01.007
Matshes, E., Burbridge, B., Sher, B., Mohamed, A., & Juurlink, B. (2005). *Human Osteology & Skeletal Radiology: An Atlas and Guide*. CRC Press.
Miles, A. E. W. (2001). The Miles method of assessing age from tooth wear revisited. *Journal of Archaeological Science*, *28*(9), 973-982. https://doi.org/0.1006/jasc.2000.0652
Monge Calleja, Á. M., Aranda, C. M., Santos, A. L., & Luna, L. H. (2020). Evaluation of the auricular surface method for non-adult sex estimation on the Lisbon documented collection. *American Journal of Physical Anthropology*, *172*(3), 500-510. https://doi.org/10.1002/ajpa.24012
Navega, D., Vicente, R., Vieira, D. N., Ross, A. H., & Cunha, E. (2015). Sex estimation from the tarsal bones in a Portuguese sample: a machine learning approach. *International Journal of Legal Medicine*, *129*(3), 651-659. https://doi.org/10.1007/s00414-014-1070-5
Nikita, E. (2014). Age-associated Variation and Sexual Dimorphism in Adult Cranial Morphology: Implications in Anthropological studies. *International Journal of Osteoarchaeology*, *24*(5), 557-569. https://doi.org/10.1002/oa.2241
Nikita, E. (2017). *Osteoarchaeology: A Guide to the Macroscopic Study of Human Skeletal Remains*. Academic Press.
Oosterbeek, L. (1987). Gruta dos Ossos. *Informcão Arqueológica*, *8*, 80-81.
Oosterbeek, L. (1993a). Gruta dos Ossos (Tomar) Um ossuário do Neolítico final. *Boletim Cultural de Tomar*, *18*, 11-28.
Oosterbeek, L. (1993b). Nossa Senhora das Lapas: Excavation of prehistoric cave burials in central Portugal. *Papers from the Institute of Archaeology*, *4*, 49-62.
Oosterbeek, L. (1994a). *Echoes from the East: The western network. An insight to unequal and combined development, 7000-2000 B.C. PhD Dissertation*. University College.
Oosterbeek, L. (1994b). *Echoes from the East: the Western Network. North Ribatejo (Portugal): an insight to unequal and combined development, 7000-2000 BC* University of London, University College London (United Kingdom)].

Oosterbeek, L. (2003). Megaliths in Portugal: the western network revisited. In G. Burenhult (Ed.), *Stones and bones. Formal disposal of the dead in Atlantic Europe during the Mesolithic-Neolithic interface 6000-3000 b.C.* (pp. 27-37). British Archaeological Reports - International Series.

Oosterbeek, L., Cruz, A. R., Pena dos Reis, R., Botón García, F., Allué Martí, E., Migliavacca, M., & Mozzi , P. (2000). Novos Dados Crono-Estratigráficos e Paleo-Ambientais do Pleistoceno e do Holoceno no Alto Ribatejo. *ARKEOS*, *9*, 23-36.

Oosterbeek, L., Garcês, S., & Almeida, N. J. (2018). A l'aube de la mondialisation : Paysages rupestres. In M. O. M. Hertrampf & B. Nickel (Eds.), *Kultur - Lanclschaft - Raum: Dynamiken literarischer Inszenierungen von Kulturlandschaften* (pp. 19-37). Stauffenburg Verlag.

Oosterbeek, L., Pereira, T., & Almeida, N. J. (2020). Moving Tasks Across Shapes: Reassessing the Mechanisms of the Agropastoralist Spread in Central Portugal. *ARKEOS*, *50*, 1-513.

Oosterbeek, L., & Tomé, T. (2012). Evidence of traumatic skeletal injuries in the collective burial caves of the Nabão Valley, central Portugal. In R. Schulting & L. Fibiger (Eds.), *Sticks, Stones, and Broken Bones: Neolithic Violence in a European Perspective* (pp. 303-316). Oxford University Press. https://doi.org/10.1093/acprof:osobl/9780199573066.003.0016

Oosterbeek, L. M. (1997). *Echoes from the East : Late Prehistory of the North Ribatejo*. CEIPHAR - Centro Europeu de Investigação da Pré-História do Alto Ribatejo.

Ortner, D. J. (2003). *Identification of Pathological Conditions in Human Skeletal Remains* (2nd ed.). Academic Press.

Peckmann, T. R., Meek, S., Dilkie, N., & Rozendaal, A. (2016). Determination of sex from the patella in a contemporary Spanish population. *Journal of forensic and legal medicine*, *44*, 84-91. https://doi.org/10.1016/j.jflm.2016.09.007

Price, T. D., & Burton, J. H. (2011). *An Introduction to Archaeological Chemistry* (1 ed.). Springer. https://doi.org/10.1007/978-1-4419-6376-5

Relvado, C., & Anselmo, D. P. (2016). *Relatório Antropológico da Campanha de Escavação 2016*.

Ribeiro, C. (2018). *Abrigo do Morgado Superior: Relatório Antropológico da Campanha de Escavação de 2017*.

Sacragi, A., & Ikeda, T. (1995). Sex Identification from the Distal Fibula. *International Journal of Osteoarchaeology*, *5*, 139-143.

Sampietro, M. L., Lao, O., Caramelli, D., Lari, M., Pou, R., Martí, M., Bertranpetit, J., & Lalueza-Fox, C. (2007). Palaeogenetic evidence supports a dual model of Neolithic spreading into Europe. *Proceedings of the Royal Society B: Biological Sciences*, *274*(1622), 2161-2167. https://doi.org/10.1098/rspb.2007.0465

Saunders, S. R., & Hoppa, R. D. (1997). Sex allocation from long bone measurements using logistic regression. *Canadian Society of Forensic Science Journal*, *30*(2), 49-60. https://doi.org/10.1080/00085030.1997.10757086

Schaefer, M., Black, S. M., & Scheuer, L. (2009). *Juvenile Osteology: A Laboratory and Field Manual*. Academic Press.

Scheuer, L., & Black, S. (2004). *The Juvenile Skeleton*. Academic Press.

Schoeneberger, P. J., Wysocki, D. A., & Benham, E. C. (2012). *Field book for describing and sampling soils, Version 3.0*. Government Printing Office. Natural Resources Conservation Service, National Soil Survey Centre.

Scott, E. C. (1979). Dental Wear Scoring Technique. *American Journal of Physical Anthropology*, *51*(2), 213-217. https://doi.org/10.1002/ajpa.1330510208

Silva, A. M. (1995). Sex assessment using the calcaneus and talus. *Antropologia portuguesa*, *13*, 107-119.

Silva, A. M. (1996). *O hipogeu de Monte Canelas I (IV-III milénios AC): estudo paleobiológico da população humana exumada* University of Coimbra]. Coimbra.

Silva, A. M. (2007). Late Neolithic/Chalcolithic Portuguese populations: example of the contribution of anthropological and molecular data to the knowledge of prehistoric populations. *Advances in molecular biology and evolution and it applications to biological anthropology*, 289-301.

Simonoff, J. S. (1996). *Smoothing Methods in Statistics*. Springer-Verlag. https://doi.org/10.1007/978-1-4612-4026-6

Smith, B. H. (1991). Standards of Human Tooth Formation and Dental Age Assessment. *Advances In Dental Anthropology*, 143-168.

Spencer-Wood, S. M., & Camp, S. L. (2013). Introduction to Historical and Archaeological Perspectives on Gender Transformations: From Private to Public. In S. M. Spencer-Wood (Ed.), *Historical and Archaeological Perspectives on Gender Transformations: From Private to Public* (pp. 1-22). Springer. https://doi.org/10.1007/978-1-4614-4863-1_1

Steele, D. G. (1976). The Estimation of Sex on the Basis of the Talus and Calcaneus. *American Journal of Physical Anthropology*, *45*(3), 581-588. https://doi.org/10.1002/ajpa.1330450323

Stojanovski, D., Roffet-Salque, M., Casanova, E., Knowles, T., Oosterbeek, L., Evershed, R. P., Cruz, A., Thissen, L., & Arzarello, M. (2020). Anta 1 de Val da Laje–the first direct view of diet, dairying practice and socio-economic aspects of pottery use in the final Neolithic of central Portugal. *Quaternary International*, *542*, 1-8. https://doi.org/10.1016/j.quaint.2020.02.016

Sulzmann, C. E., Buckberry, J. L., & Pastor, R. F. (2008). The Utility of Carpals for Sex Assessment: A Preliminary Study. *American Journal of Physical Anthropology: The Official Publication of the American Association of Physical Anthropologists*, *135*(3), 252-262. https://doi.org/https://doi.org/10.1002/ajpa.20738

Szécsényi-Nagy, A., Roth, C., Brandt, G., Rihuete-Herrada, C., Tejedor-Rodríguez, C., Held, P., García-Martínez-de-Lagrán, Í., Arcusa Magallón, H., Zesch, S., & Knipper, C. (2017). The maternal genetic make-up of the Iberian Peninsula between the Neolithic and the Early Bronze Age. *Scientific Reports*, *7*(1), 15644.

Tomé, T. (2006). *Reflexos da Vida na Morte: Paleobiologia das populações do Neolítico Final/Calcolítico do Vale do Nabão – Gruta dos Ossos*. Mater Dissertation. Universidade de Trás-os-Montes e Alto Douro

Tomé, T. (2010). *Até que a Morte nos Reúna: Paleobiologia e Antropologia Funerária da Transição para Agro-Pastoralismo na Bacia do Tejo e Sudoeste Peninsular* Universidade de Trás-os-Montes e Alto Douro.]. Vila Real.

Tomé, T. (2012). *Gruta do Morgado Superior: Relatório Antropológico da Campanha de Escavação de 2012*. G. Q. e. P.-H. d. C. d. Geociências.

Tomé, T., Almeida, N. J., Silva, A. M., Saladié, P., & Oosterbeek, L. (2013). Uma perspectiva osteoarqueológica sobre duas grutas neolíticas do vale do Nabão (Alto Ribatejo, Portugal central). *ARKEOS*, *34*, 131.

Tomé, T., & Cunha, C. (2013). *Gruta do Morgado Superior: Relatório da Campanha de Escavação de 2013*

Tomé, T., & Oosterbeek, L. (2011). One region, two systems? A paleobiological reading of cultural continuity over the agro-pastoralist transition in the North Ribatejo. In P. Bueno, E. Cerrillo-Cuenca, & A. Gonzalez (Eds.), *From the origins: the prehistory of the Inner Tagus Region* (pp. 43-54). Archaeopress. https://doi.org/https://doi.org/10.30861/9781407307770

Tomé, T., & Silva, A. M. (2013). Prácticas Funerárias na Pré-História Recente do Alto Ribatejo: Ponto da situação. *ARKEOS*, *34*, 95-107.

Wapler, U., Crubézy, E., & Schultz, M. (2004). Is cribra orbitalia synonymous with anemia? Analysis and interpretation of cranial pathology in Sudan. *American Journal of Physical Anthropology: The Official Publication of the American Association of Physical Anthropologists*, *123*(4), 333-339. https://doi.org/10.1002/ajpa.10321

Waterman, A. J., Tykot, R. H., & Silva, A. M. (2016). Stable isotope analysis of diet-based social differentiation at late prehistoric collective burials in South-Western Portugal. *Archaeometry*, *58*(1), 131-151. https://doi.org/10.1111/arcm.12159

White, T. D., Black, M. T., & Folkens, P. A. (2012). *Human Osteology* (3rd ed.). Elsavier Academic Press. https://doi.org/10.1016/b978-0-12-374134-9.50001-5

White, T. D., & Folkens, P. A. (2005). *The Human Bone Manual*. Elsevier Academic Press.

Žalaitė, I., Maurer, A.-F., Grimes, V., Silva, A. M., Ribeiro, S., Santos, J. F., Dias, C. B., & Valera, A. C. (2018). Diet and mobility of fauna from Late Neolithic–Chalcolithic site of Perdigões, Portugal. *Journal of Archaeological Science: Reports*, *19*, 674-685. https://doi.org/10.1016/j.jasrep.2018.03.033

8. Annexes

Annex 1. Distribution of GMS material (all categories) among all the excavated squares. Note that those with a W at the end are non-coordinated material from sieves.

Row Labels	No. of Entries	Percentage
E53	12	0.06%
E54	1	0.01%
F52	17	0.09%
F53	23	0.12%
F53W	173	0.93%
F54	39	0.21%
G52	15	0.08%
G53	25	0.13%
G53W	98	0.53%
G54	36	0.19%
GMI-SUP	1	0.01%
H52	59	0.32%
H53	60	0.32%
H53W	104	0.56%
H54	19	0.10%
H54AM	1	0.01%
H54W	30	0.16%
H55	1	0.01%
I50	16	0.09%
I51	1407	7.55%
I52	1113	5.97%
I53	42	0.23%
I53W	73	0.39%
I54W	21	0.11%
J50	2059	11.05%
J51	3498	18.77%
J52	1157	6.21%
J53	306	1.64%
J54	25	0.13%
J55	10	0.05%
J56	2	0.01%
K50	478	2.57%
K51	5263	28.24%
K51W	8	0.04%
K52	841	4.51%
K53	176	0.94%
K54	19	0.10%

Row Labels	No. of Entries	Percentage
K55	5	0.03%
K57	2	0.01%
L50	36	0.19%
L51	755	4.05%
L52	321	1.72%
L53	217	1.16%
L57	4	0.02%
L58	1	0.01%
NN	8	0.04%
SUPW	58	0.31%
Grand Total	**18635**	**100.00%**

Annex 2. Guidelines for phalanx identification summarizing Case and Heilman, and Ricklan's guidelines (Christensen, 2009, P. 86)

Bone	View	Description
PP1	Palmar	The lateral edge of the proximal facet faces toward the opposite side the bone is from (Case and Heilman [1])
		The most proximal point is on the side the bone is from (Case and Heilman [1])
	Distal	dorsal up: Place the bone on a flat surface, holding the proximal end down firmly. The distal end does not contact the flat surface opposite the side the bone is from (Case and Heilman [1])
		dorsal up: The largest part of the distal articular surface is on the side the bone is from (Ricklan [3])
	Proximal	dorsal up: The side with the least amount of articular surface is the side the bone is from (present study)
PP2	Palmar	The mass of the proximal end is greater on the side the bone is from (Case and Heilman [1])
		The most distal point on the bone is opposite the side the bone is from (Case and Heilman [1])
	Distal	dorsal up: Place the bone on a flat surface, holding the proximal end down firmly. The distal end does not contact the flat surface on the side the bone is from (Case and Heilman [1])
		dorsal up: The largest part of the distal articular surface is opposite the side the bone is from (Ricklan [3])
PP3	Palmar	The mass of the proximal end is greater on the side the bone is from (Case and Heilman [1])
		The most distal point on the bone is opposite the side the bone is from (Case and Heilman [1])
	Distal	With the palmar aspect down, the largest part of the distal articular surface is opposite the side the bone is from (Ricklan [3])
PP4	Proximal	palmar up: The greatest vertical height on the proximal end is found on the side the bone is from. Use finger pressure on the shaft to keep the bone from rolling. The bone also tends to roll toward the side the bone is from (Case and Heilman [1])
		palmar up: The more angular of the two tubercles is on the side the bone is from (present study)
PP5	Dorsal	The margin of the superodistal facet extends more proximally on the side the bone is from (Case and Heilman [1])
		The most distal point on the bone is opposite the side the bone is from (Case and Heilman [1])
		The mass of the proximal base is greater on the side the bone is from (Case and Heilman [1])
	Palmar	The most distal point on the bone is on the side the bone is from (Ricklan [3])
IP2	Dorsal	The projection of the superior margin of the proximal facet is off-center opposite the side the bone is from (Case and Heilman [1])
	Proximal	palmar up: Lay the bone on a flat surface. The side of the proximal base highest above the flat surface is on the side the bone is from (Case and Heilman [1])
		dorsal up: The larger of the two facet areas is on the side the bone is from (Ricklan [3])
IP3	Dorsal	The projection of the superior margin of the proximal facet is off-center opposite the side the bone is from (Case and Heilman [1])
	Proximal	palmar up: Lay the bone on a flat surface. The side of the proximal base highest above the flat surface is on the side the bone is from (Case and Heilman [1])
		distal up: The larger of the two facet areas is on the side the bone is from (Ricklan [3])
IP4	Dorsal	The most distal point on the bone is on the side the bone is from (Case and Heilman [1])

Bone	View	Description
		The shaft of the bone exhibits deeper curvature opposite the side the bone is from (Case and Heilman [1]) Occasionally, the projection of the superior margin of the proximal facet is off-centre opposite the side the bone is from (present study)
IP5	Dorsal	The most distal point on the bone is on the side the bone is from (Case and Heilman [1])
		The shaft of the bone exhibits deeper curvature opposite the side the bone is from (Case and Heilman [1])
DP1	Dorsal	One-half of the proximal facet partially faces toward the side the bone is from (Case and Heilman [1])
		The most proximal point on the bone is opposite the side the bone is from (Case and Heilman [1])
DP2	Proximal	dorsal up: The smaller of the two facets is on the side the bone is from (Case and Heilman [1])
		dorsal up: The facet height narrows more on the side the bone is from (Case and Heilman [1])
	Palmar	A line tangent to the medial- and lateral-most edges of the proximal articular surface trends distally opposite the side the bone is from (Ricklan [3])
DP3	Proximal	dorsal up: The smaller of the two facets is on the side the bone is from (Case and Heilman [1])
		dorsal up: The facet height narrows more on the side the bone is from (Case and Heilman [1])
	Palmar	A line tangent to the medial- and lateral-most edges of the proximal articular surface trends distally opposite the side the bone is from (Ricklan [3])
DP4	Proximal	dorsal up: The smaller of the two facets is on the side the bone is from (Case and Heilman [1])
		dorsal up: The facet height narrows more on the side the bone is from (Case and Heilman [1])
	Palmar	A line tangent to the medial- and lateral-most edges of the proximal articular surface trends distally on the side the bone is from (Ricklan [3])
DP5	Dorsal	The shaft of the bone exhibits deeper curvature opposite the side the bone is from (Case and Heilman [1])
	Palmar	Palmar: A line tangent to the medial- and lateral-most edges of the proximal articular surface trends distally on the side the bone is from (Ricklan [3])

Annex 3. Equations for sex allocation with Upper limbs (Albanese, 2013, P. 1415)

N	Clavicle		Humerus		Ulna		Radius			Constant
	Max Length	Cranial-Caudal Diameter	Vertical Head Diameter	Epicondylar Breadth	Anterior-Posterior Diameter	Diameter at Max Crest	Max Length	Sagittal Diameter	Max Head Diam.	
1	0.042	0.595	0.346	0.193	0.825					-48.806
2	0.051	0.684	0.315	0.282					0.363	-52.753
3	0.066	0.689	0.414	0.262						-49.855
4			0.294	0.273	1.162				0.3	-50.367
5		0.551	0.267	0.262	1.153				0.294	-53.83
6	0.109	0.613			1.04	0.524	-0.062		0.863	-48.207
7					1.18	0.487			0.83	-41.309
8	0.126	0.637					-0.059	1.083	0.958	-44.338
9	0.098	0.618			0.889	0.468				-39.164
10			0.409	0.29				0.802		-43.852
11			0.363	0.272	0.943					-43.508
12		0.582	0.361	0.23	0.911					-46.413
13		0.676	0.459	0.328						-45.865
14			0.363	0.272	0.943					-43.508
15		0.565	0.396	0.267				0.655		-45.936
16	0.055	0.585	0.37	0.22				0.579		-49.399

Annex 4. Inventory of identified material by chrono-cultural period.

Skeletal Element	Neolithic	Neo. / Chalc.	Chalcolithic	Chalc./ Early Bronze Age	Early Bronze Age	Und.	Total
I (Incisor)	8	25	162	15	1	3	214
di (Dec. Incisor)		3	14	1			18
C (Canine)	2	8	39	4			53
dc (Dec. Canine)		3	2	1			6
P (Premolar)	9	23	113	11	1	1	158
M (Molar)	3	34	168	11	1		217
dm (Dec. Molar)		1	5				6
Frontal			4				4
Parietal	1		3			1	5
Temporal		5	6				11
Occipital	1		4				5
Maxilla			9				9
Zygomatic	2		1				3
Sphenoid			1			1	2
Mandible		1	18				19
Vertebra	13	74	158	13			258
Cervical	3	5	26	1			35
Thoracic	4	2	16				22
Lumbar			11				11
Sternum		1	4				5
Rib	15	47	186	9	1		258
Clavicle	1	7	26	2			36
Scapula	2		9				11
Humerus	1	6	16	1			24
Radius	2	4	26				32
Ulna	2	4	21	1			28
Carpal		2	20				22
Lunate	2	9	16	2			29
Capitate	1	8	29	1			39
Pisiform		10	7				17
Scaphoid		10	30	2			42
Trapezoid	3	6	10	2			21
Triquetral	2	3	11	2			18
Trapezium	1	6	13				20
Hamate	2	6	18	4			30
Metacarpal	8	28	120	8	2		166
Hand Phalanx	1	19	71	5			96

Skeletal Element	Neolithic	Neo. / Chalc.	Chalcolithic	Chalc./ Early Bronze Age	Early Bronze Age	Und.	Total
Proximal Hand Phalanx	10	19	110	8	2	1	150
Intermediate Hand Phalanx	9	28	80	8		2	127
Distal Hand Phalanx	7	27	72	10	1	2	119
Sacrum		2	6	1			9
Os Coxae	2	5	13	2			22
Iliac Body		2	6				8
Pubic Body	1		1		1		3
Ischial Body			3				3
Femur	1		27	1			29
Patella	5	13	29	8			55
Tibia	2	2	20	2			26
Fibula	3	6	22				31
Talus	5	10	25				40
Calcaneus	3	6	22			1	32
Cuboid	1	4	25	3			33
Navicular	7	4	36	3			50
Medial (First) Cuneiform	2	4	16	3			25
Intermediate (Second) Cuneiform		8	14		2	1	25
Lateral (Third) Cuneiform	2	3	15	1			21
Metatarsal	21	32	171	14	2		240
Foot Phalanx		1	3				4
Proximal Foot Phalanx	10	23	144	13		5	195
Intermediate Foot Phalanx	3	11	33	3		1	51
Distal Foot Phalanx	1	14	56	2	1		74
Splinter (bone)	11	156	333	12		1	513
Splinter (Long bone)	19	128	281	14	1		443
U	1	17	47	7	1		73
Total	215	885	3003	211	17	20	4351

Annex 5. Minimal number of individuals (mature).

Element	Left	Right	Unpaired
I1	**41**	31	
I2	42	**45**	
P3	16	**24**	
P4	6	**15**	
M1	14	**17**	
M2	8	**13**	

Element	Left	Right	Unpaired
M3	1	**2**	
Maxilla	**1**	1	
Temporal	**4**	2	
Frontal			3
Occipital			4
Mandible			6
Sphenoid			1
C1			6
C2			**8**
C7			1
Zygomatic		1	
1st Rib	**4**	3	
Clavicle	**11**	8	
Scapula	**1**	1	
Humerus	2	**6**	
Radius	5	**7**	
Ulna	3	**8**	
Lunate	10	**16**	
Hamate	**13**	11	
Pisiform	4	8	
Capitate	17	**19**	
Scaphoid	**28**	12	
Sternum			0
Triquetral	**11**	6	
Trapezoid	**10**	9	
Trapezium	**10**	8	
MC1		**1**	
MC2	3	**4**	
MC3	**5**	4	
MC4	1	**3**	
MC5		**1**	
Os Coxae	**4**	2	
Femur	3	**6**	
Patella	22	**27**	
Tibia	1	**2**	
Fibula	**7**	3	
Talus	13	**16**	
Calcaneus	**11**	11	
Cuboid	12	**18**	
Navicular	**27**	17	
1st Cun.	**15**	10	
2nd Cun.	6	**13**	
3rd Cun.	5	**15**	
MT1	14	**11**	
MT2	**17**	15	
MT3	9	**12**	
MT4	16	**17**	
MT5	8	**13**	
MNI	41	**45**	8

Annex 6. Minimal number of individuals (juvenile).

Row Labels	Left	Right	Unpaired
I1	1	**2**	
I2	**1**	1	
di1	**2**	2	
di2	4	**6**	
C	**2**	1	
dc	**3**	2	
P3	**2**	2	
P4	1	**2**	
M1	7	**10**	
M2	8	**9**	
M3		**1**	
dm1		**2**	
Iliac Body		**1**	
Ischial Body	**2**		
Pubic Body	**2**		
Clavicle	**4**	2	
Humerus	**1**		
Radius	1	**2**	
Ulna	**2**		
Lunate	**1**		
Sternum			3
Trapezium		1	
MT2	**1**		
MT5	**2**		
Femur	**1**	2	
Tibia	**1**	4	
Fibula	**3**		
Talus	**2**		
2nd Cun.	**1**		
MT5	**1**		
Sacrum			2
MNI	8	**10**	3

Annex 7. Distribution of age range groups by chrono-cultural period.

Age Range	Neo.	L. Neo. / E. Chalc.	Neo. / Chalc.	Chalc.	Chalc./ E. Bronze A.	E. Bronze A.
0 to 04				1		
0 to 06				1		
<0.1				1		
0.2 to 14			1			
0.2 to 4			1			
0.5 to 6.5				1		
0.6 - 7			3	13	1	
01 to 06				1		
01 to 07			1	1		
01 to 08				1	1	
01 to 10				1		

Age Range	Neo.	L. Neo. / E. Chalc.	Neo. / Chalc.	Chalc.	Chalc./ E. Bronze A.	E. Bronze A.
01 to 16			3	4		
01.2 to 01.3				1		
<02			1			
02 to 03				1		
02 to 04				7		
02 to 05			1	1		
02 to 06			1			
02 to 08				1	1	
02 to 12				1		
02 to 15			1			
02 to 16	3		13	80	7	
02 to 18			2			
<03				3		
03 to 04			1	2		
03 to 05			1	1		
03 to 06				2		
03 to 08				2	1	
03 to 12			1			
03 to 15			1			
03 to 16				1		
03.1 to 0.32					1	
03.1 to 03.2				2		
<04			3	1		
04 to 04.1				3		
04 to 05			1	1		
04 to 08				1		
04 to 12				1		
04 to 16			1			
04 to0 4.1	1					
04.8 to 04.9				4		
05 to 05.2				1		
05 to 05.3				5		
05 to 16				1		
05.4 to 05.5			1	4		
05.4 to05.5				1		
05.7 to 16.6				2		
05.8 to 06.1				1		
<06	1			2		
06 to 07	1			1		
06 to 08				1		
06 to 14			1	1		
06 to 18				1		

Age Range	Neo.	L. Neo. / E. Chalc.	Neo. / Chalc.	Chalc.	Chalc./ E. Bronze A.	E. Bronze A.
06 to12			1	2		
06.1 to 06.4			1			
06.1 to0 6.4				1		
06.2 to 06.9				1		
06.6 to 06.8				1		
07 to 07.7				1		
07 to 14				1		
07.2 to 07.3			1	2		
07.3 to 07.6			1	1	1	
07.4 to 07.8				1		
07.7 to 08.8				1		
<08			4	2		1
08 to 10				1		
08 to 12				1		
08 to 14				1		
08 to 15				4		
08 to 16			2	13		
08 to 19				6		
08 to 20				2		
08.4 to 08.7				3	1	
08.7 to 09.3			1			
09 to 11			1			
09.5 to 09.8			3	3		
10 to 16				1		
10.3 to 10.6				2	1	
10.6 to 12.4				1		
11 to 11.4				1		
11 to 16				3		
12 to 16			2	6	2	
12 to 17				2		
12 to 18				1		
12 to 19				1		
12 to 20			1	1		
12 to 21				1		
<13			1	1		
13 to 15				1		
13 to 18			1			
<14			4	4		
14 to 14.1				1		
14 to 16			1	2		
14 to 18				1		
14 to 19				1		

Age Range	Neo.	L. Neo. / E. Chalc.	Neo. / Chalc.	Chalc.	Chalc./ E. Bronze A.	E. Bronze A.
14 to 20				4	2	
14 to 21			1	1		
<15			3	1		
<16	1		7	19		
16 to 21			1			
16.4 to 16.9				1		
<17				2		
18 to 20				1		
18 to 21				1		
3 to 12			3	2	1	
<20			1	2		
<25				1		
30 +	1					
35.2 to 38.2	1			1		
Total	**9**		**80**	**277**	**20**	**1**

Annex 8. Abnormal characteristics distribution by location and chrono-cultural period.

Row Labels	Neo.	Neo. / Chalc.	L. Neo. / E. Chalc.	Chalc.	Chalc./ E. Bronze A.
Abnormal shape resulting from biomechanical stress on poorly mineralized bone	**2**	**4**		**16**	**1**
Body				1	
Diaphysis	1	1		3	
Diaphysis (Lateral)				1	
Diaphysis (Medial)				1	
Distal Epiphysis		1			
Distal Joint Surface	1	2		6	
Non-Articular Surface				1	1
Periosteal				1	
Proximal Joint Surface				2	
Abnormal shape resulting from defects in growth and development		**3**		**6**	
Body		1		1	
Diaphysis				1	
Distal Epiphysis		1			
Distal Joint Surface				1	
Lateral Articular Facet		1			
Proximal Epiphysis				2	
Proximal Joint Surface				1	
Abnormal shape resulting from poor alignment following a fracture				**2**	
Body				1	
Distal Joint Surface				1	
Clear border with sclerosis				**1**	
Proximal Joint Surface				1	

General porous destruction			**2**	
Periosteal			1	
Proximal Epiphysis			1	
Lesions on spongy bone		**1**		
Non-Articular Surface		1		
No margin or clear border		**1**		
Proximal Joint Surface		1		
Plaque			**2**	
Diaphysis			1	
Periosteal			1	
Trauma (Fracture)	**1**	**4**	**4**	
Body			1	
Diaphysis		1		
Distal Apophyses			1	
Distal Epiphysis		3	1	
Proximal Epiphysis	1		1	
(blank)				
(blank)				
Grand Total	**3**	**13**	**33**	**1**

Annex 9. Abnormal lesions distribution by location and chrono-cultural period.

Row Labels	Neo.	Neo. / Chalc.	Chalc.	Chalc./ E. Bronze A.	E. Bronze A.
Eburnation_B				**1**	
Non-Articular Surface				1	
Enthesophyte		**2**	**4**		
Distal Joint Surface			1		
Lateral Articular Facet		1			
Palmar		1	1		
Periosteal			1		
Proximal Joint Surface			1		
Fusion of joint	**1**	**1**	**4**		
Distal Joint Surface	1	1	4		
Osteophyte	**6**	**9**	**39**	**1**	**1**
Body		1			
Cortical		2	1		
Diaphysis				1	
Diaphysis (Lateral and Medial)	4	5	25		
Diaphysis (Lateral)			1		
Diaphysis (Medial)	1				
Distal Epiphysis			6		
Distal Joint Surface			1		
Medial Articular Facet		1			
Palmar	1				

Periosteal			1		
Proximal Joint Surface			4		1
Pores_A			**1**		
Cortical			1		
Sclerosis			**1**		
Diaphysis			1		
Syndesmophyte	**1**		**5**		
Cortical	1		5		
Grand Total	**8**	**12**	**54**	**2**	**1**